UNIVERSITÀ DEGLI STUDI DI MILANO

DIPARTIMENTO DI BIOLOGIA E GENETICA PER LE SCIENZE MEDICHE
SCUOLA DI DOTTORATO IN SCIENZE BIOMEDICHE CLINICHE E SPERIMENTALI
CURRICULUM IN BIOLOGIA APPLICATA ALLE SCIENZE MEDICHE

Smac-Mimetic- and TRAIL- based combinations as therapeutic strategies for *KRAS*-mutated cancers

SETTORE BIO/13 - BIOLOGIA APPLICATA

DOTTORANDA
Annalisa Conti

RELATORE
Prof. Carmelo Carlo-Stella

CORRELATORE
Dott. Domenico Delia

COORDINATORE DEL DOTTORATO
Prof. Massimo Locati

Anno Accademico 2013-2014

Smac-Mimetic- and TRAIL- based combinations as therapeutic strategies for *KRAS*-mutated cancers

THESIS

SUBMITTED TO THE

UNIVERSITÀ DEGLI STUDI DI MILANO

FOR THE DEGREE OF

DOCTOR OF PHILOSOPHY

Annalisa Conti

2014

The thesis work was carried out at

FONDAZIONE IRCCS Istituto Nazionale Tumori Milano, Milan (Italy).
Department of Experimental Oncology and Molecular Medicine
Molecular Mechanisms of Cell Cycle Control Unit
Head of the lab, Dr Domenico Delia.
(1st January 2012 – 30th April 2012, 1st August 2014 – 31st December 2014).

UNIVERSITY COLLEGE LONDON (UCL) Cancer Institute, London (United Kingdom).
Paul's O'Gorman Building
Centre for Cell Death, Cancer and Inflammation (CCCI)
Head of the lab, Prof. Henning Walczak.
(1st May 2014 – 31st July 2014).

The thesis work was funded by

Italian Association for Cancer Research (AIRC)

Italian Foundation for Cancer Research (FIRC)

Telethon

Cancer Research UK

Dr. Mildred-Scheel Stiftung/Deutsche Krebshilfe

Acknoledgements

First of all I would like to thank Dr. Domenico Delia for mentoring and supporting my scientific career so far and Prof. Carmelo Carlo-Stella for having supervised my thesis.
I would like to thank Daniele Lecis, my first and closest labmate, for his precious advice and patient working with me, for spending together hard and funny times in the lab since I joined the group. Although we have worked together for few months, I would like to thank Maria Teresa Majorini for cheering me up every time throughout her smiles, warm hugs and morning croissants. Then, I thank my desk neighbor, Laura Zannini for our early-morning chats and practical suggestions, Luigi Carlessi for being so playful, Clara Ricci for her sympathy and availability. Together with them, I thank Enrico Fontanella, Alessandro Corti, Martina Magni, Antonio Fiorino, Elena Fusar Poli and Vincenzo Ruscica. Furthermore, I thank my lab-neighbors, Maria Chiara Anania and Paola Romeo for their kindness and for the unforgettable leisure time spent together.

I would like to thank Prof. Henning Walczak for hosting me in his group. Then, I would like to thank Silvia von Karstedt and Johannes Lemke for sharing their projects with me and for having lots of fun in the lab. Furthermore, I would like to thank Nieves Peltzer for being a special friend rather than a collegue, together with Lucia Taraborrelli for still being with me. Then I thank Maurice Darding for his useful opinions and sweetness; Hartwing Torsten for reminding me that “Every little thing is gonna be all right”; Antonella Montinaro for supplying poppy flower muffins and being always helpful; Aida Borr for her hugs every morning; Sebastian Kupka and Matthias Reichert for bearing me singing in the lab and Eva Reiser, even though for a short time, for being such a sweet desk- and bench- mate. I really thank all the members of the lab for making me experience such a multiculture atmosphere.

I thank the Italian Foundation for Cancer Research for funding my fellowship at UCL.

I also thank Prof. Alberto Bardelli, Dr. Onno Kranenburg, Dr. Anna Trauzold and Prof. Julian Downward for providing me with various cell lines studied in this thesis, Prof. Pierfausto Seneci for providing Smac-Mimetic SM83, Prof. Martino Bolognesi for supplying recombinant proteins and Prof. Stephen J. Elledge for providing the inducible lentivirus employed as vehicle to express mutated KRas.

I thank Dr. Serenella Pupa for encouraging me in any situations and for all her precious suggestions.

Moreover, I thank Dr. Elda Tagliabue for being always interested in my scientific growth and for all the cell lines she kindly provided.

I would like to thank Prof. Cesare Bartolucci for following my scientific growth always with great curiosity and attention since I started university.

I would like to thank Jenny Di Nunzio for believing in me and sustaining me everytime. Thank you for such an awesome time spent together.

Furthermore, I would like to thank Francesca Ripamonti, Silvia Mancinelli and Gaia Ghedini for being always with me.

I do thank my parents, Massimiliano and Loredana, and my brother Lorenzo for trusting and supporting me and above all for their unconditional love.

Abstract

One third of human cancers are driven by oncogenic mutations in the *KRAS* loci. In particular, *KRAS* lesions are predominantly found in the most recalcitrant cancer types of internal organs such as pancreas, colon and lungs. A vast variety of signaling pathways is aberrantly activated downstream mutated *KRAS*, thus rendering tumours highly aggressive in terms of disease progression, chemoresistance and metastatic potential. Although several attempts have been made to design effective treatment strategies to eradicate these tumours, poor patients' prognosis still remains a key issue in clinical oncology. One of the main limitations of therapies that selectively target kinase-signaling pathways is the emergence of secondary drug resistance. Therefore, new therapeutic approaches are based on combinatorial therapies, which concomitantly hit the tumour from different sides.

Herein, we firstly show a synthetic lethal interaction of Smac-mimetic 83 (SM83) and Camptothecin (CPT) in presence of mutated *KRAS* employing a model of premalignant tumour cells. Mechanistically, we find that knock-in introduction of mutated *KRAS* upregulates Noxa via MAPK ERK2. At the same time, SM83, targeting the inhibitors of apoptosis proteins (IAPs) displaces caspase and enhances TNF-mediated cell death. Thus, specific *KRAS* mutations offer an unusual death-prone scenario in which, together with SM83, CPT efficiently triggers the mitochondrial apoptotic pathway in premalignant cells. Contrarily, in colorectal cancer settings the combination of SM83 and CPT is not lethal when *KRAS* is mutated suggesting that other pathways are aberrantly activated and render cancer cells resistant to death.

Secondly, we propose a novel therapeutic strategy based on selective inhibition of Cyclin Dependent kinase 9 (CDK9) and concomitant induction of apoptosis via death ligand TRAIL in *KRAS*-mutated non-small cell lung cancer (NSCLC) cell lines. We indeed demonstrate that SNS-032, the most specific and clinically used inhibitor of CDK9, strongly synergizes with TRAIL in killing a panel of human TRAIL-resistant NSCLC cell lines. Moreover, we provide evidence of the efficacy of this novel combination *in vivo*. In fact, SNS-032 and TRAIL co-treatment totally eradicates established lung tumours. However, as the mice engrafted are immunosuppressed, this model does not provide any information regarding the interaction of the treatment with the murine immune system. Therefore, to further validate the efficacy of our novel combination, we establish an autochthonous mouse model of NSCLC. Preliminary *in*

vitro treatments with TRAIL and CDK9 inhibitor confirm the efficacy of the combination; nevertheless, the setting of the *in vivo* experiments is still ongoing.

Despite several combinatorial approaches have been so far entered clinical trials, patients often relapse and metastasis is still the main cause of cancer-related deaths especially in presence of mutated *KRAS,* which provides cancer cells with high metastasising potential. Therefore, we finally focus on the mechanisms by which *KRAS*-mutated tumours metastasize. Indeed, we point out that endogenous TRAIL and TRAIL-R2-mediated signaling is required to promote migration, invasion and metastasis via activation of Rac-1/PI3K signaling axis in *KRAS*-mutated cancers. Interestingly, we provide genetic *in vivo* evidence that mouse TRAIL-R is a key driver of cancer progression and metastasis.

Significance: *KRAS*-mutated cancers are still refractory to current targeted therapies. Therefore, we propose two drug-combination approaches, which aim to induce cell death in tumour cells: whereas SM83 in combination with CPT acts at premalignant stages of cancer development, CDK9 inhibition is capable to overcome TRAIL resistance in NSCLC even *in vivo*, thereby supporting further preclinical investigations. Moreover, we provide new insights on the mechanisms regulating the metastatic process mediated by endogenous TRAIL/TRAIL-R2 pathway. We thus envisage both TRAIL and TRAIL-R2 as potential candidate-targets in clinic.

Table of contents

1 Introduction

1.1 Apoptosis

Apoptosis is a programmed process of cell death triggered to eliminate non-functional cells during developmental stages and tissue homeostasis [Steller, 1995]. Remarkably, induction of apoptosis constitutes an attractive approach to kill cancer cells and could offer a chance to prevent tumorigenesis and eradicate tumours already established. However, tumour cells evolve a variety of strategies to limit or circumvent apoptosis [Hanahan and Weinberg, 2011]. Therefore, apoptosis resistance represents one of the six hallmarks of cancer originally proposed in 2000 by Hannah and Weinberg [Hanahan and Weinberg, 2000]. Accordingly, most current anti-cancer therapies aim to target signalling factors, which govern apoptotic resistance.

In contrast to necrosis, a form of cell death that results from acute tissue injury and provokes an inflammatory response, apoptosis is precisely regulated [Newsom-Davis *et al*, 2009]. There are two well-characterised apoptotic pathways in mammalian cells: the intrinsic and the extrinsic pathway, which both depend on the balance between pro- and anti- apoptotic downstream effectors. The intrinsic apoptotic pathway is caused by unbalanced homeostasis and intracellular stresses such as oxidative stress and DNA damage [Galluzzi *et al*, 2012]. In response to these stimuli, cells employ mithocondria and their related proteins to orchestrate and activate a protein complex called apoptosome, thus leading to cell death. As this pathway relies on mithochondria, it is also referred to as the 'mitochondrial' apoptosis pathway [Green and Kroemer, 2004]. The extrinsic apoptotic pathway is mediated by the interaction of death ligands belonging to Tumour Necrosis Factor (TNF) superfamily with their cognate receptors, the TNF-Receptors (TNF-R) family members located in the plasmatic membrane. The binding between death ligands and their receptors leads to the recruitment of several adaptor proteins that act in concert forming the Death Induced Signalling Complex DISC [Scaffidi *et al*, 1998], a phenomenon which was first described for the CD95/CD95 Ligand (L) system [Kischkel *et al*, 1995]. This event initiates an intracellular signal transduction cascade that results into apoptosis. Cells undergoing both DISC- and mitochondria-

mediated apoptosis engage the activation of 'initiator' caspases, which then activate 'effector' caspases. Caspases are cysteine-dependent, aspartate-specific proteases that can be rapidly activated by proteolitic cleavage [Falschlehner *et al*, 2007].

1.1.2 Type I *versus* Type II cells

Depending on the pathway employed to induce apoptosis, cells can be classified in two different groups. In cells termed 'type I cells', assembly of the DISC is stable and robust enough to fully activate caspase-8 which, in turn, directly and completely activates the processing of caspase-3 into its cleaved form, thus enabling apoptosis [Chaigne-Delalande *et al*, 2008, Dickens *et al*, 2012]. In so-c alled 'type II cells', DISC-activation is not sufficient to immediately trigger caspase-3 activation and consequent induction of apoptosis. Hence, cells additionally require the mithocondrial machinery to die. To make mitochondria death-promoting organs, caspase-8 cleaves Bcl-2 homology 3 (BH3) interacting-domain death agonist (Bid) [Kantari and Walczak, 2011]. The resulting truncated (t) form of Bid, tBid, mediates the activation of Bcl-2-associated X protein (Bax) and Bcl-2 homologous antagonist/killer (Bak), two pro-apoptotic Bcl-2 family members, which subsequently lead to mithocondrial outer membrane permeabilisation (MOMP) [Waterhouse *et al*, 2002, Wei *et al*, 2001, Westphal *et al*, 2014].

This phenomenon allows the release of cytochrome-c that, together with cytosolic Apaf-1 and pro-caspase-9, forms the apoptosome. Consequent activation of caspase-9 drives processing of effector caspase-3 and -7, resulting in apoptosis induction [Barnhart *et al*, 2003]. In this scenario, X-linked inhibitor of apoptosis protein (XIAP), one of the members of the inhibitor of apoptosis proteins (IAPs) family, can tightly bind active caspase-3, -7 [Barnhart *et al*, 2003, Chai *et al*, 2001] and -9 [Srinivasula *et al*, 2001], thus blocking the final steps of the apoptosis process. Nevertheless, mithocondria permeabilisation allows the Second Mitochondria-derived Activator of Caspases/Direct IAP Binding protein with LOw isoelectric point (SMAC/DIABLO) to translocate to the cytoplasm and neutralise XIAP, thus preventing caspase inhibition [Verhagen *et al*, 2000]. Moreover, mithocondria release additional pro-apoptotic factors belonging to BH3-only proteins such as Bcl-2-like protein 11 (Bim), p53 upregulated modulator of apoptosis (PUMA) and Noxa (damage in latin) [Zhang *et al*, 2013], which can enhance

apoptotic process unless antagonised, by the anti-apoptotic proteins such as B-cell lymphoma 2 (Bcl-2), B-cell lymphoma-extra large (Bcl-xL), Myeloid leukemia cell differentiation protein (Mcl-1), which will be described in details in Paragraph 1.2.7.
A schematic overview of the apoptosis pathways is shown in Figure 1.

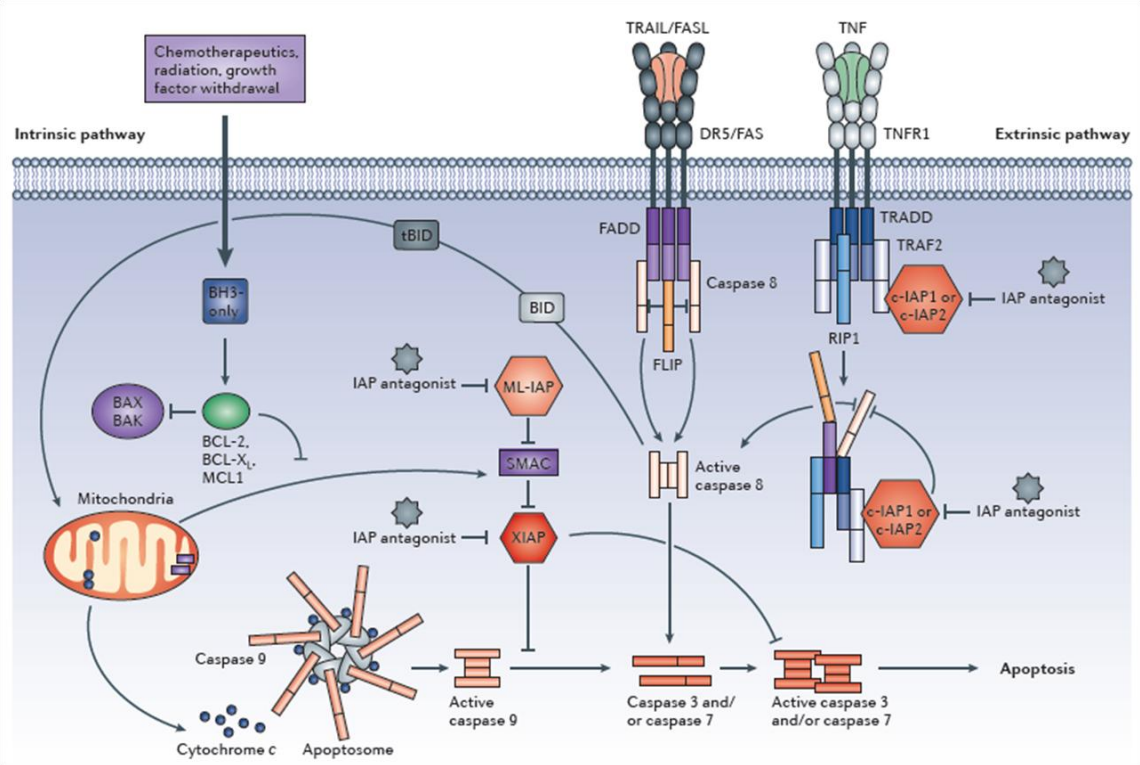

Figure 1 | Overview of cell death pathways [Fulda and Vucic, 2012].

1.2 The TNF/TNF-R superfamily

One of the key molecules in tumour immunology and pro-inflammatory signalling is TNF. In 1975, Carswell *et al*. made the interesting finding that tumour-bearing mice produce a bacterially-induced substance, later named TNF due to its capability to induce necrotic death of tumours [Carswell *et al*, 1975]. The discovery of *Lymphotoxin* (LT), which shares high homology with TNF and even binds the same receptor at high concentrations, has given the first hints of the existence of a family comprising related proteins such as TNF, LT and possibly others. These studies allowed the discovery of a whole range of cellular factors involved in the regulation of the immune system, which are homologous to TNF and therefore classified in the TNF-superfamily (TNF-SF) of cytokines. Interestingly, the TNF-SF members bind to the cognate receptors, referred to as the TNF-receptor superfamily (TNF-R-SF), which comprises more members than the TNF-SF, suggesting that some ligands can bind to several receptors. The TNF-R-SF members are characterized by the repetition of up to six cysteine rich domains (CRD) in the extracellular portion of the type I transmembrane proteins. Moreover, six TNF-R-SF members contain intracellular domains which have been described to be required for cell death-induction and are therefore called death domains (DDs) of which the most intensively studied are TNF-receptor 1 (TNF-R1), CD95 and Tumour necrosis factor-related apoptosis-inducing ligand-receptor 1/2 (TRAIL-R1/2). Although TNF-R1 contains a DD, it primarily induces gene induction via the mitogen activated protein kinase (MAPK) pathway and activation of the transcription factor Nuclear factor KappaB (NF-κB) [Wajant *et al*, 2003]. It is interesting to note that local high-doses of TNF can destroy tumour blood vessels but at the same time induce angiogenic factors [Kollias *et al*, 1999, Lejeune *et al*, 1998]. Contrarily, continuous presence of low-doses of TNF and consequential NF-κB activation have been shown to be tumour-promoting in mouse models of skin, liver, colorectal and pancreatic cancer [Egberts *et al*, 2008, Pikarsky *et al*, 2004, Popivanova *et al*, 2008, Scott *et al*, 2003].

CD95 (APO-1/Fas) is another member of the TNF-R-SF which was initially thought to primarily induce apoptosis and recently discovered to trigger also necroptosis. In 1995, Kischkel *et al*. immuno-precipitatied the protein complex DISC which forms at the DD of CD95 upon CD95L stimulation of intact cells [Kischkel *et al*, 1995]. This complex

comprises FADD [Boldin *et al*, 1995, Chinnaiyan *et al*, 1995] and caspase-8 [Boldin *et al*, 1996, Muzio *et al*, 1996].

Another member of the TNF-SF, named TNF-related apoptosis inducing Ligand (TRAIL) was later demonstrated to induce apoptosis in a way similar to CD95L [Pitti *et al*, 1996, Wiley *et al*, 1995]. Due to its high sequence homology to CD95L, a similar mechanism of DISC forming at the DD of the receptor was suggested. TRAIL-induced apoptotic and non-apoptotic signalling will be discussed in the following chapters more in detail.

Since TRAIL and CD95L are potent apoptosis-inducing agents, they sparked a lot of interest regarding the development of cancer therapeutics. However, apoptosis induction by CD95L turned out to be clinically inapplicable since systemic administration of an agonistic monoclonal antibody against CD95 is highly toxic and leads to severe liver damage in mice [Ogasawara *et al*, 1993]. CD95 is highly expressed on hepatocytes, likely explaining the hepatotoxicity [Tanaka *et al*, 1997]. A hexameric version of CD95L has been shown to be less hepatotoxic and is therefore currently in phase-I clinical trials (www.clinicaltrials.gov.). On the contrary, TRAIL potently induces apoptosis in tumour cells but not in normal cells [Walczak *et al*, 1999]. Ongoing clinical trials employing recombinant TRAIL or agonistic antibodies specific for TRAIL-R1 or TRAIL-R2 have not reported any gross toxicity so far [Newsom-Davis *et al*, 2009]. These findings placed TRAIL in the centre of attention within the TNF-SF concerning bio-therapeutic agents for cancer therapy [Johnstone *et al*, 2008, Wajant *et al*, 2002].

1.2.1 TNF/TNF-Rs signalling: between gene activation and cell death

TNF can trigger two apparently divergent cellular responses through the interaction with its cognate membrane receptors: gene activation and cell death [Wajant *et al*, 2003]. One of the most surprising observations about this cytokine is that it can kill only very few cells [Walczak, 2011]. In general, it contributes to stimulation of immunity [Aggarwal, 2003, Hayden and Ghosh, 2008, Wajant *et al*, 2003], and can also sustain cancer and play a role in tumour immune evasion [Verhoef *et al*, 2007].

Upon TNF binding, the cytosolic portion of TNF-R1-trimers recruits the receptor interacting protein 1 (RIP1) and TNFR1-associated death domain (TRADD) [Emmerich

et al, 2011a, Walczak *et al*, 2011]. TRADD then serves as an adapter protein for TNFR-associated factor 2 (TRAF2), which in turn associates with cellular IAP 1 (cIAP1) and cIAP2. Once this core complex is assembled, several ubiquitination events promote full assembly and functionality of the TNF-receptor signalling complex (TNF-RSC). The E3-ligase activity of cIAP1/2 forms ubiquitin chains that provide the binding sites for the recruitment of Linear Ubiquitin Chain Assembly Complex (LUBAC) to the TNF-RSC [Emmerich *et al*, 2011a, Haas *et al*, 2009]. LUBAC is a heterotrimer composed of HOIL-1, HOIP and SHARPIN [Gerlach *et al*, 2011, Ikeda *et al*, 2011] as shown in Figure 2.

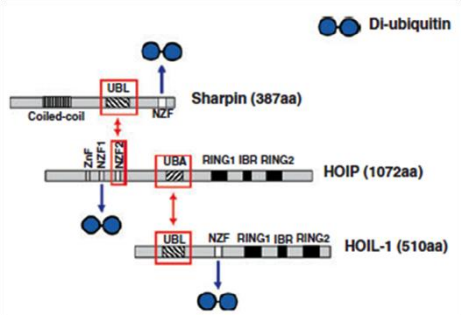

Figure 2 | Schematic representation of the interactions between the three LUBAC components and with ubiquitin [Walczak, 2011].

As illustrated in Figure 3, LUBAC attaches Met1-linked (also known as linear) Di-Ubiquitin chains to NF-kB essential modulator (NEMO) and RIP1, thus strengthening the TNF-RSC [Gerlach *et al*, 2011, Schmukle and Walczak, 2012]. Ubiquitination by cIAPs and LUBAC enables recruitment of the Inhibitor of kB (IkB) kinase (IKK) and TNF-associated kinase (TAK)/TAB complexes, leading to the activation of canonical NF-kB and MAPKs, respectively [Emmerich *et al*, 2011a]. LUBAC activity is not essential for TNF-induced activation of NF-kB; nevertheless, by retaining RIP1, TRAF2, cIAP1/2 and TAK1 in the complex, it extends the half-life of the TNF-RSC. Hence, LUBAC is important for regulating the strength of the signal transduction and gene expression, and for preventing TNF-induced apoptosis [Emmerich *et al*, 2011b]. Interestingly, it has been recently published that LUBAC and its linear-ubiquitin-forming activity are required for maintaining vascular integrity during embryogenesis by preventing TNF-R1-mediated endothelial cell death [Peltzer *et al*, 2014]. This further highlights the importance of LUBAC-mediated gene induction.

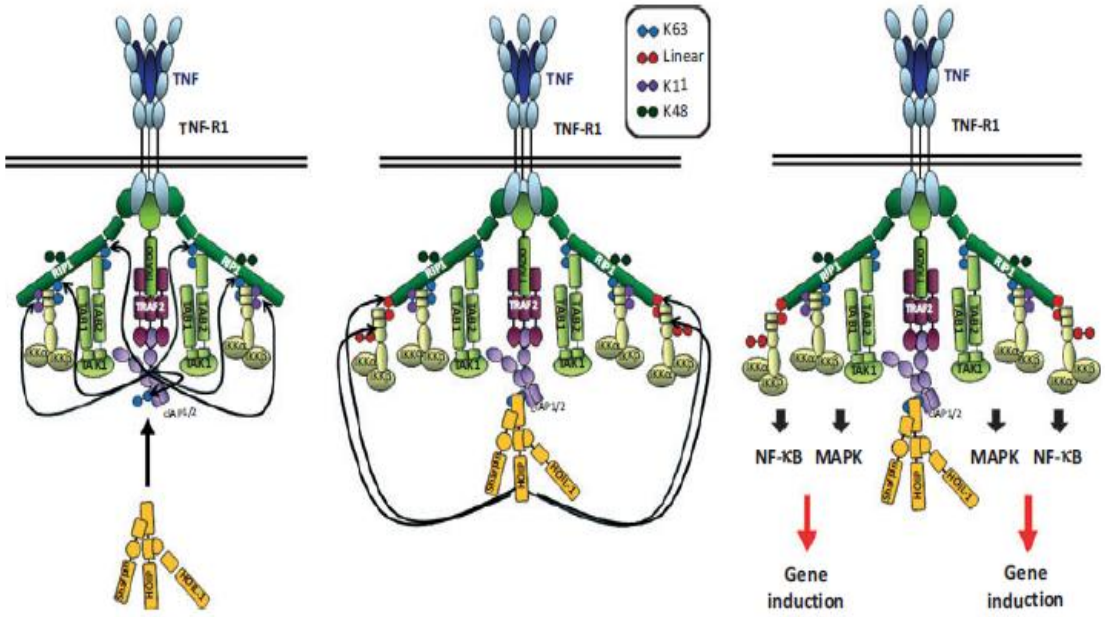

Figure 3 | Model of TNF-RSC proposed by Walczak [Walczak, 2011]**.**

1.2.2 Regulation of LUBAC at the TNF-RSC

Unlike other death ligands, TNF does not kill cells in most circumstances and instead stimulates NF-κB and MAPKs, leading to cell survival and stimulation of inflammation. Interestingly, gene expression induced by LUBAC can be 'switched-off' by either preventing the recruitment of LUBAC to the TNF-R complex or impeding LUBAC-mediated ubiquitination and consequently activation/stabilisation of its targets. Firstly, treatment with IAP targeting compounds named Smac-Mimetics (SMs) known to induce rapid auto-ubiquitination and proteosomal degradation of cIAPs [Vince *et al*, 2007], can block gene induction [Gerlach *et al*, 2011]. Secondly, linear ubiquitin activity associated to LUBAC can be modulated by deubiquitinases (DUBs). In particular, it has recently been discovered a previously unnoticed human DUB called OTULIN, belonging to the ovarian tumour (OTU) DUB family, which hydrolises linear ubiquitin chains of LUBAC [Keusekotten *et al*, 2013]. Furthermore, Gumby was identified as another member of the OUT linear DUB family, which interacts with HOIP, thus regulating LUBAC-mediated

Wnt signaling [Rivkin *et al*, 2013]. An additional DUB, named cylindromatosis (CYLD) can cleave linear polyubiquitin chains on HOIP and, together with OTULIN, synergistically suppresses LUBAC-mediated linear polyubiquitination and TNF-induced NF-kB activation [Takiuchi *et al*, 2014]. Additionally, A20 is a potent inhibitor of NF-kB whose mechanism of action is still unknown. Intriguingly, A20 is characterised by two ubiquitin-editing domains that cooperate in their activity: the N-terminal domain, which is a de-ubiquitinating (DUB) enzyme of the OTU family, removes ubiquitin chains from RIP1, while the C-terminal domain functions as a ubiquitin ligase by polyubiquitinating RIP1, thereby targeting RIP1 for proteasomal degradation [Wertz *et al*, 2004]. TNF-RSC is then destabilised and, as a consequence, NF-kB signaling is downregulated. Although the regulation of the linear ubiquitin chain generation by LUBAC is not well characterised yet, these findings highlight that OTULIN, Gumby, CYLD and A20 can be so far considered as NF-kB switch-off players, thus representing another way to balance signalling pathways downstream of the TNF-R.

A summary of the outcome generated by the presence or the absence of LUBAC at the TNF-RSC is shown in Figure 4.

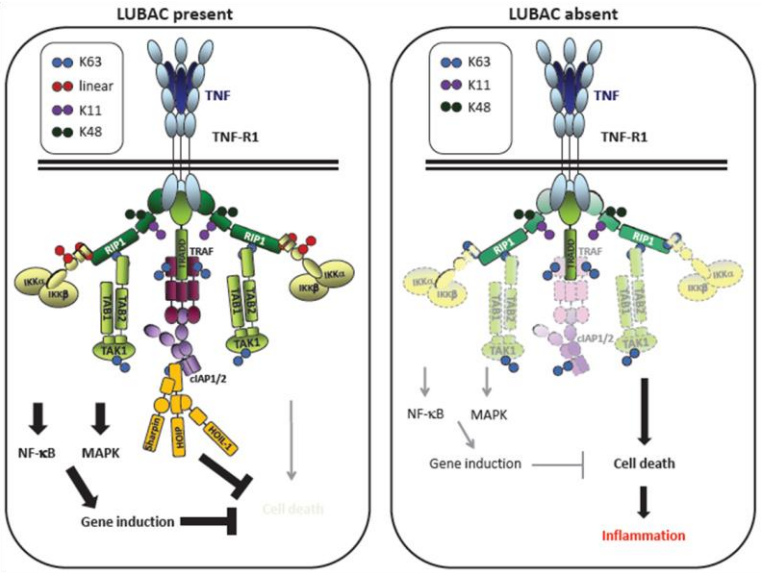

Figure 4 | Model of TNF-R1 signaling with and without LUBAC [Walczak *et al*, 2012]**.**

1.2.3 TNF-induced necroptosis

Beside influencing TNF-induced gene activation, in the absence of cIAPs, TNF stimulates the formation of a secondary cytoplasmic complex, named Complex II which contains RIP1, FADD and Caspase-8 [Micheau and Tschopp, 2003, Petersen *et al*, 2007]. In most cases, activated Complex II leads to apoptosis, however, in some cells, exposure to caspase inhibitors or intracellular factors like cellular FLICE-like inhibitory protein (cFLIP) which prevents caspase-8 activation switches the apoptotic response to necrosis [He *et al*, 2009]. It is currently in use the term necroptosis as a cell death mechanism that complements the conventional cell death pathway, apoptosis, in multicellular organisms. Receptor interacting Protein 3 (RIP3) is the key effector of necroptosis and exerts its role phosphorylating and consequently activating RIP1, and the pseudokinase Mixed Lineage Kinase Domain-Like (MLKL) [Sun *et al*, 2012]. Yet, the molecular events following RIP3-mediated phosphorylation of MLKL required to induce cell death still need to be elucidated [Hildebrand *et al*, 2014].

1.2.4 TRAIL/TRAIL-R system

When human TRAIL was identified as a CD95L homologous molecule its transcript was found to share 65% sequence identity with murine TRAIL and to be expressed in many tissues with the highest expression in spleen, thymus, prostate and lung [Wiley *et al*, 1995]. Among all death-inducing ligands of the TNF-SF, the TRAIL/TRAIL-R system seems to be the most complex with five different receptors for TRAIL being reported [Newsom-Davis *et al*, 2009]. Nevertheless, only two of them are able to transmit an apoptotic signal, namely TRAIL-R1 (DR4) and TRAIL-R2 (DR5) [Walczak *et al*, 1997]. Two additional receptors, which are incapable of transmitting an apoptotic signal, TRAIL-R3 and TRAIL-R4 [Degli-Esposti *et al*, 1997], were subsequently cloned and characterised. Whilst TRAIL-R3 lacks a DD, TRAIL-R4 only comprises a truncated DD and can induce activation of NF-kB upon overexpression [Degli-Esposti *et al*, 1997]. Both receptors have been suggested to act as “decoy” receptors not only by sequestring TRAIL molecules and thereby decreasing the probability of this ligand to bind TRAIL-R1 and TRAIL-R2 [Riccioni *et al*, 2005], but also by negatively influencing TRAIL-DISC

formation [Merino *et al*, 2006]. However, these observations were made only in overexpression systems. A decoy function of these receptors still needs to be confirmed in physiological settings. Lastly, TRAIL also binds a soluble receptor called osteoprotegerin (OPG) which is involved in regulation of bone formation and normally functions as a decoy receptor for Receptor Activator of Nuclear factor Kappa B Ligand (RANKL). RANKL is the natural ligand for Receptor Activator of Nuclear factor Kappa B (RANK), which, upon ligand-induced interaction on osteoclasts, activates NF-kB resulting in osteoclast-mediated bone resorption [Wilson, 2011]. Consequently, TRAIL binding to OPG prevents RANKL binding to OPG thereby promoting RANKL binding to RANK which leads to an increase in bone resorption [Vitovski *et al*, 2007]. Moreover, a role of OPG in cancer cell survival, by functioning as a TRAIL decoy receptor, has also been proposed [Holen *et al*, 2002].

1.2.5 TRAIL-induced apoptosis

Upon binding of TRAIL to its respective DD-containing receptors, receptor trimerisation and subsequent recruitment of FADD, caspase-8 and -10 as well as cFLIP are triggered [Sprick *et al*, 2000]. DISC formation leads pro-caspases-8 and -10 to cluster around adaptor proteins at the intracellular portion of the death receptor. The clustering and not the cleavage of the pro-domains of pro-caspases leads to their activation [Salvesen and Riedl, 2008]. Furthermore, the ubiquitin ligase Cullin 3 (CUL3) was shown to associate with caspase-8 upon TRAIL stimulation and to mediate poly-ubiquitination of caspase-8, which is required for caspase-8 aggregation and activation [Jin *et al*, 2009]. Following their activation, initiator caspases are cleaved in an autocatalytic process, generating large and small subunits. These large and small subunits form active hetero-tetramers, which activate the downstream effector caspases-3 and -7 [Stennicke *et al*, 1998]. Cleavage of their substrates leads to the key morphological changes observed during apoptosis.

1.2.6 TRAIL-induced necroptosis

Although necroptosis was originally discovered as a TNF-mediated cell death, soon thereafter it was found that cell death triggered by CD95L and TRAIL can, under certain circumstances, also be necroptotic [Vandenabeele *et al*, 2010]. It was further shown that Necrostatin-1 (Nec-1), an inhibitor of RIP1 kinase activity, can block this kind of cell death [Degterev *et al*, 2005]. The molecular mechanisms of necroptosis at least as far as we understand to date, have been reviewed [Vandenabeele *et al*, 2010].

1.2.7 Mechanisms of resistance to TRAIL-induced cell death

In order to escape TRAIL-induced cell death, tumour cells engage anti-apoptotic mechanisms at DISC- and mitochondria- levels.

The protein cFLIP is responsible for preventing DISC activation and is characterised by three splice variants: cFLIP-long ($cFLIP_L$), cFLIP-short ($cFLIP_S$) and cFLIP-Raji ($cFLIP_R$). The first isoform, if expressed at low levels, favours pro-caspase-8 recruitment to the DISC [Micheau and Tschopp, 2003], otherwise, as well as $cFLIP_S$ and $cFlip_R$, it exerts its anti-apoptotic activity competing with caspase-8 and -10 for binding to FADD, thereby obstructing the DISC-mediated induction of apoptosis [Krueger *et al*, 2001]. These isoforms can also interfere with the necroptosis pathway: whereas $cFLIP_S$, preventing caspase-8 recruitment to the DISC, enhances caspase-8 enrollment to RIP1/3 complex, thus leading to necroptosis induction, $cFLIP_L$ sequesters caspase-8 and, as a result, impedes the activation of RIP1/3-mediated necroptosis [Feoktistova *et al*, 2011, Oberst *et al*, 2011, Tenev *et al*, 2011]. Mechanisms of resistance to mitochondria-mediated apoptosis assume high importance in type II cells that usually necessitate of this organelle to undergo apoptosis. MOMP is governed by the interaction of the so-called Bcl-2 family members: Bax and Bak, together with the BH3-only proteins such as Bid, Bim, PUMA and Noxa act as pro-apoptotic factors and Bcl-2, Bcl-xL and Mcl-1 as pro-survival factors [Shamas-Din *et al*, 2013]. All together these molecules orchestrate the response to apoptotic stimuli, hence the resulting balance tightly regulates the cell fate between survival and death. Accordingly, cancer cells aberrantly express the Bcl-2 family members via down-regulating and up-regulating respectively pro- and anti-

apoptotic effectors. This cancer cell strategy to escape apoptosis partially explains why type II tumour cells are resistant to conventional chemotherapy and/or radiotherapy. Concerning TRAIL-based therapy, several groups demonstrated that both overexpression of Bcl-2, Bcl-X_L or Mcl-1 and lack of Bax and Bak can be responsible for TRAIL-resistance in many cancer cell types as reviewed by Lemke *et al.* [Lemke *et al*, 2014b]. Another family of proteins, which play a role in resistance to TRAIL-induced cell death is represented by IAPs. A detailed description in terms of their structure, functions and relevance in cancer therapy is intensively expanded in Paragraph 1.3 and 1.4.

1.2.8 Roles of TRAIL/TRAIL-Rs in promoting tumour growth and metastasis

Recombinant TRAIL can selectively kill tumour cells *in vivo* [Ashkenazi *et al*, 1999, Walczak *et al*, 1999]. These findings have initiated the development of TRAIL and other TRAIL-R agonists for clinical applications as novel promising anti-cancer drugs.

More recent studies have, however, revealed that many tumour cell lines and, importantly, the majority of primary tumours, are resistant to TRAIL-induced apoptosis [Todaro *et al*, 2008]. This can in part explain the limited therapeutic benefit of TRAIL-R agonists in clinical trials [Micheau *et al*, 2013]. Moreover, recent preclinical findings indicate pro-survival, proliferation and even metastatic activity of TRAIL, suggesting more caution when applying TRAIL-R agonists, particularly as single agents [Azijli *et al*, 2012]. In fact, TRAIL- and TRAIL-R agonists-based combination therapies are required in order to additionally block non-apoptotic TRAIL signalling pathways.

More in detail, as shown in Figure 5, TRAIL can induce survival and proliferation by activation of Src [Azijli *et al*, 2012] and of MAPK family members such as c-Jun N-terminal kinases (JNK), p38 MAPK [Varfolomeev *et al*, 2005] and Extracellular signal-Regulated Kinase 1 and 2 (ERK1/2) [Belyanskaya *et al*, 2008]. Moreover, proliferation, together with migration of primary human vascular endothelial cells can be positively regulated by TRAIL stimuli of the Phosphoinositide 3-kinase (PI3K)/AKT axis [Secchiero *et al*, 2003, Secchiero *et al*, 2004]. Another effector, which plays a role in TRAIL-mediated non-cell death signaling is NF-kB [Harper and Adams, 2001, Varfolomeev *et al*, 2005, Wajant, 2004].

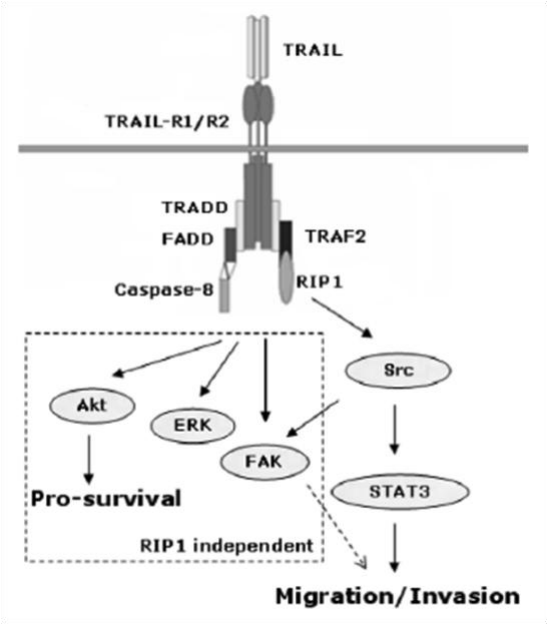

Figure 5 | Schematic representation of the identified kinases involved in non-canonical TRAIL signaling [Azijli *et al*, 2012].

In line with these findings, it has been shown that TRAIL-mediated proliferation is completely abrogated by blockage of NF-kB activation in a model of TRAIL-resistant cancer cells [Ehrhardt *et al*, 2003]. Current studies reveal that the effectors downstream TRAIL signalling responsible for survival and proliferation are also involved in promoting migration, invasion and metastasis, thus favouring tumour aggressiveness [Azijli *et al*, 2012]. In fact, TRAIL-R2-mediated signaling is also shown to promote lymph node and lung metastasis in an orthotopic model of triple negative breast cancer, thereby suggesting the employment of monoclonal antibody targeting TRAIL-R2 as effective therapeutic strategy for metastatic breast cancer [Malin *et al*, 2011]. On the contrary, it has been published that TRAIL-R inhibits lymph node metastases without affecting primary tumour formation in a mouse model of multistage skin tumorigenesis [Grosse-Wilde *et al*, 2008]. In this paper, they also demonstrated that adherent TRAIL-R-expressing skin carcinoma cells were TRAIL-resistant *in vitro* but were sensitive to TRAIL upon detachment by inactivation of the ERK signaling pathway [Grosse-Wilde and Kemp, 2008]. Since detachment from primary tumour is an obligatory step in metastasis, this could be a mechanism by which TRAIL-R exerts its metastasis suppressor role. However, other groups demonstrate the opposite concept, which

supports the idea of TRAIL/TRAIL-R as a tumour-promoter system [Bertsch *et al*, 2014, Haselmann *et al*, 2014].

Furthermore, it has been reported that treatment with TRAIL was capable of promoting liver metastasis of Bcl-X_L-overexpressing, TRAIL-apoptosis-resistant human orthotopic Pancreatic Ductal AdenoCarcinoma (PDAC) xenografts [Trauzold *et al*, 2006]. Likewise, it was previously demonstrated that *KRAS*-mutated colorectal cancer cell lines are more resistant to TRAIL-induced apoptosis than their isogenic *KRAS*-wild-type (WT) counterparts and, instead, exhibit increased migration when exposed to recombinant TRAIL [Hoogwater *et al*, 2010]. Further studies to support the potential negative implication for TRAIL in cancer therapy confirm that TRAIL promotes cell migration and invasion by a NF-kB-dependent pathway in human Cholangiocarcinoma (CCA) cells [Ishimura *et al*, 2006]. Interestingly, even Thyroid hormone Receptors (TRs) have been shown to induce TRAIL expression, and TRAIL thus synthesised acts in concert with simultaneously synthesised Bcl-X_L to promote metastasis, but not apoptosis in TR-overexpressing hepatoma cell lines [Chi *et al*, 2012].

In summary, these findings highlight that treating certain TRAIL-resistant cancers with TRAIL/TRAIL-R agonists might even worse disease prognosis [Lemke *et al*, 2014b]. It is therefore imperative to investigate in depth the molecular mechanisms based on TRAIL-mediated non-cell death pathway in order to pre-empt it.

1.3 Inhibitor of apoptosis proteins (IAPs) family.

IAP family is formed by eight members: Survivin, cIAP1, cIAP2, XIAP, NAIP, Livin, Apollon and ILP-2 (Figure 6). The defining feature of IAPs is the presence of one or more baculoviral IAP repeat (BIR) domains, which mediate protein-protein interactions with other IAPs or with caspases, hindering their activity.

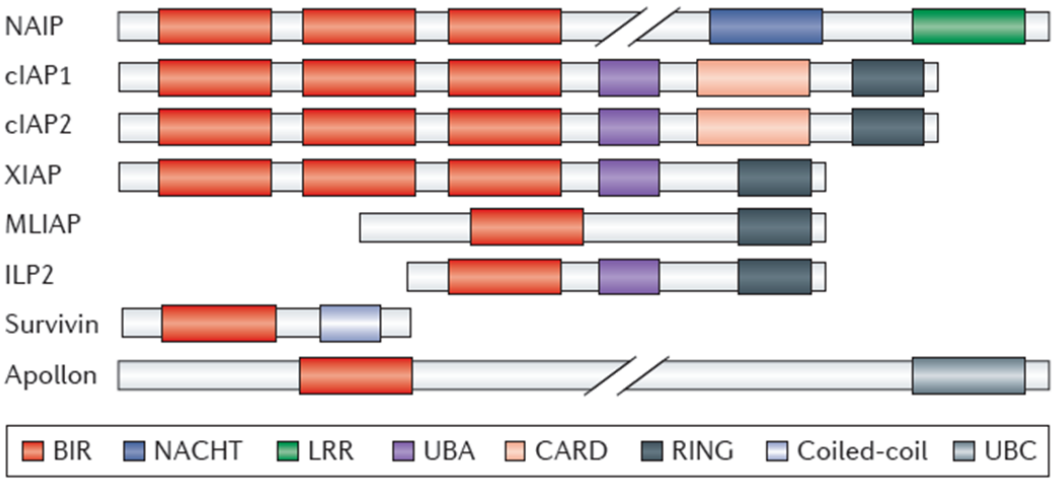

Figure 6 | Structural organization of the human IAP family members [Fulda and Vucic, 2012].

XIAP is shown to be a potent inhibitor of caspase -3, -7 [Chai *et al*, 2001, Riedl *et al*, 2001] and -9 [Srinivasula *et al*, 2001]. Other IAPs, as cIAP1 and cIAP2, interact with caspases, but the biological significance of this event is less understood [Eckelman and Salvesen, 2006].

XIAP, cIAP1 and cIAP2 are also characterised by a C-terminal Really Interesting New Gene (RING) domain endowed with E3-ubiquitin ligase activity. The dimerisation of the RING domain of cIAP1 and cIAP2 activates these proteins [Darding *et al*, 2011, Feltham *et al*, 2011], allowing the regulation of several signalling cascades involved not only in cell death but also in inflammation, cell proliferation and migration [Damgaard and Gyrd-Hansen, 2011, Gyrd-Hansen and Meier, 2010, Lopez *et al*, 2011]. Intriguingly, cIAP1 has been shown to be essential for maintaining endothelial cell survival and blood vessel homeostasis during vascular development, thereby providing an additional target

pathway for the control of angiogenesis [Santoro *et al*, 2007]. The proteins cIAP1 and cIAP2 also contain an UB-associated (UBA) domain for binding to poly-Ubiquitin chains and a caspase recruitment domain (CARD). The role of CARD is not well understood yet, but, together with the BIR3 domain, it is known to inhibit the E3-ligase activity of cIAP1, preventing RING dimerization as shown in Figure 7 [Lopez *et al*, 2011].

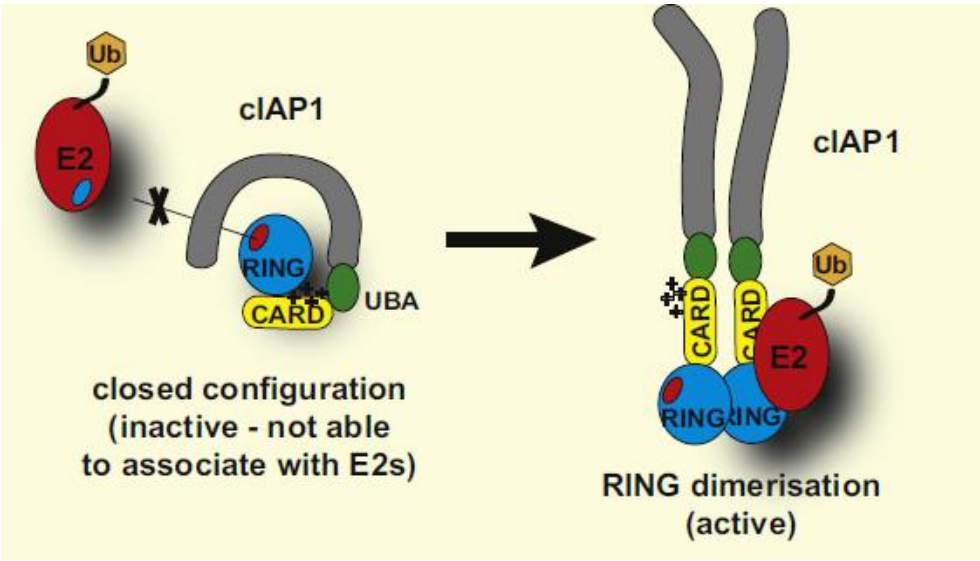

Figure 7 | **Model of RING dimerization** [Lopez *et al*, 2011, Lopez *et al*, 2011]

IAPs are frequently overexpressed in cancer and contribute to chemoresistance, disease progression and poor prognosis [Gyrd-Hansen and Meier, 2010]. In addition, the comprehension that IAPs help tumour cells to bypass the apoptotic programme suggested that IAPs are promising targets for therapeutic intervention and lead to the development of small pharmacological IAP-targeting compounds named Smac-Mimetics (SMs) to be employed in clinical oncology.

1.4 Design of Smac-Mimetics as IAPs-targeting compounds

SMs were originally designed to target XIAP, preventing its inhibition on caspases by favouring their displacement from the BIR domains of XIAP. In fact, SM compounds, mimicking the N-terminal IAP-binding motif (AVPI tetrapeptide: Alanine-Valine-Proline-Isoleucine) of mature Smac/Diablo [Oost *et al*, 2004, Seneci *et al*, 2009, Sun *et al*, 2004], selectively bind the BIR2 and BIR3 domains of XIAP [Mastrangelo *et al*, 2008].
The monomeric SMs are smaller, more stable and pass easier through the cellular barriers [Bianchi 2012], while the dimeric SMs [Cossu *et al*, 2012, Lecis *et al*, 2012, Manzoni *et al*, 2012], composed by two AVPI-mimicking molecules, are less favourable as drugs due to their heavy mass. Nonetheless, because of their ability to target simultaneously two BIR domains of the same protein [Cossu *et al*, 2009], dimeric SMs are usually more active in inducing cell death [Sun *et al*, 2008]. Furthermore, SMs target cIAP1 and cIAP2 [Cossu *et al*, 2010] and trigger their self-ubiquitilation and proteosomal degradation [Petersen *et al*, 2007, Varfolomeev *et al*, 2007, Vince *et al*, 2007]. However, the absence of cIAP1- and cIAP2- E3 ligase activity does not allow auto-ubiquitilation in response to SM treatment [Darding *et al*, 2011]. Besides controlling caspases, cIAPs display other activities: cIAP1 and cIAP2 regulate NF-kB by ubiquitylation and proteosomal degradation of NF-kB-induced kinase (NIK) thus leading to the suppression of the non-canonical NF-kB signalling [Darding *et al*, 2011, Haas *et al*, 2009]. As shown in Figure 8A, by causing the degradation of cIAPs, SMs stimulate the non-canonical NF-kB signalling thereby inducing the production of high amount of TNF, an NF-kB target, which overstimulates TNF-R1; RIP1 is then released from TNF-R1 and subsequently incorporated into a complex with caspase-8 and FADD thus promoting cell death [Varfolomeev *et al*, 2007]. This response can be engaged only by cells sensitive to SM as single agent [Petersen *et al*, 2007].

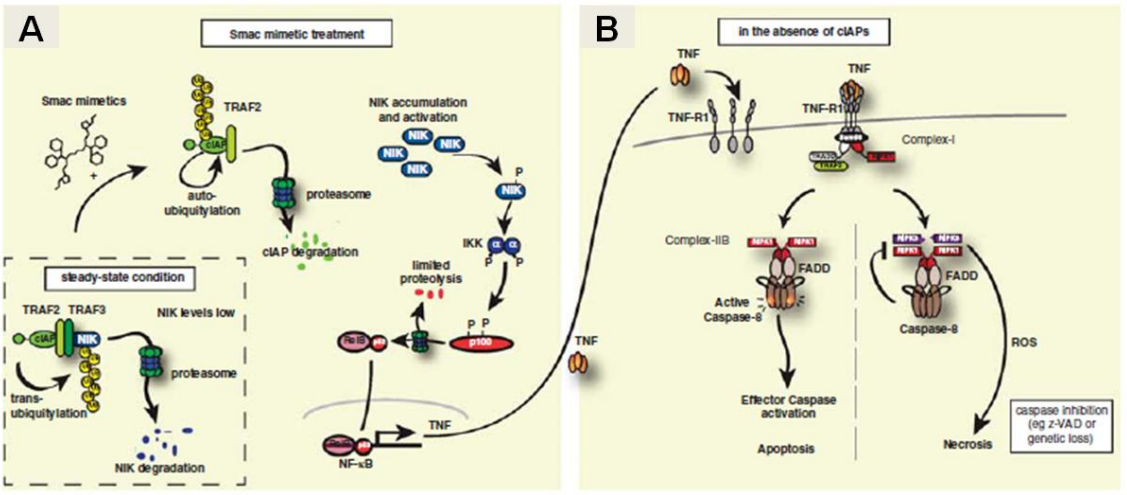

Figure 8 | SM-induced cell death by non-canonical NF-kB-mediated transcription of TNF [Darding and Meier, 2012].

Unluckily, few cancer cells can be treated by SMs as single agents [Gatti *et al*, 2014, Scavullo *et al*, 2013]. On the contrary, despite TNF-R1 expression is quite ubiquitous among several cancer cell types [Wajant *et al*, 2003], most cancer cells tested to date are not responsive to SMs [Petersen *et al*, 2010]. It has been suggested that these cell lines can upregulate cIAP2 by TNF-dependent stimulation of the NF-kB pathway. Importantly, the newly generated cIAP2 is no longer subjected to SM-induced degradation because this event is dependent on the presence of cIAP1 that rapidly undergoes degradation after SM administration and is not expressed back as quickly as cIAP2 [Petersen *et al*, 2007]. Due to the similarity of the two proteins, cIAP2 might assume the role of cIAP1 in preventing further release of RIP1 from the TNFR1 [Darding and Meier, 2012, Petersen *et al*, 2010]. A further possible explanation of SM-resistant mechanisms has been recently suggested by Wang's group: breast cancer cells resistant to SM-164 downregulate Leucine-Rich repeats and immunoglobulin-like domain 1 (LRIG1), thus increasing the expression of receptor tyrosine kinases (RTKs) and attenuating SM-induced TNF gene expression [Bai *et al*, 2012]. Nevertheless, SM activity can also be independent of TNF by inducing the formation of a large complex (~2 MDa) called 'ripoptosome', composed by RIP1, FADD and Caspase-8. Its assembly requires RIP1 kinase activity and can stimulate caspase-8-mediated apoptosis as well as caspase-independent necrosis [Tenev *et al*, 2011]. The ripoptosome forms

independently of TNF, CD95L, TRAIL, death receptors and mitochondrial pathways and is regulated by cIAP1, cIAP2 and XIAP [Feoktistova *et al*, 2011, Tenev *et al*, 2011].

1.4.1 Smac-Mimetics as potential sensitisers in the treatment of cancer

Most cancer cells are resistant to SMs as monotherapy [Petersen *et al*, 2010]. Therefore, since SMs deplete cIAPs and inhibit XIAP, they can be employed as potential sensitisers towards death-inducing ligands such as TNF, TRAIL and CD95L. Indeed, it has been reported that SMs can particularly enhance cell death triggered by TNF [Gaither *et al*, 2007] and TRAIL [Li *et al*, 2004]. Focusing on the synergism between SMs and TRAIL, SM-mediated depletion of cIAP1 can favour TRAIL-induced apoptosis, because cIAP1 is a determinant of TRAIL resistance, as recently demonstrated by Guicciardi and co-workers [Guicciardi *et al*, 2011]. Notably, SMs have shown broad preclinical activity in sensitising cancer cells especially to TRAIL-induced apoptosis *in vitro* and *in vivo* in a variety of cancer types [Fakler *et al*, 2009, Fulda *et al*, 2002, Lecis *et al*, 2010, Raulf *et al*, 2014]. In line with this, a clinical trial in ovarian cancer patients has been started to test the efficacy of SM Birinapant in combination with the TRAIL-R2 agonist Conatumumab and also the preclinical results support the employability of this kind of combination in clinic [Lemke *et al*, 2014b]. Despite the great interest towards the development of SMs and the presence of many groups that are studying their mechanism of activity, there are still some aspects that need to be clarified. Why some cancer cells respond to SMs as monotherapy and others require the addition of TRAIL to be killed is a key issue facing cancer therapy.

There is a huge spectrum of possible SM-based combinations employed in the treatment of several tumour types. For instance, SM (i) can synergise with Cytarabine, Etoposide and with TRAIL in human leukemic cell lines [Servida *et al*, 2011], (ii) can stimulate melanoma cell death in combination with TRAIL in the presence of the proteasome inhibitor Bortezomib [Lecis *et al*, 2010], (iii) can enhance the anti-proliferative effects of ErbB antagonists such as Trastuzumab, Lapatinib and Gefitinib in breast cancer [Foster *et al*, 2009] and (iv) can sensitise prostate cancer cells to TRAIL-induced apoptosis via modulation of both IAPs and NF-kB. Wang's group developed the bivalent SM-164 [Lu *et*

al, 2008] which has been shown to be active with recombinant TRAIL in a panel of 19 human breast, prostate and colon cancer cell lines *in vitro* and in a breast cancer xenograft model *in vivo* [Lu *et al*, 2011]. SM JP1201 from Minna's lab is able to act in an IAP-dependent but TNF-independent manner to sensitise non-small cell lung cancer NSCLC to multiple chemotherapeutic agents such as Doxorubicin, Erlotinib, Gemcitabine, Paclitaxel, Vinorelbine and Carboplatin [Greer *et al*, 2011]. Likewise, it has recently been shown that SM BV6 can sensitise glucocorticoid-triggered cell death by promoting ripoptosome formation in Acute Lymphoblastic Leukemia (ALL) [Belz *et al*, 2014]. Furthermore, Probst *et al* found that the combination effects resulting from SM and various chemotherapeutics (Gemcitabine, Cisplatin, SN38, Paclitaxel, 5-Fluorouracil and Etoposide) is caused by a multifacing mechanism involving either inhibition of cell proliferation by the chemotherapy agents and an enhanced autocrine TNF feedback loop by the SM/chemotherapy agent combination [Probst *et al*, 2010]. Interestingly, SMs also synergise with a diabody format of tumour-targeted TRAIL termed DbαEGFR-scTRAIL from Pfizenmeier's lab, comprising single-stranded TRAIL (scTRAIL) molecules and the variable domains of a humanised variant of the EGFR blocking antibody Cetuximab [Moller *et al*, 2014].

1.4.2 Role of Smac-Mimetics in cancer-related inflammation and immune response

Tissue stress and malfunction, key characteristics of human tumours, can induce an inflammatory response that is similar to the one elicited by invading microbes, in particular necrotic death of tumours stimulates macrophage recruitment and triggers tissue repair and modelling, which in turn fuels tumour growth [Gyrd-Hansen and Meier, 2010]. Since cIAPs are involved in inflammation, SMs can modulate immune response in the treatment of cancer. It has been published that oncolytic viruses as well as microbial RNA and DNA (Poly (I:C) and CpG, respectively) induce bystander death of cancer cells treated with SM compounds, death that is mediated by interferon beta (IFNβ), TNF and/or TRAIL. This combinatorial treatment results in tumour regression and extended survival [Beug *et al*, 2014]. Furthermore, IAPs have lately emerged as important

regulators of innate immune signalling downstream of Pattern Recognition Receptors (PRRs), such as Toll-like-receptor 4 (TLR-4), the Nucleotide-binding Oligomerisation Domain 1 (NOD1)- and NOD2- receptors and the Retinoic acid-Inducible Gene-I-Receptor (RIG-I-R), thus activating NF-kB, p38 and JNK [Bertrand *et al*, 2009, Damgaard and Gyrd-Hansen, 2011].

Taken together these findings support the idea that, even though SMs were originally designed to enhance cancer cell death and since their targets (IAPs) are components of receptor complexes involved in immunity, SMs can play novel roles in modulating immune system-related responses within cancer treatment.

1.4.3 SM83-mediated host-induced inflammatory response eradicates xenograft cancer ascites

We newly described the synthesis of novel dimeric molecules that target XIAP, cIAP1 and cIAP2. One of these molecules, SM83, inhibited the growth of SM-sensitive human mammary adenocarcinoma MDA-MB-231 and Rhabdomyosarcoma Kym-1, but not of other cell lines [Cossu *et al*, 2012, Lecis *et al*, 2012, Manzoni *et al*, 2012]

We recently published [Lecis *et al*, 2013] that SM83, when administered in monotherapy, by targeting tumour-associated macrophages, increases the survival of two murine xenograft models of cancer ascites: athymic nude mice injected intraperitoneally with IGROV-1 human ovarian carcinoma cells and immunocompetent BALB/c mice injected with murine Meth A sarcoma cells. SM83 rapidly killed ascitic IGROV-1 and Meth A cells *in vivo*, nevertheless was ineffective against the same cells *in vitro*. IGROV-1 cells in nude mice were killed within the ascites by a non-apoptotic, TNF-dependent mechanism. SM83 administration triggered a rapid inflammatory event characterised by host secretion of TNF, interleukin-1beta (IL-1β) and interferon-γ (IFN-γ). This inflammatory response was associated with the reversion of the phenotype of tumour-associated macrophages from a pro-tumoural M2- to a pro-inflammatory M1-like state. SM83 treatment was also associated with a massive recruitment of neutrophils that, however, was not essential for the antitumoural activity of this compound.

Therefore, our work shows that SM83 displays different mechanisms of action *in vitro* and *in vivo*, and that *in vivo* it exerts its antitumoural activity by stimulating the immune

system. In conclusion, our data demonstrate that the SM SM83 is active in monotherapy by promoting inflammation and immunogenic cell death. These observations likely provide an explanation for why SMs increase the effectiveness of standard therapies, namely by stimulating the immune system. Finally, the evidence that SMs can induce an inflammatory response and activate the immune system provides an interpretation of why SMs can be more effective *in vivo* than *in vitro*.

1.4.4 Smac-Mimetics as regulators of migration, invasion and metastases

Since IAPs have been related to the control of cell motility, migration, invasion and metastasis, it is relevant for cancer therapy to understand whether SM-mediated targeting of IAPs can affect the steps of the metastatic process, even because this issue is still controversial. Different works proposed that IAPs both positively and negatively control these processes [Fulda, 2013, Fulda, 2014]. Whereas Fulda's group sustains that SM BV6 at non-toxic concentrations promotes the migration and invasion of Glioblastoma cells (GBCs) via non-canonical NF-kB signaling [Tchoghandjian *et al*, 2013], Tomonaga demonstrates that LUBAC-mediated activation of NF-kB contributes to lung metastasis in osteosarcoma cells, thereby suggesting that treatment with IAP antagonists would prevent this event [Tomonaga *et al*, 2012]. Furthermore, it has been reported that SMs, beside acting on TNF-R pathway, can switch-off TRAIL-mediated NF-kB-induced upregulation of Matrixmetalloprotease 9 (MMP9), thus blocking one of the first stages of metastatisation in CCA cells [Fingas *et al*, 2010]. Apart from influencing NF-kB pathway in regulating migration and invasion, it has been published that cIAP1 and XIAP can directly bind to Rac-1 to promote its poly-Ubiquitilation and proteosomal degradation. Hence, SM treatment leads to an increase of Rac-1 protein levels in primary and tumour cells, thus guiding to an elongated morphology and enhanced cell migration [Oberoi *et al*, 2012]. Conversely, a Survivin/XIAP complex has been shown to activate NF-kB, which, in turn, leads to an increased gene expression of fibronectin, a more intense signaling by beta (β) 1 Integrins and a high activation of cell motility kinases Focal adhesion kinase (FAK) and Src [Mehrotra *et al*, 2010]. Another study supports the idea that XIAP promotes Heat Shock Protein 90 (Hsp90)-mediated

ubiquitination and, consequently, de-stabilisation of C-RAF kinase, thereby negatively modulating the migration capacity of the cell [Dogan *et al*, 2008]. On the other hand, in a model of colorectal cancer, XIAP was found to downregulate RhoGDP dissociation inhibitor RhoGDI SUMOylation, thus leading to a marked reduction of β-actin polymerisation and cytoskeleton formation [Liu *et al*, 2011]. Consistently, cell migration and invasion were also decreased. In accordance to these findings, XIAP can recruit alpha (α) 5-Integrin, Caveolin 1 and FAK to form a multicomplex that regulates endothelial cell migration via a mechanism that involves shear-dependent ERK activation [Kim *et al*, 2010]. Interestingly, a study conducted by Pascal Meier's lab demonstrates that depletion of cIAP1 and/or treatment with SMs mostly decreases migration capability of triple-negative breast cancer cell lines. Moreover, his group showed that specific loss of cIAP1 determines vascular tree degeneration *in vivo*, thus suggesting that cIAP1 can be considered as a promoter of motility and maintenance of vascular integrity [Lopez *et al*, 2011]. Hence, SMs might potentially interfere with both the migratory capacity of cancer cells and tumour vasculature in a negative manner.
In conclusion, we might presume that most of the discrepancy observed with respect to pro- and anti-migratory effects of IAPs could be attributed to the difference in the cell types employed, as many of the migration-regulating molecules controlled by IAPs could promote or inhibit migration in a context-dependent manner [Oberoi-Khanuja *et al*, 2013].

1.4.5 Clinical testing of Smac-Mimetics

So far, five distinct SM compounds have been evaluated in clinical early trials. The first-in-human phase-I dose-escalation study of LCL161 was conducted in patients with advanced solid malignancies [Infante *et al*, 2014]. In these settings, it was responsible for toxic adverse effects such as cytokine release syndrome (CRS), thus supporting the idea that cytotoxicity is still a major drawback for many SMs in the cancer clinic. Moreover, in preclinical cancer models, a variety of rationally designed SMs-based combinations have been developed, involving chemotherapeutic drugs, signal transduction inhibitors and radiotherapy. An ongoing phase-I clinical study of Birinapant (TL32711) combined with multiple chemotherapeutics evaluates tolerability and clinical

activity for solid tumours. This trial indicates that such combination may be tolerable and yield clinical benefits [Krepler *et al*, 2013].

In summary, since SMs, in monotherapy or combination, have entered the stage of clinical evaluation as cancer therapeutics, a better understanding of the various cellular effects will be decisively needed for their rational use in the treatment of cancer.

1.5 Ras in cancer

Ras is a 21 KDa protein belonging to the Ras subfamily, which comprises small GTP-hydrolysing proteins, GTPases, considered as molecular switches. When bound to GTP, these enzymes are active and transmit signals to downstream molecules. They possess weak intrinsic GTPase activity, which is however too slow in causing rapid signalling processes and therefore requires acceleration mediated by GTPase Activating Proteins (GAPs). When bound to GDP, Ras proteins are inactive and require assistance from Guanosine Exchange Factors (GEFs) in order to be loaded with GTP and to be activated [Bos, 1989]. Supported by GAPs and GEFs, Ras proteins can undergo rapid cycles of activation and facilitated self-inactivation, which is crucial for controlling Ras signalling dose.

30% of all cancers bear activating mutations in Ras [Bos, 1989]. These Ras-driven cancers are the example of what can happen when the tight network of Ras activity regulation is perturbed. Spontaneous single amino acid mutations in the GTP binding pocket of Ras at codon 12, 13 or 61 result in failure of GAP binding and, in turn, constitutively activated Ras, which is intrinsically very slow in hydrolysing bound GTP [Downward, 2003]. Consequently, downstream signalling pathways are hyperactivated in Ras-mutated cancers providing them with the ability to grow independently of growth factor stimulation and attachment, and thereby increase proliferation and migration rate.

The proteins of the Ras subfamily are NRas, HRas and KRas [Castellano and Santos, 2011]. In human cancers KRas mutations are observed with a frequency of 21% followed by 8% mutations in NRas and 3% HRas mutations [Bos, 1989]. Ras isoforms share about 80% sequence homology and mainly differ in their C-terminal so-called Hyper Variable Region (HVR) that contains lipid anchoring post-translational modifications which are required for membrane-anchoring of Ras proteins [Karnoub and Weinberg, 2008]. Ras isoforms are ubiquitously expressed in all the tissues with some preferential localisations [Leon *et al*, 1987]. Based on overexpression experiments it was originally believed that different Ras isoforms might have overlapping and redundant functions. However, studies in isoform-specific knock-out mice have demonstrated that KRas deficiency [Johnson *et al*, 2001], but not NRas [Umanoff *et al*, 1995] or HRas [Esteban *et al*, 2001], is embryonically lethal. KRas knock-out mice die between embryonic day 12 and 14 and present anaemia and liver defects [Johnson *et al*, 2001].

Although these results suggest that KRas can fulfil a unique function during development, it is also possible that its expression pattern during embryogenesis is distinct from the other isoforms, which are not present in that particular tissue at sufficient levels to compensate the loss of KRas. Besides the evidence from knock-out mice, different cancers typically are characterised by distinct Ras isoform mutations supporting the idea of isoform-specific effects. NRas mutations have high incidence in acute leukaemia, whereas HRas mutations are mostly found in bladder, thyroid and kidney cancer [Castellano and Santos, 2011]. KRas mutations are predominantly found in the most aggressive cancer types of internal organs such as 95% of all pancreatic cancers [Jaffee *et al*, 2002], 50% of colon cancers [Grady and Markowitz, 2002] and about 30% of lung cancers [Mitsuuchi and Testa, 2002].

1.5.1 Ras isoform-specific signaling

All Ras isoforms respond to the basic signalling principle that an upstream activator which can be a non-receptor or receptor tyrosine kinase such as platelet-derived growth factor receptor (PDGFR) is activated by ligand binding [Downward, 2003]. The receptor tyrosine kinase auto-phosphorylates and provides a binding site to recruit the adaptor molecule growth- factor-receptor-bound protein 2 (Grb2) via its SH2 domain. Grb2 in turn recruits the Ras GEF Son of sevenless (Sos), which binds to Grb2's SH3 domain [Bos, 1989]. Due to the resulting membrane-proximal localisation of Sos it is now placed within the membrane-associated Ras molecules. Furthermore, Sos facilitates GDP release from Ras molecules, which, as a result of chemical equilibrium, then bind with GTP, present at much higher concentrations in the cytosol. GTP-bound Ras subsequently activates a variety of downstream signalling molecules until the GTP is hydrolysed by Ras, which serves as an auto-inactivatory function for self-regulation [Downward, 2003].

KRas mutational status is nowadays screened in colon cancer patients in order to determine whether they would benefit from an Epithelial Growth Factor Receptor (EGFR)-blocking treatment, which is only effective when wild-type KRas is expressed downstream of EGFR and therefore responsive to upstream blocking. Downstream of Ras molecules, a vast variety of pathways has been described to be activated and ERK

and PI3K pathways are the most widely studied. Additional Ras effector pathways were also discovered [Cellurale *et al*, 2011, Meylan *et al*, 2009, Shields *et al*, 2000]. ERK activation is triggered via GTP-bound Ras that interacts with one of the Raf kinase isoforms (Raf1/cRaf, BRAF or ARAF). Activated Rafs trigger downstream activation of MEK1/2 kinases, which in turn activate ERK1/2. Again, different Ras isoforms were shown to have preferences between Raf isoforms. KRas is a much more potent activator of Raf1 than HRas whereas HRas is more potent in activating PI3K [Yan *et al*, 1998]. Furthermore, KRas was shown to be more efficient than HRas in activating the small GTPase Rac-1 [Walsh and Bar-Sagi, 2001], a member of the Rho GTPase-family regulating cell motility. Both H- and K-Ras can induce NF-κB activation upon overexpression whereas N-Ras is a rather weak inducer of NF-κB [Millan *et al*, 2003]. Considering the high sequence similarity between the isoforms with main differences only present in the C-terminal HVR, it is plausible that the post-translational modifications present in this region, deriving from tissue expression pattern and intracellular localization, are decisive for isoform-specific signalling.

1.5.2 Mutant KRas promotes enhanced motility

There are multiple reasons why *KRAS*-mutated cancers are highly metastatic. Enhanced KRas-mediated downstream signalling provides the increased capacity to proliferate, migrate, invade and survive anoikis. The metastatic process requires initial invasion and migration of tumour cells into the surrounding tissue and, importantly, crossing of the endothelial barrier to enter the bloodstream, a process termed intravasation [McCarthy, 2009]. While travelling in the bloodstream, cancer cells need to overcome anoikis (i.e. avoid cell death due to detachment) and evade recognition by the immune system. For long-term survival in the body they will however need to adhere again, cross the endothelial barrier and migrate into the tissue at a secondary site. This step is referred to as extravasation [Pantel and Brakenhoff, 2004]. As can be seen from the described requirements, the capacity to migrate and invade is both important at the initiating intravasation step as well as the final extravasation step. Although PI3K-signalling downstream of Ras has been mainly associated with cell survival and proliferation it can also promote Ras-mediated migration either via activation of the small GTPase Rac-1

[Nimnual *et al*, 1998] or independently of Rho-family GTPases [Cain and Ridley, 2009]. A PI3K-independent mechanism of Ras-mediated Rac-1 activation has been characterised in which the Rac-1 GEF T-cell lymphoma invasion and metastasis-inducing protein 1 (Tiam1) directly binds Ras via a Ras-binding domain and activates Rac-1 even in cells expressing PI3K- binding mutants of Ras [Lambert *et al*, 2002].

1.5.3 Synthetic lethal interactions associated to oncogenic *KRAS*

KRAS-mutated cancers are notoriously difficult to be treated in clinic. Small molecule Ras inhibitors, which have been developed to decrease Ras activity, have, however, only led to marginal success so far [Sebti and Adjei, 2004]. At the moment, new targeted therapeutic strategies consists in inhibiting common proteins aberrantly regulated in *KRAS*-mutated cancers: therapies include inhibition of MEK in combination with inhibition of Bcl-2/Bcl-xL or PI3K, STK33, TAK1, GATA2, CDC6, APC/C, and PLK1 [Faber *et al*, 2014]. In order to exploit *KRAS* oncogene addiction and circumvent the problem that inhibition of neither KRas nor KRas-downstream effectors is potent enough, an approach of synthetic lethality was used to develop therapeutic strategies against *KRAS*-mutated cancers. The concept of synthetic lethality was first coined in a study in Drosophila showing that two single mutations alone can be viable, while the combination of both is lethal [DOBZHANSKY, 1946]. Consequently, synthetic lethal drugs can target factors that are only essential for cell survival in combination with Ras-mutation in cells, but are dispensable for the survival of cells, which are Ras wild-type [Hartman *et al*, 2001]. Accordingly, factors that mediate oncogene addiction and therefore result in synthetic lethality when inhibited can be identified in comparative screens of Ras mutated and Ras wild-type cells [Weidle *et al*, 2011].

One recently published study has tested a combinatorial treatment designed from the results of a genome-wide siRNA screen that searched for factors whose inhibition would induce cell death specifically in KRas-mutated cancer cells. This screen identified addiction to the transcription factor GATA2, which upregulates TRAF6, ROCK1, CDC42 and ephrin type-A receptor 3 (EPHA3) specifically in KRas-mutated cells, as well as proteasome components in mutated and wild-type cells. A co-treatment of ROCK

inhibition with proteasome inhibition significantly reduced lung tumour burden in a KRas-driven lung tumour model [Kumar *et al*, 2012]. Another siRNA screen performed in *KRAS*-transformed colorectal cancer cells compared with their derivatives lacking this oncogene reveals that either topoisomerase inhibitors or proteasome inhibitors can be efficient in killing selectively *KRAS*-mutated tumours [Steckel *et al*, 2012]. A different approach to study synthetic lethal interactions reveals that knock-in (KI) of single or multiple cancer alleles in non-transformed human cells can sensitise or protect cells to pathway-targeted drugs i.e. MEKK inhibitors, mTORC inhibitors and PI3K inhibitors, currently used in clinical trials [Di Nicolantonio *et al*, 2008, Di Nicolantonio *et al*, 2008, Di Nicolantonio *et al*, 2010]. This KI technology can then be used as a tool to study the molecular mechanisms originating from common cancer lesions, thus providing a pharmacogenomic platform for the rational design of targeted therapies. An interesting study by Engelman' s lab demonstrated that combined Bcl-X_L and MEK inhibition induces dramatic apoptosis in a panel of *KRAS*-mutated cancer cell lines and promotes marked tumour regression in *KRAS*-mutant xenografts and in a genetically engineered *KRAS*-driven lung cancer mouse model [Corcoran *et al*, 2013]. Along with this finding, novel ideas have been recently developed regarding the employment of targeted therapies to treat these *KRAS*-mutated recalcitrant tumours. Firstly, in January 2014, Engelman's group published that Mcl-1-mediated TORC1/2 inhibition via AZD8055 sensitises *KRAS*-/*B-RAF*-mutated but not wild-type colorectal cancers to Bcl-2 family inhibitor ABT-263 [Faber *et al*, 2014]. Soon after, in June 2014, the same group elucidated the cellular mechanisms through which several subtypes of non-small cell lung cancers are still resistant to the standard-of-care therapy i.e. MEK- and PI3K-inhibitors (MEKi/PI3Ki). This group indeed identified in the downregulation of Bim and PUMA the main cause of the limited effectiveness of MEKi/PI3Ki-based conventional therapeutic strategy [Hata *et al*, 2014]. A different and singular synthetic lethal interaction proposed for the treatment of lung cancer involves SM and TRAIL in *KRAS*-mutated cell lines. Hyperactivation of KRas led to upregulation of TRAIL-R1/-R2 and downregulation of Decoy Receptors on one side and MAPK-mediated repression of cFLIP on the other side. Furthermore, concomitant SM-inhibition of XIAP enhances TRAIL-induced apoptosis, thus completely killing tumour cells and reducing tumour burden *in vivo* [Huang *et al*, 2011]. Another example of how selective can be KRas lesions in favouring cell death, has been reported by Matallanas *et al* who show that mutant *KRAS* activates the MST2-LATS21-mediated apoptotic pathway. However, the

co-expression of *KRAS* and MST2 is necessary to trigger apoptosis, otherwise WT-*KRAS* allele would repress this pro-apoptotic signaling via AKT [Matallanas *et al*, 2011].

So far, many targeted therapeutic strategies have been developed in order to treat *KRAS*-mutated cancers. However, it is difficult to predict which approaches are more likely to enter the clinic trials in oncology. Even the most potent treatment(s) may not be vastly efficient for a certain type of cancer as there are different subsets of *KRAS*-mutant cancers, which are susceptible to particular combinations even though the tumour arises from the same tissue of origin.

2 Aims of the thesis

Task I

- Explore possible synthetic lethal interaction(s) between combination of SM83/CPT and cancer-associated mutation of *KRAS* in human premalignant cells and elucidate the molecular mechanisms of this phenomenon.
- Study whether SM83/CPT combination is efficient in killing *KRAS*-mutated cancer cells, with particular focus on colorectal cancer cell lines.

This task was carried out at Istituto Nazionale dei Tumori di Milano.

Task II

- Test whether the specific inhibition of CDK9 in combination with TRAIL would synergistically and selectively kill human non-small cell lung cancer cells *in vitro* and *in vivo* highly resistant to TRAIL.
- Estabilish an autochthonous lung tumour model to evaluate the efficacy of combined CDK9 inhibition and TRAIL.

This task was carried out at UCL, as part of Johannes Lemke's Medical Internship.

Task III

- Clarify whether the endogenous TRAIL/TRAIL-R2 system may promote invasion/migration/metastasis in *KRAS*-mutated cancers
- Investigate which effectors are involved in TRAIL/TRAIL-R2-mediated pro-metastatic signalling pathway.

This task was carried out at UCL, as part of Silvia von Karstedt's PhD project.

3 Matherial & Methods

3.1 Material – Task I

3.1.1 Cell lines

Isogenic human mammary epithelial cell lines HME +/+, HME D13/+ and MCF10A together with the isogenic colorectal cancer cell lines SW48 +/+ and SW48 D13/+, HCT116 +/- and HCT116 D13/-, Lim1215 +/+ and Lim1215 D13/+, DLD-1 D13/- and DLD-1 +/- were kindly provided by Prof. Alberto Bardelli [Di Nicolantonio *et al*, 2008, Di Nicolantonio *et al*, 2008, Misale *et al*, 2012]. HME isogenic pairs and MCF10A cell lines were cultured in DMEM-F12 from Gibco, supplemented with 10% FBS from LONZA, 2mM Glutamine from LONZA, 20 ng/ml EGF from Immunological Science, 10 ug/ml Insulin from Sigma, 500 ug/ml hydrocortisone from Sigma. SW48 and DLD-1 isogenic pairs were cultured with DMEM from GIBCO, supplemented with 10% FBS and 2 mM Glutamine. Lim1215 isogenic pairs were cultured with RPMI from LONZA, supplemented with 10% FBS, 2 mM Glutamine and 1 ug/ml Insulin. HCT116 were cultured in RPMI, supplemented with 2mM Glutamine, Sodium Pyruvate, and Non-Essential Amino Acids (NEAA) from LONZA. All cell lines were mycoplasma-free as determined by *Takara* Mycoplasma Detection Kit (Clontech).

3.1.2 Reagents

3.1.2.1 Buffers and Solutions

- Blocking Buffer:
  4% milk powder (CalBiochem),
  0.01% Tween-20 (Sigma),
  1X PBS.
- Freezing medium (for cells), Lysis Buffer I (for lysis): see Paragraph 3.3.2.1.

- Lysis Buffer II (it additionally allows the lysis of the nuclei): 10% SDS (LONZA).
- MES and MOPS (Running Buffers) were purchased from Invitrogen.
- Transfer Buffer (blotting):
  1X NuPage Transfer Buffer (Invitrogen),
  10% MetOH (VWR Chemicals),
  water.
- 10X PBS (pH = 7.4) (LONZA).
- PBS/Tween-20:
  0.05% Tween-20,
  1X PBS.
- Antibody solution:
  5% Albumin from Bovine Serum (BSA) (Sigma),
  0,01% Tween-20,
  0,01% Sodium Azide purchased from Sigma,
  1X PBS.
- ECL-HRP Linked Secondary Antibodies (Novex).
- Peroxide Buffer LiteAb*lot* – PLUS/ - EXTEND/ - TURBO (Euroclone).
- Hyperfilms (Amersham).

3.1.2.2 Antibodies

α-pan-RAS from CalBiochem, α-β-Actin and α-ERK1/2 from Sigma, α-Cleaved-PARP, α-Cleaved-Caspase-3, α-phospho ERK1/2 (Thr202/Tyr204), α-pAKT and AKT were purchased from Cell Signaling, α-cIAP1 from R&D Systems, α-cIAP2 and α-XIAP from BD Biosciences, α-Caspase-8 from Enzo Life Sciences and α-Noxa from CalBiochem.

3.1.2.3 Inhibitors

z-VAD(OMe)-FMK was purchased by BIOMOL, Necrostatin-1 from Enzo Life Sciences. PD98059 and UO126 were purchased from CalBiochem, LY294002 from Sigma, Triciribine from Selleckem.
Infliximab and Enbrel were provided by Ospedale Policlinico (Milan).

SM83 was synthetised at CISI Institute by Prof. Pierfausto Seneci [Manzoni *et al*, 2012; Lecis *et al*, 2012].
CPT was purchased from Sigma.

3.1.2.4 Production of mutated KRas expression vector

The vector pINDUCER20 was kindly provided by Prof. Stephen J. Elledge. These vectors as used as vehicles, which enable cDNA induction in mammalian cells [Meerbrey *et al*, 2010]. In our experiments mutant KRas (G13D) was cloned in the pINDUCER20 and its expression was induced by Doxocycline.

3.2 Methods – Task I

3.2.1 Preparation of cell lysates

Cells were harvested by centrifugation at 4500 rpm for 5 minutes at 4°C. After washing once with PBS, lysates were prepared by resuspending cell pellets in 60-100 µl cell lysis buffer I or II supplemented with 1 x Complete™ protease inhibitors (Roche Diagnostics) and phosphatase inhibitors (cocktail I and II) according to the manufacturer's instructions. If lysis is performed in Buffer I, after 30 min incubation on ice, the lysates were centrifuged at 13000 rpm for 20 min at 4°C, cleared supernatants were transferred to a new tube and frozen at -20 °C. If lysis is performed in Buffer II, lysates were boiled at 99°C, sonicated at 30% intensity for 10'' at RT. Then the lysates were centrifuged at 13000 rpm for 20 min at RT and cleared supernatants were transferred to a new tube and frozen at -20 °C.

3.2.2 Determination of protein concentration

To determine the protein concentration of cell lysates, the bicinchonic acid (BCA)-containing protein assay was applied according to the manufacturer's instructions (QuantumMicro Protein purchased from Euroclone). In a 96-well plate, 2 ul lysate were incubated with 148 ul water and BSA was used as standard protein is titrated up to 15 ug/ul. To 150 ul of final volume, 150 ul BCA solution was added. The plate was then placed at 37 °C for 20 minutes, followed by absorption measurement at 485 nm using TECAN Ultra Microplate reader (Thermo Labsystems).

3.2.3 SDS polyacrylamide gel electrophoresis (SDS-PAGE)

Proteins were separated according to size using pre-cast 4-12% Bis-Tris-NuPAGE gels (Invitrogen). Cell lysates were mixed with 4x reducing SDS-Sample buffer containing 10% β-mercaptoethanol (Sigma) and heated for 10 min at 93°C. As molecular weight standard, Page Ruler Plus Pre-Stained Protein Ladder (Euroclone) was used. The electrophoretic separation was achieved by applying a constant voltage of 80 V for 7 minutes and subsequently 120 V for 150 minutes. MES buffer was used for the separation of proteins smaller than 30 kDa, MOPS buffer was used for the separation of all other proteins.

3.2.4 Western blot analysis

Cells were treated as indicated and then lysed in Buffer I or II. Proteins were separated by SDS-PAGE (NuPAGE) and analysed by western blotting. PVDF membranes (Millipore) were incubated with PBS-tween for 5', blocking buffer for 30' and then incubated overnight with the indicated primary antibodies.

3.2.5 Cell viability assay

96-well Optical Bottom Plate, Polymer Base White (Thermo Scientific) were used. At Day 1, 10000 cells per well were seeded in 100 ul medium. At day 2, cells were treated adding the indicated drug(s) in 10 ul volume per well. At day 3, cell viability was determined using the CellTiter Glo assay (Promega) according to the manufacturer's instructions.

3.2.6 siRNA-mediated knockdown (reverse protocol)

To achieve transient knockdowns of target proteins, siRNA single sequences were purchased from Qiagen. RNAi MAX purchased by Invitrogen was used as transfection reagent. Briefly, for 12-well plate (1 well), 3,25 µl RNAi MAX and 200 µl Optimem (GIBCO) were mixed and incubated for 5 minutes at RT. Subsequently, 3,25 µl siRNA of a 20 µM stock were added, mixed and incubated for further 30 minutes at RT. The 200 µl transfection mix was placed into one well and 0,15 x 10^6 cells seeded in 800 uL on top of the transfection mix. Cells were incubated for 72 hours for the knockdowns to be efficient in all cases. If the KD is followed by treatment with compounds, the treatment is scheduled 24 hours after the KD.

3.2.7 Ras-GTP pull-down assay

2.5 x 10^6 cells were seeded into 10 cm dishes. The next day, cells were incubated with and without 250 ng/ml of Dox. Cell lysis and Ras-GTP pulldown was performed: Cells were then lysed in 500 µl IP-lysis buffer supplemented with a cocktail of protease inhibitors. To fully detach lysed cells, they were scratched of the plates using a cell scraper and transferred into tubes for 30 minute lysis at 4 °C on a rotator. Afterwards, the lysates were centrifuged at 13000 rpm for 30 min and cleared supernatants were transferred to a new tube. After protein adjustment of the lysate, Ras-GTP was precipitated by using anti-RBD-beads (Sigma) overnight. The following day, beads were washed 5 times with IP-lysis buffer and precipitated protein complexes were eluted from

the beads via boiling in SDS-Sample buffer for 10 minutes at 80°C. Proteins were separated by SDS-PAGE (NuPAGE) and analysed by western blotting.

3.3 Material – Task II and III

3.3.1 Cell lines and human samples

Isogenic colorectal cancer cell line DLD-1, DKO4 and HCT116 [Shirasawa *et al*, 1993] were kindly provided by O. Kranenburg, pancreatic cancer cell lines Panc Tu I and Colo357 by A. Trauzold. The human lung adenocarcinoma panel of *KRAS*-mutated and WT cell lines (H460, H441, H522, H322, H23 and Calu-1) by J. Downward. A549-luc cells were purchased from Caliper Life Science. The murine NSCLC cell lines 802T4, 394T4 and 482T2 derived from lung tumours of KP mice. DLD-1, DKO4, HCT116, Hkh-2 cells were cultured in DMEM supplemented with 10% FCS and 2 mM Glutamine, Panc Tu I, Colo357, 802T4, 394T4 and 482T2 in RPMI1640 supplemented with 10% FCS, 2 mM Glutamine and 1 mM sodium pyruvate and the human lung cancer cell line panel including A549-luc cells in RPMI1640 supplemented with 10% FCS. All cell lines were mycoplasma-free as determined by *MycoAlert*™ Mycoplasma Detection Kit (LONZA).
Human biopsies employed for H&E, CDK9 and TTF-1 staining derive from NSCLC patients. The UCL Biobank Ethical Committee approved the employement of human samples for that experiment.

3.3.2 Reagents

3.3.2.1 Buffers and Solutions

- Blocking Buffer:
  5% milk powder,
  0.05% Tween-20,
  PBS.

- Freezing medium (for cells):
  90% FCS (v/v),
  10% DMSO (v/v).
- Lysis Buffer (cell lysates and IP):
  30 mM Tris-Base (pH 7.4),
  120 mM NaCl,
  2 mM EDTA,
  2 mM KCl,
  10% Glycerol (v/v),
  1% Triton X-100 (v/v) (IP-LB1),
  COMPLETE protease-inhibitor cocktail.
- MES running buffer:
  50 mM MES,
  50 mM Trizma Base,
  1 mM EDTA.
- MOPS Running Buffer (pH = 7.7):
  50 mM MOPS,
  50 mM Tris-Base,
  3.5 mM SDS,
  1.0 mM EDTA.
- PBS (pH = 7.4):
  137 mM NaCl,
  8.1 mM Na_2HPO_4,
  2.7 mM KCl,
  1.5 mM KH_2PO_4.
- PBS/Tween:
  137 mM NaCl
  8.1 mM Na_2HPO_4
  2.7 mM KCl
  1.5 mM KH_2PO_4
  0.05% Tween-20,
  PBS (v/v).
- Stripping Buffer (pH = 2.3) (Western blots): 50 mM Glycin in H_2O.

- Transfer Buffer (Western blots):
  192 mM Glycin,
  25 mM Tris-Base,
  0.01% EDTA,
  10% Methanol (v/v).

3.3.2.2 Antibodies

α-KRAS was purchased from Santa Cruz, α-β-Actin from Sigma, α-Rac1 from Millipore, α-TRAIL-R2 from Cell Signaling for knockdown detection and from ProSci for SEC, α-TRAIL from Alexis and α-TRAIL-R1 from ProSci, α-pAKT and AKT were purchased from Cell Signaling and α-PTEN from Santa Cruz; α-RNA-Pol II, α-pSer2 was purchased from Convance; α-Caspase-3 and α-cIAP from R&D Systems; α-Caspase-8 (C15) from Enzo; α-PARP was purchased from BD Bioscience; α-Caspase-9 from MBL; α-Bid was from or Cell Signalling (Rabbit) or R&D Systems (Goat).

3.3.2.3 Inhibitors

GDC-0941 was purchased from Selleck Chemicals and z-VAD(OMe)-FMK was purchased from Abcam. SNS-032 was purchased from Selleck Chemicals, Dinaciclib was purchased by Haoyuan Chemoexpress Co..

3.3.2.4 Recombinant proteins

Recombinant TRAIL was used as an isoleucine zipper-tagged version of the extracellular domain of human TRAIL (izTRAIL) and was produced in *E. coli*, purified as described previously [Ganten *et al*, 2009], izTRAIL was LPS-free after purification as tested by Limulus amebocyte lysate (LAL) assay (LONZA). MoTAP-TRAIL was produced in *E. coli*, purified in our laboratory.

3.4 Methods – Task II and III

3.4.1 Preparation of cell lysates

Half of the cells were detached and washed for transwell migration as described in 3.4.10, then were harvested by centrifugation at 45000 rpm for 2 minutes at 4°C. After washing once again with PBS, lysates were prepared by resuspending cell pellets in 40 ul cell lysis buffer supplemented with 1 x Complete™ protease inhibitors (Roche Diagnostics) and phosphatase inhibitors (cocktail I and II from Sigma) according to the manufacturer's instructions. After 30 min of incubation on ice, the lysates were centrifuged at 13000 rpm for 20 min at 4°C, cleared supernatants were transferred to a new tube and frozen at -20 °C.

3.4.2 Determination of protein concentration

To determine the protein concentration of cell lysates, the bicinchonic acid (BCA)-containing protein assay was applied according to the manufacturer's instructions (Pierce). 2 ul lysate were incubated with 100 ul BCA solution at 37 °C for 20 minutes, followed by absorption measurement at 560 nm using a Multiskan Ascent plate-reader (Thermo Labsystems). All sample volumes were adjusted to equal concentrations according to differences in absorption.

3.4.3 SDS polyacrylamide gel electrophoresis (SDS-PAGE)

Proteins were separated according to size based on the method by Laemmli (Laemmli, 1970) using pre-cast 4-12% Bis-Tris-NuPAGE gels (Invitrogen). Cell lysates were mixed with 4x and immunoprecipitations with 2x reducing SDS-Sample buffer and heated for 10 min at 80 °C. As a molecular weight standard, SeeBlueTM Plus2 Pre-Stained marker (Novex) was used. The electrophoretic separation was achieved by applying a constant voltage of 80 V for 7 minutes and subsequently 180 V for 50 minutes. MES buffer was

used for the separation of proteins smaller than 30 KDa, MOPS buffer was used for the separation of all other proteins.

3.4.4 Western blot analysis

Cells were treated as indicated and then lysed in IP-lysis buffer (30 mM Tris-HCl [pH 7.4], 120 mM NaCl, 2 mM EDTA, 2 mM KCl, 1% Triton X-100, 1× COMPLETE protease-inhibitor cocktail) at 4°C for 30 min. Proteins were separated by SDS-PAGE (NuPAGE) and analysed by western blotting. Membranes were stripped with 50 mM glycine (pH 2.3) before reprobing with other antibodies.

3.4.5 Stripping of western blot membranes

All Western blot membranes had to be incubated with more than one primary antibody. Therefore, after successful signal detection, previous antibodies were removed by incubating the membranes with stripping buffer at RT for 15 minutes. The low pH of the stripping buffer alters protein conformation resulting in release of antibody/antigen-binding. The membranes were washed 3 times with PBS/Tween, followed by incubation in blocking solution and a new round of probing.

3.4.6 Cell viability assay

Cell viability was determined using the Cell Titer Glo assay (Promega) according to the manufacturer's instructions. See Paragraph 3.2.5.

3.4.7 siRNA-mediated knockdown (reverse protocol)

To achieve transient knockdowns of target proteins, siRNA smart-pools purchased from Thermo Scientific or single sequences if indicated were used. Dharmafect was used as

transfection reagent. Briefly, per six-well (1 well), 1.5 ul Dharmafect and 200 ul FCS-free RPMI were mixed and incubated for 5 minutes at RT. Subsequently, 2.2 ul siRNA of a 20 uM stock were added, mixed and incubated for further 20 minutes at RT. The 200 ul transfection mix was placed into one well of a fresh 6-well plate and 1.5 x 10^5 cells seeded on top of the transfection mix. Cells were incubated for 48 hours for the knockdowns to be efficient in all cases.

3.4.8 Coomassie staining of protein gels – Task II

Proteins were stained with Coomassie staining solution for visualisation. Firstly, SDS had to be rinsed from the gel, by either 15 min washing or brief cooking of the gel in deionised H_2O. Then, the gel was transferred into the Coomassie staining solution and cooked in the microwave to accelerate staining. After sufficient staining, for example overnight, the background was reduced by periodic rinsing in deionised H_2O. The stained gel was scanned for documentation and dried with gel drying solution for long term storage. To increase the staining of lowly abundant proteins the gel was rinsed in 20 % NaCl overnight.

3.4.10 Migration assay – Task III

Migration assays were performed using the xCELLigence System (Acea Biosciences, Inc.) that uses specially designed microtiter plates containing gold microelectrodes to measure electrical impedance of cells adhering to electrodes in real time. Increased impedance of background control wells was subtracted from all other values, the increase in electrical impedance/migration of control siRNA-transfected/control vector-infected cells was then defined as 100% migration and relative migration of all other transfected samples was calculated as compared to control-transfected cells, accordingly. Migration plates (CIM 16) are based on the Boyden chamber principle, the lower surface of the filter is covered with microelectrodes measuring cells that have migrated through the pores and adhere to the lower surface of the filter in real-time. Briefly, the lower chambers of a CIM 16 plate were filled with media containing 2% FCS

as chemoattractant, the upper part was assembled and 30 ul of FCS-free medium was added to the top wells. The plate was then equilibrated at 5% CO_2 and 37°C for 1 h. Cells were trypsinized and washed three times in FCS-free medium. Then, 8 x 10^5 cells were resuspended in 1 ml FCS-free medium and 100 ul cell suspension was added to each well after a background measurement without cells was performed. Four wells without cells (FCS-free medium only) were included as assay background control. Cells were left to settle in the top well of the plates at room temperature for 30 minutes and then plates were returned to the RTCA-DP xCELLigence system and impedance measurements were taken every minute. Cells that had been transfected with siRNA were left to migrate for a total of 6h.

3.4.11 Invasion assay – Task III

Invasion assays were performed using the xCELLigence System (Acea Biosciences, Inc.) that measures cell impedance in real-time (see Migration assay). In this assay, E-plates were used which do not follow a Boyden chamber principle but are regular wells (16-wells, each with the size of a 96-well) that contain gold electrodes at the bottom of the well. Wells were coated with 30 ul of 1:10-diluted Matrigel (BD) and left to set in the incubator for 1 hour. Importantly, matrigel was diluted in medium containing 10% FCS to promote invasion. In the meantime cells were prepared as described for the migration assay. Again, before adding washed cells to the well, a background measurement was taken. After adding cells, they were left for 30 minutes at room temperature to settle. Wells without cells and the non-invasive cell line NIH3T3 were included as controls in each experiment. E-plates were then returned to the RTCA-DP xCELLigence system to take measurements every minute for a total of 6 h. Cell Index measurements increase as a function of cells that have passed through the matrigel and have reached the electrodes. Background of wells without cells was subtracted and control transfected cells were set to 100% migration and relative migration of TRAIL-R2 knockdown cells and NIH3T3 was calculated accordingly. Subsequently, the matrigel layer was removed and cells adhering to electrodes were stained by crystal violet and washed with PBS.

3.4.12 Size exclusion chromatography (SEC) – Task III

5 x 10^6 cells were lysed in 240 µl of IP-lysis buffer (30 mM Tris-HCl [pH 7.4], 120 mM NaCl, 2 mM EDTA, 2 mM KCl, 1% Triton X-100, 1X COMPLETE protease-inhibitor cocktail, 10 mM $MgCl_2$) at 4°C for 20 minutes. Subsequently, lysates were cleared by centrifugation and additional centrifugal spin filtration (0.2 um). At this point lysates were either stored at -80°C or fractionated using the Superose™ 6 PC 3.2/30 (GE Healthcare). Briefly, the column was equilibrated with 2 column volumes (2x 2,4 ml) of running buffer (20 mM HEPES, 120 mM NaCl, 2 mM EDTA, 2 mM KCl, 5% (w/v) sucrose, 1% Triton X-100, [pH 7.5]). Lysates were then injected and collected in 50 ul fractions. 12 ul of fractions 9-32 were analyzed by western blotting.

3.4.13 Re-expression of wild type version of TRAIL-R2 – Task III

A549-luc pLKO.1 and shTRAIL-R2 (targeting the 3'UTR) cells were transfected with either pcDNA3.1 or full length TRAIL-R2 (long isoform) inserted into pcDNA3.1 using Lipofectamine 2000 (Invitrogen, Paisley, UK) according to the manufacturer's instructions. After 24 h incubation, cells were subjected to migration assays or to SDS-PAGE and subsequent western blot.

3.4.14 Immunohistochemistry & Immunofluorescence – Task II

For preparation of lung tissue sections, mice were sacrificed 3.5 weeks after cell injection according to Guidance on Operation of Animals [Scientific Procedures] Act 1986. From each mouse the upper lobe of the left lung was removed, fixed in 10% formalin (Sigma) for one week and then transferred to 70% ethanol. Paraffin embedding, preparation of sections and H&E stainings were performed as part of a histological staining service at the National Heart & Lung Institute. Sections were de-waxed and rehydrated by passing the slides through xylene and descending grades of alcohol then rinsed in water. The slides were incubated for 15 minutes with 0.6% hydrogen peroxide solution for IHC. Slides were rinsed and immersed in 0.1 M citrate buffer (pH 6.0) and microwaved for 15 minutes (750 watts) for antigen retrieval. Slides were then

immediately cooled under running water and rinsed in PBS. 100 ul of Protein Block was added to each slide for 5 minutes. After rinsing with 0.05% PBS/Tween 20 solution for 5 minutes, the slides were incubated with 100 ul of the primary antibody at 4^{o}C overnight. Paraffin sections of lungs from KP mice were stained for CDK9 (Cell Signaling) at a 1/100 dilution for IF. Following overnight incubation, slides were washed with 0.05% PBS/Tween 20 solution. The sections were then incubated with secondary antibody for 30 minutes (IHC) or 1 h (IF) at room temperature and again washed three times. The sections were developed using the ABC kit (Vector laboratories) before being counterstained by haematoxylin for 2 minutes and rinsed in water for 5 minutes for IHC. Slides were then dehydrated in ascending grades of alcohol and cleared in 3 changes of xylene (IHC). Finally, the sections were mounted using Di-N-Butyle Phthalate in Xylene (DPX) mounting solution and covered with a glass coverslip (IHC) or mounted in DAPI (ProLong® Golds antifade reagent with DAPI, Invitrogen) (IF). For negative controls, duplicate slides from each case were used. These slides were incubated with 100 µl antibody diluent instead of primary antibody/secondary antibody. H&E stainings were examined by an experienced pathologist (Mona A. El-Bahrawy) who was blinded to the study design.
CDK9 and TTF-1 for human samples were IHC-stained by UCL Hospital Service.

Histological Quantifications.
Lung metastasis burden (xenograft) was quantified by counting all nodules within a central 50x microscopic field. All histopathological analyses were performed by an experienced pathologist (Mona A. El-Bahrawy), who was blinded to the study design.

3.4.15 Transformation of competent *E.Coli*

Competent bacteria previously generated in the laboratory were thawed on ice and 5 ul of plasmid DNA (stable knockdown constructs) were added followed by further incubation on ice for 30 min. Afterwards, a heat-shock was performed at 42 ºC for 90 seconds and the bacteria were again incubated on ice for 5 minutes. Subsequently, 200 ul SOC medium were added and the bacteria suspension was incubated at 37 ºC for 60 minutes. Finally, bacteria were plated onto previously cast LB agar plates containing the

respective antibiotic and incubated overnight at 37 ºC. Single clones were picked the next day for further expansion of plasmid containing bacteria.

Isolation of plasmid DNA.

For the preparation of plasmid DNA, 300 ml overnight bacteria cultures were inoculated and harvested the next day by centrifugation at 4500 rpm for 30 minutes. The resulting pellets were processed using the E.Z.N.A. Plasmid Maxi kit (OMEGA bio-tek) according to the manufacturer's protocol.

3.4.16 Animal Experiment

6 to 12-week old female Fox Chase® SCID Beige Mice (Charles River, Germany) were injected with 2 x 10^6 A549-luc cells via the lateral tail vein. After one week all mice were imaged for bioluminescence using the Ivis Spectrum (Caliper Life Science). Photons per second (Photon Flux) were quantified using the Ivis Spectrum software. Mice with established tumour burden were included in the study and randomized into the treatment groups (8 mice per group). Subsequently, mice were treated for 4 consecutive days with daily i.p. injections of 600 ug SNS-032 (or 300 ug Dinaciclib) (30 mg/KG) and/or 100 ug izTRAIL (or 50 ug in the Dinaciclib experiment) (5 mg/KG) or 200 ul Buffer as control. After three weeks tumor burden was quantified by bioluminescence imaging. For preparation of lung tissue sections, mice were sacrificed according to Guidance on Operation of Animals [Scientific Procedures] Act 1986. Lungs were removed, fixed in 10% formalin for one week and then transferred to 70% ethanol. Paraffin embedding, preparation of sections and H&E stainings were performed as part of a histological staining service at the National Heart & Lung Institute. H&E stainings were examined and quantified by an experienced pathologist (Mona A. El-Bahrawy) who was blinded to the study. Tumor burden was quantified as percentage of tumor tissue in the lung. SCID beige mice were maintained in individually ventilated cages (IVCs), received autoclaved food, water and bedding according to the institutional guidelines under a UK Home Office project license. The required risk assessments were obtained for this study.

KP mice were from Charles River (USA) and were infected following the protocol described by Dupage et al. [DuPage *et al*, 2009]. That optimisation of that protocol is still

ongoing in our lab. AdenoCre for infection was purchased by Gene Transfer Vector Code from the University of Iowa.

3.4.17 *In vivo* Bioluminescence imaging

Starting on day 1 after cell injection all mice were imaged weekly for bioluminescence. 1 gram D-luciferin was purchased from Caliper Life Science and solved in DPBS at a final concentration of 30 mg/ml and syringe filtered through 0,2 µm. Subsequently, luciferin was aliquoted (700 µl) and frozen at -80 °C. To avoid batch-to-batch variability, all luciferin used in this study came from the same batch and was only frozen once. Prior to imaging, each mouse was anaesthetised by 4% Isofluorane gas and received 100 µl subcutaneous injection of 3 mg luciferin per 20 g mouse. For maintenance of anaesthesia, Isofluorane dose was reduced to 1.5%. 10 minutes after luciferin injections bioluminescence images were acquired using the Ivis Spectrum at 1 minute exposure time (Caliper Life Science). Afterwards, mice recovered from anaesthesia in a 37 °C heating chamber. Photons per second were quantified using the Ivis Spectrum software.

3.4.18 Statistical analysis – Task II

Data were analysed using GraphPad Prism 5 software (GraphPad Software). Statistical significance between groups was determined using unpaired Student's t-test. A p-value of <0.05 was considered significant and indicated with *p<0.05, **p<0.01, *** p<0.005 and **** p < 0.0001.

3.4.19 Statistical analysis – Task III

Data were analyzed using GraphPad Prism 5 software (GraphPad Software). Results are expressed as means ± SEM. Statistical significance between groups was determined using Student's t-test and/or one-way analysis of variance (ANOVA),

followed by the Bonferroni post-test. A p-value of <0.05 was considered significant and indicated with **p<0.01 and ***p<0.001. ns = non-significant.

3.5 Purification of recombinant murine TRAIL (iz-mu-TRAIL) – Task II

The purification of iz-mu-TRAIL was adapted and optimised from the protocol for the purification of the human version iz-hu-TRAIL which was established in our laboratory based on the protocol published by Ashkenazi in 1999 [Ashkenazi *et al*, 1999]. After bacterial lysis, a two step chromatographic purification was applied, first a hydroxyapatite column followed by a Ni-NTA (nickel Nitrilotriacetic acid) column, which is usually used to purify His-tagged proteins. Even though iz-mu-TRAIL does not contain any affinity tag, it seems to bind to the Ni-NTA resin quite efficiently by an unknown mechanism. To remove lipopolysaccharides (LPS) from the protein preparations we used the detergent triton-X-114 as described below.

Bacterial lysis:

10 L of bacterial cultures were used for one purification. Lysis took place on ice in phosphate based bacterial lysis buffer (100 ml/1 L bacterial culture).

Lysis buffer:

- 50 mM potassium phosphate buffer (pH = 7.4),
- 200 mM NaCl,
- 100 mM KCl,
- 10% glycerol,
- 0,5% triton-X-100,

add freshly before lysis:

- 2 mM DTT,
- 100 µM AEBSF,
- 5 µM E-64,
- 1 µM Pepstatin.

When the pellet was nearly dissolved, 5 U/ml of benzonase and 50 ug/ml lysozyme were added. This increases the lysis capacity even though the Rosetta TM(DE3) pLysS strain already contains an endogenous lysozyme encoded on the pLysS plasmid. For further lysis and DNA shearing, the solution was sonified 5 to 6 times (1 min, duty cycle 30, output control 40) on ice. In between, the lysate was stirred on ice for 10 to 15 min. The lysate can be stored on -20◦C, but is ideally processed freshly. To pellet still unlysed bacteria and cell debris, the solution was first centrifuged at 4,600 rpm for 30 min (4◦C) and afterwards at 15,000 rpm for 30min (4◦C), to remove the inclusion bodies. The lysate can then be stored overnight on ice until the first step of the purification on the next day. Before loading onto the column, the solution was filtered with 0.45 um syringe filters to remove potentially precipitated protein.

Hydroxyapatite Purification

Hydroxyapatite ($Ca(PO_4)_3OH)_2$ is a special form of calcium phosphate that can be used as a matrix for chromatographic purification of proteins. Protein binding is facilitated by interac- tions of basic amino acids with Ca^{2+} and acidic and neutral residues with the PO^{3-} groups.

Elution occurs by increasing the phosphate concentration. Hydroxyapatite (type I) with 40 um particle size was packed in a 100 ml column volume (CV). To maintain protein activity throughout the procedure, purification was performed at 4°C in the cold room. Samples and protein containing fractions were kept on ice. All buffers were degassed, 0.22 um filtered and cooled to 4◦C before the purification. Reducing reagents like DTT (dithiothreitol) and β-ME (β-mercaptoethanol) were added freshly to all buffers to prevent disulfide bridge formation during the purification. The maximum pressure during the whole purification was not higher then 0.3 MPa on the column.

The hydroxyapatite column was equilibrated overnight with 5 to 6 CV of Hydroxy-Equili bration buffer (50 mM potassium phosphate) with 0.2 - 1 ml/min. The filtered bacterial lysate was then loaded onto the column at 3 ml/min and the flow-through collected for further analysis. The flow rate was then increased to 5 ml/min for all further steps. To reduce protein loss in the application volume, the sample container was rinsed twice with 50 to 100ml of bacterial lysis buffer, which was also applied to the column. To remove unbound proteins, contaminants and inactive target protein, the column was washed with 3CV of 200 mM potassium phosphate buffer (Hydroxy-Wash buffer). For elution 4CV of Hydroxy-Elution buffer (400 mM potassium phosphate) were used and 10 ml

fractions collected. To analyse protein content of the fractions, every third or second fraction was analysed in an SDS-PAGE. The iz-mu-TRAIL containing fractions (typically fraction E8-E25) were stored on ice in the cold room overnight for the Ni-NTA purification on the next day.

The following buffers were used during the described procedure.

1. *Hydroxyapatite equilibration buffer:*
   50 mM Potassiumphosphate pH 7,4,
   100 mM NaCl,
   Vacuum filtration (0.22 µm filters) to degas buffer afterwards add:
   0,02% Tween 20.
   Right before purification add 2 mM β-mercaptoethanol.
2. *Hydroxyapatite wash buffer 1:*
   200 mM Potassiumphosphate pH 7,4,
   100 mM NaCl.
   Vacuum filtration (0.22 µm filters) to degas buffer afterwards add:
   0,02% Tween 20,
   0.1% Triton x 114.
   Right before purification add 2 mM β-mercaptoethanol.
3. *Hydroxyapatite wash buffer 2:*
   200 mM Potassiumphosphate pH 7,4,
   100 mM NaCl.
   Vacuum filtration (0.22 µm filters) to degas buffer afterwards add:
   0,02% Tween 20.
   Right before purification add 2 mM β-mercaptoethanol.
4. *Hydroxyapatite elution buffer:*
   400 mM Potassium phosphate pH7,4,
   100 mM NaCl.
   Vacuum filtration (0.22 µm filters) to degas buffer afterwards add:
   0,02% Tween 20.
   Right before purification add 2 mM β-mercaptoethanol.

Ni-NTA purification

In the Ni-NTA purification, protein interactions occur due to complexes of the NTA-matrix with Ni^{2+} ions and histidine (His) residues in proteins. In the case of iz-mu.TRAIL, which does not contain a His-tag, internal residues, other amino acids or the tertiary structure, usually complexing a zinc ion, could contribute to the binding effect.

The eluates from the hydroxyapatite column containing the target protein were pooled, filtered with a 0.22 um syringe filter and loaded onto the Ni-NTA column (100 ml column volume) that had been equilibrated with the respective buffer beforehand (for 3-5 CV). The flow rate for this column was always 3 ml/min, as it is not possible to run the Ni-NTA column with higher pressures. The flow-through was collected for further analysis. The same buffer as the equilibration buffer was used to wash the column with 3 CV. A buffer containing a low imidazol concentration eluted the purified protein.

To check for presence of iz-mu-TRAIL, an SDS-PAGE was carried out with a sample of every second fraction. The respective fractions were then pooled and dialysed in two steps. To remove the imidazol and other buffer constituents in which the protein is unstable, it was dialysed in 5 L maintenance buffer (without arginine) overnight and then another 24 h in 3 L maintenance buffer in the presence of 0.5 M arginine. The protein could then be sterile filtered and the protein content measured at on optical density (OD) of 280 nm wavelength in the Nanodrop photometer. As the extinction coefficient of iz-mu-TRAIL is close to one, the OD280 directly correlates with the amount of protein. The protein was then aliquoted and frozen at -80◦C.

The following buffers were used during this purification step.

1. *Ni-NTA equilibration buffer* pH= 8:
   50 mM Tris –HCl pH 7,4,
   200 mM NaCl,
   100 mM KCl.
   Vacuum filtration (0.22 µm filters) to degas buffer afterwards add:
   10% Glycerol,
   0,5% Triton x100.
   Prior to use add 2 mM β- Mercaptoethanol.
2. *Ni-NTA wash buffer:*
   50 mM Tris- HCl pH 8,

200 mM NaCl,

100 mM KCl,

15 mM imidazole.

Vacuum filtration (0.22 µm filters) to degas buffer afterwards add:

10% Glycerol,

0,5% Triton x100,

0.1% Triton x 114,

Prior to use add 2 mM β-Mercaptoethanol.

3. *Ni-NTA elution buffer* pH= 8:

   20 mM Tris-HCl pH 8,

   300 mM NaCl,

   170 mM imidazole.

   Vacuum filtration (0.22 µm filters) to degas.

   Prior to use add 2 mM β-Mercaptoethanol.

4. Maintenance buffer I:

   20 mM Tris-HCl pH 8,

   100 mM NaCl,

   0,005% Tween 20.

   Prior to use add 2 mM β-Mercaptoethanol.

5. Maintenance buffer II:

   20 mM Tris-HCl pH 8,

   100 mM NaCl,

   0,005% Tween 20,

   0.5 M Arginine.

   Prior to use add 2 mM β-Mercaptoethanol.

Proteins that are produced in bacteria are most likely to be contaminated with endotoxin, also called LPS, which is a constituent of the bacterial cell wall. If the recombinant protein is intended to be used *in vivo*, it is indispensable to check and remove traces of LPS from these preparations.

Two different strategies of LPS removal were adopted. Firstly, already purified iz-mu-TRAIL batches were bound onto the hydroxyapatite column and the LPS removed from the preparation with a 0.1% triton-X-114 containing buffer. Secondly, further iz-mu-

TRAIL batches were purified using additional steps with 0.1% triton-X-114 in the wash buffer during both purifications.

LPS removal from protein preparation

For LPS removal of already purified iz-mu-TRAIL batches, the general protocol of hydroxyapatite purification was used. The protein was pooled from the aliquots and diluted 1:2 into equilibration buffer to facilitate binding to the column. Then, it was bound onto the equilibrated column, and 3 CV of the equilibration buffer containing 0.1% (v/v) triton-X- 114 were rinsed over the column at 3 ml/min to increase the contact time. To remove the triton-X-114 from the column and the protein again, 3 CV of the equilibration buffer without triton-X-114 were run over the column at 4.5 ml/min. Afterwards the protein was eluted as usual and dialysed in maintenance buffer with arginine for at least 24 h. This procedure was repeated when the LPS values (determined by LAL test) were still too high. In the usual purification protocol in both purification steps an additional washing step with wash buffers containing 0.1% triton-X-114 were added. First 3 CV of buffer plus triton-X-114 and then at least 3 CV of buffer without triton-X-114 were applied before elution.

Comassie staining

A typical result of the two-step purification is illustrated in figure 9. To analyse the protein content of the different fractions, samples were subjected to SDS-PAGE and the proteins were stained with coomassie. The first lane of Figure 9A shows a dilution of the bacterial lysate containing several different bacterial proteins. A substantial amount of iz-mu-TRAIL running at approximately 25 KDa was found in this fraction. During the application of the lysate, the flow-through containing only very little of the target protein was collected. Then, the potassium phosphate concentration was increased in the washing buffer to remove contaminating proteins. In later wash fractions, iz-mu-TRAIL was leaking from the column. Yet, activity tests of these fractions showed that this protein is mostly inactive and probably not properly folded (data not shown). The protein was eluted by increasing potassium phosphate concentration. The fractions containing iz-muTRAIL were then collected, pooled and applied on the Ni-NTA column (see curly brackets in Figure 9A). The purification success on the first column can be judged by comparing the first two lanes of Figure 9B. The target protein was concentrated and the contaminating proteins from the crude bacterial extract were removed to a great extend.

The Ni-NTA column was then used to further reduce contaminations. As it can be seen in figure 10 B, a few contaminants were still present in the relevant elution fractions. The fractions containing the purified iz-mu-TRAIL were pooled and subjected to dialysis in an appropriate maintenance buffer, containing arginine for stabilisation.

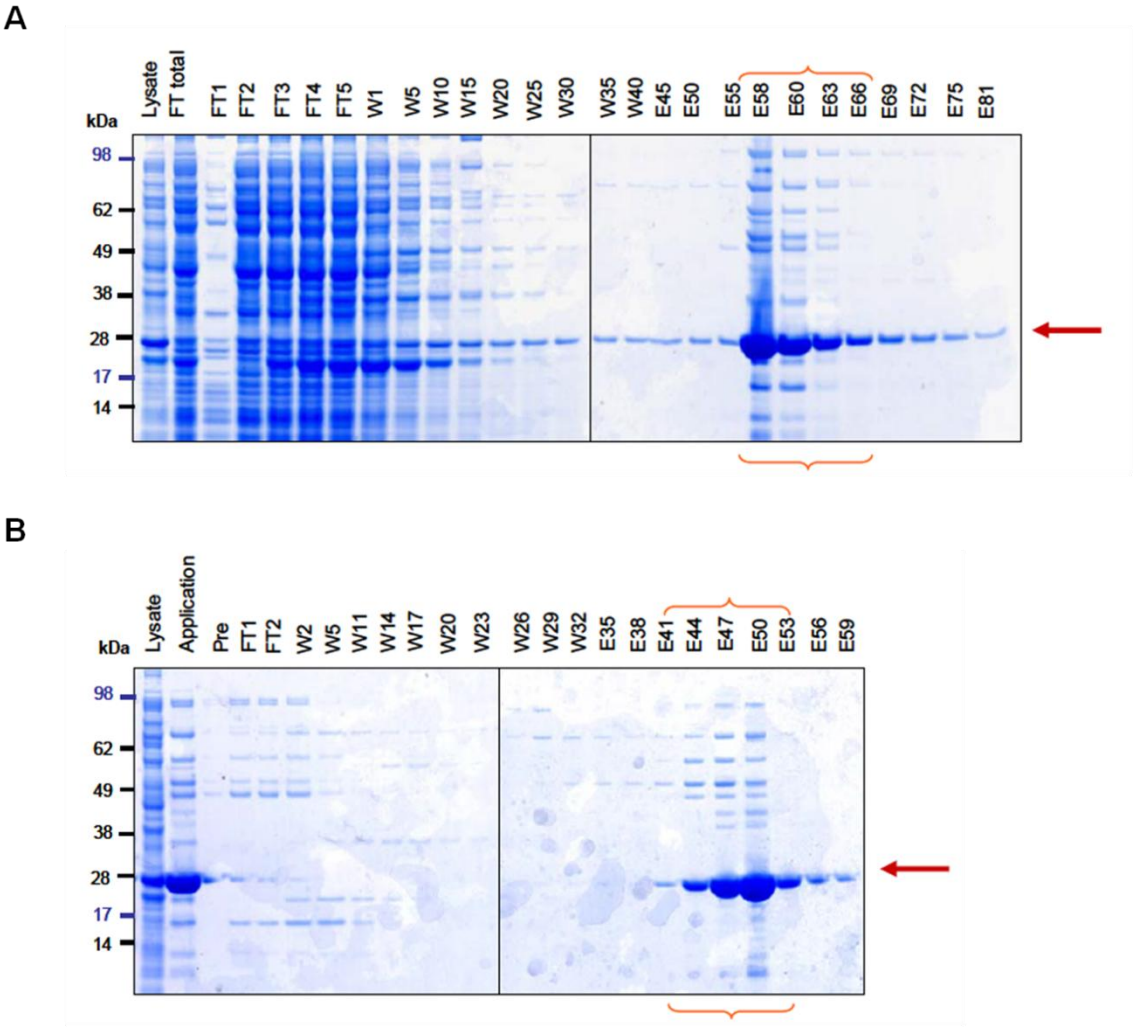

Figure 9 | Two-steps purification of iz-mu-TRAIL. (a) Hydroxyapatite purification. (b) Ni-NTA purification. 10 ul of different purification fractions were supplemented with reducing sample buffer and separated by SDS-PAGE in MES buffer. Samples were: bacterial lysate (1:10 diluted in sample buffer), preflow (Pre), flow-through (FT), wash fractions (W) and elution fractions (E). The target protein iz-mu-TRAIL at a size of 25 KDa is marked with an arrow. The curly brackets indicate the fractions pooled for the second purification step (application) or for dialysis of the final protein.

Activity of iz-mu-TRAIL.

After the purification, we tested whether the newly produced ligand was active. At that moment, we did not have any TRAIL-sensitive murine cancer cell line available. Therefore, a TRAIL-resistant hepatocellular cancer cell (HCC) line mutated for NRAS and p19 was treated with Dinaciclib and iz-mu-TRAIL.

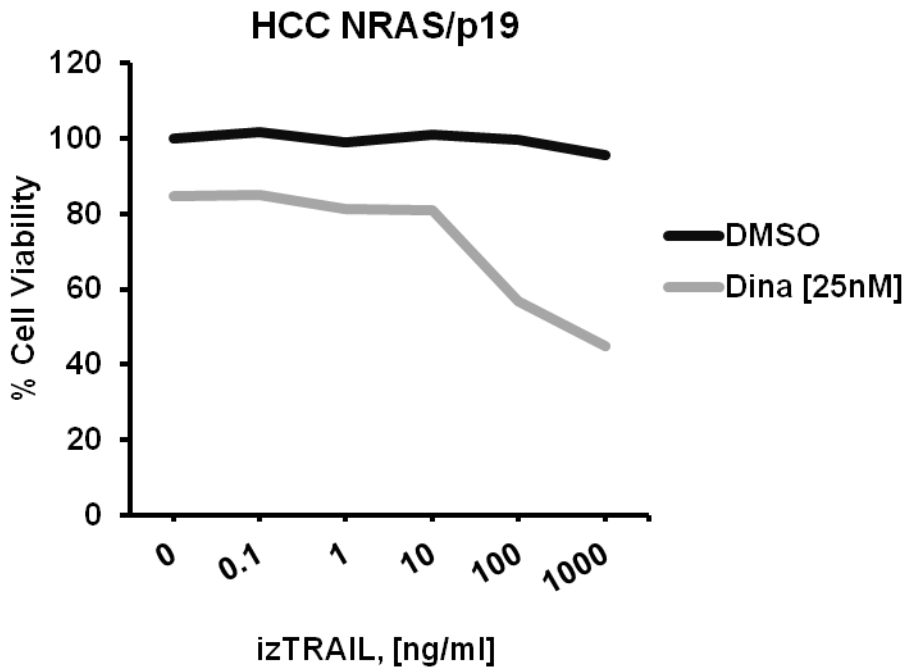

Figure 10 | Iz-mu-TRAIL is active. HCC NRAS/p19 were pre-incubated with Dinaciclib [25nM] and treated with iz-mu-TRAIL at the indicated concentrations. After 24 hours cell viability was performed. Dina: Dinaciclib.

4 Results

4.1 Smac-Mimetic in combination with Camptothecin selectively kills pre-malignant epithelial cells mutated for *KRAS*

Since most cancer cells are resistant to SMs as single agents, SM is commonly employed as a sensitiser for either death ligands [Li *et al*, 2004] or chemotherapeutics [Probst *et al*, 2010]. This is the reason why we aimed to find a drug that, in combination with SM, triggers a strong cell death. To this end, in collaboration with the Institute of Cancer Research (ICR) in London, we performed an *in vitro* pharmacological screen to test the capability of a new SM, named SM83 and designed by our collaborators of the CISI Institute [Cossu *et al*, 2012, Lecis *et al*, 2012, Manzoni *et al*, 2012], to induce cell death by targeting IAPs in the presence or absence of a library of 3000 pharmacological compounds. Interestingly, the drug which best synergises with SM83 was the Topoisomerase I inhibitor Camptothecin (CPT) [Tomicic and Kaina, 2013].

Importantly, the ideal cancer drug targets are those essential in tumour cells bearing oncogenic mutations and cause synthetic lethality with cancer-specific genetic lesions. *KRAS* is frequently mutated in human cancers and therapies currently available to treat patients are not efficient. This led us to search for synthetic lethal interactions between drug-combinations and proteins frequently mutated in cancer cells with particular focus on aberrant activation of *KRAS*. For this reason, we tested whether the combination of SM83 and CPT could be effective in killing cells bearing oncogenic mutation in *KRAS*. Therefore, we selected hTERT-immortalised human mammary epithelial (hTERT-HME) cell lines, which were subjected to targeted introduction via homologous recombination (Knock-In technology) of a specific point mutation at one *KRAS* allele (G13D or D13, HME KRasG13D) whereas the other allele was still wild-type (WT or +, HME WT) (see Paragraph 3.1.1). Biochemical analysis demonstrated that this insertion strongly activated *KRAS* by permanently switching the corresponding mutated protein into the GTP-bound active state [Di Nicolantonio *et al*, 2008].

Surprisingly, we found that SM83 in combination with 1 uM of CPT profoundly induced cell death in HME D13/+ contrarily to the parental ones (Figure 11A). Whereas this cell death was blocked by pre-treatment with pan-caspase inhibitor zVAD, the necroptosis inhibitor Necrostatin-1 (Nec-1) failed to rescue cell death, thus suggesting that HME D13/+ died apoptotically (Figure 11B). In line with these results, HME D13/+ cells treated with both SM83 and CPT showed a drastic increase in the cleavage of Poly (ADP-ribose) polymerase (PARP), caspase-3 and caspase-8 (Figure 11C). SM83 was active in depleting cIAP1 and cIAP2 as shown in Figure 11D.

These results demonstrate that the combination of SM83 with CPT and not the same drugs as single agents strongly and selectively kills *KRAS*-mutated normal cells.

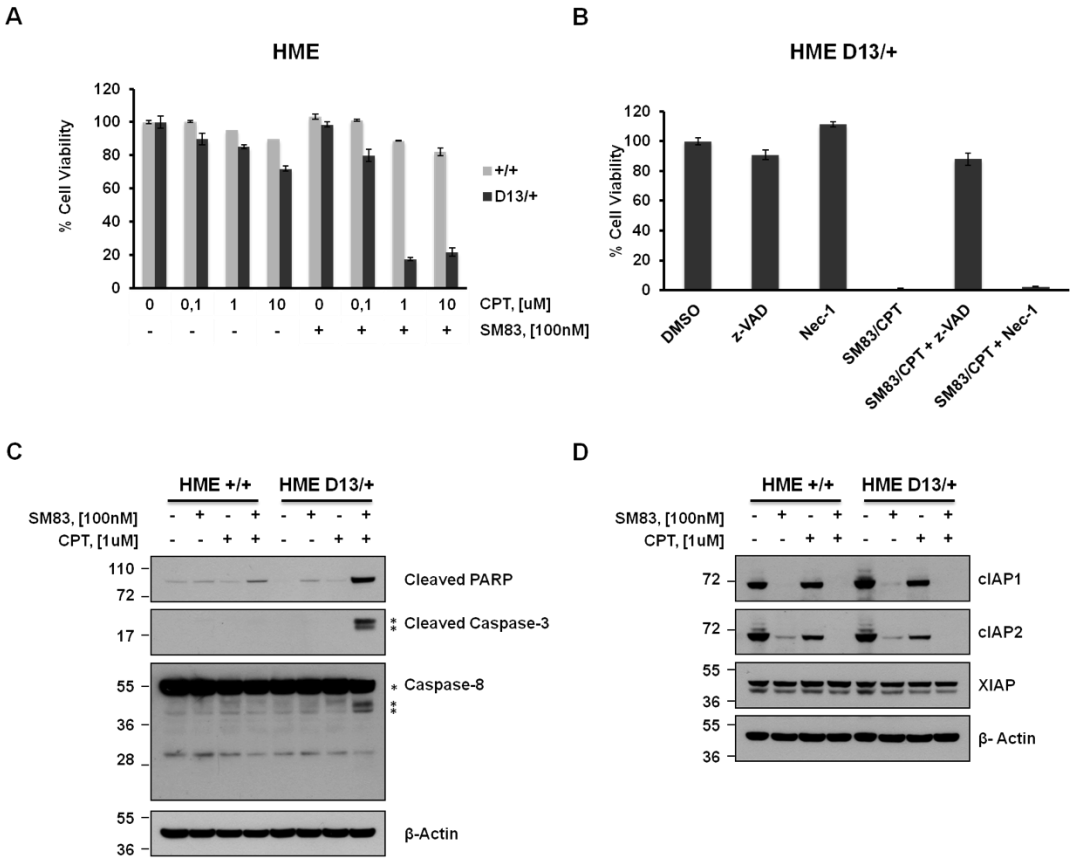

Figure 11 | Combined SM83 and CPT induce apoptosis in *KRAS*-mutated HME cell line. (a) HME +/+ and HME D13/+ cells were treated with DMSO, SM83 and CPT at the indicated concentrations. Cell viability was quantified by Cell Titer Glo assay after 24 h. One representative of four independent experiments is shown. (b) HME +/+ and HME D13/+ cells were preincubated with DMSO, z-VAD [50 uM], Nec-1 [20 uM] for 1 h and subsequently stimulated with SM83 [100 nM] and CPT [1 uM]. Cell viability was determined after 24 h. (c,d) HME +/+ and HME D13/+ cells were treated with DMSO, SM83, CPT at the indicated concentrations for 6 h. Cells were lysed and subjected to western blotting. (b, c, d) One representative of two independent experiments is shown.

4.1.1 Oncogenic *KRAS* confers sensitivity to SM83 and CPT

The strong cell death of HME D13/+ is exclusively observed in the concomitant presence of three factors: mutated *KRAS*, SM83 and CPT. Firstly, we aimed to address how much the *KRAS* lesion contributes to SM83/CPT-sensitivity. HME D13/+ were then depleted for mutated *KRAS* and treated with SM83 and CPT. As shown in Figure 12A, knock-down (KD) of mutated *KRAS* partially rescued SM83/CPT-induced cell death. However, we could not exclude that the amount of KRas protein remained after the KD was sufficient to compensate the phenotype as shown in Figure 13B, right panel. To further test whether mutated *KRAS* was indeed responsible for SM83/CPT-induced apoptosis, HME and another human mammary epithelial cell line MCF10A were transduced with a doxocycline (Dox)-inducible lentivector (pInducer20) encoding for either KRasG13D (pInducer20 KRasG13D) or control (pInducer20 MOCK). The map of this expression vector is shown in Figure 12B. After 48 hours of induction with Dox [250 ng/ml], HME and MCF10A pInducer20 KRasG13D nicely expressed hyperactivated *KRAS* as shown in Figure 12C for HME. Strikingly and in line with the results obtained for HME D13/+ cells, KRasG13D-induced-expressing cells (HME and MCF10A) showed high sensitivity to the combination of SM83 and CPT (Figure 12D and 12E respectively) while MOCK-induced-expressing cells were not affected.

Taken together, these data demonstrate that the presence of mutated KRas markedly confers high sensitivity to combined SM83/CPT in our models of pre-malignant cell lines.

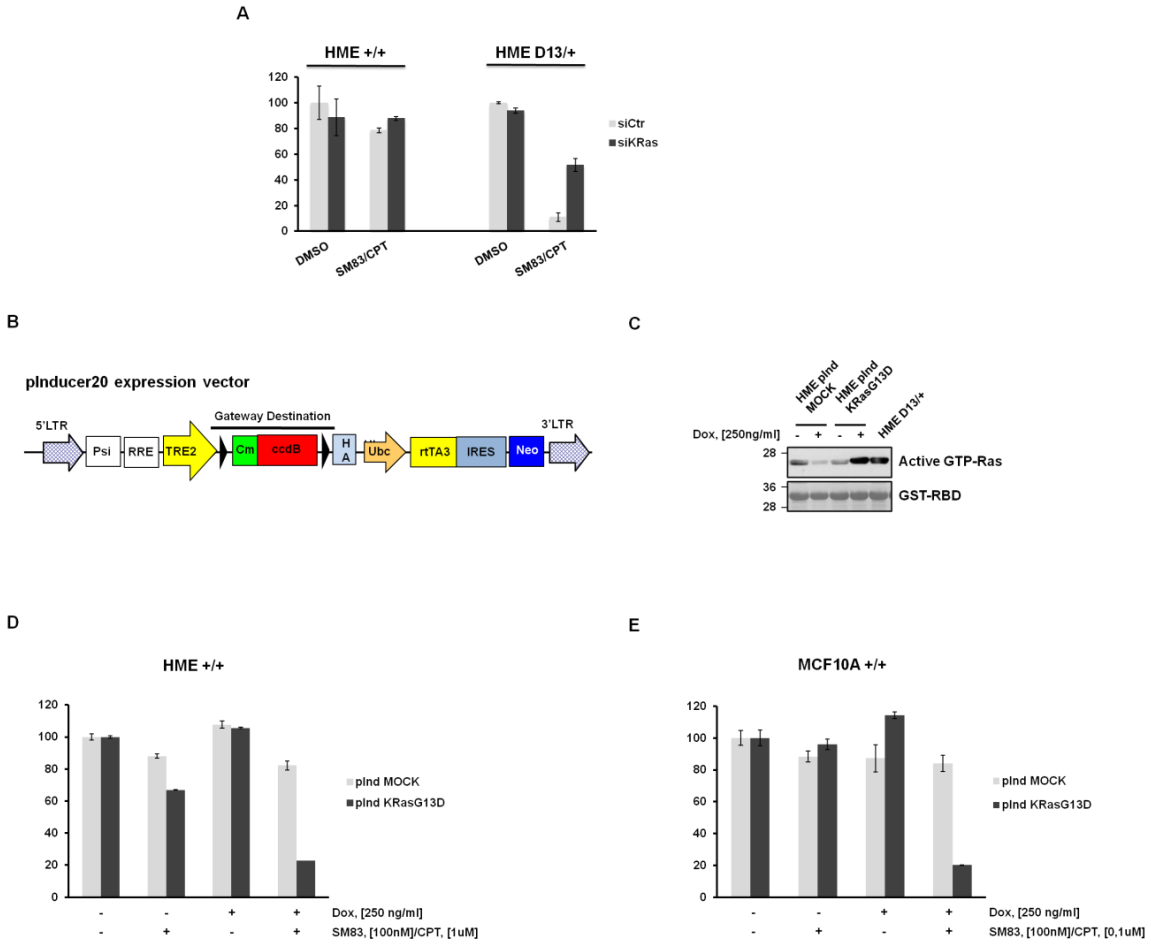

Figure 12 | Mutated *KRAS* confers sensitivity to SM83 and CPT co-treatment. (a) HME +/+ and HME D13/+ were transfected with siRNA targeting KRas for 72 h and subsequently treated with SM83 [100 nM] and CPT [1 uM]. Cell viability was determined after 24 h. (b) Map of the pInducer20 expressing vector. (c) HME pInd MOCK and HME pInd KRasG13D were incubated with Dox [250 ng/ml] for 48 hours and subjected to pull-down (PD) assay for activated Ras (Ras-GTP). Cells were subjected to western blotting. HME D13/+ were used as positive control for activated KRas. (d) HME pInd MOCK and HME pInd KRasG13D were pre-incubated with Dox [250 ng/ml] for 48 hours and treated with SM83 [100 nM] and CPT [1 uM]. Cell viability was determined after 24 h. (e) MCF10A pInd MOCK and MCF10A pInd KRasG13D were pre-incubated with Dox [250 ng/ml] for 48 hours and treated with SM83 [100 nM] and CPT [0,1 uM]. Cell viability was determined after 24 h. (a, c, d, e) One representative of two independent experiments is shown. pInd: pInducer20. GST-RBD: Ras Binding Domain bound to a GST resin.

4.1.2 *KRAS*-induced upregulation of Noxa sensitises cells to SM83/CPT co-treatment

At this point, we demonstrated that the presence of mutated *KRAS* provides a background, which favours SM83/CPT-induced cell death. However, the molecular mechanisms engaged by this oncogenic mutation to enhance apoptosis in pre-malignant cells still need to be investigated. So far, several groups reported that either mutated *RAS* or DNA damage inducing agents can upregulate pro-apoptotic and downregulate anti-apoptotic proteins belonging to Bcl-2 family. More in details, Seamus Martin's lab published that expression of oncogenic *HRAS* V12 leads to extensive autophagy by increasing the expression of Noxa [Elgendy *et al*, 2011]. Another group demonstrated that oncogenic *KRAS* sensitises colorectal tumour cells to oxaliplatin and 5-fluorouracil by upregulating Noxa [de Bruijn *et al*, 2010]. In line with this, recent studies conducted in melanoma cells revealed that the BH3-mimetic ABT-737, in combination with cytotoxic drugs that induce Noxa or repress Mcl-1 protein levels, may be an attractive therapeutic strategy [Lucas *et al*, 2012]. In this last example KRas mutation is not involved, however, the reports mentioned above suggest taking into consideration that the balance among pro- and anti-apoptotic factors associated to mitochondria might be modulated by oncogenic lesions in cancer cells.

Therefore, we aimed to study whether the presence of KRasG13D in HME cells correlated with increased expression of Noxa, thus leading to more sensitisation in the presence of SM83 and CPT. In order to answer this question we firstly analysed Noxa protein levels in pre-malignant cell lines at basal conditions and, as expected, levels of Noxa in HME D13/+ were higher than in HME +/+ as shown in Figure 13A, left panel. In line with this finding, either HME or MCF10A pInducer20 KRasG13D, upon Dox treatment, expressed mutated *KRAS* and this was associated with robust upregulation of Noxa protein levels already after 48 hours of *KRAS*-induction (Figure 13A, right panel). Both HME +/+ and Dox-treated HME/MCF10A pInducer20 MOCK cells failed to induce Noxa expression (Figure 13A, right panel) and survived upon SM83/CPT combination as previously shown in Figure 12D and 12E, confirming that the increased expression of Noxa and cell death observed under these conditions tightly correlated with the presence of mutated *KRAS*. To address whether the upregulation of NOXA driven by mutated *KRAS* was responsible for SM83/CPT-induced cell death, we knocked-down

Noxa in HME D13/+ (KI) and treated them with the combination. As the viability assay in Figure 13B, left panel illustrates, the full loss of Noxa (Figure 13B, right panel) nearly totally rescued cell death.

Overall, these data suggest that expression of Noxa is tightly regulated by mutated KRas and plays a role in the KRas pathway to promote cell death upon SM83 and CPT treatment.

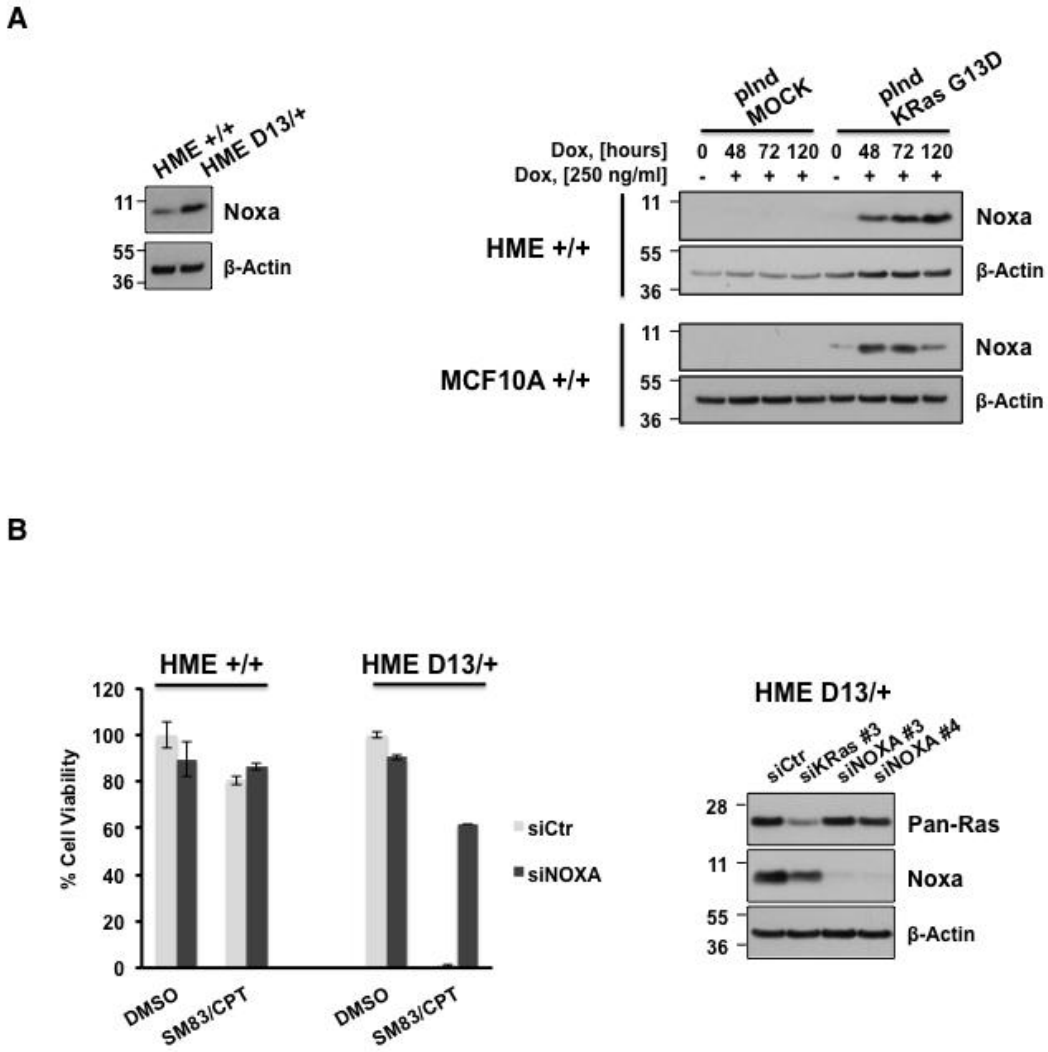

Figure 13 | Noxa expression increases in *KRAS*-mutated HME favouring SM83/CPT-induced cell death. (a, left panel) HME +/+ and HME D13/+ were lysed and subjected to western blot. (a, right panel) HME/MCF10A pInd MOCK and pInd KRasG13D were incubated with Dox [250 ng/ml] for the indicated time [hours] and

subjected to western blotting. (b, left panel) HME +/+ and HME D13/+ were transiently transfected with siRNA targeting NOXA for 48 h and subsequently treated with SM83 [100 nM] and CPT [1u M]. Cell viability was determined after 24 h. (b, right panel) HME D13/+ were transfected with siRNA targeting KRas and Noxa for 48 h and subsequently subjected to western blot analysis to verify the KD efficiency. One representative of two independent experiments is shown.

4.1.3 *KRAS*-induced upregulation of Noxa is mediated by MAPK signaling axis.

Our evidences support the idea that mutated KRas enhances SM83/CPT-induced cell death via markedly upregulation of Noxa. However, which specific effectors within KRas pathway are directly involved in controlling expression of Noxa have not been identified yet. Notoriously, KRas activates multiple critical effectors such as MEK/ERK, PI3K/AKT, NF-kB pathways in order to drive tumour development and maintenance [Montagut and Settleman, 2009]. Therefore, we focused on exploring whether KRasG13D-induced expression of Noxa required MEK/ERK- and/or PI3K/AKT-signaling and whether these intermediate players would, in turn, affect SM83/CPT-induced cell death. First, HME D13/+ cell lines and their WT counterparts were pre-treated with two different inhibitors of the upstream ERK-activating kinase MEK, PD98059 and UO126 both of which approximately fully rescued SM83/CPT-induced cell death (Figure 14A) and, intriguingly, reduced KRasG13D-mediated overexpression of Noxa (Figure 14B). Conversely, pre-treatment with AKT inhibitor Triciribine and PI3K inhibitor LY294002 did not exert any evident effect on SM83/CPT-induced cell death (Figure 14A) and did not alter Noxa levels (Figure 14B), thus suggesting that PI3K/AKT, the other side of the KRas downstream signalling, is not responsible for *KRAS*-driven sensitivity to SM83 and CPT. To further confirm that the effectors ERK1/2 downstream mutated KRas are dispensable for Noxa modulation and given that the inhibitors might have possible off-target effects, we transiently silenced ERK1 and ERK2 and checked for Noxa protein levels. As clearly shown in Figure 14C, Noxa protein levels were, as expected, decreased in the absence of KRas. Intriguingly, selective loss of ERK2 itself downregulated Noxa. We then wondered whether SM83 and CPT as single agents or in combination would affect

ERK1/2 phosphorylation-status, thus influencing KRas-mediated activation of these MAPKs. Under basal conditions the amount of phosphorilated-ERK1/2 (pERK1/2) in HME D13/+ cell line is higher than in the WT counterpart, but SM83 increased pERK1/2 only modestly, while CPT either alone or combined with SM83 even decreased, thought moderately, pERK1/2.

In conclusion, we propose a model where downstream oncogenic KRas, the MAPK ERK2 is the main responsible for upregulation of Noxa, thus favouring the pro-apoptotic response upon treatment with SM83 plus CPT.

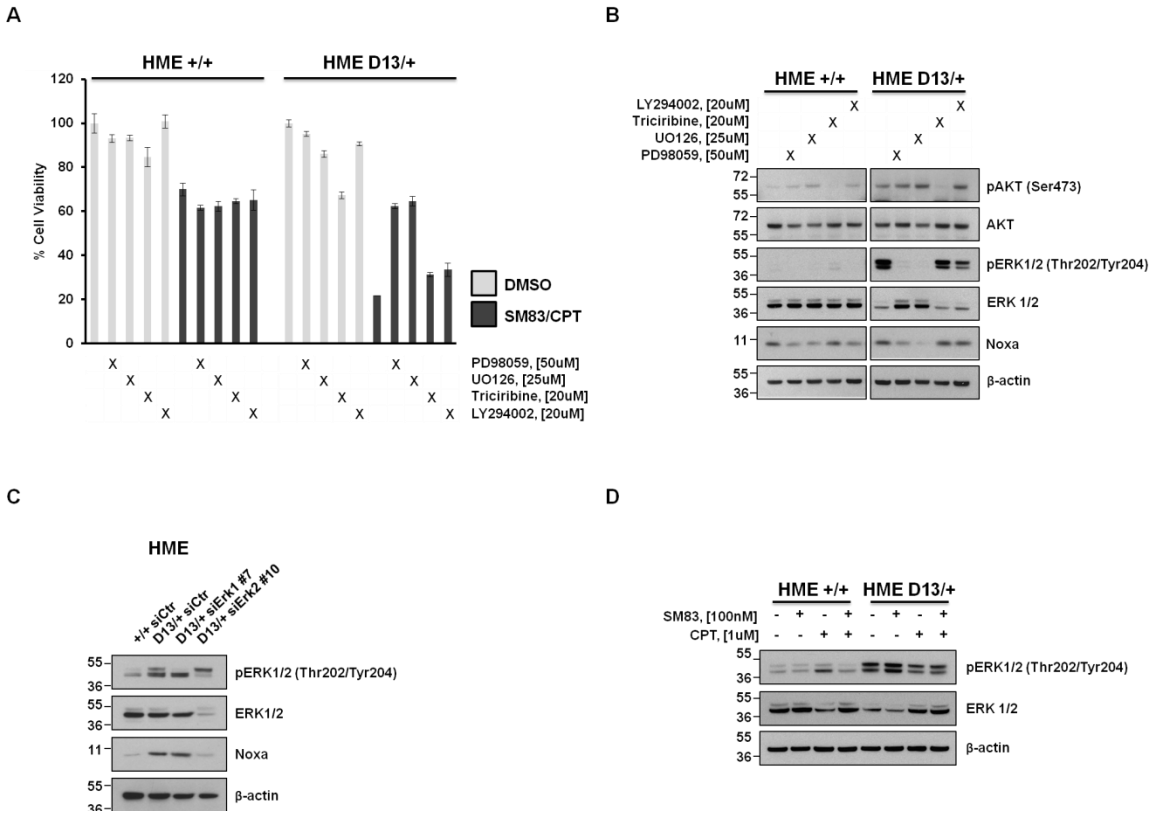

Figure 14 | MAPK ERK2 is the KRas main effector responsible for Noxa-induction. (a) HME +/+ and HME D13/+ cell lines were pre-incubated with the following inhibitors PD98059, UO126, Triciribine and LY294002 at the indicated concentrations for 2 hours and subsequently treated with SM83 [100 nM] and CPT [1 uM]. Cell viability was quantified after 24 h. One representative of three independent experiments is shown. (b) HME +/+ and HME D13/+ cell lines were treated with the following inhibitors PD98059, UO126, Triciribine and LY294002 at the indicated concentrations for 2 hours and

subsequently subjected to western blotting. (c) HME +/+ and HME D13/+ were transiently transfected with the indicated siRNAs for 72 hours and subsequently subjected to western blotting. (d) HME +/+ and HME D13/+ cells were treated with DMSO, SM83, CPT and the combination at the indicated concentrations for 6h. Cells were lysed and subjected to western blotting. (b, c, d,) One representative of two independent experiments is shown.

4.1.4 TNF/TNF-Rs system partially cooperates to SM83/CPT-induced cell death in *KRAS*-mutated cells

Beyond the fact that KRas can regulate NF-kB signaling [Montagut and Settleman, 2009], it is known that SM-mediated downregulation of cIAP1/2 leads to the stabilisation of NIK and NF-kB-induced transcription of TNF which, in turn, kills cells in an autocrine fashion [Petersen *et al*, 2007].

Therefore, we hypothesised that expression of TNF might be induced by SM83 in a cell system where the presence of mutated *KRAS* might already positively impact on endogenous/secreted TNF amount and/or on the endogenous TNF-Rs expression at the cell surface, thus facilitating cell death upon combined SM83 and CPT. To this end, we pre-treated HME WT and HME KRasG13D with Infliximab (IFX), a monoclonal antibody targeting human TNF as well as Enbrel, thereby blocking the interaction between TNF and its cognate receptors. As a result, both IFX (Figure 15A) and Enbrel (Figure 15B) partially rescued SM83/CPT-induced cell death in *KRAS*-mutated HME.

Therefore, we can conclude that TNF is one of the mediators of cell death, nevertheless, whether *KRAS*-mutated cells, compared to the WT counterparts are characterised by high basal levels of TNF or by high surface expression of TNF-Rs still needs to be clarified.

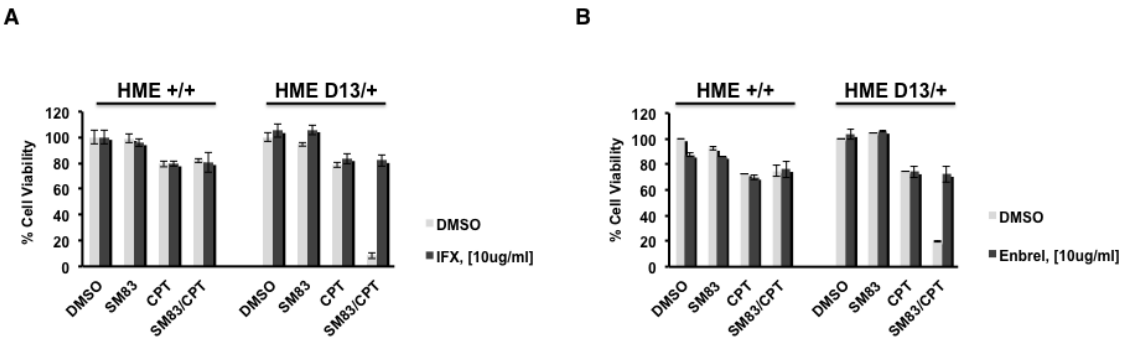

Figure 15 | TNF/TNF-R contribute to SM83/CPT-induced cell death in *KRAS*-mutated HME cell line. HME +/+ and HME D13/+ cell lines were pre-incubated with either IFX [10 ug/ml] (a) or Enbrel [10 ug/ml] (b) for 1 hour and subsequently treated with SM83 [100 nM] and CPT [1 uM]. Cell viability was quantified after 24 h. One representative of three independent experiments is shown.

4.1.5 Sensitivity to SM83/CPT is *KRAS*-independent in a panel of colorectal cancer cell lines.

We then investigated whether the findings described with SM83 and CPT-treated HME KRasG13D are true also for cancer cells carrying the same mutation.

Therefore, we hypothesised that colorectal cancer cells containing oncogenic *KRAS* would be more sensitive to SM83/CPT than their WT counterparts. For this aim, we chose a panel of isogenic colorectal cancer (CRC) cell lines: SW48 and Lim1215 bear either *KRAS*-WT alleles (+/+) or one allele of the two is mutated (D13/+) by KI technology; HCT116 and DLD-1 bear either one allele mutated (D13), which can be accompanied by the knock-out (KO) of the wild-type resulting in the D13/- genotype or one allele wild-type (+) and the other one is null (-) resulting in the +/- genotype. Notably, after the treatments, SW48 (Figure 16A), Lim1215 (Figure 16B) and HCT116 (figure 16C) were sensitive to combined SM83 and CPT independently of the mutational status of KRAS. In particular, even at 10 uM CPT the combination with SM83 did not kill more than 50% of the cells. Conversely, DLD-1 showed a quite different response from the others (Figure 16D): DLD-1 bearing mutated *KRAS* was more resistant than DLD-1

which followed targeted disruption of the D13 (+/-) and, overall, this cell line was completely resistant to the combination.

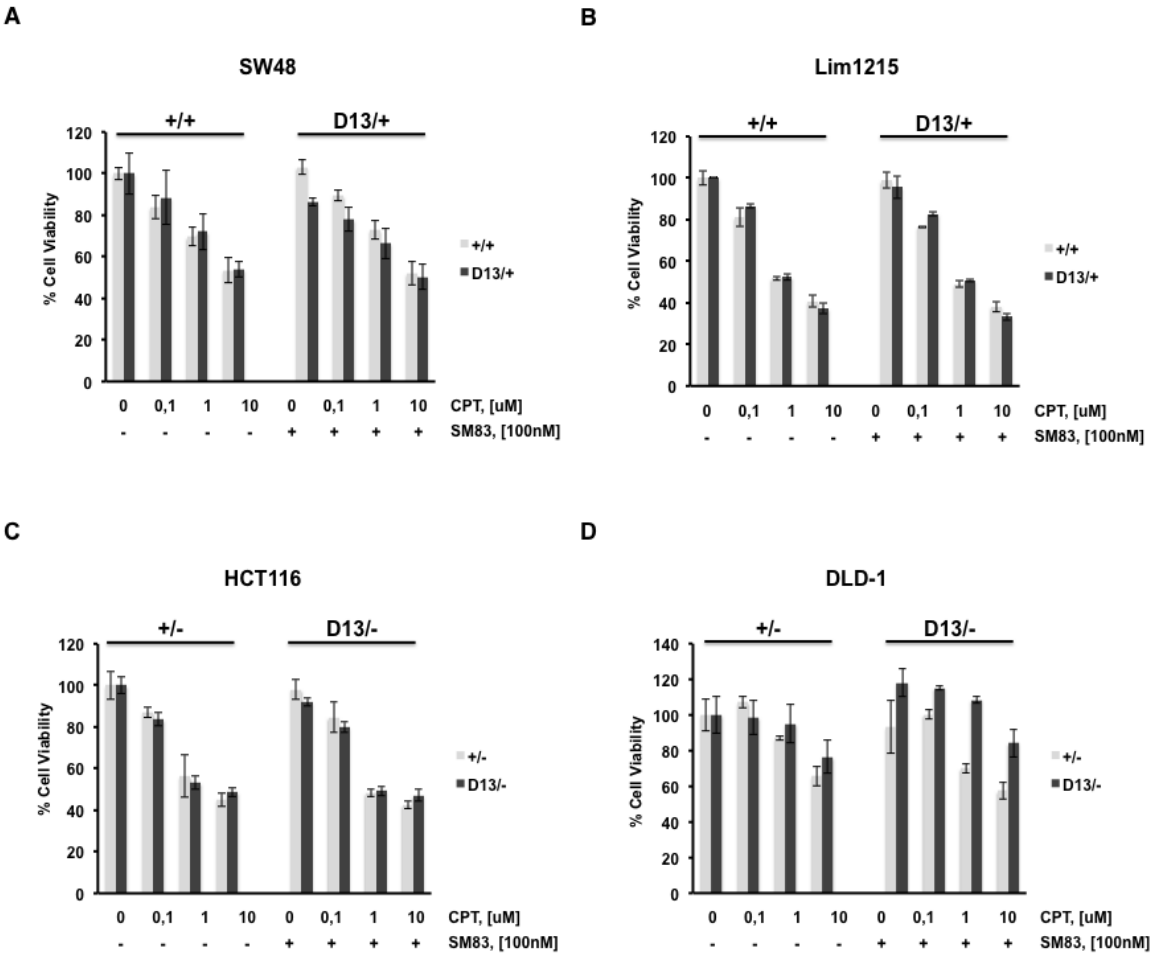

Figure 16 | Response to SM83/CPT does not depend on the mutational status of KRas in a panel of isogenic CRC cell lines. SW48 +/+ and SW48 D13/+ (a), Lim1215 +/+ and Lim1215 D13/+ (b), HCT116 +/- and HCT116 D13/- (c) and DLD-1 D13/- and DLD-1 +/- (d) cell lines were treated with DMSO and the combination of SM83 and CPT at the indicated concentrations. Cell viability was quantified after 24 h. One representative of three independent experiments is shown.

4.1.6 Noxa levels do not differ on the basis of *KRAS* mutational status in CRC cell lines

We then asked why mutation of *KRAS* is not associated with sensitivity to SM83 and CPT. Since we found that Noxa-mediated cell death in human normal cells was KRasG13D dependent, we then hypothesised that colorectal cancer cells bearing oncogenic KRas did not upregulate Noxa, thereby resulting in a similar outcome in presence of WT and mutated *KRAS*. As Figure 17 shows, Noxa protein levels were not altered by the presence of KRasG13D even in the absence of the WT one (D13/- genotype) i.e. HCT116 and DLD-1.

To summarize, in normal immortalized cell lines (HME and MCF10A) the mutation of *KRAS* confers sensitivity to combination therapy, while in colorectal cancer cell lines it does not. In conclusion, the sensitivity to treatment observed in colorectal cancer cell lines is KRasG13D-independent, while the robust synergism detected in HME and MCF10A is KRasG13D-dependent and is triggered by MAPK ERK2-mediated upregulation of Noxa.

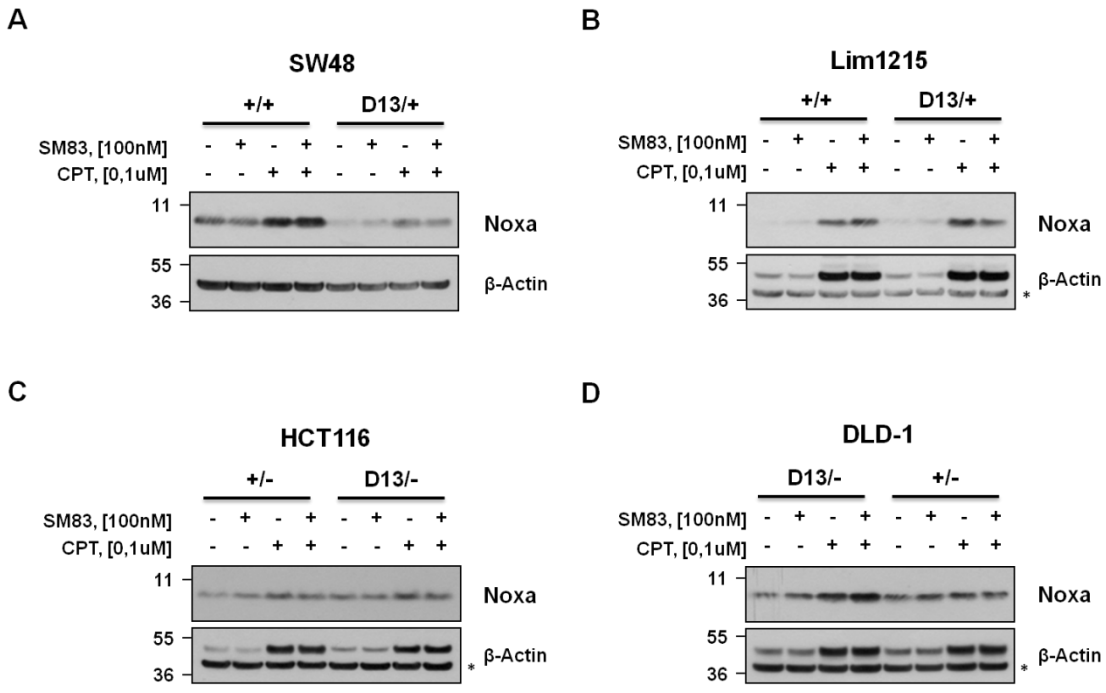

Figure 17 | Noxa protein levels are not upregulated by the presence of mutated *KRAS*. SW48 +/+ and SW48 D13/+ (a), Lim1215 +/+ and Lim1215 D13/+ (b), HCT116 +/- and HCT116 D13/- (c), DLD-1 D13/- and DLD-1 +/- (d) cell lines were treated with DMSO, SM83, CPT and the combination at the indicated concentrations for 6 h. Cells were lysed and subjected to western blotting. One representative of two independent experiments is shown. (*) indicates the antibody specificity.

4.2 Cyclin Dependent Kinase 9 inhibition overcomes TRAIL-resistance in *KRAS*-mutated non-small cell lung cancer

TRAIL can induce apoptosis in many cancer cells without causing toxicity *in vivo* [Ashkenazi *et al*, 1999, Walczak *et al*, 1999]. Since most primary human cancers are TRAIL-resistant [Todaro *et al*, 2008], future TRAIL-based therapies will require the addition of sensitising agents that remove crucial blocks in the TRAIL apoptosis pathway. PI3K are components of signalling pathways which promote tumour growth, migration, invasion and metastasis. Consequently, PI3K inhibitors have emerged as a novel class of agents currently used in clinical trials as single agents or as potential TRAIL-sensitiser candidates.

Intriguingly, recently data published by Johannes Lemke [Lemke *et al*, 2014a] show that PIK-75, an inhibitor of the p110α isoform of PI3K, is an exceptionally potent TRAIL-apoptosis sensitiser. Surprisingly, PI3K inhibition is not responsible for this activity. A kinome-wide *in vitro* screen reveals that PIK-75 strongly inhibits a panel of 27 kinases. Within this panel, CDK9 has been identified as responsible for TRAIL-resistance of cancer cells. Indeed, CDK9 inhibition by SNS-032, a small molecule inhibitor already in clinical trials [Conroy *et al*, 2009], could strongly sensitise tumour cells to TRAIL-induced apoptosis. Mechanistically, SNS-032-mediated CDK9 inhibition induced transcriptional suppression of cFlip and Mcl-1, thus facilitating cell death at DISC- and mitochondria-levels as represented in Figure 18.

There are several CDKs inhibitors currently used in clinical trial. We therefore evaluated a novel combinatorial therapy consisting of TRAIL and the clinically used CDK9 inhibitor SNS-032. Despite it inhibits CDK2, CDK7 and CDK9 among other CDKs and kinases, its inhibitory capacity is about 10-fold selective for CDK9 (the half maximal inhibitory concentration IC50 = 4 nM) over the others. Furthermore, this combination is not hepatotoxic at the killing concentrations of the co-treatment.

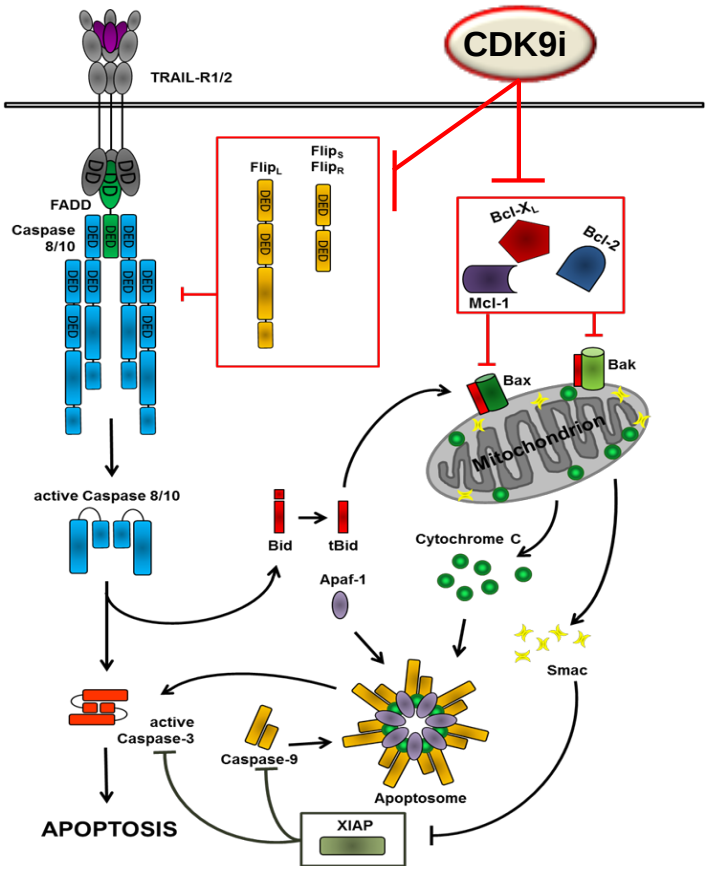

Figure 18 | Proposed model of the molecular mechanisms of CDK9 inhibition-mediated TRAIL sensitisation.

4.2.1 Combination of TRAIL and SNS-032 kills a panel of human NSCLC cell lines

As published by Lemke et al., TRAIL and SNS-032 were highly efficient in killing A549, a human non-small cell lung cancer cell line. To investigate whether this co-treatment may be applicable more broadly, we tested the combination on a panel of TRAIL-resistant NSCLC cell lines [Kumar *et al*, 2012]. Upon 10 ng/ml of TRAIL together with 300 nM of SNS-032, all cell lines tested were potently sensitised (Figure 19).

Therefore, we demonstrate that SNS-032/TRAIL combination can be extended to a broad range of *KRAS*-mutated NSCLC cell lines.

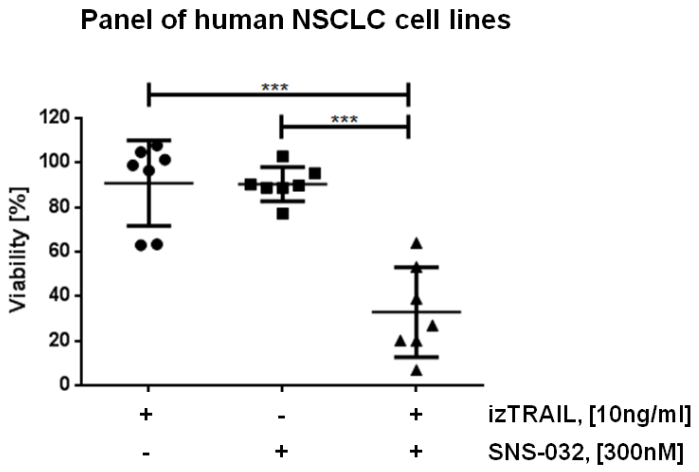

Figure 19 | Human NSCLC cell lines are sensitive to combined SNS-032 and TRAIL. Seven different NSCLC cell lines were pre-incubated with SNS-032 [300 nM] for 1 h and subsequently stimulated with izTRAIL (10 ng/ml). Cell viability was quantified after 24 h. The graph represents means of three independent experiments ± SEM; individual dots represent means of three experiments of one cell line. *** $P < 0.0005$; Student's t-test.

4.2.2 TRAIL combined with CDK9 inhibition eradicates orthotopic lung tumours *in vivo*

Having demonstrated the efficacy of TRAIL with SNS-032 *in vitro*, we evaluated whether it is active also *in vivo*. To this end, we induced lung tumours via tail vein injection of A549 cells stably expressing luciferase (A549-luc). After seven days, mice were randomised to obtain similar amounts of tumour burden in each group and subsequently a four-day treatment regime was applied with either vehicle, TRAIL, SNS-032 or the combination of SNS-032 and TRAIL (Figure 20A). Whereas TRAIL treatment alone had a slight growth inhibitory effect, and SNS-032 only marginally affected lung tumour burden, combined treatment with TRAIL and SNS-032 completely eradicated established lung tumours in most mice as determined by *in vivo* bioluminescence imaging (Figure 20B). Furthermore, histopathological inspection of lung sections confirmed the results obtained by *in vivo* imaging (Figure 20C). Strikingly and in line with

the bioluminescence data, 7 out of 8 mice receiving TRAIL combined with SNS-032 were histologically tumour-free after the treatment cycle.

Therefore, the novel treatment strategy of TRAIL and CDK9 inhibition may lead to the design of highly powerful and cancer-selective therapeutics.

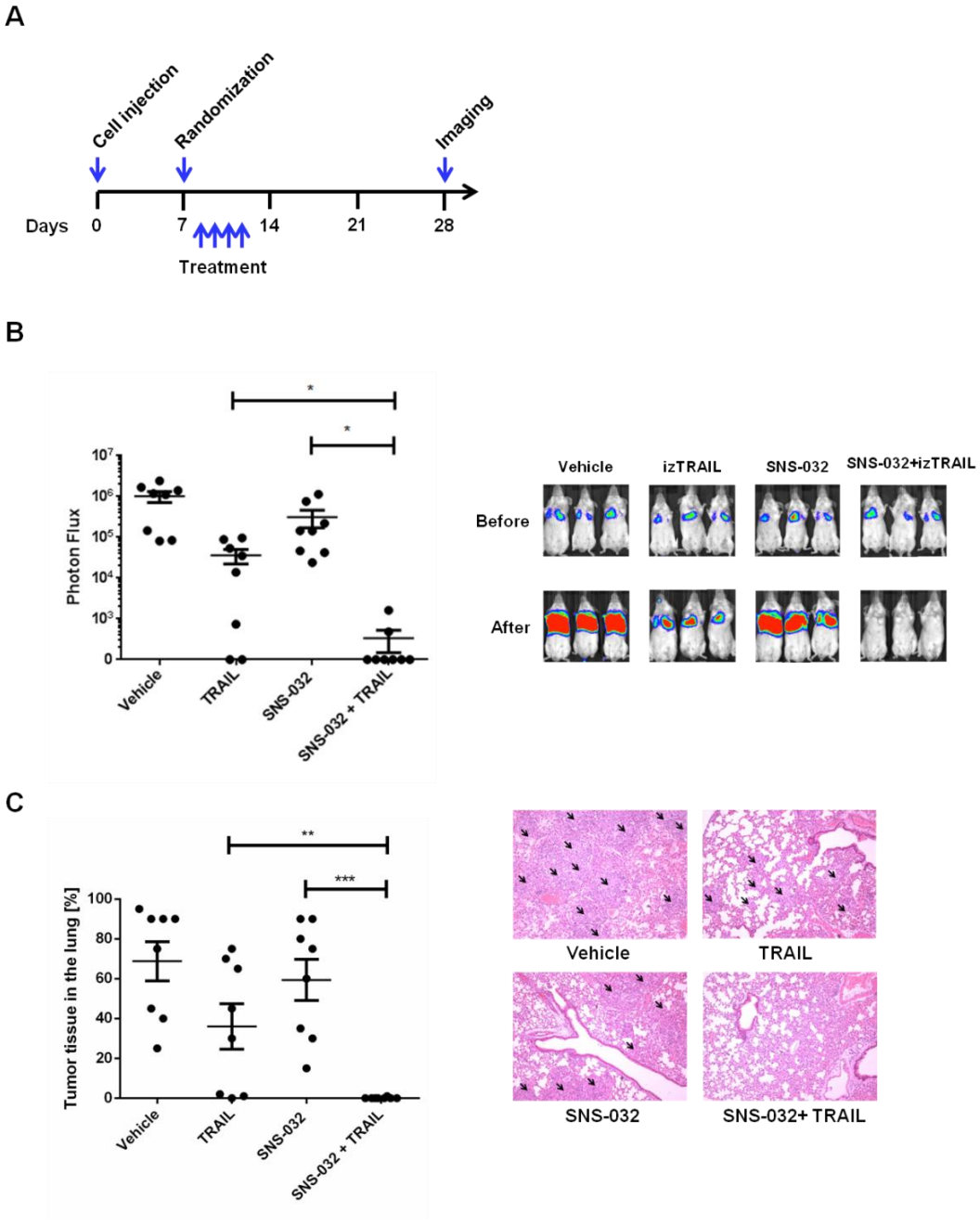

Figure 20 | TRAIL/SNS-032 co-treatment eradicates orthotopic lung tumours *in vivo*. (a) Experimental treatment schedule is shown. (b) Tumour burden was quantified by bioluminescence imaging (Photon Flux) one week after injection of $2x10^6$ A549-Luc cells and three weeks after treatment. Dots represent individual mice (n=8 per group) +/- SEM. Three representative mice from each group are shown. (c) Paraffin sections of lungs from all mice were stained with H&E and subjected to microscopical analysis quantifying the percentage of total lung area occupied by tumour tissue. Dots represent lungs from individual mice, (n=8 per group) +/- SEM. Representative histological images are shown (arrows indicate tumour tissue). * $p < 0.05$; ** $p < 0.01$, *** $p < 0.0005$, Student's t-test.

4.2.3 Establishment of autochthonous lung tumours that have a tumour supporting microenvironment

The strength of this novel combination has been evaluated in an orthotopic lung tumour. However, the injection of a human NSCLC cell line into an immunodeficient mouse does not closely resemble human NSCLC dynamics. Therefore, we next focused on analysing the efficacy of CDK9 inhibition in combination with TRAIL in an autochthonous mouse model where the mouse is genetically engineered to develop NSCLC that mimics the genetic and histophatological features of the human disease [Meuwissen and Berns, 2005]. In principle, autochthonous tumours arise from few somatic cells that, upon Cre-recombinase delivery, become transformed in their natural location, surrounded by a normal tissue microenvironment [Frese and Tuveson, 2007]. As shown in Figure 21, the mouse genome is engineered to contain LoxP DNA elements, 'flox', that either surround exons critical to a tumour suppressor gene or surround a synthetic 'stop' element, 'Lox-Stop-Lox' ('LSL'), inserted in front of an oncogene. LoxDNA elements are under the control of Cre-recombinase that, once delivered to the appropriate cell type, can turn-off tumour suppressor genes or turn-on oncogenes, thus generating the tumour [Frese and Tuveson, 2007].

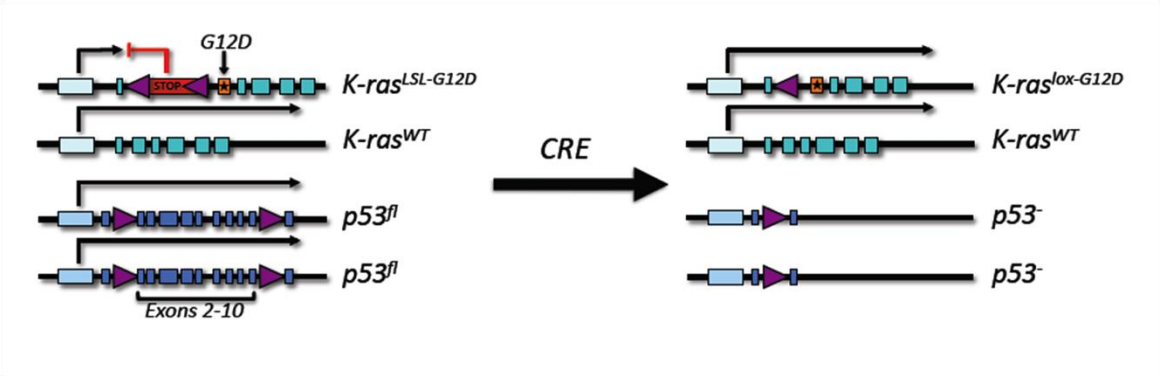

Figure 21 | Genetically controlled events in a mouse model of lung cancer. [DuPage *et al*, 2009]

Common mutations in NSCLC are activating mutation in *KRAS* (10-30%) and loss of function in p53 (50-70%) [Herbst *et al*, 2008]. Tyler Jacks's lab generated an oncogenic mutation in *KRAS*, G12D in the endogenous locus of the gene. Then, a LSL cassette was engineered into the first intron of the *KRAS* gene (*K-Ras*$^{LSL\text{-}G12D}$), thereby preventing the expression of the mutant *KRAS* allele until the stop elements are removed by the activity of Cre recombinase [DuPage *et al*, 2009]. Since the cassette creates a null allele and given that *KRAS* null mice are embrionically lethal, mice can only be heterozygous for the *K-Ras*$^{LSL\text{-}G12D}$ allele [Johnson *et al*, 1997]. To more recapitulate the p53 loss of function mutations, Tyler Jacks's lab generated a conditional point mutation version of p53, R172H under the control of LSL (*p53*$^{LSL\text{-}R172H}$) as described for KRas [DuPage *et al*, 2009].

To summarize, in order to develop NSCLC in mice, Cre recombinase needed to be virally delivered to the lungs, thus sporadically allowing the cells to express mutant K-Ras and p53 alleles. To this end, mice had to inhale adenoviruses engineered to express Cre (Ad-Cre) either by intranasal (IN) instillation (Figure 22) or intratracheal (IT) intubation as described in details by Tyler Jacks [DuPage *et al*, 2009].

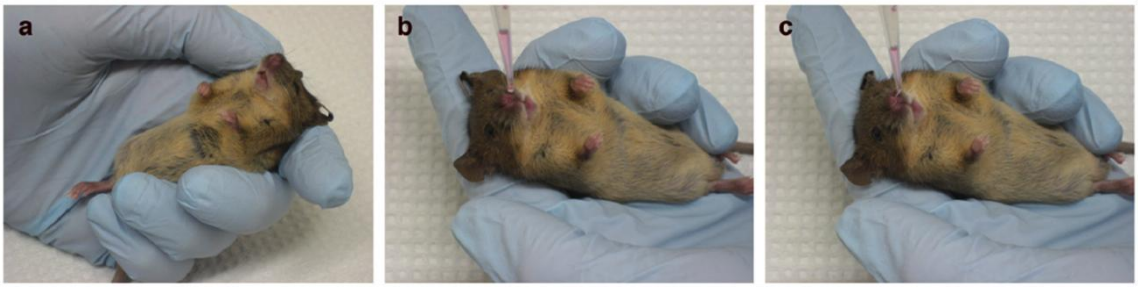

Figure 22 | Intranasal infection technique. [DuPage *et al*, 2009]

For our study, we decided to employ the *K-Ras*$^{LSL\text{-}G12D/+}$ (K) and *p53*$^{LSL\text{-}R172H/+}$ (P), KP conditional mouse model of NSCLC where the IN delivery method was chosen to introduce Ad-Cre according to the Tyler Jacks's method. The first experiment aimed to understand how many weeks after Cre recombinase infections were necessary to assure the development of the tumour. Mice were then sacrificed at 8, 12 and 16 weeks after Cre infection. Therefore, based on the amount of tumour burden detected by the histology, we set out that 12 weeks might be the mouse-age to start the treatment with either vehicle, TRAIL, CDK9 inhibitor or the combination. Yet, the optimisation of the protocol of infection and the treatment schedule are still ongoing.

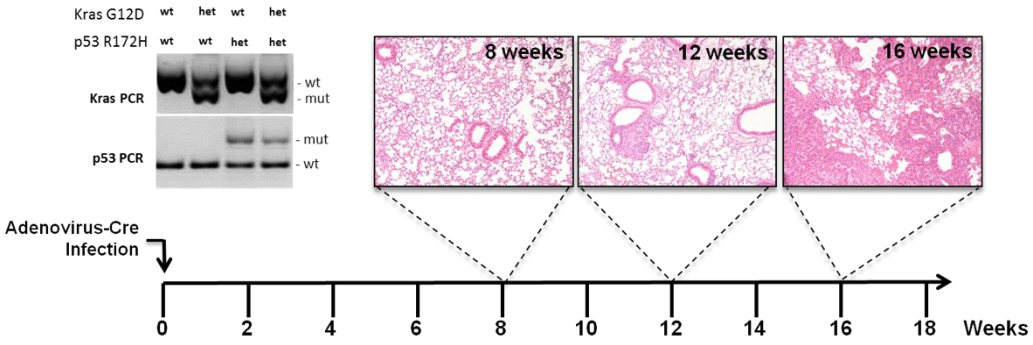

Figure 23 | Experimental schedule of Ad-Cre-mediated growth of NSCLC in KP mice. Mice were IN-infected with Ad-Cre. 8-, 12- and 16-weeks-old mice were sacrificed and paraffin sections of lungs from all mice were stained with H&E. The top left panel shows the genotype of mice used in this study.

Murine tumours derived from the KP mouse model were supposed to be treated with a recombinant murine form of izTRAIL (iz-mu-TRAIL). Therefore, a highly active form of murine TRAIL was generated and from here it is named izTRAIL.
Interestingly, a database search revealed that the extracellular domain of murine TRAIL is only a few amino acids longer than its human homologue. The cloning of iz-mu-TRAIL was already performed in our lab. However, purification of iz-mu-TRAIL was essential to produce a high amount of the ligand to perform both *in vitro* and *in vivo* experiments. Purification method is described in details in Matherial & Methods chapter, Paragraph 3.5.

4.2.4 Dinaciclib-mediated CDK9-inhibition combined with TRAIL kills murine NSCLC cell lines while SNS-032 does not

So far, *in vitro and in vivo* experiments were performed by using SNS-032 as CDK9 inhibitor. Since this molecule is able to specifically downregulate the human form of CDK9, we could not employ SNS-032 to test this combination either in murine NSCLC cell lines or in the new established autochthonous mouse model. Therefore, we chose to employ another CDK9 inhibitor, Dinaciclib.
Dinaciclib (MK-7965, formerly SCH7277965) is a novel, potent, small-molecule inhibitor of CDK1, CDK2, CDK5 and CDK9 with IC50 values in the 1 nM to 4 nM range, and inhibits CDK4, CDK6, and CDK7 at IC50 values from 60 nM to 100 nM range [Parry *et al*, 2010, Paruch *et al*, 2010]. A first-in-human phase I dose escalation study of Dinaciclib shows that its initial bioactivity and the observed disease stabilization support further evaluation as a treatment option for patients with advanced solid malignancies [Nemunaitis *et al*, 2013]. Importantly, it has been reported that Dinaciclib has direct anti-leukemia cytotoxicity, but effects are of short duration, suggesting that it needs to be combined with chemotherapy or other novel agents [Gojo *et al*, 2013]. In line with this findings, it has been recently conducted a phase II randomised clinical study where Dinaciclib does not exert any antitumour activity as monotherapy in patients with advanced NSCLC [Stephenson *et al*, 2014].
We therefore proposed to evaluate the anticancer activity of Dinaciclib in combination with TRAIL in our model of NSCLC. We firstly compared the effect of Dinaciclib to SNS-

032 on the inhibition of murine CDK9. To this end, 802T4, a murine NSCLC cell line derived from KP mouse model, was treated with either Dinaciclib or SNS-032. Strikingly, western blot analysis for Ser2 Phosphorilation of RNA Pol II revealed that 25 nM of Dinaciclib were sufficient to completely inhibit murine CDK9 within 6 hours while SNS-032 did not have any effects (Figure 24A). To investigate whether this novel CDK9 inhibitor was efficient in synergising with TRAIL, we treated 802T4 cell line with the combination and immediately after 24 hours, 100 ng/ml of iz-mu-TRAIL almost completely killed these cells in combination with 100 nM Dinaciclib (Figure 24B). As expected and in line with the western blot data showed in Figure 24A, 802T4 were resistant even at 500 nM of SNS-032 in combination with TRAIL.

Hence, we demonstrate that Dinaciclib is active in inhibiting murine CDK9 and sensitises murine NSCLC cell lines to TRAIL-induced cell death. Accordingly, Dinaciclib can be considered as a preferential CDK9 inhibitor to be employed in our next experiments.

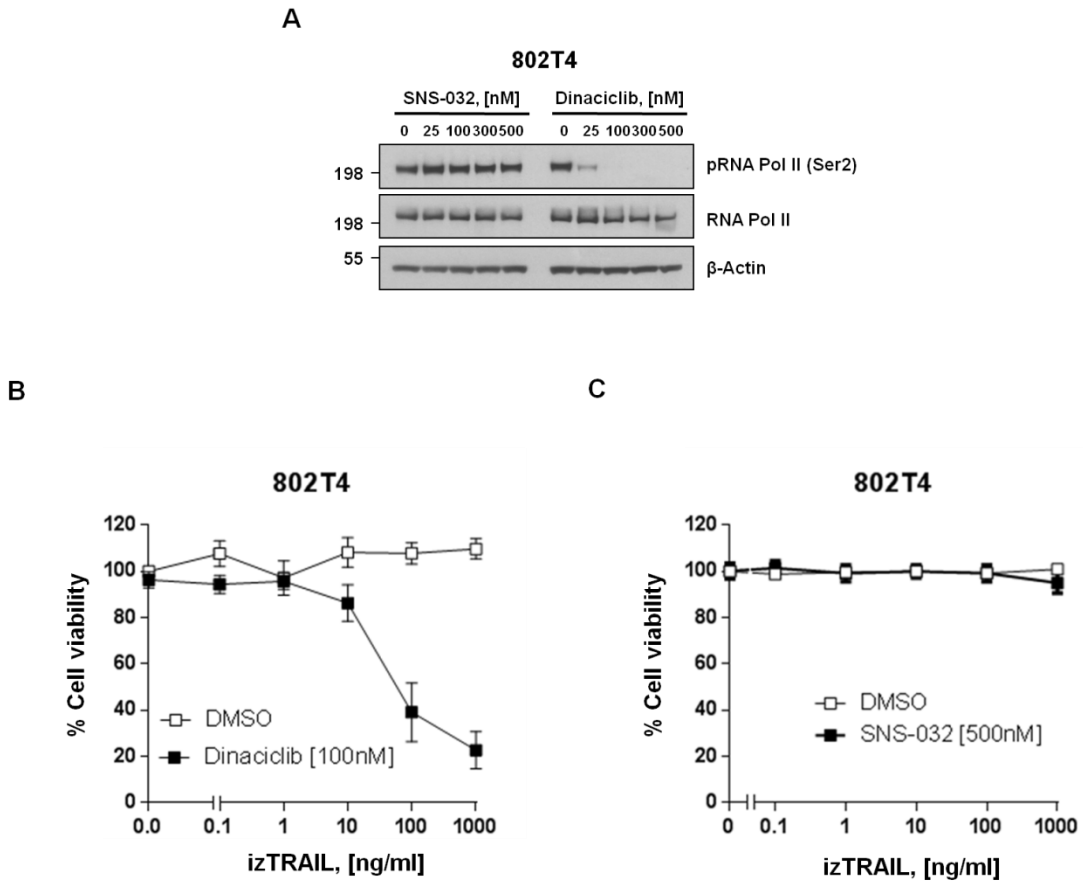

Figure 24 | Dinaciclib inhibits murine CDK9 and sensitises 802T4 to TRAIL-induced cell death. (a) 802T4 cells were treated with SNS-032 or Dinaciclib at the indicated concentrations for 6 h. Cells were lysed and subjected to western blotting. (b) 802T4 cells were pre-incubated with Dinaciclib [100 nM] for 1h and subsequently stimulated with izTRAIL at the indicated concentrations. Cell viability was quantified after 24 h. (c) 802T4 cells were pre-incubated with SNS-032 [500 nM] for 1 h and subsequently stimulated with izTRAIL at the indicated concentrations. Cell viability was quantified after 24 h. One representative of three independent experiments is shown.

4.2.5 Dinaciclib sensitises human NSCLC to TRAIL-induced apoptosis *in vitro*

Despite Dinaciclib was employable in the autochthonous mouse model, its effects on inhibiting human CDK9 and on killing human NSCLC cell lines in combination with iz-hu-TRAIL needed to be tested. For this reason, A549 were treated with increasing doses of Dinaciclib and 25 nM concentration was enough to prevent Ser2 phosphorilation of RNA Pol II after 6 hours, while SNS-032 needed 10-fold more to do so (Figure 25A). Notably, 25 nM Dinaciclib was sufficient to kill A549 in combination with 10 ng/ml of TRAIL as shown in Figure 25B while it was previously shown by Lemke *et al.* that these cells needed 300 nM of SNS-032 to obtain the same effect. Furthermore, we demonstrated that A549 died apoptotically upon Dinaciclib and TRAIL co-treatment; in fact, cleaved-caspases together with cleaved-PARP and tBid are detectable only when TRAIL was added to Dinaciclib (Figure 25C). Moreover, this novel CDK9 inhibitor combined with TRAIL was also active in killing a panel of human NSCLC cell lines as well as SNS-032 as shown below (Figure 25D).

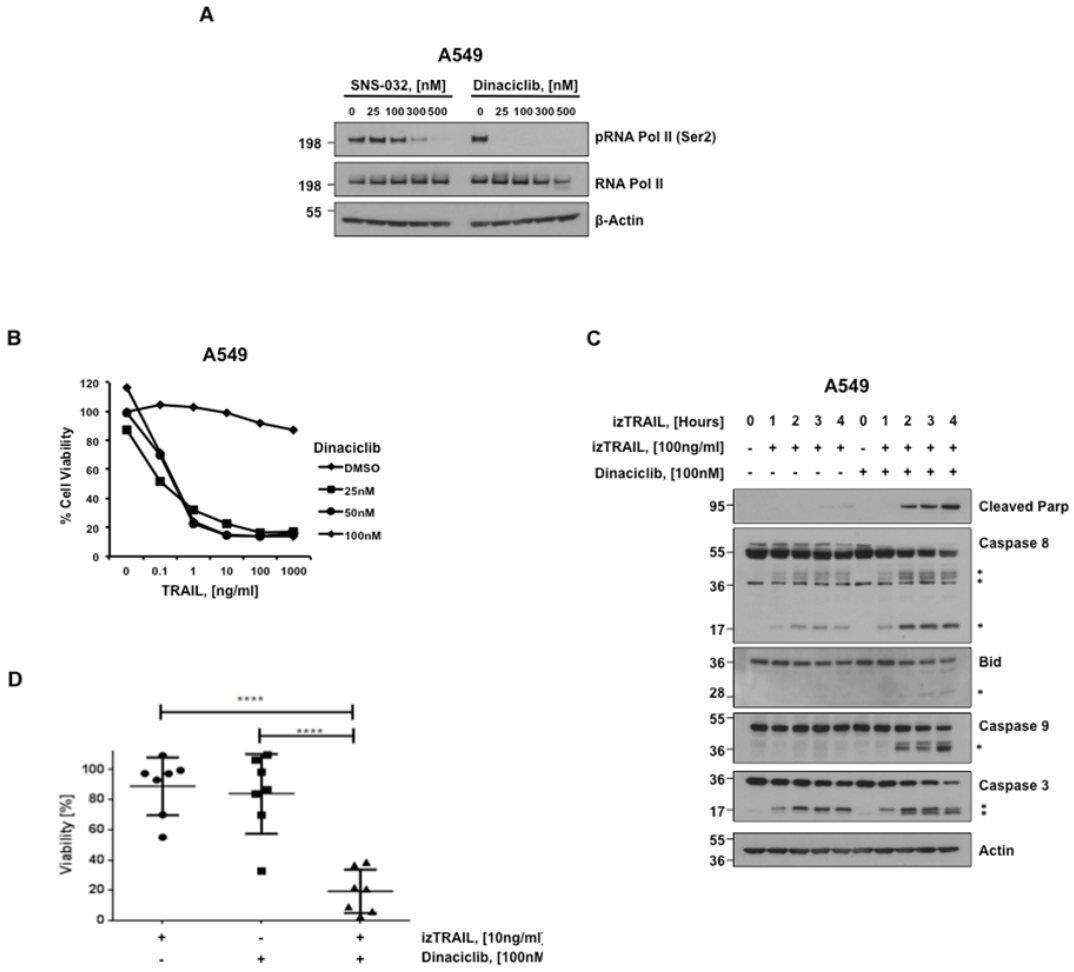

Figure 25 | Dinaciclib inhibits human CDK9 and sensitises A549 cells to TRAIL-induced apoptosis *in vitro*. (a) A549 cells were treated with SNS-032 or Dinaciclib at the indicated concentrations for 6 h. Cells were lysed and subjected to western blotting. (b) A549 cells were pre-incubated with SNS-032 for 1 h and subsequently stimulated with izTRAIL at the indicated concentrations. Cell viability was quantified after 24 h. (c) A549 cells were pre-incubated with Dinaciclib [100 nM] for 1 h and subsequently stimulated with izTRAIL [100 ng/ml] for the indicated time points. Cells were lysed and subjected to western blotting. (d) Six different NSCLC cell lines were pre-incubated with SNS-032 [100 nM] for 1 h and subsequently stimulated with izTRAIL (10 ng/ml). Cell viability was quantified after 24 h. The graph represents means of three independent experiments ± SEM; individual dots represent means of three experiments of one cell line. **** $P < 0.0001$; Student's t-test. (*) indicates the cleaved form. One representative of three independent experiments is shown.

4.2.6 TRAIL combined with Dinaciclib eradicates orthotopic lung tumours *in vivo*

Finally, to evaluate the effect of Dinaciclib and TRAIL in an orthotopic xenograft *in vivo*, lung tumours were induced via tail vein injection of A549-luc. The experiment was carried out as shown in Figure 20A. Photon flux images and the hystopathological analysis showed that TRAIL alone already had an effect on tumour regression while Dinaciclib alone did not (Figure 26). However, in mice treated with the combination there was no sign of tumour.

Therefore, Dinaciclib in combination with TRAIL was effective even towards human NSCLC *in vivo*.

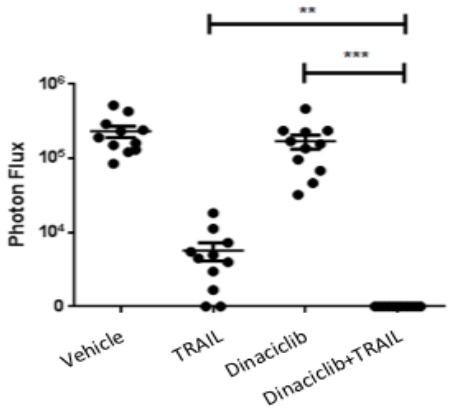

Figure 26 | Combination of Dinaciclib and TRAIL eradicates orthotopic lung tumours *in vivo*. Tumor burden was quantified by bioluminescence imaging (Photon Flux) one week after injection of $2x10^6$ A549-Luc cells and three weeks after treatment. Dots represent individual mice (n=8 per group) +/- SEM. Three representative mice from each group are shown. ** $p < 0.01$; *** $p < 0.0005$, Student's t-test.

4.2.7 Not all murine NSCLC cell lines are sensitive to combined TRAIL and Dinaciclib

We next examined whether TRAIL in combination with Dinaciclib was active in killing several murine NSCLC cell lines as 802T4. We then treated two murine NSCLC cell lines 394T4 and 482T1, together with 802T4 with Dinaciclib at 100 nM and an escalation dose of izTRAIL up to 1 ug/ml. After 24 hours, whereas 802T4 cells were, as expected, strongly sensitive to Dinaciclib and TRAIL (Figure 27A) confirming the results shown in Figure 24B, 394T4 were slightly sensitive only at high doses of TRAIL (Figure 27B) and 482T1 were resistant even at 1 ug/ml of TRAIL (Figure 27C).

This finding indicates that Dinaciclib/TRAIL co-treatment may not be efficient in killing all murine NSCLC cell lines, thus anticipating that the employment of this combination in an autochtonous mouse models may need the addition of a sensitising agent(s).

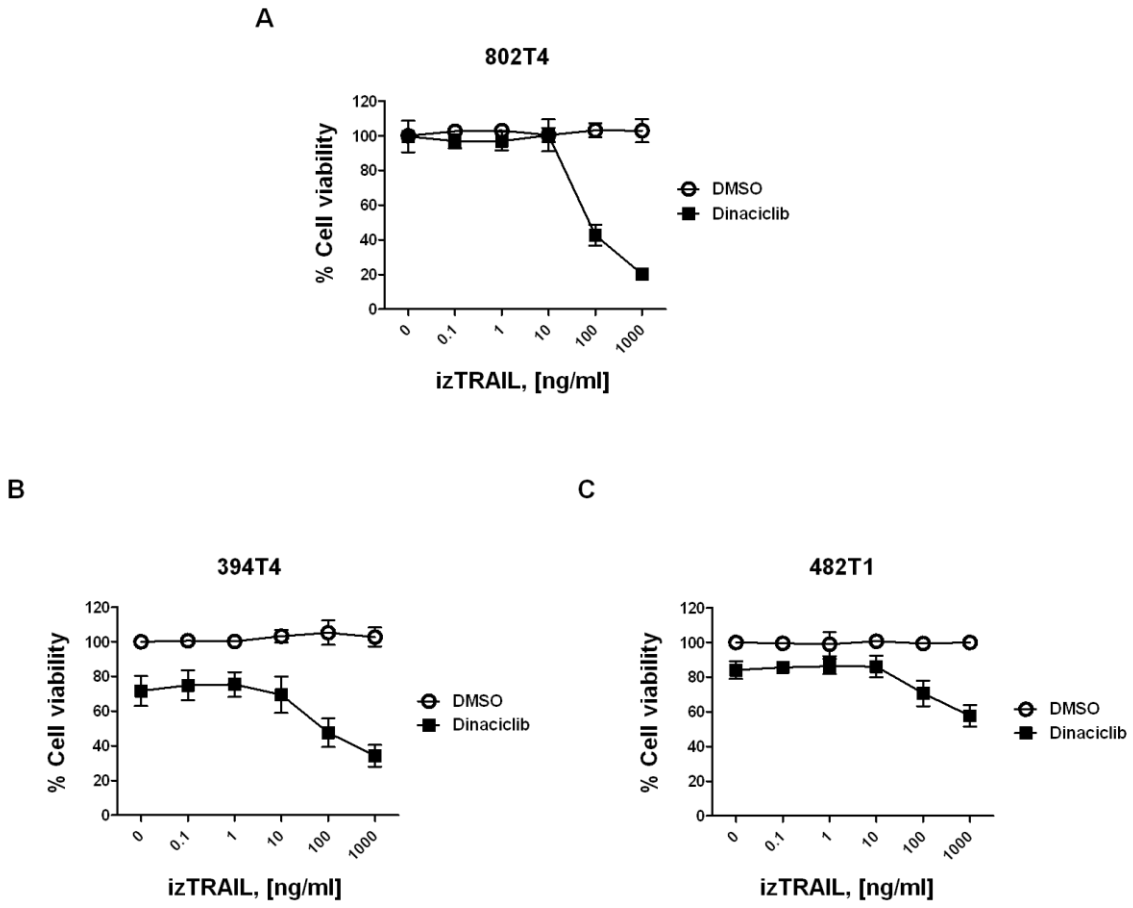

Figure 27 | Treatment with both TRAIL and Dinaciclib does not have high cytotoxic activity in 394T4 and 482T4 cell lines. (a) 802T4, (b) 394T4, (c) 482T1 cell lines were pre-incubated with Dinaciclib [100 nM] for 1 h and subsequently stimulated with iz-mu-TRAIL at the indicated concentrations. Cell viability was quantified after 24 h. One representative of three independent experiments is shown.

Therefore, we evaluated the possibility to add a further agent in order to overcome the resistance to Dinaciclib and TRAIL engaged by some NSCLC cell lines. Since SMs are known to be potent TRAIL sensitisers [Li *et al*, 2004], we pre-treated 394T4 (Figure 28A) and 482T1 (Figure 28B) with SM83 at 100 nM and then with izTRAIL. We also included 802T4 (Figure 28C) even though they are already sensitive to the combination to check whether SM83 can further sensitise to TRAIL/Dinaciclib co-treatment. The results obtained from this experiment showed that SM83 did not further enhance TRAIL-induced apoptosis.

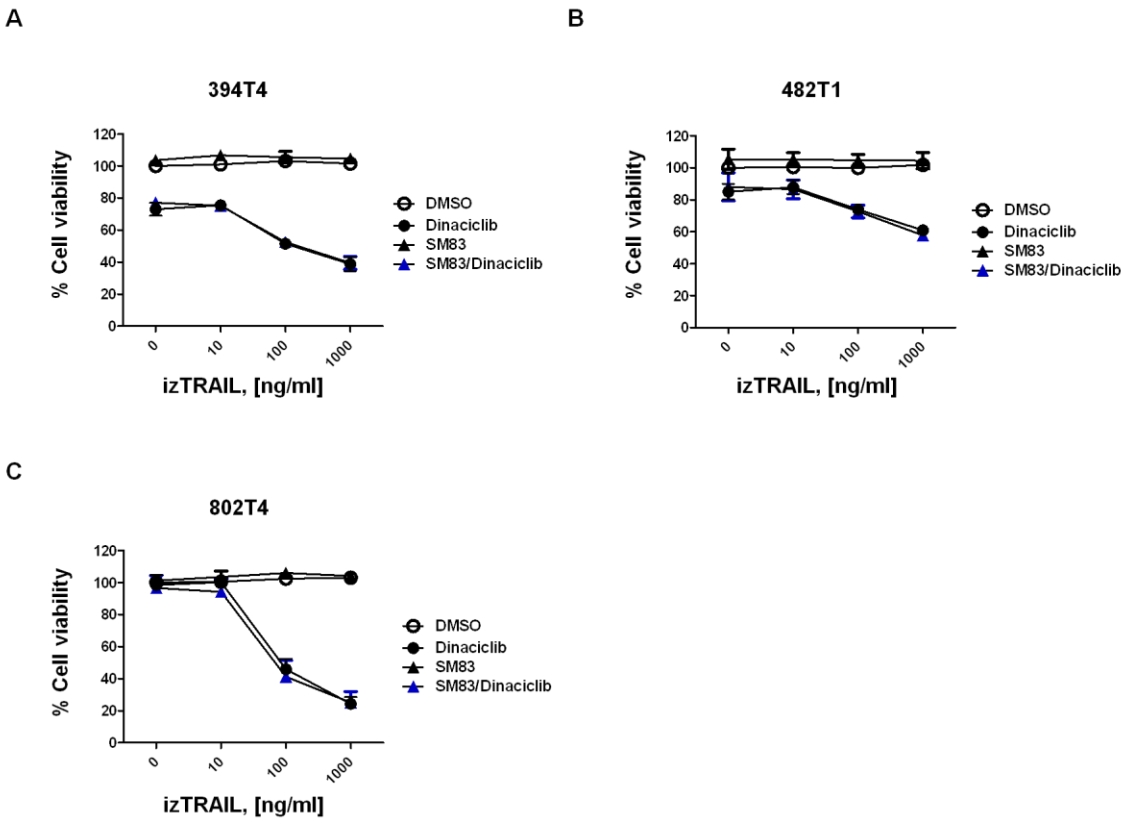

Figure 28 | SM83 does not synergise with TRAIL. (a) 394T4 (b) and 482T4 (c) 802T4 cell lines were pre-incubated with Dinaciclib [100 nM] for 1 h and subsequently stimulated with SM83 [100 nM] and izTRAIL at the indicated concentrations. Cell viability was quantified after 24 h. One representative of three independent experiments is shown.

4.2.8 CDK9 is overexpressed in NSCLC

SNS-032- or Dinaciclib-mediated CDK9 inhibition represents our proposed strategy to overcome TRAIL resistance in NSCLC. We then asked whether this protein might be overexpressed selectively in NSCLC thus providing a strong rationale of targeting CDK9 in the treatment of this tumour.

Therefore, we performed immunofluorescence for CDK9 on the lungs of 16-weeks-old mice from the KP model together with hematoxylin and eosin to identify tumour areas. As shown in Figure 29A, tumours delimited by the white line were CDK9 positive. In line with these *in vivo* data, tumour biopsies from NSCLC patients overexpressed CDK9, thus supporting the idea that CDK9 might be considered as a biomarker in clinic in order to study this newly Dinaciclib-based targeted therapeutic strategy. To address whether CDK9 positivity in the human samples is tumour-specific, the biopsies were stained also for TTF-1, a human marker for lung adenocarcinoma by immunohistochemistry (IHC) as shown in Figure 29B. High positivity for CDK9 is exclusively related to TTF-1 positive areas, thus suggesting that combined TRAIL/CDK9 inhibition treatment could be combined to TRAIL-based therapy.

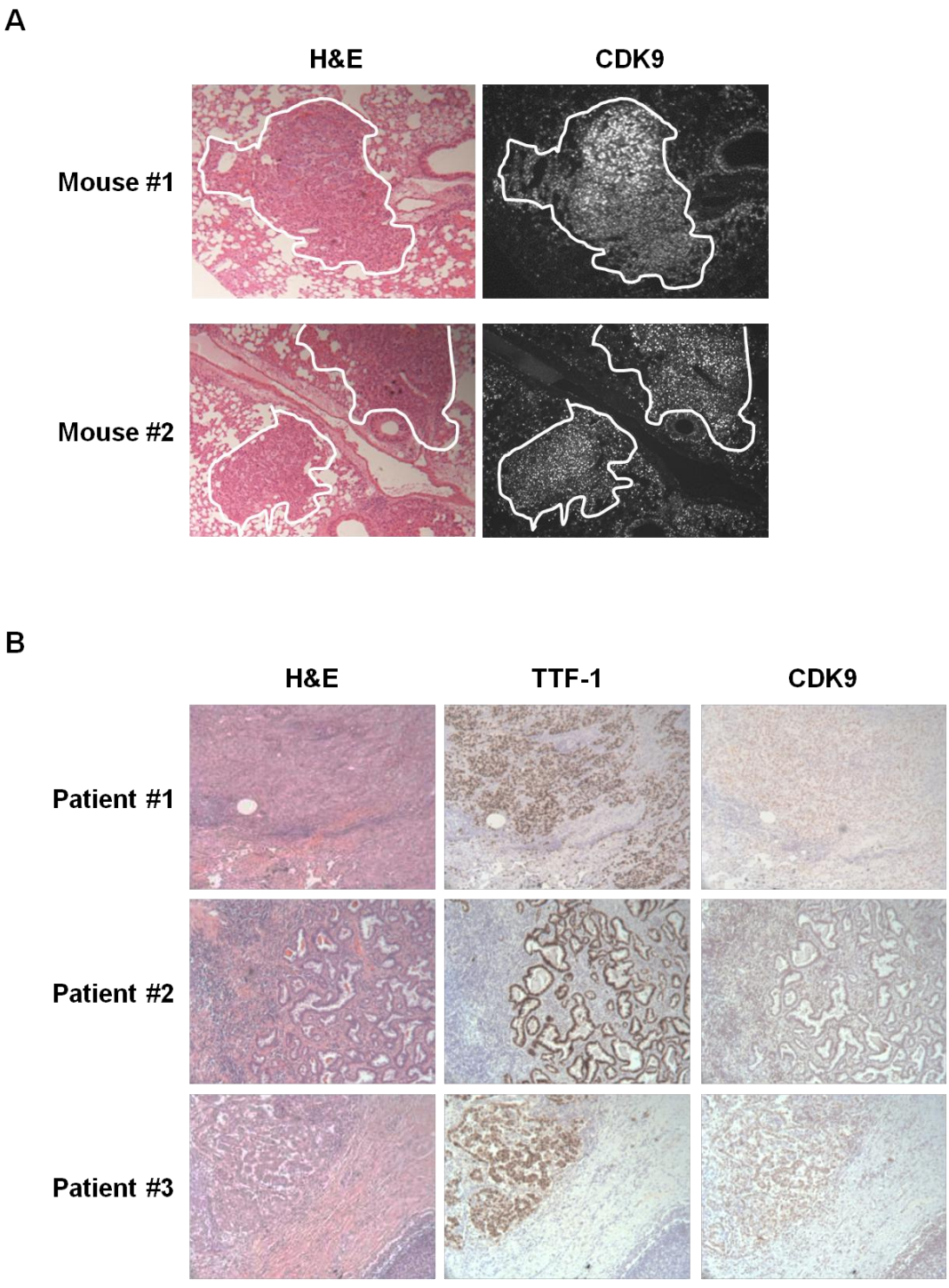

Figure 29 | CDK9 is overexpressed in murine and human NSCLC. (a) Paraffin sections of lungs from 16-weeks-old mice were stained with H&E and with CDK9 by immunofluorescence. The white line defines the area of the tumour. (b) Biopsies from three representative NSCLC patients were stained for H&E, CDK9 and TTF-1.

4.3 Endogenous TRAIL/TRAIL-R2 complex promotes metastasis progression in *KRAS*-mutated cancers via Rac-1/PI3K signaling axis

TRAIL can selectively kill tumour cells *in* vivo [Ashkenazi *et al*, 1999, Walczak *et al*, 1999]. These findings have initiated the development of TRAIL and other TRAIL-R agonists for clinical application as novel cancer therapeutics [Lemke *et al*, 2014b]. More recent studies have however revealed that many tumour cell lines and, importantly, the majority of primary tumours are resistant to TRAIL-induced apoptosis [Koschny *et al*, 2007, Todaro *et al*, 2008]. Hence, besides inducing apoptosis, exogenous TRAIL has also been shown to activate non-apoptotic signaling. These findings highlight potential risks of a TRAIL-based therapy as a single agent for patients with TRAIL-resistant and/or *KRAS*-mutated cancers. Furthermore, cancer cells usually do not down-regulate TRAIL-R suggesting a biological role of this receptor favouring cancer progression In accordance to this hypothesis, many cancers even upregulate TRAIL-Rs, and therefore we hypothesised the existence of a yet unknown cancer-beneficial role of the endogenous TRAIL/TRAIL-R system. TRAIL-Rs and TRAIL are often highly expressed in renal, breast, metastatic head and neck, NSCLC and PDAC with the latter almost always harboring oncogenic *KRAS* mutations [Elrod *et al*, 2010, Ganten *et al*, 2009, Macher-Goeppinger *et al*, 2009, Sanlioglu *et al*, 2007a, Sanlioglu *et al*, 2007b].

Within Silvia von Karstedt's PhD project, preliminary data from an experimental lung metastasis model *in vivo* show that depleting TRAIL-R2 or blocking TRAIL by TRAIL-R2-Fc reduces lung metastasis. However, proliferation, cell death, vascularization and anoikis are not affected. Furthermore, immunosuppressed mice transplanted with human pancreatic cancer cells depleted for TRAIL-R2 develop fewer or no liver metastasis, whilst primary tumour growth is not influenced, suggesting that a pro-metastatic process is prevented by disabling the endogenous TRAIL/TRAIL-R2 system (von Karstedt *et al*, *submitted*).

4.3.1 Endogenous TRAIL-R2 drives cell autonomous migration and invasion in *KRAS*-mutated tumour cell lines

It has been previously published that treatment with TRAIL can induce migration in *KRAS*-mutated but not *KRAS*-wild type (WT) colorectal cancer cell lines [Hoogwater *et al*, 2010]. Therefore, we hypothesised that TRAIL/TRAIL-R2 control *KRAS*-mutated cells migration. To address this point, we performed migration assays in isogenic colon carcinoma cell lines with mutated or WT *KRAS* [Shirasawa *et al*, 1993], in the presence or absence of endogenous TRAIL-R2. As expected, *KRAS*-mutated cells showed increased migration capacity relative to their *KRAS*-WT counterparts (Figure 30A). Strikingly, KD of TRAIL-R2 abrogated the entire enhanced migratory capacity of mutated *KRAS* cells. To test whether TRAIL-R2 was responsible for the induction of migration in *KRAS*-mutated cells, we reconstituted A549 shTRAIL-R2 cells with TRAIL-R2 expression. Indeed, reconstitution of TRAIL-R2 expression led to rescued migration to normal levels (Figure 30B). Migration and invasion are two fundamental steps for cancer metastasis formation. Therefore, we next tested whether absence of endogenous TRAIL-R2 affects also invasion. Indeed, TRAIL-R2-KD blunted invasion to nearly the same low level exhibited by the non-invasive cell line NIH3T3 in DLD-1 (colon), Colo357 (pancreas) and A549 (lung) cells, representing the three most common cancer types with *KRAS* mutations (Figure 30C and Figure 30D, representative images of cells that have passed through a matrigel layer).

Thus, endogenous TRAIL-R2 drives cell-autonomous migration and invasion in *KRAS*-mutated cells irrespective of tissue of origin.

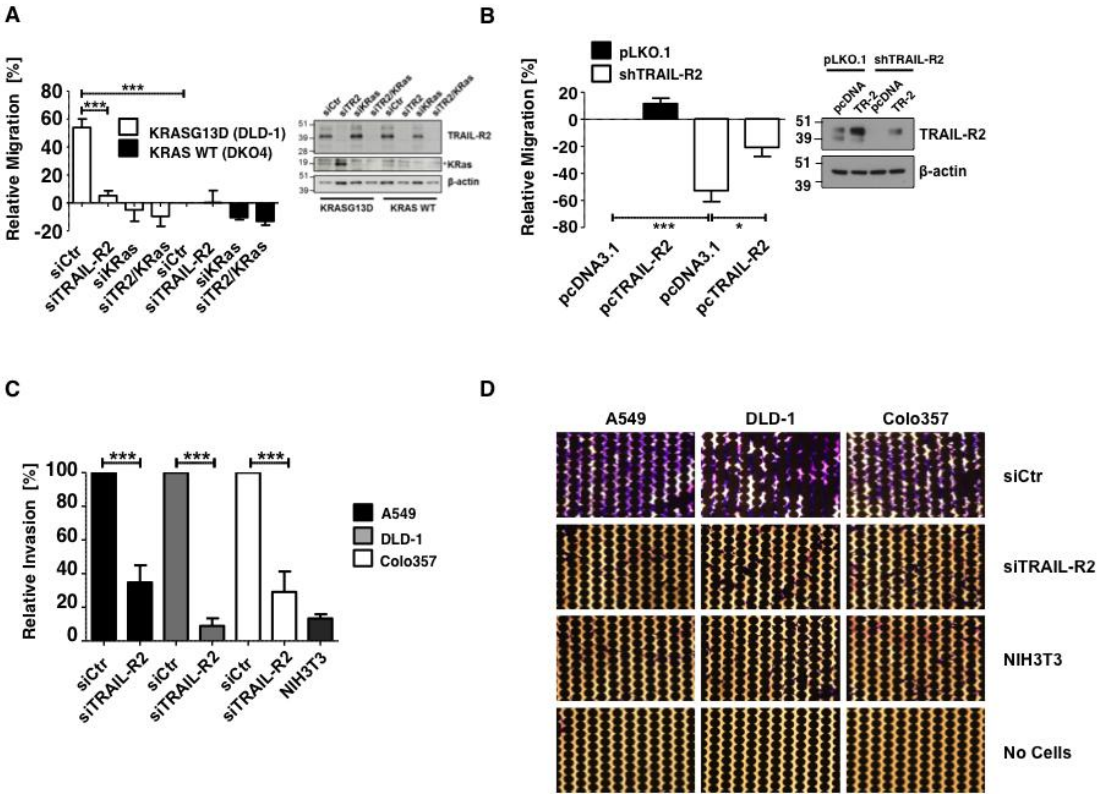

Figure 30 | TRAIL-R2 drives migration and invasion of *KRAS*-mutated cancer cells. (a, left panel) Isogenic *KRAS*-mutated (DLD-1) and *KRAS*-WT (DKO4) cells were transfected with the siRNA targeting KRAS and TRAIL-R2 for 48 h and subsequently subjected to migration assays. Migration was normalised to control transfected DKO4 cells. (a, right panel) Representative western blot is shown. (b, left panel) A549-luc pLKO.1 and shTRAIL-R2 were transiently transfected with either vector (pcDNA3.1) or with a TRAIL-R2 overexpression construct (pcTRAIL-R2) for 24 hours and subsequently subjected to migration assays. (b, right panel) Representative western blots are shown. (c) *KRAS*-mutated A549-luc, DLD-1 and Colo357 cells were transfected with the siRNA targeting TRAIL-R2 for 48 hours and subjected to invasion assays. (d) Matrigel layers were removed and cells that had passed through and adhered to the electrodes were stained by crystal violet. Representative images are shown.

All figures represent means of three independent experiments +/- SEM, individual dots represent means of three experiments of one cell line. * $p < 0.05$ and *** $p < 0.0001$ (Student's t-test (a and b) or ANOVA (c)).

4.3.2 TRAIL and TRAIL-R2 form an endogenous non-apoptotic complex

Since TRAIL/TRAIL-R2 was responsible for enhanced migration of *KRAS*-mutated cells, we investigated whether this effect is caused by the formation of an endogenous TRAIL/TRAIL-R2 complex. Interestingly, when subjecting lysates of *KRAS*-mutated cells at basal condition to Size Exclusion Chromatography (SEC) we found that in all cell lines tested a subfraction of endogenous TRAIL-R2 could be detected in high molecular weight fractions along with endogenous TRAIL (Figure 31A). Moreover, siRNA-mediated KD of TRAIL led to a shift of TRAIL-R2 from high molecular weight fractions to the size range of trimerised TRAIL-R2 (Figure 31B).

Thus, we could conclude that endogenous cancer-cell-expressed TRAIL and TRAIL-R2 can bind to each other and the resulting native complex may be responsible for the enhanced migration in *KRAS*-mutated cell lines.

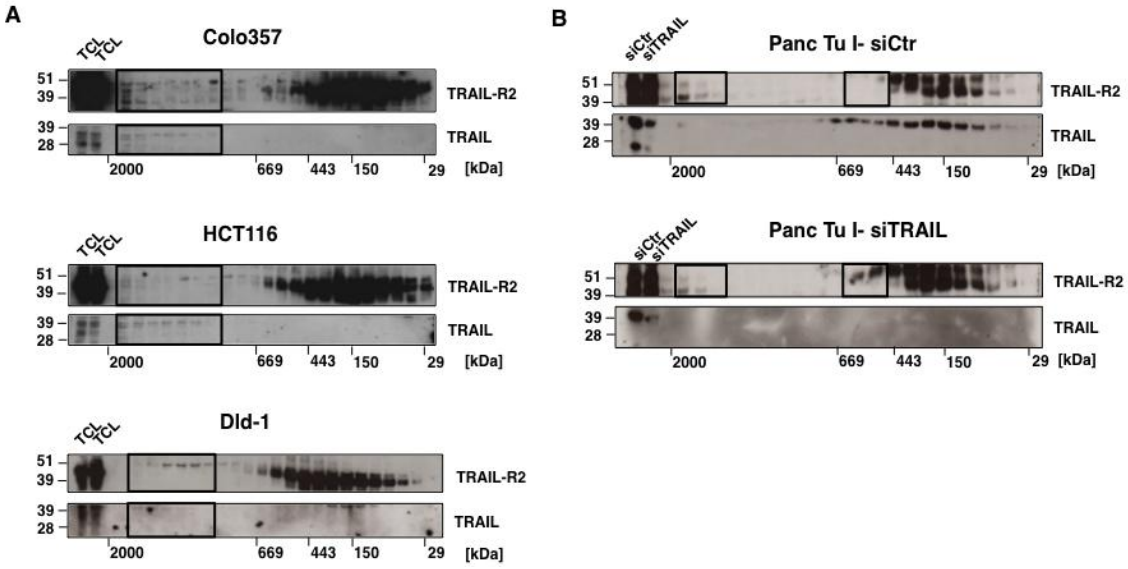

Figure 31 | Endogenous TRAIL and TRAIL-R2 constitute a native complex. (a) Native lysates of the indicated cell lines were fractionated by SEC. Fractions 9-32 were then subjected to western blotting. (b) Panc Tu I cells were transfected with siRNAs for 48 hours as indicated and subjected to lysis, SEC fractionation and western blotting as above. Representative western blots from two independent experiments are shown.

4.3.3 Endogenous TRAIL/TRAIL-R2 complex drives Rac-1/PI3K-mediated migration

The study of the mechanisms controlled by TRAIL/TRAIL-R2 revealed that constitutive activation of Rac-1 was reduced by TRAIL-R2-KD. Moreover, silencing of Rac-1 reduced migration to a similar extent as TRAIL-R2-KD, yet no additional reduction was achieved by co-suppression of TRAIL-R2 and Rac-1, implying that endogenous TRAIL/TRAIL-R2 and Rac-1 acted in the same pathway. Based on these results, it was concluded that *KRAS*-mutated cells employ constitutive endogenous TRAIL/TRAIL-R2 signaling to activate Rac-1 for migration (data not shown).

Rac-1 activation has been described to be mediated either in a PI3K-dependent [Nimnual *et al*, 1998] or -independent manner [Lambert *et al*, 2002]. Therefore, we first tested whether the cell lines used, with particular focus on A549, required constitutive PI3K activity for migration. To do so, we employed the pan-PI3K inhibitor GDC-0941. Interestingly, PI3K inhibition suppressed basal migration and, importantly, when we suppressed Phosphatase and tensin homolog (PTEN), which counteracts PI3K activity reducing the pool of PIP3 [Ali *et al*, 1999], cells increased migration in a PI3K activity-dependent manner (Figure 32A). Based on these results, we next hypothesised whether basal PI3K activity might be dependent on TRAIL-R2 and Rac-1. Firstly, we observed a marked reduction of constitutive phosphorylation of AKT when TRAIL-R2 expression was suppressed in A549 (Figure 32B), Panc Tu I and DLD-1 (data not shown) cells, thereby proving that PI3K activity is modulated by TRAIL-R2 at basal conditions. Secondly, Rac1-KD also suppressed basal AKT phosphorylation to a similar extent to TRAIL-R2-KD (Figure 32B). In line with these findings, PI3K-dependent migration induced by PTEN-KD was also entirely reversed by either TRAIL-R2- or Rac-1- KD in A549 (Figure 32C), Panc Tu I and DLD-1 cells (data not shown). So far, we demonstrated that the constitutive phosphorylation of AKT is affected by TRAIL-R2 and with less extend by Rac-1 in three *KRAS*-mutated cell lines representing non-small cell lung cancer (NSCLC), colorectal cancer (CRC) and pancreatic ductal adenocarcinoma (PDAC), thus showing that endogenous TRAIL-R2 and Rac-1 enables PI3K activation which is required for migration of *KRAS*-mutated cancer cells. However, since cancer cells are normally exposed to pro-survival signals in the microenvironment, we still needed to clarify whether AKT phosphorylation induced by exogenous stimuli could be

affected by the presence of TRAIL-R2 and Rac-1. Interestingly, we observed that A549, Panc Tu I and DLD-1, after one hour of stimulation with serum, showed increased levels of phosphorylated AKT that were then diminished by the absence of TRAIL-R2 (Figure 32D). Since Rac-1-KD was not efficient, we could not verify whether Rac-1 really modulated the phosphorylation of AKT upon external stimuli.

We therefore propose a model in which *KRAS*-mutated cancer cells, TRAIL-R2 and Rac-1 are upstream of PI3K activity in a cell-autonomous migration pathway triggered by endogenous TRAIL/TRAIL-R2.

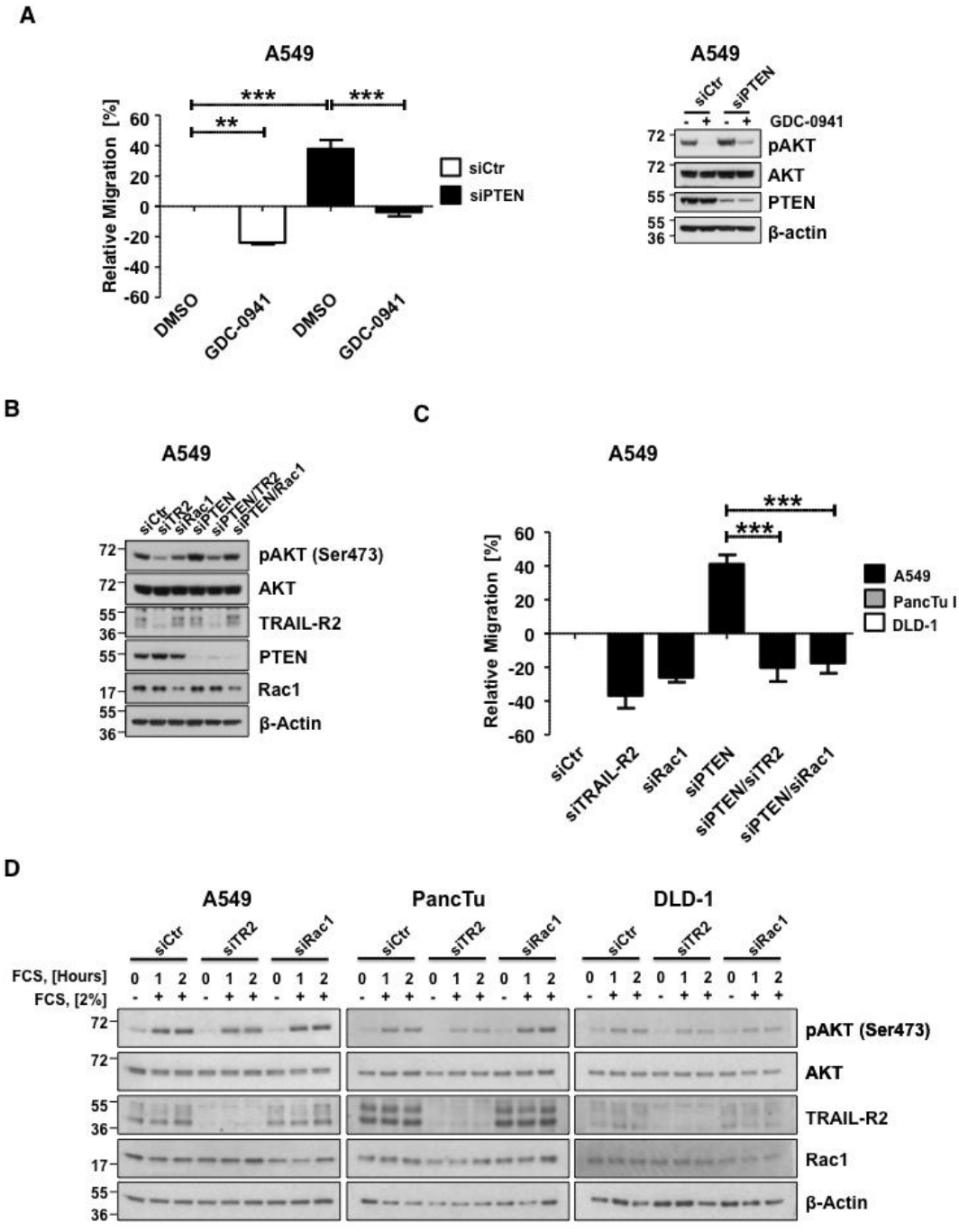

Figure 32 | Endogenous TRAIL-R2 promotes activation of a pro-migratory Rac1/PI3K signaling axis. (a, left panel) A549-luc cells were transfected with PTEN-targeting siRNAs and subsequently subjected to migration assays in the presence or absence of GDC-0941 [1 uM]. (a, right panel) A representative western blot is shown. (b) A549-luc and PancTu cells were transfected with the indicated siRNAs for 48 hours and subjected to western blot. (c) A549-luc cells were transfected as indicated in panel b and

subjected to migration assays. (d) A549, PancTu and DLD-1 were transfected with TRAIL-R2-targeting siRNA, subsequently stimulated with FCS [2%] for the indicated time points and subjected to western blot. One representative of three independent experiments is shown. (a, b, c) Values are means +/- SEM of three independent experiments. ** $p < 0.01$ and *** $p < 0.0001$ (ANOVA).

These results place both TRAIL-R2 and Rac-1 upstream of PI3K activity in the cell-autonomous migration pathway triggered by endogenous TRAIL/TRAIL-R2. Thus, we propose a model in which endogenous TRAIL/TRAIL-R2 promote a Rac1/PI3K signaling axis which drives migration, invasion and metastasis of *KRAS*-mutated cancers (Figure 33).

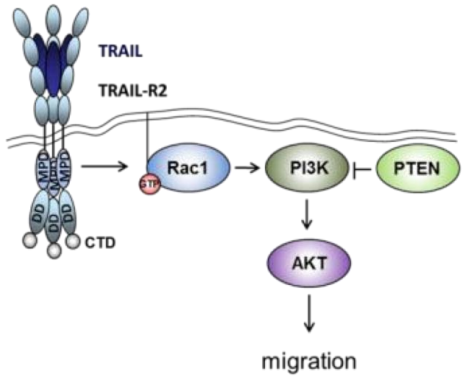

Figure 33 | Proposed model of invasion/migration/metastasis signalling mediated by endogenous TRAIL/TRAIL-R2.

Herein, we have demonstrated that in *KRAS*-mutated cancer cells TRAIL and TRAIL-R2 constitute an endogenous complex that can promote migration by activating the downstream non-apoptotic effectors Rac-1 and PI3K. Therefore, targeting TRAIL-R2 and/or non-apoptotic effectors might represent a strategy to convert the pro-migratory pathway into a pro-apoptotic outcome upon treatment with exogenous TRAIL.

5 Discussion

Task I - Smac-Mimetic in combination with Camptothecin selectively kill pre-malignant human epithelial cells mutated for KRAS.

Here we newly show that SM83 in combination with CPT induces apoptosis in human normal cells mutated for *KRAS*. Mechanistically, oncogenic *KRAS* leads to MAPK ERK2-mediated upregulation of Noxa, thus enhancing, together with SM83, CPT-induced apoptosis.

Since most cancer cells are resistant to SM as single agent, SM is commonly employed as a sensitiser for either death ligands [Li *et al*, 2004] or chemotherapeutics [Probst *et al*, 2010]. Hence, we aimed to find a drug that, in combination with SM, would strongly trigger cell death. Among potential chemotherapeutics identified from the screening at ICR, Camptothecin emerged as the top candidate. CPT is the inhibitor of the nuclear Topoisomerase I (TOP1) and exerts its activity causing DNA double strand breaks, thereby triggering p53-dependent apoptosis [Tomicic *et al*, 2010]. Two derivates are currently approved for clinical treatment: Topotecan, mainly employed for second line therapy of small cell lung cancer (SCLC) and ovarian cancer and Irinotecan for colorectal cancer [Venditto and Simanek, 2010]. Despite the high initial response rates, the majority of patients relapse early to these conventional chemotherapies [Hamilton *et al*, 2014]. Of note, the fact that SM has been reported to synergise with DNA damage inducers such as Cisplatin, 5-Fluorouracil, Etoposide and analogs of camptothecin [Foster *et al*, 2009, Greer *et al*, 2011, Servida *et al*, 2011] strongly supported the result from our screening.

Moreover, the killing potency of SM83 and CPT was even increased in the context of KRas knocked-in mutations in normal human cell lines. Indeed, when inducing KRasG13D expression in cells, which normally owed the WT-KRas, the KRas lesion triggered a robust apoptosis event upon combined SM83 and CPT treatment. Mechanistically, we identify that SM83/CPT-mediated cell death of pre-malignant *KRAS*-mutated cells is executed by activation of a MAPK signaling axis; in particular ERK2 upregulates Noxa and renders the cells more prone to apoptosis. Importantly and in line with our hypothesis, it has been published that mutations of the other Ras family

member *HRAS* plays a role in inducing autophagic cell death via Noxa upregulation [Elgendy *et al*, 2011]. Furthermore, it has been shown that transient overexpression of mutated *KRAS* positively regulates Noxa via ERK1/2 signalling, thereby sensitising to platinum-based chemotherapy [Sheridan *et al*, 2010]. Importantly, we show that treatment with MEKK inhibitors prevents SM83/CPT-induced apoptosis, in contrast with the conventional therapeutic approaches based on the employment of MEKK inhibitors as anti-cancer drugs [Hata *et al*, 2014]. Intriguingly, as shown in Figure 14, whereas depletion of ERK2 downregulates Noxa, depletion of ERK1 does not affect Noxa in *KRAS*-mutated HME cells, suggesting that ERK1 and ERK2 play dual roles in regulating Noxa levels, with ERK2 ultimately favouring KRasD13-induce apoptosis upon SM83/CPT co-treatment. Our findings suggest that the MAPK ERK2-mediated upregulation of Noxa renders the cells more prone to pro-apoptotic stimuli. Therefore, ERK2 inhibition would protect HME KRasG13D cells from combined SM83/CPT treatment. This opens a scenario in which ERK1 and ERK2 play different and even opposite functions, in line with what previously observed by others, describing a a mutual regulation between the two molecules downstream KRas signalling [Guegan *et al*, 2013]. Nevertheless, whether ERK2 displays a pro-apoptotic function in KRas signaling pathway is still to be proven.

Studying the molecular mechanisms responsible for SM83/CPT-induced cell death, we investigated the role played by each component of this triad SM-CPT-KRasG13D. However, whereas CPT intervention is exerted by inducing intrinsic apoptosis and mutated *KRAS* by upregulating Noxa, in our hands SM83 manly consists in inhibiting XIAP in order to release caspases. Of note, SM-depletion of cIAP1 and cIAP2 leads to the transcription of TNF, which can then kill cells in an autocrine manner [Petersen *et al*, 2007]. With our work, we demonstrated that TNF blocking by either Infliximab or Enbrel, *KRAS*-mutated cells survive to SM83/CPT combination. This suggests that cells engage other parallel responses to our treatment besides KRas-induced upregulation of Noxa. Whether cell death is caused by (i) high basal levels of TNF or (ii) hyperproduction of TNF or (iii) by high surface levels of TNF-Rs is still not clarified. Moreover, we still have not investigated whether *KRAS*-mutated cells (and not the WT cells) express basal high level of TNF or TNF-Rs that confer more susceptibility to the combinatorial treatment. The comprehension of these points would completely explain the molecular mechanisms responsible for synthetic lethal interaction between combined SM83/CPT and oncogenic *KRAS*.

Of note, synthetic lethality can selectively kill cancer cells while sparing normal cells. A therapeutic treatment based on synthetic lethality would thus be in theory extremely not toxic. As mutational activation of KRAS occurs in approximately 30% of human cancers in general [Bos, 1989, Malumbres and Barbacid, 2003] and 50% of colorectal adenocarcinoma [Grady and Markowitz, 2002], targeting KRas activation with the proposed combined SM83 and CPT treatment would be a potential new approach for these recalcitrant tumours. Therefore, we tested this combination using a panel of isogenic colorectal cancer cell lines bearing oncogenic and wild type KRas. First, since cancer cells engage several pro-survival pathways to escape apoptosis, it is surprising that they are as sensitive as *KRAS*-mutated HME cells to SM83 and CPT. In fact, cell death detected through cell viability assays was about 30% less than the premalignant cells. Furthermore, there were no differences in terms of cell death between KRas G13D- and WT- cancer cells, meaning that the observed sensitivity was independent of the *KRAS* mutational status. When we checked for Noxa levels in WT and mutated KRas colorectal cancer cells, they were comparable between mutated and WT isogenic pairs. Therefore, we can speculate several hypotheses: (i) *KRAS*-mediated upregulation of Noxa is antagonised by simultaneous upregulation of anti-apoptotic factors such as members of the Bcl-2 family or (ii) MAPKs, responsible for upmodulation of NOXA, are blocked by PI3K/AKT axis known to be markedly activated in cancer cells. Another possible explanation relies on (iii) the final equilibrium between death and survival, meaning that, in both *KRAS*-mutated and WT cancer cells, aberrant pro-survival signals deriving from mutation in PI3K or EGFR counterbalance the pro-apoptotic stimuli promoted by mutated *KRAS*. This would mean that activating mutations of oncogenes like *KRAS* are accompanied by the development of other mutations in transformed cells and for example HCT116 and DLD-1 cells bearing PI3KCA mutations seem to support this idea. Accordingly, we can consider that the introduction of mutations in immortalized human cells of epithelial origin (HME, MCF10A) is not sufficient to confer transforming properties and these cells are therefore sensitised to treatment, having no “protecting” mutations in other pathways.

Taken together our results show pre-clinical evidence of synthetic lethal interaction among SM83, CPT and constitutive hyperactivation of *KRAS* in pre-malignant epithelial cells. This interaction relies on the effects at different levels: mutated *KRAS* upregulates Noxa via MAPK ERK2; SM83 prevents caspases blockage by inhibiting XIAP and, depleting cIAPs, enhances TNF-mediated cell death. Thus, specific *KRAS* mutations

and SM83 greatly offer a death-prone scenario in which pre-malignant cells efficiently die via CPT-mediated triggering of the mitochondrial apoptotic pathway. Although in the colorectal cancer setting the combination of SM83 and CPT is not highly efficient, we may employ this co-treatment as a 'scaffold' combination, which can be sensitised by a further agent. Alternatively, SM83/CPT can represent itself a sensitising combination to treat *KRAS*-mutated cells resistant to conventional therapies such as MEKK/PI3K/mTORC inhibitors.

Task II – CDK9 inhibition overcomes TRAIL-resistance in KRAS-mutated NSCLC.

Preliminary data show that the p110α-inhibitor PIK-75 potently sensitises to TRAIL-induced apoptosis. Surprisingly PI3K inhibition is not responsible for this effect. A kinome-wide screen reveals that PIK-75 exerts off-target effects on a panel of 27 kinases in addition to p110α. Further investigations show that the main target inhibited by PIK-75 and responsible for TRAIL sensitisation is CDK9. Intriguingly, analysis of the molecular mechanisms at the basis of this potent synergism showed that CDK9 blocks the DISC and the mitochondria acting on cFLIP and Mcl-1. In fact, SNS-032-mediated CDK9 inhibition leads to concomitant downregulation of cFLIP and Mcl-1, thereby facilitating DISC- and mitochondria-mediated apoptosis [Lemke *et al*, 2014a].
Here, we demonstrate that selective inhibition of CDK9 via SNS-032, an inhibitor targeting CDK9 preferentially among other cell cycle CDKs [Conroy *et al*, 2009], synergises with TRAIL not only in A549, the human NSCLC cell line selected to perform the experiment, but also in an panel of human NSCLC cell lines. Therefore, the strong killing effect of this combination can be extended to a broad range of *KRAS*-mutated NSCLC cell lines. Importantly, our results show that CDK9 inhibition in combination with TRAIL cannot kill primary human hepatocytes (PHH) [Lemke *et al*, 2014a]. Notably, the concentration of SNS-032 sufficient for effective sensitisation of cancer cells to TRAIL-induced apoptosis is easily reached and sustained in the plasma of patients [Tong *et al*, 2010]. Moreover, we provide *in vivo* evidence of the potency of this novel treatment strategy. In fact, a four-day treatment with SNS-032 and TRAIL combination totally eradicates established lung tumours. However, the xenograft model used lacks a complete murine tumour microenvironment as SCID beige mice, for instance, lack activated T and mature Natural Killer (NK) cells, two major cell types described to

express TRAIL [Mirandola *et al*, 2004, Takeda *et al*, 2005]. In order to address whether exogenous TRAIL and paracrine microenvironment-associated factors are required to eradicate the tumour, we employed an autochthonous mouse model of NSCLC, named the KP conditional mouse model [DuPage *et al*, 2009, Hingorani *et al*, 2005]. Since SNS-032 is not able to inhibit murine CDK9 and, as a consequence, it does not synergise with TRAIL to trigger apoptosis in murine NSCLC cell lines, we chose another potent CDK9 inhibitor, Dinaciclib, already employed in clinical trials [Nemunaitis *et al*, 2013, Stephenson *et al*, 2014]. We demonstrated that it is active by inhibiting not only human but also murine CDK9. However, the IC50 of Dinaciclib towards CDK9 is similar to other CDKs [Parry *et al*, 2010, Paruch *et al*, 2010], a fact that has to be considered for the *in vivo* experiment. The effects of Dinaciclib in mice might be caused by the inhibition of other CDKs. Yet, to prove that Dinaciclib effect is caused selectively by CDK9 inhibition, we proposed another approach, i.e. the injection of BALB/c mice with murine NSCLC cell line inducible knocked-down for murine CDK9. The depletion of CDK9 will then be induced once the tumour is established simultaneously to TRAIL treatment. Moreover, the fact that Dinaciclib targets also other CDKs might in part explain the reason why we found that even at very low concentrations it synergises with TRAIL in killing a panel of human NSCLC cell lines. On the contratry, SNS-032 needs 6-fold more concentration to provoke the same killing effect. However, when we tested Dinaciclib and TRAIL co-treatment in two further murine NSCLC cell lines derived from the KP mice, they were only partially sensitive, thus suggesting that the combination in not potent enough to induce apoptosis. Therefore, we tried to add to the combination our developed SM83 [Lecis *et al*, 2012, Manzoni *et al*, 2012], which is known to synergise with TRAIL (data not shown), without success. We speculate that these cells can either engage anti-apoptotic factors or be intrinsically resistant due to the presence of additional oncogenic mutations helping to escape cell death. Hence, it would be reasonable to include other types of TRAIL sensitisers such as ABT-263 [Tse *et al*, 2008], ABT-199 [Touzeau *et al*, 2014] belonging to BH3-mimetic, Bortezomib [Lecis *et al*, 2010], chemotherapeutic agents like Cisplatin [Xu *et al*, 2011, Yin *et al*, 2011] in order to overcome this resistance also *in vivo*. In this study, we also prove that CDK9 is overexpressed in NSCLC. In particular, both lung tumours from 16-week old mice and human lung tumours biopsies show high expression of CDK9 as compared to the normal lung tissue surrounding the tumour nodules. In human samples, the positivity for CDK9 is specific for lung tumour areas as the co-staining for TTF-1, which selectively marks lung adenocarcinoma

demonstrates. Hence, detection of CDK9 overexpression makes this protein a candidate marker for NSCLC, which might then be responsive to our proposed combinatorial therapy.

In conclusion, we herein propose a newly targeted therapeutic strategy that may overcome TRAIL resistance in a cancer-selective manner. However, further preclinical and ultimately clinical studies using TRAIL and CDK9 inhibitor could be considered for the treatment of NSCLC.

Task III – The Endogenous TRAIL/TRAIL-R2 complex promotes metastasis progression in KRAS-mutated cancers via Rac-1/PI3K signaling axis.

In this task, we show that endogenous TRAIL and TRAIL-R2-mediated signaling is required to promote migration, invasion and metastasis via activation of the Rac-1/PI3K signaling axis in *KRAS*-mutated cancer. This oncogenic mutation represents a key feature of pancreatic, colorectal and lung cancers [Bos, 1989], tumours mostly highly aggressive. Furthermore, we provide genetic *in vivo* evidence that mouse TRAIL-R (mTRAIL-R) is a key driver of cancer progression and metastasis in an autochtonous mouse model of lung cancer and two autochtonous mouse models of pancreatic cancer (data not shown). Moreover, high TRAIL-R2 expression correlates with shortened metastasis-free survival in *KRAS*-mutated colorectal cancer patients, thus supporting the idea that TRAIL-R2, endogenously expressed by *KRAS*-mutated cancer cells is responsible for metastatisation (Von Karstedt *et al., submitted*). Since metastasis is the main reason for cancer related deaths [Hanahan and Weinberg, 2011], from a therapeutic point of view, our finding indicates both TRAIL and TRAIL-R2 as potential targets in clinic. At the same time, treatment with recombinant TRAIL has been commonly shown to selectively kill tumour cells *in vivo* without causing toxicity [Walczak *et al*, 1999], thus beginning the development of TRAIL and other TRAIL-R agonists for clinical application as novel cancer therapeutics [Lemke *et al*, 2014b]. Therefore, our study, which suggests a tumour-promoting role of endogenous TRAIL/TRAIL-R2 seems to be in contrast with the standard concept which supports an anti-tumour activity of TRAIL and TRAIL-R agonists. Nonetheless, if the tumour is sensitive to TRAIL-induced cell death, a therapy based on TRAIL or TRAIL-R agonists would be reasonable in order to eradicate the tumour. Otherwise, when cancer cells physiologically employ

TRAIL/TRAIL-R2 to invade, migrate and form metastasis as demonstrated by our experiments, endogenous TRAIL/TRAIL-R2 system and even paracrine TRAIL stimuli by the tumour microenvironment should be antagonized by a designed therapeutic strategy. Mechanistically, we identify that TRAIL-R2-mediated cell-autochtonous migration of *KRAS*-mutated cancer cells is independent of the canonical cell death-inducing machinery. The non-apoptotic role of TRAIL/TRAIL-R has already been described [Azijli *et al*, 2012]. However, we enlighten a correlation between PI3K and Rac-1 effectors downstream TRAIL-R2 which create a circuit governing migration and invasion of cancer cells. Hence, it would be object of interest to delineate the precise molecular mechanisms that directly or indirectly connect these effectors in order to orchestrate the events that determine the aggressiveness of *KRAS*-mutated tumours. Interestingly and in line with the model we propose, a recent publication has demonstrated the selective requirement of KRAS/PI3K activation in pancreatic cancer [Eser *et al*, 2013] and tumours from KP mice were shown to harbor elevated Rac-1 activity [Johnsson *et al*, 2014] highlighting once more the importance of targeting this pathway. Although further investigations are needed to explore this pathway more in depth, we give new insights in the non-canonical TRAIL/TRAIL-R system as promoter of cancer progression, invasion and metastasis in *KRAS*-mutated cancers. Therefore, we provide potential cancer-therapy targets that might be clinically considered in the treatment of these recalcitrant tumours.

In conclusion, the whole thesis is focused on colorectal, lung and pancreatic cancers, which are all characterised by the presence of the oncogenic *KRAS* lesion. Task I and Task II propose two different approaches to kill *KRAS*-mutated colorectal and lung cancer cell lines respectively. These targeted therapeutic strategies rely on apoptosis induction triggered by either a genotoxic stress (CPT) or a death ligand (TRAIL). Whereas the first task is mainly a mechanistic study, which tries to explain the synthetic lethal interaction between SM, CPT and mutated *KRAS* in a context of pre-malignancy, the second task provides a combination based on inhibiting CDK9 to enhance TRAIL-induced apoptosis in an already transformed cell (NSCLC). Although several combinatorial approaches have been entered clinical trials so far, patients relapse early as *KRAS*-mutated cancers are known for their high capacity to metastatise. Task III indeed explain why, mechanistically, *KRAS*-mutated cancers are aggressive: they

physiologically employ endogenous TRAIL/TRAIL-R2 system together with downstream effectors PI3K and Rac-1 to migrate, invade and, as a final result, metastatise.

Therefore, this thesis propose two complementary frontlines to completely eradicate *KRAS*-mutated cancers: on one side, the aim is killing tumour cells by the employment of targeted drug combinations, on the other side, the purpose is to block the endogenous migratory/invasion capacity of the cancer cell, thereby preventing metastatisation, which still remains the main cause of cancer-related death.

6 Appendix

6.1 Abbreviations

A	Alanine
Ad-Cre	Adenovirus engeneered to express Cre
ATP	Adenosin-triphosphate
Bak	Bcl-2 homologous antagonist/killer
Bax	Bcl-2–associated X protein
Bcl 2	B-cell lymphoma 2
Bcl-xL	B-cell lymphoma-extra large
Bid	BH3 interacting-domain death agonist
Bim	Bcl-2-like protein 11
CARD	Caspase recruitment domain
CCA	Cholangiocarcinoma
CDK	Cyclin-dependent kinase
cFLIP	Cellular FLICE-Inhibitory Protein
cIAP	Cellular inhibitor of apoptosis protein
CPT	Camptothecin
CRC	Colorectal cancer
CUL-3	Cullin-3
CYLD	Cylindromatosis
Da	Dalton
DD	Death Domain
DISC	Death inducing signaling complex
DMEM	Dulbecco’s modified Eagle’s medium
DUB	Deubiquitinase

EGF	Epithelial Growth Factor
EGFR	Epithelial Growth Factor receptor
ER	Endoplasmic reticulum
ERK	Extracellular signal related kinase
FACS	Fluorescence-Associated Cell Sorting
FADD	Fas associated death domain
FBS	Fetal Bovine Serum
FCS	Fetal calf serum
GAP	GTPase-Activating Protein
GATA2	GATA binding protein 2
GEF	GTP-Exchanging Protein
Grb2	Growth-factor-receptor-bound protein 2
GTP	Guanosine-triphosphate
H	Histidine
HBS	Hepes buffered saline
HME	Human mammary epithelial cell line
HOIL-1	Haeme-oxidized IRP2 ubiquitin ligase 1
HOIP	HOIL-1-interacting protein
HRP	Horseradish-peroxidase
hTERT	Human telomerase reverse transcriptase
HVR	Hyper variable region
I	Isoleucine
IAP	Inhibitor of apoptosis protein
IF	Immunofluorescence
IFN	Interferon
IKK	Inhibitor of kappaB kinase
IKK	IκB Inhibitor of kappaB
IL	Interleukin
IN	Intranasal instillation

IT	Intratracheal inalation
KP	*K-Ras*$^{LSL-G12D/+}$ and *p53*$^{LSL-R172H/+}$ mouse model
KRas	Kirsten rat sarcoma viral oncogene homologue
L	Lysine
LPS	Lipopolysaccharide
LT	Lymphotoxin
LUBAC	Linear ubiquitin chain assembly complex
MAPK	Mitogen-activated protein kinase
Mcl-1	Myeloid leukemia cell differentiation protein
mTOR	mammalian target of rapamycin
mTRAIL-R	murine TRAIL-R
NEAA	Non-essential amino acid
NEMO	NF-κB essential modulator
NF-kB	Nuclear factor kappaB
NK	Natural Killer
Noxa	‘damage’ in latin
NSCLC	non-small cell lung cancer
OPG	Osteoprotegerin
OTULIN	OTU deubiquitinase with linear linkage specificity
P	Proline
P-TEFb	Positive transcriptional elongation factor b
PAGE	Polyacrylamid gel electrophoresis
PARP	Poly ADP ribose polymerase
PBS	Phosphate buffered saline
PDAC	Pancreatic Ductal Adenocarcinoma
PI3K	Phosphoinositide 3-kinase
PUMA	p53 upregulated modulator of apoptosis
RANK	Receptor activator of NF-κB
RANKL	Receptor activator of NF-κB Ligand

RIP	Receptor interacting protein
RIP 3	Receptor interacting protein 3
RIPK1	Receptor interacting protein kinase 1
RNA-Pol II	RNA-Polymerase II
RNAi	RNA interference
ROCK	Rho-associated protein kinase
RTK	Receptor tyrosine kinases
S	Serine
SEM	Standard Error Mean
SHARPIN	SHANK-associated RH-domain-interacting protein
siRNA	Small interfering RNA
SM	SMAC-mimetic
Smac/DIABLO	Second mitochondria-derived activator of caspase/ Direct IAP-binding protein with low isoelectric point
Sos	Son of Sevenless
Src	Schmidt-Ruppin A-2 viral oncogene homolog
TAB	TAK1 binding protein
TAK	TGF-β-activated kinase 1
tBid	truncated Bid
Thr	Threonine
TLR	Toll-like receptor
TNF	Tumor Necrosis Factor
TNF-SF	Tumour necrosis factor-superfamily
TNF-SF-R	Tumour necrosis factor receptor-superfamily receptor
TR	Tyroid hormaone receptor
TRADD	TNF-R1-associated death domain
TRAF	TNF-receptor associated factor
TRAIL	Tumor necrosis factor-related apoptosis-inducing ligand
Tyr	Tyrosine
V	Valine

Wnt	Wingless proto-oncogene
WT	wild-type
XIAP	X-linked inhibitor of apoptosis protein

6.2 Figures

7 Bibliography

Aggarwal BB (2003). Signalling pathways of the TNF superfamily: a double-edged sword. *Nat Rev Immunol* **3**: 745-756, doi:10.1038/nri1184 [doi]

Ali IU, Schriml LM, Dean M (1999). Mutational spectra of PTEN/MMAC1 gene: a tumor suppressor with lipid phosphatase activity. *J Natl Cancer Inst* **91**: 1922-1932

Ashkenazi A, Pai RC, Fong S, Leung S, Lawrence DA, Marsters SA, Blackie C, Chang L, McMurtrey AE, Hebert A, DeForge L, Koumenis IL, Lewis D, Harris L, Bussiere J, Koeppen H, Shahrokh Z, Schwall RH (1999). Safety and antitumor activity of recombinant soluble Apo2 ligand. *J Clin Invest* **104**: 155-162, doi:10.1172/JCI6926 [doi]

Azijli K, Yuvaraj S, Peppelenbosch MP, Wurdinger T, Dekker H, Joore J, van Dijk E, Quax WJ, Peters GJ, de Jong S, Kruyt FA (2012). Kinome profiling of non-canonical TRAIL signaling reveals RIP1-Src-STAT3-dependent invasion in resistant non-small cell lung cancer cells. *J Cell Sci* **125**: 4651-4661, doi:10.1242/jcs.109587 [doi]

Bai L, McEachern D, Yang CY, Lu J, Sun H, Wang S (2012). LRIG1 modulates cancer cell sensitivity to Smac mimetics by regulating TNFalpha expression and receptor tyrosine kinase signaling. *Cancer Res* **72**: 1229-1238, doi:10.1158/0008-5472.CAN-11-2428 [doi]

Barnhart BC, Alappat EC, Peter ME (2003). The CD95 type I/type II model. *Semin Immunol* **15**: 185-193

Belyanskaya LL, Ziogas A, Hopkins-Donaldson S, Kurtz S, Simon HU, Stahel R, Zangemeister-Wittke U (2008). TRAIL-induced survival and proliferation of SCLC cells is mediated by ERK and dependent on TRAIL-R2/DR5 expression in the absence of caspase-8. *Lung Cancer* **60**: 355-365, doi:S0169-5002(07)00671-X [pii]

Belz K, Schoeneberger H, Wehner S, Weigert A, Bonig H, Klingebiel T, Fichtner I, Fulda S (2014). Smac mimetic and glucocorticoids synergize to induce apoptosis in childhood ALL by promoting ripoptosome assembly. *Blood* **124**: 240-250, doi:10.1182/blood-2013-05-500918 [doi]

Bertrand MJ, Doiron K, Labbe K, Korneluk RG, Barker PA, Saleh M (2009). Cellular inhibitors of apoptosis cIAP1 and cIAP2 are required for innate immunity signaling by the pattern recognition receptors NOD1 and NOD2. *Immunity* **30**: 789-801, doi:10.1016/j.immuni.2009.04.011 [doi]

Bertsch U, Roder C, Kalthoff H, Trauzold A (2014). Compartmentalization of TNF-related apoptosis-inducing ligand (TRAIL) death receptor functions: emerging role of nuclear TRAIL-R2. *Cell Death Dis* **5**: e1390, doi:10.1038/cddis.2014.351 [doi]

Beug ST, Tang VA, LaCasse EC, Cheung HH, Beauregard CE, Brun J, Nuyens JP, Earl N, St-Jean M, Holbrook J, Dastidar H, Mahoney DJ, Ilkow C, Le Boeuf F, Bell JC, Korneluk RG (2014). Smac mimetics and innate immune stimuli synergize to promote tumor death. *Nat Biotechnol* **32**: 182-190, doi:10.1038/nbt.2806 [doi]

Boldin MP, Goncharov TM, Goltsev YV, Wallach D (1996). Involvement of MACH, a novel MORT1/FADD-interacting protease, in Fas/APO-1- and TNF receptor-induced cell death. *Cell* **85**: 803-815, doi:S0092-8674(00)81265-9 [pii]

Boldin MP, Varfolomeev EE, Pancer Z, Mett IL, Camonis JH, Wallach D (1995). A novel protein that interacts with the death domain of Fas/APO1 contains a sequence motif related to the death domain. *J Biol Chem* **270**: 7795-7798

Bos JL (1989). Ras Oncogenes in Human Cancer: a Review. *Cancer Res* **49**: 4682-4689

Cain RJ and Ridley AJ (2009). Phosphoinositide 3-kinases in cell migration. *Biol Cell* **101**: 13-29, doi:10.1042/BC20080079 [doi]

Carswell EA, Old LJ, Kassel RL, Green S, Fiore N, Williamson B (1975). An endotoxin-induced serum factor that causes necrosis of tumors. *Proc Natl Acad Sci U S A* **72**: 3666-3670

Castellano E and Santos E (2011). Functional specificity of ras isoforms: so similar but so different. *Genes Cancer* **2**: 216-231, doi:10.1177/1947601911408081 [doi]

Cellurale C, Sabio G, Kennedy NJ, Das M, Barlow M, Sandy P, Jacks T, Davis RJ (2011). Requirement of c-Jun NH(2)-terminal kinase for Ras-initiated tumor formation. *Mol Cell Biol* **31**: 1565-1576, doi:10.1128/MCB.01122-10 [doi]

Chai J, Shiozaki E, Srinivasula SM, Wu Q, Datta P, Alnemri ES, Shi Y (2001). Structural basis of caspase-7 inhibition by XIAP. *Cell* **104**: 769-780, doi:S0092-8674(01)00272-0 [pii]

Chaigne-Delalande B, Moreau JF, Legembre P (2008). Rewinding the DISC. *Arch Immunol Ther Exp (Warsz)* **56**: 9-14, doi:10.1007/s00005-008-0002-9 [doi]

Chi HC, Chen SL, Liao CJ, Liao CH, Tsai MM, Lin YH, Huang YH, Yeh CT, Wu SM, Tseng YH, Chen CY, Tsai CY, Chung IH, Chen WJ, Lin KH (2012). Thyroid hormone

receptors promote metastasis of human hepatoma cells via regulation of TRAIL. *Cell Death Differ* **19**: 1802-1814, doi:10.1038/cdd.2012.58 [doi]

Chinnaiyan AM, O'Rourke K, Tewari M, Dixit VM (1995). FADD, a novel death domain-containing protein, interacts with the death domain of Fas and initiates apoptosis. *Cell* **81**: 505-512, doi:0092-8674(95)90071-3 [pii]

Conroy A, Stockett DE, Walker D, Arkin MR, Hoch U, Fox JA, Hawtin RE (2009). SNS-032 is a potent and selective CDK 2, 7 and 9 inhibitor that drives target modulation in patient samples. *Cancer Chemother Pharmacol* **64**: 723-732, doi:10.1007/s00280-008-0921-5 [doi]

Corcoran RB, Cheng KA, Hata AN, Faber AC, Ebi H, Coffee EM, Greninger P, Brown RD, Godfrey JT, Cohoon TJ, Song Y, Lifshits E, Hung KE, Shioda T, Dias-Santagata D, Singh A, Settleman J, Benes CH, Mino-Kenudson M, Wong KK, Engelman JA (2013). Synthetic lethal interaction of combined BCL-XL and MEK inhibition promotes tumor regressions in KRAS mutant cancer models. *Cancer Cell* **23**: 121-128, doi:10.1016/j.ccr.2012.11.007 [doi]

Cossu F, Malvezzi F, Canevari G, Mastrangelo E, Lecis D, Delia D, Seneci P, Scolastico C, Bolognesi M, Milani M (2010). Recognition of Smac-mimetic compounds by the BIR domain of cIAP1. *Protein Sci* **19**: 2418-2429, doi:10.1002/pro.523 [doi]

Cossu F, Mastrangelo E, Milani M, Sorrentino G, Lecis D, Delia D, Manzoni L, Seneci P, Scolastico C, Bolognesi M (2009). Designing Smac-mimetics as antagonists of XIAP, cIAP1, and cIAP2. *Biochem Biophys Res Commun* **378**: 162-167, doi:10.1016/j.bbrc.2008.10.139 [doi]

Cossu F, Milani M, Vachette P, Malvezzi F, Grassi S, Lecis D, Delia D, Drago C, Seneci P, Bolognesi M, Mastrangelo E (2012). Structural insight into inhibitor of apoptosis proteins recognition by a potent divalent smac-mimetic. *PLoS One* **7**: e49527, doi:10.1371/journal.pone.0049527 [doi]

Damgaard RB and Gyrd-Hansen M (2011). Inhibitor of apoptosis (IAP) proteins in regulation of inflammation and innate immunity. *Discov Med* **11**: 221-231

Darding M, Feltham R, Tenev T, Bianchi K, Benetatos C, Silke J, Meier P (2011). Molecular determinants of Smac mimetic induced degradation of cIAP1 and cIAP2. *Cell Death Differ* **18**: 1376-1386, doi:10.1038/cdd.2011.10 [doi]

Darding M and Meier P (2012). IAPs: guardians of RIPK1. *Cell Death Differ* **19**: 58-66, doi:10.1038/cdd.2011.163 [doi]

de Bruijn MT, Raats DA, Hoogwater FJ, van Houdt WJ, Cameron K, Medema JP, Borel Rinkes IH, Kranenburg O (2010). Oncogenic KRAS sensitises colorectal tumour cells to chemotherapy by p53-dependent induction of Noxa. *Br J Cancer* **102**: 1254-1264, doi:10.1038/sj.bjc.6605633 [doi]

Degli-Esposti MA, Smolak PJ, Walczak H, Waugh J, Huang CP, DuBose RF, Goodwin RG, Smith CA (1997). Cloning and characterization of TRAIL-R3, a novel member of the emerging TRAIL receptor family. *J Exp Med* **186**: 1165-1170

Degterev A, Huang Z, Boyce M, Li Y, Jagtap P, Mizushima N, Cuny GD, Mitchison TJ, Moskowitz MA, Yuan J (2005). Chemical inhibitor of nonapoptotic cell death with therapeutic potential for ischemic brain injury. *Nat Chem Biol* **1**: 112-119, doi:nchembio711 [pii]

Di Nicolantonio F, Arena S, Gallicchio M, Zecchin D, Martini M, Flonta SE, Stella GM, Lamba S, Cancelliere C, Russo M, Geuna M, Appendino G, Fantozzi R, Medico E, Bardelli A (2008). Replacement of normal with mutant alleles in the genome of normal human cells unveils mutation-specific drug responses. *Proc Natl Acad Sci U S A* **105**: 20864-20869, doi:10.1073/pnas.0808757105 [doi]

Di Nicolantonio F, Arena S, Tabernero J, Grosso S, Molinari F, Macarulla T, Russo M, Cancelliere C, Zecchin D, Mazzucchelli L, Sasazuki T, Shirasawa S, Geuna M, Frattini M, Baselga J, Gallicchio M, Biffo S, Bardelli A (2010). Deregulation of the PI3K and KRAS signaling pathways in human cancer cells determines their response to everolimus. *J Clin Invest* **120**: 2858-2866, doi:10.1172/JCI37539 [doi]

Di Nicolantonio F, Martini M, Molinari F, Sartore-Bianchi A, Arena S, Saletti P, De Dosso S, Mazzucchelli L, Frattini M, Siena S, Bardelli A (2008). Wild-type BRAF is required for response to panitumumab or cetuximab in metastatic colorectal cancer. *J Clin Oncol* **26**: 5705-5712, doi:10.1200/JCO.2008.18.0786 [doi]

Dickens LS, Boyd RS, Jukes-Jones R, Hughes MA, Robinson GL, Fairall L, Schwabe JW, Cain K, Macfarlane M (2012). A death effector domain chain DISC model reveals a crucial role for caspase-8 chain assembly in mediating apoptotic cell death. *Mol Cell* **47**: 291-305, doi:10.1016/j.molcel.2012.05.004 [doi]

DOBZHANSKY T (1946). Genetics of natural populations; recombination and variability in populations of Drosophila pseudoobscura. *Genetics* **31**: 269-290

Dogan T, Harms GS, Hekman M, Karreman C, Oberoi TK, Alnemri ES, Rapp UR, Rajalingam K (2008). X-linked and cellular IAPs modulate the stability of C-RAF kinase and cell motility. *Nat Cell Biol* **10**: 1447-1455, doi:10.1038/ncb1804 [doi]

Downward J (2003). Targeting RAS signalling pathways in cancer therapy. *Nat Rev Cancer* **3**: 11-22, doi:10.1038/nrc969 [doi]

DuPage M, Dooley AL, Jacks T (2009). Conditional mouse lung cancer models using adenoviral or lentiviral delivery of Cre recombinase. *Nat Protoc* **4**: 1064-1072, doi:10.1038/nprot.2009.95 [doi]

Eckelman BP and Salvesen GS (2006). The human anti-apoptotic proteins cIAP1 and cIAP2 bind but do not inhibit caspases. *J Biol Chem* **281**: 3254-3260, doi:M510863200 [pii]

Egberts JH, Cloosters V, Noack A, Schniewind B, Thon L, Klose S, Kettler B, von Forstner C, Kneitz C, Tepel J, Adam D, Wajant H, Kalthoff H, Trauzold A (2008). Anti-tumor necrosis factor therapy inhibits pancreatic tumor growth and metastasis. *Cancer Res* **68**: 1443-1450, doi:10.1158/0008-5472.CAN-07-5704 [doi]

Ehrhardt H, Fulda S, Schmid I, Hiscott J, Debatin KM, Jeremias I (2003). TRAIL induced survival and proliferation in cancer cells resistant towards TRAIL-induced apoptosis mediated by NF-kappaB. *Oncogene* **22**: 3842-3852, doi:10.1038/sj.onc.1206520 [doi]

Elgendy M, Sheridan C, Brumatti G, Martin SJ (2011). Oncogenic Ras-induced expression of Noxa and Beclin-1 promotes autophagic cell death and limits clonogenic survival. *Mol Cell* **42**: 23-35, doi:10.1016/j.molcel.2011.02.009 [doi]

Elrod HA, Fan S, Muller S, Chen GZ, Pan L, Tighiouart M, Shin DM, Khuri FR, Sun SY (2010). Analysis of death receptor 5 and caspase-8 expression in primary and metastatic head and neck squamous cell carcinoma and their prognostic impact. *PLoS One* **5**: e12178, doi:10.1371/journal.pone.0012178 [doi]

Emmerich CH, Schmukle AC, Haas TL, Gerlach B, Cordier SM, Rieser E, Walczak H (2011a). The linear ubiquitin chain assembly complex forms part of the TNF-R1 signalling complex and is required for effective TNF-induced gene induction and prevents TNF-induced apoptosis. *Adv Exp Med Biol* **691**: 115-126, doi:10.1007/978-1-4419-6612-4_12 [doi]

Emmerich CH, Schmukle AC, Walczak H (2011b). The emerging role of linear ubiquitination in cell signaling. *Sci Signal* **4**: re5, doi:10.1126/scisignal.2002187 [doi]

Eser S, Reiff N, Messer M, Seidler B, Gottschalk K, Dobler M, Hieber M, Arbeiter A, Klein S, Kong B, Michalski CW, Schlitter AM, Esposito I, Kind AJ, Rad L, Schnieke AE, Baccarini M, Alessi DR, Rad R, Schmid RM, Schneider G, Saur D (2013). Selective requirement of PI3K/PDK1 signaling for Kras oncogene-driven pancreatic cell plasticity and cancer. *Cancer Cell* **23**: 406-420, doi:10.1016/j.ccr.2013.01.023 [doi]

Esteban LM, Vicario-Abejon C, Fernandez-Salguero P, Fernandez-Medarde A, Swaminathan N, Yienger K, Lopez E, Malumbres M, McKay R, Ward JM, Pellicer A, Santos E (2001). Targeted genomic disruption of H-ras and N-ras, individually or in combination, reveals the dispensability of both loci for mouse growth and development. *Mol Cell Biol* **21**: 1444-1452, doi:10.1128/MCB.21.5.1444-1452.2001 [doi]

Faber AC, Coffee EM, Costa C, Dastur A, Ebi H, Hata AN, Yeo AT, Edelman EJ, Song Y, Tam AT, Boisvert JL, Milano RJ, Roper J, Kodack DP, Jain RK, Corcoran RB, Rivera MN, Ramaswamy S, Hung KE, Benes CH, Engelman JA (2014). mTOR inhibition specifically sensitizes colorectal cancers with KRAS or BRAF mutations to BCL-2/BCL-XL inhibition by suppressing MCL-1. *Cancer Discov* **4**: 42-52, doi:10.1158/2159-8290.CD-13-0315 [doi]

Fakler M, Loeder S, Vogler M, Schneider K, Jeremias I, Debatin KM, Fulda S (2009). Small molecule XIAP inhibitors cooperate with TRAIL to induce apoptosis in childhood acute leukemia cells and overcome Bcl-2-mediated resistance. *Blood* **113**: 1710-1722, doi:10.1182/blood-2007-09-114314 [doi]

Falschlehner C, Emmerich CH, Gerlach B, Walczak H (2007). TRAIL signalling: decisions between life and death. *Int J Biochem Cell Biol* **39**: 1462-1475, doi:S1357-2725(07)00052-0 [pii]

Feltham R, Bettjeman B, Budhidarmo R, Mace PD, Shirley S, Condon SM, Chunduru SK, McKinlay MA, Vaux DL, Silke J, Day CL (2011). Smac mimetics activate the E3 ligase activity of cIAP1 protein by promoting RING domain dimerization. *J Biol Chem* **286**: 17015-17028, doi:10.1074/jbc.M111.222919 [doi]

Feoktistova M, Geserick P, Kellert B, Dimitrova DP, Langlais C, Hupe M, Cain K, MacFarlane M, Hacker G, Leverkus M (2011). cIAPs block Ripoptosome formation, a RIP1/caspase-8 containing intracellular cell death complex differentially regulated by cFLIP isoforms. *Mol Cell* **43**: 449-463, doi:10.1016/j.molcel.2011.06.011 [doi]

Fingas CD, Blechacz BR, Smoot RL, Guicciardi ME, Mott J, Bronk SF, Werneburg NW, Sirica AE, Gores GJ (2010). A smac mimetic reduces TNF related apoptosis inducing ligand (TRAIL)-induced invasion and metastasis of cholangiocarcinoma cells. *Hepatology* **52**: 550-561, doi:10.1002/hep.23729 [doi]

Foster FM, Owens TW, Tanianis-Hughes J, Clarke RB, Brennan K, Bundred NJ, Streuli CH (2009). Targeting inhibitor of apoptosis proteins in combination with ErbB antagonists in breast cancer. *Breast Cancer Res* **11**: R41, doi:10.1186/bcr2328 [doi]

Frese KK and Tuveson DA (2007). Maximizing mouse cancer models. *Nat Rev Cancer* **7**: 645-658, doi:nrc2192 [pii]

Fulda S (2014). Targeting inhibitor of apoptosis proteins for cancer therapy: a double-edge sword? *J Clin Oncol* **32**: 3190-3191, doi:10.1200/JCO.2014.56.8741 [doi]

Fulda S (2013). The dark side of TRAIL signaling. *Cell Death Differ* **20**: 845-846, doi:10.1038/cdd.2013.36 [doi]

Fulda S and Vucic D (2012). Targeting IAP proteins for therapeutic intervention in cancer. *Nat Rev Drug Discov* **11**: 109-124, doi:10.1038/nrd3627 [doi]

Fulda S, Wick W, Weller M, Debatin KM (2002). Smac agonists sensitize for Apo2L/TRAIL- or anticancer drug-induced apoptosis and induce regression of malignant glioma in vivo. *Nat Med* **8**: 808-815, doi:10.1038/nm735 [doi]

Gaither A, Porter D, Yao Y, Borawski J, Yang G, Donovan J, Sage D, Slisz J, Tran M, Straub C, Ramsey T, Iourgenko V, Huang A, Chen Y, Schlegel R, Labow M, Fawell S, Sellers WR, Zawel L (2007). A Smac mimetic rescue screen reveals roles for inhibitor of apoptosis proteins in tumor necrosis factor-alpha signaling. *Cancer Res* **67**: 11493-11498, doi:67/24/11493 [pii]

Galluzzi L, Kepp O, Kroemer G (2012). Mitochondria: master regulators of danger signalling. *Nat Rev Mol Cell Biol* **13**: 780-788, doi:10.1038/nrm3479 [doi]

Ganten TM, Sykora J, Koschny R, Batke E, Aulmann S, Mansmann U, Stremmel W, Sinn HP, Walczak H (2009). Prognostic significance of tumour necrosis factor-related apoptosis-inducing ligand (TRAIL) receptor expression in patients with breast cancer. *J Mol Med (Berl)* **87**: 995-1007, doi:10.1007/s00109-009-0510-z [doi]

Gatti L, Sevko A, De Cesare M, Arrighetti N, Manenti G, Ciusani E, Verderio P, Ciniselli CM, Cominetti D, Carenini N, Corna E, Zaffaroni N, Rodolfo M, Rivoltini L, Umansky V, Perego P (2014). Histone deacetylase inhibitor-temozolomide co-treatment inhibits melanoma growth through suppression of Chemokine (C-C motif) ligand 2-driven signals. *Oncotarget* **5**: 4516-4528, doi:2065 [pii]

Gerlach B, Cordier SM, Schmukle AC, Emmerich CH, Rieser E, Haas TL, Webb AI, Rickard JA, Anderton H, Wong WW, Nachbur U, Gangoda L, Warnken U, Purcell AW, Silke J, Walczak H (2011). Linear ubiquitination prevents inflammation and regulates immune signalling. *Nature* **471**: 591-596, doi:10.1038/nature09816 [doi]

Gojo I, Sadowska M, Walker A, Feldman EJ, Iyer SP, Baer MR, Sausville EA, Lapidus RG, Zhang D, Zhu Y, Jou YM, Poon J, Small K, Bannerji R (2013). Clinical and laboratory studies of the novel cyclin-dependent kinase inhibitor dinaciclib (SCH 727965) in acute leukemias. *Cancer Chemother Pharmacol* **72**: 897-908, doi:10.1007/s00280-013-2249-z [doi]

Grady WM and Markowitz SD (2002). Genetic and epigenetic alterations in colon cancer. *Annu Rev Genomics Hum Genet* **3**: 101-128, doi:10.1146/annurev.genom.3.022502.103043 [doi]

Green DR and Kroemer G (2004). The pathophysiology of mitochondrial cell death. *Science* **305**: 626-629, doi:10.1126/science.1099320 [doi]

Greer RM, Peyton M, Larsen JE, Girard L, Xie Y, Gazdar AF, Harran P, Wang L, Brekken RA, Wang X, Minna JD (2011). SMAC mimetic (JP1201) sensitizes non-small cell lung cancers to multiple chemotherapy agents in an IAP-dependent but TNF-alpha-

independent manner. *Cancer Res* **71**: 7640-7648, doi:10.1158/0008-5472.CAN-10-3947 [doi]

Grosse-Wilde A and Kemp CJ (2008). Metastasis suppressor function of tumor necrosis factor-related apoptosis-inducing ligand-R in mice: implications for TRAIL-based therapy in humans? *Cancer Res* **68**: 6035-6037, doi:10.1158/0008-5472.CAN-08-0078 [doi]

Grosse-Wilde A, Voloshanenko O, Bailey SL, Longton GM, Schaefer U, Csernok AI, Schutz G, Greiner EF, Kemp CJ, Walczak H (2008). TRAIL-R deficiency in mice enhances lymph node metastasis without affecting primary tumor development. *J Clin Invest* **118**: 100-110, doi:10.1172/JCI33061 [doi]

Guegan JP, Ezan F, Theret N, Langouet S, Baffet G (2013). MAPK signaling in cisplatin-induced death: predominant role of ERK1 over ERK2 in human hepatocellular carcinoma cells. *Carcinogenesis* **34**: 38-47, doi:10.1093/carcin/bgs317 [doi]

Guicciardi ME, Mott JL, Bronk SF, Kurita S, Fingas CD, Gores GJ (2011). Cellular inhibitor of apoptosis 1 (cIAP-1) degradation by caspase 8 during TNF-related apoptosis-inducing ligand (TRAIL)-induced apoptosis. *Exp Cell Res* **317**: 107-116, doi:10.1016/j.yexcr.2010.10.005 [doi]

Gyrd-Hansen M and Meier P (2010). IAPs: from caspase inhibitors to modulators of NF-kappaB, inflammation and cancer. *Nat Rev Cancer* **10**: 561-574, doi:10.1038/nrc2889 [doi]

Haas TL, Emmerich CH, Gerlach B, Schmukle AC, Cordier SM, Rieser E, Feltham R, Vince J, Warnken U, Wenger T, Koschny R, Komander D, Silke J, Walczak H (2009). Recruitment of the linear ubiquitin chain assembly complex stabilizes the TNF-R1

signaling complex and is required for TNF-mediated gene induction. *Mol Cell* **36**: 831-844, doi:10.1016/j.molcel.2009.10.013 [doi]

Hamilton G, Klameth L, Rath B, Thalhammer T (2014). Synergism of cyclin-dependent kinase inhibitors with camptothecin derivatives in small cell lung cancer cell lines. *Molecules* **19**: 2077-2088, doi:10.3390/molecules19022077 [doi]

Hanahan D and Weinberg RA (2011). Hallmarks of cancer: the next generation. *Cell* **144**: 646-674, doi:10.1016/j.cell.2011.02.013 [doi]

Hanahan D and Weinberg RA (2000). The hallmarks of cancer. *Cell* **100**: 57-70, doi:S0092-8674(00)81683-9 [pii]

Harper JW and Adams PD (2001). Cyclin-dependent kinases. *Chem Rev* **101**: 2511-2526, doi:cr0001030 [pii]

Hartman JL,4th, Garvik B, Hartwell L (2001). Principles for the buffering of genetic variation. *Science* **291**: 1001-1004

Haselmann V, Kurz A, Bertsch U, Hubner S, Olempska-Muller M, Fritsch J, Hasler R, Pickl A, Fritsche H, Annewanter F, Engler C, Fleig B, Bernt A, Roder C, Schmidt H, Gelhaus C, Hauser C, Egberts JH, Heneweer C, Rohde AM, Boger C, Knippschild U, Rocken C, Adam D, Walczak H, Schutze S, Janssen O, Wulczyn FG, Wajant H, Kalthoff H, Trauzold A (2014). Nuclear death receptor TRAIL-R2 inhibits maturation of let-7 and promotes proliferation of pancreatic and other tumor cells. *Gastroenterology* **146**: 278-290, doi:10.1053/j.gastro.2013.10.009 [doi]

Hata AN, Yeo A, Faber AC, Lifshits E, Chen Z, Cheng KA, Walton Z, Sarosiek KA, Letai A, Heist RS, Mino-Kenudson M, Wong KK, Engelman JA (2014). Failure to induce

apoptosis via BCL-2 family proteins underlies lack of efficacy of combined MEK and PI3K inhibitors for KRAS-mutant lung cancers. *Cancer Res* **74**: 3146-3156, doi:10.1158/0008-5472.CAN-13-3728 [doi]

Hayden MS and Ghosh S (2008). Shared principles in NF-kappaB signaling. *Cell* **132**: 344-362, doi:10.1016/j.cell.2008.01.020 [doi]

He S, Wang L, Miao L, Wang T, Du F, Zhao L, Wang X (2009). Receptor interacting protein kinase-3 determines cellular necrotic response to TNF-alpha. *Cell* **137**: 1100-1111, doi:10.1016/j.cell.2009.05.021 [doi]

Herbst RS, Heymach JV, Lippman SM (2008). Lung cancer. *N Engl J Med* **359**: 1367-1380, doi:10.1056/NEJMra0802714 [doi]

Hildebrand JM, Tanzer MC, Lucet IS, Young SN, Spall SK, Sharma P, Pierotti C, Garnier JM, Dobson RC, Webb AI, Tripaydonis A, Babon JJ, Mulcair MD, Scanlon MJ, Alexander WS, Wilks AF, Czabotar PE, Lessene G, Murphy JM, Silke J (2014). Activation of the pseudokinase MLKL unleashes the four-helix bundle domain to induce membrane localization and necroptotic cell death. *Proc Natl Acad Sci U S A*, doi:201408987 [pii]

Hingorani SR, Wang L, Multani AS, Combs C, Deramaudt TB, Hruban RH, Rustgi AK, Chang S, Tuveson DA (2005). Trp53R172H and KrasG12D cooperate to promote chromosomal instability and widely metastatic pancreatic ductal adenocarcinoma in mice. *Cancer Cell* **7**: 469-483, doi:S1535-6108(05)00128-5 [pii]

Holen I, Croucher PI, Hamdy FC, Eaton CL (2002). Osteoprotegerin (OPG) is a survival factor for human prostate cancer cells. *Cancer Res* **62**: 1619-1623

Hoogwater FJ, Nijkamp MW, Smakman N, Steller EJ, Emmink BL, Westendorp BF, Raats DA, Sprick MR, Schaefer U, Van Houdt WJ, De Bruijn MT, Schackmann RC, Derksen PW, Medema JP, Walczak H, Borel Rinkes IH, Kranenburg O (2010). Oncogenic K-Ras turns death receptors into metastasis-promoting receptors in human and mouse colorectal cancer cells. *Gastroenterology* **138**: 2357-2367, doi:10.1053/j.gastro.2010.02.046 [doi]

Huang S, Ren X, Wang L, Zhang L, Wu X (2011). Lung-cancer chemoprevention by induction of synthetic lethality in mutant KRAS premalignant cells in vitro and in vivo. *Cancer Prev Res (Phila)* **4**: 666-673, doi:10.1158/1940-6207.CAPR-10-0235 [doi]

Ikeda F, Deribe YL, Skanland SS, Stieglitz B, Grabbe C, Franz-Wachtel M, van Wijk SJ, Goswami P, Nagy V, Terzic J, Tokunaga F, Androulidaki A, Nakagawa T, Pasparakis M, Iwai K, Sundberg JP, Schaefer L, Rittinger K, Macek B, Dikic I (2011). SHARPIN forms a linear ubiquitin ligase complex regulating NF-kappaB activity and apoptosis. *Nature* **471**: 637-641, doi:10.1038/nature09814 [doi]

Infante JR, Dees EC, Olszanski AJ, Dhuria SV, Sen S, Cameron S, Cohen RB (2014). Phase I Dose-Escalation Study of LCL161, an Oral Inhibitor of Apoptosis Proteins Inhibitor, in Patients With Advanced Solid Tumors. *J Clin Oncol* **32**: 3103-3110, doi:10.1200/JCO.2013.52.3993 [doi]

Ishimura N, Isomoto H, Bronk SF, Gores GJ (2006). Trail induces cell migration and invasion in apoptosis-resistant cholangiocarcinoma cells. *Am J Physiol Gastrointest Liver Physiol* **290**: G129-36, doi:00242.2005 [pii]

Jaffee EM, Hruban RH, Canto M, Kern SE (2002). Focus on pancreas cancer. *Cancer Cell* **2**: 25-28, doi:S1535610802000934 [pii]

Jin Z, Li Y, Pitti R, Lawrence D, Pham VC, Lill JR, Ashkenazi A (2009). Cullin3-based polyubiquitination and p62-dependent aggregation of caspase-8 mediate extrinsic apoptosis signaling. *Cell* **137**: 721-735, doi:10.1016/j.cell.2009.03.015 [doi]

Johnson L, Greenbaum D, Cichowski K, Mercer K, Murphy E, Schmitt E, Bronson RT, Umanoff H, Edelmann W, Kucherlapati R, Jacks T (1997). K-ras is an essential gene in the mouse with partial functional overlap with N-ras. *Genes Dev* **11**: 2468-2481

Johnson L, Mercer K, Greenbaum D, Bronson RT, Crowley D, Tuveson DA, Jacks T (2001). Somatic activation of the K-ras oncogene causes early onset lung cancer in mice. *Nature* **410**: 1111-1116, doi:10.1038/35074129 [doi]

Johnsson AK, Dai Y, Nobis M, Baker MJ, McGhee EJ, Walker S, Schwarz JP, Kadir S, Morton JP, Myant KB, Huels DJ, Segonds-Pichon A, Sansom OJ, Anderson KI, Timpson P, Welch HC (2014). The Rac-FRET mouse reveals tight spatiotemporal control of Rac activity in primary cells and tissues. *Cell Rep* **6**: 1153-1164, doi:10.1016/j.celrep.2014.02.024 [doi]

Johnstone RW, Frew AJ, Smyth MJ (2008). The TRAIL apoptotic pathway in cancer onset, progression and therapy. *Nat Rev Cancer* **8**: 782-798, doi:10.1038/nrc2465 [doi]

Kantari C and Walczak H (2011). Caspase-8 and bid: caught in the act between death receptors and mitochondria. *Biochim Biophys Acta* **1813**: 558-563, doi:10.1016/j.bbamcr.2011.01.026 [doi]

Karnoub AE and Weinberg RA (2008). Ras oncogenes: split personalities. *Nat Rev Mol Cell Biol* **9**: 517-531, doi:10.1038/nrm2438 [doi]

Keusekotten K, Elliott PR, Glockner L, Fiil BK, Damgaard RB, Kulathu Y, Wauer T, Hospenthal MK, Gyrd-Hansen M, Krappmann D, Hofmann K, Komander D (2013). OTULIN antagonizes LUBAC signaling by specifically hydrolyzing Met1-linked polyubiquitin. *Cell* **153**: 1312-1326, doi:10.1016/j.cell.2013.05.014 [doi]

Kim J, Ahn S, Ko YG, Boo YC, Chi SG, Ni CW, Go YM, Jo H, Park H (2010). X-linked inhibitor of apoptosis protein controls alpha5-integrin-mediated cell adhesion and migration. *Am J Physiol Heart Circ Physiol* **299**: H300-9, doi:10.1152/ajpheart.00180.2010 [doi]

Kischkel FC, Hellbardt S, Behrmann I, Germer M, Pawlita M, Krammer PH, Peter ME (1995). Cytotoxicity-dependent APO-1 (Fas/CD95)-associated proteins form a death-inducing signaling complex (DISC) with the receptor. *EMBO J* **14**: 5579-5588

Kollias G, Douni E, Kassiotis G, Kontoyiannis D (1999). The function of tumour necrosis factor and receptors in models of multi-organ inflammation, rheumatoid arthritis, multiple sclerosis and inflammatory bowel disease. *Ann Rheum Dis* **58 Suppl 1**: I32-9

Koschny R, Holland H, Sykora J, Haas TL, Sprick MR, Ganten TM, Krupp W, Bauer M, Ahnert P, Meixensberger J, Walczak H (2007). Bortezomib sensitizes primary human astrocytoma cells of WHO grades I to IV for tumor necrosis factor-related apoptosis-inducing ligand-induced apoptosis. *Clin Cancer Res* **13**: 3403-3412, doi:13/11/3403 [pii]

Krepler C, Chunduru SK, Halloran MB, He X, Xiao M, Vultur A, Villanueva J, Mitsuuchi Y, Neiman EM, Benetatos C, Nathanson KL, Amaravadi RK, Pehamberger H, McKinlay M, Herlyn M (2013). The novel SMAC mimetic birinapant exhibits potent activity against human melanoma cells. *Clin Cancer Res* **19**: 1784-1794, doi:10.1158/1078-0432.CCR-12-2518 [doi]

Krueger A, Baumann S, Krammer PH, Kirchhoff S (2001). FLICE-inhibitory proteins: regulators of death receptor-mediated apoptosis. *Mol Cell Biol* **21**: 8247-8254, doi:10.1128/MCB.21.24.8247-8254.2001 [doi]

Kumar MS, Hancock DC, Molina-Arcas M, Steckel M, East P, Diefenbacher M, Armenteros-Monterroso E, Lassailly F, Matthews N, Nye E, Stamp G, Behrens A, Downward J (2012). The GATA2 transcriptional network is requisite for RAS oncogene-driven non-small cell lung cancer. *Cell* **149**: 642-655, doi:10.1016/j.cell.2012.02.059 [doi]

Lambert JM, Lambert QT, Reuther GW, Malliri A, Siderovski DP, Sondek J, Collard JG, Der CJ (2002). Tiam1 mediates Ras activation of Rac by a PI(3)K-independent mechanism. *Nat Cell Biol* **4**: 621-625, doi:10.1038/ncb833 [doi]

Lecis D, De Cesare M, Perego P, Conti A, Corna E, Drago C, Seneci P, Walczak H, Colombo MP, Delia D, Sangaletti S (2013). Smac mimetics induce inflammation and necrotic tumour cell death by modulating macrophage activity. *Cell Death Dis* **4**: e920, doi:10.1038/cddis.2013.449 [doi]

Lecis D, Drago C, Manzoni L, Seneci P, Scolastico C, Mastrangelo E, Bolognesi M, Anichini A, Kashkar H, Walczak H, Delia D (2010). Novel SMAC-mimetics synergistically stimulate melanoma cell death in combination with TRAIL and Bortezomib. *Br J Cancer* **102**: 1707-1716, doi:10.1038/sj.bjc.6605687 [doi]

Lecis D, Mastrangelo E, Belvisi L, Bolognesi M, Civera M, Cossu F, De Cesare M, Delia D, Drago C, Manenti G, Manzoni L, Milani M, Moroni E, Perego P, Potenza D, Rizzo V, Scavullo C, Scolastico C, Servida F, Vasile F, Seneci P (2012). Dimeric Smac mimetics/IAP inhibitors as in vivo-active pro-apoptotic agents. Part II: Structural and

biological characterization. *Bioorg Med Chem* **20**: 6709-6723, doi:10.1016/j.bmc.2012.09.041 [doi]

Lejeune FJ, Ruegg C, Lienard D (1998). Clinical applications of TNF-alpha in cancer. *Curr Opin Immunol* **10**: 573-580, doi:S0952-7915(98)80226-4 [pii]

Lemke J, von Karstedt S, Abd El Hay M, Conti A, Arce F, Montinaro A, Papenfuss K, El-Bahrawy MA, Walczak H (2014a). Selective CDK9 inhibition overcomes TRAIL resistance by concomitant suppression of cFlip and Mcl-1. *Cell Death Differ* **21**: 491-502, doi:10.1038/cdd.2013.179 [doi]

Lemke J, von Karstedt S, Zinngrebe J, Walczak H (2014b). Getting TRAIL back on track for cancer therapy. *Cell Death Differ* **21**: 1350-1364, doi:10.1038/cdd.2014.81 [doi]

Leon J, Guerrero I, Pellicer A (1987). Differential expression of the ras gene family in mice. *Mol Cell Biol* **7**: 1535-1540

Li L, Thomas RM, Suzuki H, De Brabander JK, Wang X, Harran PG (2004). A small molecule Smac mimic potentiates TRAIL- and TNFalpha-mediated cell death. *Science* **305**: 1471-1474, doi:10.1126/science.1098231 [doi]

Liu J, Zhang D, Luo W, Yu Y, Yu J, Li J, Zhang X, Zhang B, Chen J, Wu XR, Rosas-Acosta G, Huang C (2011). X-linked inhibitor of apoptosis protein (XIAP) mediates cancer cell motility via Rho GDP dissociation inhibitor (RhoGDI)-dependent regulation of the cytoskeleton. *J Biol Chem* **286**: 15630-15640, doi:10.1074/jbc.M110.176982 [doi]

Lopez J, John SW, Tenev T, Rautureau GJ, Hinds MG, Francalanci F, Wilson R, Broemer M, Santoro MM, Day CL, Meier P (2011). CARD-mediated autoinhibition of

cIAP1's E3 ligase activity suppresses cell proliferation and migration. *Mol Cell* **42**: 569-583, doi:10.1016/j.molcel.2011.04.008 [doi]

Lu J, Bai L, Sun H, Nikolovska-Coleska Z, McEachern D, Qiu S, Miller RS, Yi H, Shangary S, Sun Y, Meagher JL, Stuckey JA, Wang S (2008). SM-164: a novel, bivalent Smac mimetic that induces apoptosis and tumor regression by concurrent removal of the blockade of cIAP-1/2 and XIAP. *Cancer Res* **68**: 9384-9393, doi:10.1158/0008-5472.CAN-08-2655 [doi]

Lu J, McEachern D, Sun H, Bai L, Peng Y, Qiu S, Miller R, Liao J, Yi H, Liu M, Bellail A, Hao C, Sun SY, Ting AT, Wang S (2011). Therapeutic potential and molecular mechanism of a novel, potent, nonpeptide, Smac mimetic SM-164 in combination with TRAIL for cancer treatment. *Mol Cancer Ther* **10**: 902-914, doi:10.1158/1535-7163.MCT-10-0864 [doi]

Lucas KM, Mohana-Kumaran N, Lau D, Zhang XD, Hersey P, Huang DC, Weninger W, Haass NK, Allen JD (2012). Modulation of NOXA and MCL-1 as a strategy for sensitizing melanoma cells to the BH3-mimetic ABT-737. *Clin Cancer Res* **18**: 783-795, doi:10.1158/1078-0432.CCR-11-1166 [doi]

Macher-Goeppinger S, Aulmann S, Tagscherer KE, Wagener N, Haferkamp A, Penzel R, Brauckhoff A, Hohenfellner M, Sykora J, Walczak H, Teh BT, Autschbach F, Herpel E, Schirmacher P, Roth W (2009). Prognostic value of tumor necrosis factor-related apoptosis-inducing ligand (TRAIL) and TRAIL receptors in renal cell cancer. *Clin Cancer Res* **15**: 650-659, doi:10.1158/1078-0432.CCR-08-0284 [doi]

Malin D, Chen F, Schiller C, Koblinski J, Cryns VL (2011). Enhanced metastasis suppression by targeting TRAIL receptor 2 in a murine model of triple-negative breast cancer. *Clin Cancer Res* **17**: 5005-5015, doi:10.1158/1078-0432.CCR-11-0099 [doi]

Malumbres M and Barbacid M (2003). RAS oncogenes: the first 30 years. *Nat Rev Cancer* **3**: 459-465, doi:10.1038/nrc1097 [doi]

Manzoni L, Belvisi L, Bianchi A, Conti A, Drago C, de Matteo M, Ferrante L, Mastrangelo E, Perego P, Potenza D, Scolastico C, Servida F, Timpano G, Vasile F, Rizzo V, Seneci P (2012). Homo- and heterodimeric Smac mimetics/IAP inhibitors as in vivo-active pro-apoptotic agents. Part I: Synthesis. *Bioorg Med Chem* **20**: 6687-6708, doi:10.1016/j.bmc.2012.09.020 [doi]

Mastrangelo E, Cossu F, Milani M, Sorrentino G, Lecis D, Delia D, Manzoni L, Drago C, Seneci P, Scolastico C, Rizzo V, Bolognesi M (2008). Targeting the X-linked inhibitor of apoptosis protein through 4-substituted azabicyclo[5.3.0]alkane smac mimetics. Structure, activity, and recognition principles. *J Mol Biol* **384**: 673-689, doi:10.1016/j.jmb.2008.09.064 [doi]

Matallanas D, Romano D, Al-Mulla F, O'Neill E, Al-Ali W, Crespo P, Doyle B, Nixon C, Sansom O, Drosten M, Barbacid M, Kolch W (2011). Mutant K-Ras activation of the proapoptotic MST2 pathway is antagonized by wild-type K-Ras. *Mol Cell* **44**: 893-906, doi:10.1016/j.molcel.2011.10.016 [doi]

McCarthy N (2009). Metastasis: Route master. *Nat Rev Cancer* **9**: 610, doi:10.1038/nrc2721 [doi]

Meerbrey KL, Hu G, Kessler JD, Roartyd K, Lie MZ, Fanga JE, Herschkowitzd JI, Burrowse AE, Cicciae A, Suna T, Schmitta EM, Bernardif RJ, Fud X, Blandi CS, Cooperi TA, Schiffd R, Rosend JM, Westbrooka TF, Elledgee SJ (2011). The pINDUCER lentiviral toolkit for inducible RNA interference in vitro and in vivo. *Proc Natl Acad Sci U S A* **108**: 3665-3670, doi: 10.1073/pnas.1019736108

Mehrotra S, Languino LR, Raskett CM, Mercurio AM, Dohi T, Altieri DC (2010). IAP regulation of metastasis. *Cancer Cell* **17**: 53-64, doi:10.1016/j.ccr.2009.11.021 [doi]

Merino D, Lalaoui N, Morizot A, Schneider P, Solary E, Micheau O (2006). Differential inhibition of TRAIL-mediated DR5-DISC formation by decoy receptors 1 and 2. *Mol Cell Biol* **26**: 7046-7055, doi:26/19/7046 [pii]

Meuwissen R and Berns A (2005). Mouse models for human lung cancer. *Genes Dev* **19**: 643-664, doi:19/6/643 [pii]

Meylan E, Dooley AL, Feldser DM, Shen L, Turk E, Ouyang C, Jacks T (2009). Requirement for NF-kappaB signalling in a mouse model of lung adenocarcinoma. *Nature* **462**: 104-107, doi:10.1038/nature08462 [doi]

Micheau O, Shirley S, Dufour F (2013). Death receptors as targets in cancer. *Br J Pharmacol* **169**: 1723-1744, doi:10.1111/bph.12238 [doi]

Micheau O and Tschopp J (2003). Induction of TNF receptor I-mediated apoptosis via two sequential signaling complexes. *Cell* **114**: 181-190, doi:S009286740300521X [pii]

Millan O, Ballester A, Castrillo A, Oliva JL, Traves PG, Rojas JM, Bosca L (2003). H-Ras-specific activation of NF-kappaB protects NIH 3T3 cells against stimulus-dependent apoptosis. *Oncogene* **22**: 477-483, doi:10.1038/sj.onc.1206179 [doi]

Mirandola P, Ponti C, Gobbi G, Sponzilli I, Vaccarezza M, Cocco L, Zauli G, Secchiero P, Manzoli FA, Vitale M (2004). Activated human NK and CD8+ T cells express both TNF-related apoptosis-inducing ligand (TRAIL) and TRAIL receptors but are resistant to TRAIL-mediated cytotoxicity. *Blood* **104**: 2418-2424, doi:10.1182/blood-2004-04-1294 [doi]

Misale S, Yaeger R, Hobor S, Scala E, Janakiraman M, Liska D, Valtorta E, Schiavo R, Buscarino M, Siravegna G, Bencardino K, Cercek A, Chen CT, Veronese S, Zanon C, Sartore-Bianchi A, Gambacorta M, Gallicchio M, Vakiani E, Boscaro V, Medico E, Weiser M, Siena S, Di Nicolantonio F, Solit D, Bardelli A (2012). Emergence of KRAS mutations and acquired resistance to anti-EGFR therapy in colorectal cancer. *Nature* **486**: 532-536, doi:10.1038/nature11156 [doi]

Mitsuuchi Y and Testa JR (2002). Cytogenetics and molecular genetics of lung cancer. *Am J Med Genet* **115**: 183-188, doi:10.1002/ajmg.10692 [doi]

Moller Y, Siegemund M, Beyes S, Herr R, Lecis D, Delia D, Kontermann R, Brummer T, Pfizenmaier K, Olayioye MA (2014). EGFR-Targeted TRAIL and a Smac Mimetic Synergize to Overcome Apoptosis Resistance in KRAS Mutant Colorectal Cancer Cells. *PLoS One* **9**: e107165, doi:10.1371/journal.pone.0107165 [doi]

Montagut C and Settleman J (2009). Targeting the RAF-MEK-ERK pathway in cancer therapy. *Cancer Lett* **283**: 125-134, doi:10.1016/j.canlet.2009.01.022 [doi]

Muzio M, Chinnaiyan AM, Kischkel FC, O'Rourke K, Shevchenko A, Ni J, Scaffidi C, Bretz JD, Zhang M, Gentz R, Mann M, Krammer PH, Peter ME, Dixit VM (1996). FLICE, a novel FADD-homologous ICE/CED-3-like protease, is recruited to the CD95

(Fas/APO-1) death--inducing signaling complex. *Cell* **85**: 817-827, doi:S0092-8674(00)81266-0 [pii]

Nemunaitis JJ, Small KA, Kirschmeier P, Zhang D, Zhu Y, Jou YM, Statkevich P, Yao SL, Bannerji R (2013). A first-in-human, phase 1, dose-escalation study of dinaciclib, a novel cyclin-dependent kinase inhibitor, administered weekly in subjects with advanced malignancies. *J Transl Med* **11**: 259-5876-11-259, doi:10.1186/1479-5876-11-259 [doi]

Newsom-Davis T, Prieske S, Walczak H (2009). Is TRAIL the holy grail of cancer therapy? *Apoptosis* **14**: 607-623, doi:10.1007/s10495-009-0321-2 [doi]

Nimnual AS, Yatsula BA, Bar-Sagi D (1998). Coupling of Ras and Rac guanosine triphosphatases through the Ras exchanger Sos. *Science* **279**: 560-563

Oberoi TK, Dogan T, Hocking JC, Scholz RP, Mooz J, Anderson CL, Karreman C, Meyer zu Heringdorf D, Schmidt G, Ruonala M, Namikawa K, Harms GS, Carpy A, Macek B, Koster RW, Rajalingam K (2012). IAPs regulate the plasticity of cell migration by directly targeting Rac1 for degradation. *EMBO J* **31**: 14-28, doi:10.1038/emboj.2011.423 [doi]

Oberoi-Khanuja TK, Murali A, Rajalingam K (2013). IAPs on the move: role of inhibitors of apoptosis proteins in cell migration. *Cell Death Dis* **4**: e784, doi:10.1038/cddis.2013.311 [doi]

Oberst A, Dillon CP, Weinlich R, McCormick LL, Fitzgerald P, Pop C, Hakem R, Salvesen GS, Green DR (2011). Catalytic activity of the caspase-8-FLIP(L) complex inhibits RIPK3-dependent necrosis. *Nature* **471**: 363-367, doi:10.1038/nature09852 [doi]

Ogasawara J, Watanabe-Fukunaga R, Adachi M, Matsuzawa A, Kasugai T, Kitamura Y, Itoh N, Suda T, Nagata S (1993). Lethal effect of the anti-Fas antibody in mice. *Nature* **364**: 806-809, doi:10.1038/364806a0 [doi]

Oost TK, Sun C, Armstrong RC, Al-Assaad AS, Betz SF, Deckwerth TL, Ding H, Elmore SW, Meadows RP, Olejniczak ET, Oleksijew A, Oltersdorf T, Rosenberg SH, Shoemaker AR, Tomaselli KJ, Zou H, Fesik SW (2004). Discovery of potent antagonists of the antiapoptotic protein XIAP for the treatment of cancer. *J Med Chem* **47**: 4417-4426, doi:10.1021/jm040037k [doi]

Pantel K and Brakenhoff RH (2004). Dissecting the metastatic cascade. *Nat Rev Cancer* **4**: 448-456, doi:10.1038/nrc1370 [doi]

Parry D, Guzi T, Shanahan F, Davis N, Prabhavalkar D, Wiswell D, Seghezzi W, Paruch K, Dwyer MP, Doll R, Nomeir A, Windsor W, Fischmann T, Wang Y, Oft M, Chen T, Kirschmeier P, Lees EM (2010). Dinaciclib (SCH 727965), a novel and potent cyclin-dependent kinase inhibitor. *Mol Cancer Ther* **9**: 2344-2353, doi:10.1158/1535-7163.MCT-10-0324 [doi]

Paruch K, Dwyer MP, Alvarez C, Brown C, Chan TY, Doll RJ, Keertikar K, Knutson C, McKittrick B, Rivera J, Rossman R, Tucker G, Fischmann T, Hruza A, Madison V, Nomeir AA, Wang Y, Kirschmeier P, Lees E, Parry D, Sgambellone N, Seghezzi W, Schultz L, Shanahan F, Wiswell D, Xu X, Zhou Q, James RA, Paradkar VM, Park H, Rokosz LR, Stauffer TM, Guzi TJ (2010). Discovery of Dinaciclib (SCH 727965): A Potent and Selective Inhibitor of Cyclin-Dependent Kinases. *ACS Med Chem Lett* **1**: 204-208, doi:10.1021/ml100051d [doi]

Peltzer N, Rieser E, Taraborrelli L, Draber P, Darding M, Pernaute B, Shimizu Y, Sarr A, Draberova H, Montinaro A, Martinez-Barbera JP, Silke J, Rodriguez TA, Walczak H (2014). HOIP Deficiency Causes Embryonic Lethality by Aberrant TNFR1-Mediated Endothelial Cell Death. *Cell Rep* **9**: 153-165, doi:10.1016/j.celrep.2014.08.066 [doi]

Petersen SL, Peyton M, Minna JD, Wang X (2010). Overcoming cancer cell resistance to Smac mimetic induced apoptosis by modulating cIAP-2 expression. *Proc Natl Acad Sci U S A* **107**: 11936-11941, doi:10.1073/pnas.1005667107 [doi]

Petersen SL, Wang L, Yalcin-Chin A, Li L, Peyton M, Minna J, Harran P, Wang X (2007). Autocrine TNFalpha signaling renders human cancer cells susceptible to Smac-mimetic-induced apoptosis. *Cancer Cell* **12**: 445-456, doi:S1535-6108(07)00261-9 [pii]

Pikarsky E, Porat RM, Stein I, Abramovitch R, Amit S, Kasem S, Gutkovich-Pyest E, Urieli-Shoval S, Galun E, Ben-Neriah Y (2004). NF-kappaB functions as a tumour promoter in inflammation-associated cancer. *Nature* **431**: 461-466, doi:10.1038/nature02924 [doi]

Pitti RM, Marsters SA, Ruppert S, Donahue CJ, Moore A, Ashkenazi A (1996). Induction of apoptosis by Apo-2 ligand, a new member of the tumor necrosis factor cytokine family. *J Biol Chem* **271**: 12687-12690

Popivanova BK, Kitamura K, Wu Y, Kondo T, Kagaya T, Kaneko S, Oshima M, Fujii C, Mukaida N (2008). Blocking TNF-alpha in mice reduces colorectal carcinogenesis associated with chronic colitis. *J Clin Invest* **118**: 560-570, doi:10.1172/JCI32453 [doi]

Probst BL, Liu L, Ramesh V, Li L, Sun H, Minna JD, Wang L (2010). Smac mimetics increase cancer cell response to chemotherapeutics in a TNF-alpha-dependent manner. *Cell Death Differ* **17**: 1645-1654, doi:10.1038/cdd.2010.44 [doi]

Raulf N, El-Attar R, Kulms D, Lecis D, Delia D, Walczak H, Papenfuss K, Odell E, Tavassoli M (2014). Differential response of head and neck cancer cell lines to TRAIL or Smac mimetics is associated with the cellular levels and activity of caspase-8 and caspase-10. *Br J Cancer*, doi:10.1038/bjc.2014.521 [doi]

Riccioni R, Pasquini L, Mariani G, Saulle E, Rossini A, Diverio D, Pelosi E, Vitale A, Chierichini A, Cedrone M, Foa R, Lo Coco F, Peschle C, Testa U (2005). TRAIL decoy receptors mediate resistance of acute myeloid leukemia cells to TRAIL. *Haematologica* **90**: 612-624

Riedl SJ, Renatus M, Schwarzenbacher R, Zhou Q, Sun C, Fesik SW, Liddington RC, Salvesen GS (2001). Structural basis for the inhibition of caspase-3 by XIAP. *Cell* **104**: 791-800, doi:S0092-8674(01)00274-4 [pii]

Rivkin E, Almeida SM, Ceccarelli DF, Juang YC, MacLean TA, Srikumar T, Huang H, Dunham WH, Fukumura R, Xie G, Gondo Y, Raught B, Gingras AC, Sicheri F, Cordes SP (2013). The linear ubiquitin-specific deubiquitinase gumby regulates angiogenesis. *Nature* **498**: 318-324, doi:10.1038/nature12296 [doi]

Salvesen GS and Riedl SJ (2008). Caspase mechanisms. *Adv Exp Med Biol* **615**: 13-23, doi:10.1007/978-1-4020-6554-5_2 [doi]

Sanlioglu AD, Koksal IT, Ciftcioglu A, Baykara M, Luleci G, Sanlioglu S (2007a). Differential expression of TRAIL and its receptors in benign and malignant prostate tissues. *J Urol* **177**: 359-364, doi:S0022-5347(06)02191-4 [pii]

Sanlioglu AD, Korcum AF, Pestereli E, Erdogan G, Karaveli S, Savas B, Griffith TS, Sanlioglu S (2007b). TRAIL death receptor-4 expression positively correlates with the tumor grade in breast cancer patients with invasive ductal carcinoma. *Int J Radiat Oncol Biol Phys* **69**: 716-723, doi:S0360-3016(07)00652-9 [pii]

Santoro MM, Samuel T, Mitchell T, Reed JC, Stainier DY (2007). Birc2 (cIap1) regulates endothelial cell integrity and blood vessel homeostasis. *Nat Genet* **39**: 1397-1402, doi:ng.2007.8 [pii]

Scaffidi C, Fulda S, Srinivasan A, Friesen C, Li F, Tomaselli KJ, Debatin KM, Krammer PH, Peter ME (1998). Two CD95 (APO-1/Fas) signaling pathways. *EMBO J* **17**: 1675-1687, doi:10.1093/emboj/17.6.1675 [doi]

Scavullo C, Servida F, Lecis D, Onida F, Drago C, Ferrante L, Seneci P, Barcellini W, Lionetti M, Todoerti K, Neri A, Delia D, Deliliers GL (2013). Single-agent Smac-mimetic compounds induce apoptosis in B chronic lymphocytic leukaemia (B-CLL). *Leuk Res* **37**: 809-815, doi:10.1016/j.leukres.2013.03.016 [doi]

Schmukle AC and Walczak H (2012). No one can whistle a symphony alone - how different ubiquitin linkages cooperate to orchestrate NF-kappaB activity. *J Cell Sci* **125**: 549-559, doi:10.1242/jcs.091793 [doi]

Scott KA, Moore RJ, Arnott CH, East N, Thompson RG, Scallon BJ, Shealy DJ, Balkwill FR (2003). An anti-tumor necrosis factor-alpha antibody inhibits the development of experimental skin tumors. *Mol Cancer Ther* **2**: 445-451

Sebti SM and Adjei AA (2004). Farnesyltransferase inhibitors. *Semin Oncol* **31**: 28-39, doi:S009377540300650X [pii]

Secchiero P, Gonelli A, Carnevale E, Milani D, Pandolfi A, Zella D, Zauli G (2003). TRAIL promotes the survival and proliferation of primary human vascular endothelial cells by activating the Akt and ERK pathways. *Circulation* **107**: 2250-2256, doi:10.1161/01.CIR.0000062702.60708.C4 [doi]

Secchiero P, Zerbinati C, Rimondi E, Corallini F, Milani D, Grill V, Forti G, Capitani S, Zauli G (2004). TRAIL promotes the survival, migration and proliferation of vascular smooth muscle cells. *Cell Mol Life Sci* **61**: 1965-1974, doi:10.1007/s00018-004-4197-6 [doi]

Seneci P, Bianchi A, Battaglia C, Belvisi L, Bolognesi M, Caprini A, Cossu F, Franco E, Matteo M, Delia D, Drago C, Khaled A, Lecis D, Manzoni L, Marizzoni M, Mastrangelo E, Milani M, Motto I, Moroni E, Potenza D, Rizzo V, Servida F, Turlizzi E, Varrone M, Vasile F, Scolastico C (2009). Rational design, synthesis and characterization of potent, non-peptidic Smac mimics/XIAP inhibitors as proapoptotic agents for cancer therapy. *Bioorg Med Chem* **17**: 5834-5856, doi:10.1016/j.bmc.2009.07.009 [doi]

Servida F, Lecis D, Scavullo C, Drago C, Seneci P, Carlo-Stella C, Manzoni L, Polli E, Lambertenghi Deliliers G, Delia D, Onida F (2011). Novel second mitochondria-derived activator of caspases (Smac) mimetic compounds sensitize human leukemic cell lines to

conventional chemotherapeutic drug-induced and death receptor-mediated apoptosis. *Invest New Drugs* **29**: 1264-1275, doi:10.1007/s10637-010-9475-6 [doi]

Shamas-Din A, Kale J, Leber B, Andrews DW (2013). Mechanisms of action of Bcl-2 family proteins. *Cold Spring Harb Perspect Biol* **5**: a008714, doi:10.1101/cshperspect.a008714 [doi]

Sheridan C, Brumatti G, Elgendy M, Brunet M, Martin SJ (2010). An ERK-dependent pathway to Noxa expression regulates apoptosis by platinum-based chemotherapeutic drugs. *Oncogene* **29**: 6428-6441, doi:10.1038/onc.2010.380 [doi]

Shields JM, Pruitt K, McFall A, Shaub A, Der CJ (2000). Understanding Ras: 'it ain't over 'til it's over'. *Trends Cell Biol* **10**: 147-154, doi:S0962-8924(00)01740-2 [pii]

Shirasawa S, Furuse M, Yokoyama N, Sasazuki T (1993). Altered growth of human colon cancer cell lines disrupted at activated Ki-ras. *Science* **260**: 85-88

Sprick MR, Weigand MA, Rieser E, Rauch CT, Juo P, Blenis J, Krammer PH, Walczak H (2000). FADD/MORT1 and caspase-8 are recruited to TRAIL receptors 1 and 2 and are essential for apoptosis mediated by TRAIL receptor 2. *Immunity* **12**: 599-609, doi:S1074-7613(00)80211-3 [pii]

Srinivasula SM, Hegde R, Saleh A, Datta P, Shiozaki E, Chai J, Lee RA, Robbins PD, Fernandes-Alnemri T, Shi Y, Alnemri ES (2001). A conserved XIAP-interaction motif in caspase-9 and Smac/DIABLO regulates caspase activity and apoptosis. *Nature* **410**: 112-116, doi:10.1038/35065125 [doi]

Steckel M, Molina-Arcas M, Weigelt B, Marani M, Warne PH, Kuznetsov H, Kelly G, Saunders B, Howell M, Downward J, Hancock DC (2012). Determination of synthetic

lethal interactions in KRAS oncogene-dependent cancer cells reveals novel therapeutic targeting strategies. *Cell Res* **22**: 1227-1245, doi:10.1038/cr.2012.82 [doi]

Steller H (1995). Mechanisms and genes of cellular suicide. *Science* **267**: 1445-1449

Stennicke HR, Jurgensmeier JM, Shin H, Deveraux Q, Wolf BB, Yang X, Zhou Q, Ellerby HM, Ellerby LM, Bredesen D, Green DR, Reed JC, Froelich CJ, Salvesen GS (1998). Pro-caspase-3 is a major physiologic target of caspase-8. *J Biol Chem* **273**: 27084-27090

Stephenson JJ, Nemunaitis J, Joy AA, Martin JC, Jou YM, Zhang D, Statkevich P, Yao SL, Zhu Y, Zhou H, Small K, Bannerji R, Edelman MJ (2014). Randomized phase 2 study of the cyclin-dependent kinase inhibitor dinaciclib (MK-7965) versus erlotinib in patients with non-small cell lung cancer. *Lung Cancer* **83**: 219-223, doi:10.1016/j.lungcan.2013.11.020 [doi]

Sun H, Nikolovska-Coleska Z, Yang CY, Qian D, Lu J, Qiu S, Bai L, Peng Y, Cai Q, Wang S (2008). Design of small-molecule peptidic and nonpeptidic Smac mimetics. *Acc Chem Res* **41**: 1264-1277, doi:10.1021/ar8000553 [doi]

Sun H, Nikolovska-Coleska Z, Yang CY, Xu L, Liu M, Tomita Y, Pan H, Yoshioka Y, Krajewski K, Roller PP, Wang S (2004). Structure-based design of potent, conformationally constrained Smac mimetics. *J Am Chem Soc* **126**: 16686-16687, doi:10.1021/ja047438+ [doi]

Sun L, Wang H, Wang Z, He S, Chen S, Liao D, Wang L, Yan J, Liu W, Lei X, Wang X (2012). Mixed lineage kinase domain-like protein mediates necrosis signaling downstream of RIP3 kinase. *Cell* **148**: 213-227, doi:10.1016/j.cell.2011.11.031 [doi]

Takeda K, Cretney E, Hayakawa Y, Ota T, Akiba H, Ogasawara K, Yagita H, Kinoshita K, Okumura K, Smyth MJ (2005). TRAIL identifies immature natural killer cells in newborn mice and adult mouse liver. *Blood* **105**: 2082-2089, doi:2004-08-3262 [pii]

Takiuchi T, Nakagawa T, Tamiya H, Fujita H, Sasaki Y, Saeki Y, Takeda H, Sawasaki T, Buchberger A, Kimura T, Iwai K (2014). Suppression of LUBAC-mediated linear ubiquitination by a specific interaction between LUBAC and the deubiquitinases CYLD and OTULIN. *Genes Cells* **19**: 254-272, doi:10.1111/gtc.12128 [doi]

Tanaka M, Suda T, Yatomi T, Nakamura N, Nagata S (1997). Lethal effect of recombinant human Fas ligand in mice pretreated with Propionibacterium acnes. *J Immunol* **158**: 2303-2309

Tchoghandjian A, Jennewein C, Eckhardt I, Rajalingam K, Fulda S (2013). Identification of non-canonical NF-kappaB signaling as a critical mediator of Smac mimetic-stimulated migration and invasion of glioblastoma cells. *Cell Death Dis* **4**: e564, doi:10.1038/cddis.2013.70 [doi]

Tenev T, Bianchi K, Darding M, Broemer M, Langlais C, Wallberg F, Zachariou A, Lopez J, MacFarlane M, Cain K, Meier P (2011). The Ripoptosome, a signaling platform that assembles in response to genotoxic stress and loss of IAPs. *Mol Cell* **43**: 432-448, doi:10.1016/j.molcel.2011.06.006 [doi]

Todaro M, Lombardo Y, Francipane MG, Alea MP, Cammareri P, Iovino F, Di Stefano AB, Di Bernardo C, Agrusa A, Condorelli G, Walczak H, Stassi G (2008). Apoptosis resistance in epithelial tumors is mediated by tumor-cell-derived interleukin-4. *Cell Death Differ* **15**: 762-772, doi:10.1038/sj.cdd.4402305 [doi]

Tomicic MT, Christmann M, Kaina B (2010). Topotecan triggers apoptosis in p53-deficient cells by forcing degradation of XIAP and survivin thereby activating caspase-3-mediated Bid cleavage. *J Pharmacol Exp Ther* **332**: 316-325, doi:10.1124/jpet.109.159962 [doi]

Tomicic MT and Kaina B (2013). Topoisomerase degradation, DSB repair, p53 and IAPs in cancer cell resistance to camptothecin-like topoisomerase I inhibitors. *Biochim Biophys Acta* **1835**: 11-27, doi:10.1016/j.bbcan.2012.09.002 [doi]

Tomonaga M, Hashimoto N, Tokunaga F, Onishi M, Myoui A, Yoshikawa H, Iwai K (2012). Activation of nuclear factor-kappa B by linear ubiquitin chain assembly complex contributes to lung metastasis of osteosarcoma cells. *Int J Oncol* **40**: 409-417, doi:10.3892/ijo.2011.1209 [doi]

Tong WG, Chen R, Plunkett W, Siegel D, Sinha R, Harvey RD, Badros AZ, Popplewell L, Coutre S, Fox JA, Mahadocon K, Chen T, Kegley P, Hoch U, Wierda WG (2010). Phase I and pharmacologic study of SNS-032, a potent and selective Cdk2, 7, and 9 inhibitor, in patients with advanced chronic lymphocytic leukemia and multiple myeloma. *J Clin Oncol* **28**: 3015-3022, doi:10.1200/JCO.2009.26.1347 [doi]

Touzeau C, Dousset C, Le Gouill S, Sampath D, Leverson JD, Souers AJ, Maiga S, Bene MC, Moreau P, Pellat-Deceunynck C, Amiot M (2014). The Bcl-2 specific BH3 mimetic ABT-199: a promising targeted therapy for t(11;14) multiple myeloma. *Leukemia* **28**: 210-212, doi:10.1038/leu.2013.216 [doi]

Trauzold A, Siegmund D, Schniewind B, Sipos B, Egberts J, Zorenkov D, Emme D, Roder C, Kalthoff H, Wajant H (2006). TRAIL promotes metastasis of human pancreatic ductal adenocarcinoma. *Oncogene* **25**: 7434-7439, doi:1209719 [pii]

Tse C, Shoemaker AR, Adickes J, Anderson MG, Chen J, Jin S, Johnson EF, Marsh KC, Mitten MJ, Nimmer P, Roberts L, Tahir SK, Xiao Y, Yang X, Zhang H, Fesik S, Rosenberg SH, Elmore SW (2008). ABT-263: a potent and orally bioavailable Bcl-2 family inhibitor. *Cancer Res* **68**: 3421-3428, doi:10.1158/0008-5472.CAN-07-5836 [doi]

Umanoff H, Edelmann W, Pellicer A, Kucherlapati R (1995). The murine N-ras gene is not essential for growth and development. *Proc Natl Acad Sci U S A* **92**: 1709-1713

Vandenabeele P, Galluzzi L, Vanden Berghe T, Kroemer G (2010). Molecular mechanisms of necroptosis: an ordered cellular explosion. *Nat Rev Mol Cell Biol* **11**: 700-714, doi:10.1038/nrm2970 [doi]

Varfolomeev E, Blankenship JW, Wayson SM, Fedorova AV, Kayagaki N, Garg P, Zobel K, Dynek JN, Elliott LO, Wallweber HJ, Flygare JA, Fairbrother WJ, Deshayes K, Dixit VM, Vucic D (2007). IAP antagonists induce autoubiquitination of c-IAPs, NF-kappaB activation, and TNFalpha-dependent apoptosis. *Cell* **131**: 669-681, doi:S0092-8674(07)01348-7 [pii]

Varfolomeev E, Maecker H, Sharp D, Lawrence D, Renz M, Vucic D, Ashkenazi A (2005). Molecular determinants of kinase pathway activation by Apo2 ligand/tumor necrosis factor-related apoptosis-inducing ligand. *J Biol Chem* **280**: 40599-40608, doi:M509560200 [pii]

Venditto VJ and Simanek EE (2010). Cancer therapies utilizing the camptothecins: a review of the in vivo literature. *Mol Pharm* **7**: 307-349, doi:10.1021/mp900243b [doi]

Verhagen AM, Ekert PG, Pakusch M, Silke J, Connolly LM, Reid GE, Moritz RL, Simpson RJ, Vaux DL (2000). Identification of DIABLO, a mammalian protein that

promotes apoptosis by binding to and antagonizing IAP proteins. *Cell* **102**: 43-53, doi:S0092-8674(00)00009-X [pii]

Verhoef C, de Wilt JH, Grunhagen DJ, van Geel AN, ten Hagen TL, Eggermont AM (2007). Isolated limb perfusion with melphalan and TNF-alpha in the treatment of extremity sarcoma. *Curr Treat Options Oncol* **8**: 417-427, doi:10.1007/s11864-007-0044-y [doi]

Vince JE, Wong WW, Khan N, Feltham R, Chau D, Ahmed AU, Benetatos CA, Chunduru SK, Condon SM, McKinlay M, Brink R, Leverkus M, Tergaonkar V, Schneider P, Callus BA, Koentgen F, Vaux DL, Silke J (2007). IAP antagonists target cIAP1 to induce TNFalpha-dependent apoptosis. *Cell* **131**: 682-693, doi:S0092-8674(07)01357-8 [pii]

Vitovski S, Phillips JS, Sayers J, Croucher PI (2007). Investigating the interaction between osteoprotegerin and receptor activator of NF-kappaB or tumor necrosis factor-related apoptosis-inducing ligand: evidence for a pivotal role for osteoprotegerin in regulating two distinct pathways. *J Biol Chem* **282**: 31601-31609, doi:M706078200 [pii]

Wajant H (2004). TRAIL and NFkappaB signaling--a complex relationship. *Vitam Horm* **67**: 101-132, doi:10.1016/S0083-6729(04)67007-5 [doi]

Wajant H, Pfizenmaier K, Scheurich P (2003). Tumor necrosis factor signaling. *Cell Death Differ* **10**: 45-65, doi:10.1038/sj.cdd.4401189 [doi]

Wajant H, Pfizenmaier K, Scheurich P (2002). TNF-related apoptosis inducing ligand (TRAIL) and its receptors in tumor surveillance and cancer therapy. *Apoptosis* **7**: 449-459

Walczak H (2011). TNF and ubiquitin at the crossroads of gene activation, cell death, inflammation, and cancer. *Immunol Rev* **244**: 9-28, doi:10.1111/j.1600-065X.2011.01066.x [doi]

Walczak H, Degli-Esposti MA, Johnson RS, Smolak PJ, Waugh JY, Boiani N, Timour MS, Gerhart MJ, Schooley KA, Smith CA, Goodwin RG, Rauch CT (1997). TRAIL-R2: a novel apoptosis-mediating receptor for TRAIL. *EMBO J* **16**: 5386-5397, doi:10.1093/emboj/16.17.5386 [doi]

Walczak H, Iwai K, Dikic I (2012). Generation and physiological roles of linear ubiquitin chains. *BMC Biol* **10**: 23-7007-10-23, doi:10.1186/1741-7007-10-23 [doi]

Walczak H, Miller RE, Ariail K, Gliniak B, Griffith TS, Kubin M, Chin W, Jones J, Woodward A, Le T, Smith C, Smolak P, Goodwin RG, Rauch CT, Schuh JC, Lynch DH (1999). Tumoricidal activity of tumor necrosis factor-related apoptosis-inducing ligand in vivo. *Nat Med* **5**: 157-163, doi:10.1038/5517 [doi]

Walsh AB and Bar-Sagi D (2001). Differential activation of the Rac pathway by Ha-Ras and K-Ras. *J Biol Chem* **276**: 15609-15615, doi:10.1074/jbc.M010573200 [doi]

Waterhouse NJ, Ricci JE, Green DR (2002). And all of a sudden it's over: mitochondrial outer-membrane permeabilization in apoptosis. *Biochimie* **84**: 113-121, doi:S0300908402013792 [pii]

Wei MC, Zong WX, Cheng EH, Lindsten T, Panoutsakopoulou V, Ross AJ, Roth KA, MacGregor GR, Thompson CB, Korsmeyer SJ (2001). Proapoptotic BAX and BAK: a requisite gateway to mitochondrial dysfunction and death. *Science* **292**: 727-730, doi:10.1126/science.1059108 [doi]

Weidle UH, Maisel D, Eick D (2011). Synthetic lethality-based targets for discovery of new cancer therapeutics. *Cancer Genomics Proteomics* **8**: 159-171, doi:8/4/159 [pii]

Wertz IE, O'Rourke KM, Zhou H, Eby M, Aravind L, Seshagiri S, Wu P, Wiesmann C, Baker R, Boone DL, Ma A, Koonin EV, Dixit VM (2004). De-ubiquitination and ubiquitin ligase domains of A20 downregulate NF-kappaB signalling. *Nature* **430**: 694-699, doi:10.1038/nature02794 [doi]

Westphal D, Dewson G, Menard M, Frederick P, Iyer S, Bartolo R, Gibson L, Czabotar PE, Smith BJ, Adams JM, Kluck RM (2014). Apoptotic pore formation is associated with in-plane insertion of Bak or Bax central helices into the mitochondrial outer membrane. *Proc Natl Acad Sci U S A* **111**: E4076-85, doi:10.1073/pnas.1415142111 [doi]

Wiley SR, Schooley K, Smolak PJ, Din WS, Huang CP, Nicholl JK, Sutherland GR, Smith TD, Rauch C, Smith CA (1995). Identification and characterization of a new member of the TNF family that induces apoptosis. *Immunity* **3**: 673-682

Wilson C (2011). Osteocytes, RANKL and bone loss. *Nat Rev Endocrinol* **7**: 693, doi:10.1038/nrendo.2011.176 [doi]

Xu L, Yin S, Banerjee S, Sarkar F, Reddy KB (2011). Enhanced anticancer effect of the combination of cisplatin and TRAIL in triple-negative breast tumor cells. *Mol Cancer Ther* **10**: 550-557, doi:10.1158/1535-7163.MCT-10-0571 [doi]

Yan J, Roy S, Apolloni A, Lane A, Hancock JF (1998). Ras isoforms vary in their ability to activate Raf-1 and phosphoinositide 3-kinase. *J Biol Chem* **273**: 24052-24056

Yin S, Xu L, Bandyopadhyay S, Sethi S, Reddy KB (2011). Cisplatin and TRAIL enhance breast cancer stem cell death. *Int J Oncol* **39**: 891-898, doi:10.3892/ijo.2011.1085 [doi]

Zhang LN, Li JY, Xu W (2013). A review of the role of Puma, Noxa and Bim in the tumorigenesis, therapy and drug resistance of chronic lymphocytic leukemia. *Cancer Gene Ther* **20**: 1-7, doi:10.1038/cgt.2012.84 [doi]

8 Publications

Related to the PhD project:

1. Manzoni L, Belvisi L, Bianchi A, Conti A, Drago C, de Matteo M, Ferrante L, Mastrangelo E, Perego P, Potenza D, Scolastico C, Servida F, Timpano G, Vasile F, Rizzo V, Seneci P. **"Homo- and heterodimeric Smac mimetics/IAP inhibitors as in vivo-active pro-apoptotic agents. Part I: Synthesis"**. *Bioorg Med Chem*. 2012 Nov 15;20(22):6687-708.
2. Lemke J, von Karstedt S, Abd El Hay M, Conti A, Arce F, Montinaro A, Papenfuss K, El-Bahrawy MA, Walczak H. **"Selective CDK9 inhibition overcomes TRAIL resistance by concomitant suppression of cFlip and Mcl-1"**. *Cell Death and Diff*. 2014 Mar;21(3):491-502.doi: 10.1038/cdd.2013.179.
3. Von Karstedt S, Conti A, Montinaro A, Torsten H, Lemke J, Taraborrelli L, Grosse-Wilde A, Coy JF, El-Bahrawy MA, Bergmann F, Koschny R, Werner J, Schweiger T, Hoetzenecker K, Kenessey I,Hegedüs B, Ganten TM, Walczak H. ***"KRA*S-driven cancer progression, invasion and metastasis require constitutive endogenous TRAIL/TRAIL-R2 signalling"**. *Submitted*.

Other publications:

4. Lecis D, De Cesare M, Perego P, Conti A, Corna E, Drago C, Seneci P, Walczak H, Colombo MP, Delia D, Sangaletti S. **"Smac mimetics induce inflammation and necrotic tumour cell death by modulating macrophage activity"**. *Cell Death Dis*. 2013 Nov 14;4:e920.doi: 10.1038/cddis.2013.449.

5. Seneci P, Rizzi M, Ballabio L, Lecis D, Conti A, Carra*a C,* Licandro E**. "SPION-Smac mimetic nano-conjugates: putative pro-apoptotic agents in oncology"**. *Bioorg Med Chem Lett*. 2014 May 15;24(10):2374-8.doi: 10.1016/j.bmcl.2014.03.048.

Bioorganic & Medicinal Chemistry 20 (2012) 6687–6708

Contents lists available at SciVerse ScienceDirect

Bioorganic & Medicinal Chemistry

journal homepage: www.elsevier.com/locate/bmc

Homo- and heterodimeric Smac mimetics/IAP inhibitors as in vivo-active pro-apoptotic agents. Part I: Synthesis

Leonardo Manzoni [a], Laura Belvisi [b], Aldo Bianchi [c], Annalisa Conti [d], Carmelo Drago [c], Marilenia de Matteo [c], Luca Ferrante [c], Eloise Mastrangelo [e], Paola Perego [d], Donatella Potenza [b], Carlo Scolastico [c], Federica Servida [f], Gabriele Timpano [c], Francesca Vasile [b], Vincenzo Rizzo [c], Pierfausto Seneci [b,c,*]

[a] Istituto di Scienze e Tecnologie Molecolari (ISTM), Consiglio Nazionale delle Ricerche (CNR), Via Golgi 19, Milan I-20133, Italy
[b] Dipartimento di Chimica, Università degli Studi di Milano, Via Golgi 19, Milan I-20133, Italy
[c] CISI scrl, Via Fantoli 16/15, Milan I-20138, Italy
[d] Dipartimento di Oncologia Sperimentale e Medicina Molecolare, Fondazione IRCCS Istituto Nazionale dei Tumori, Via Amadeo 42, Milan I-20133, Italy
[e] Dipartimento di Bioscienze e CNR-IBF, Università degli Studi di Milano, Via Celoria 26, Milan I-20133, Italy
[f] Fondazione Matarelli, Dipartimento di Farmacologia, Chemioterapia e Tossicologia Medica, Università degli Studi di Milano, Via Vanvitelli 32, Milan I-20129, Italy

ARTICLE INFO

Article history:
Available online 21 September 2012

Keywords:
IAP inhibitors
Smac mimetics
Apoptosis
Oncology
Peptidomimetics

ABSTRACT

Novel pro-apoptotic, homo- and heterodimeric Smac mimetics/IAPs inhibitors based on the N-AVPI-like 4-substituted 1-aza-2-oxobicyclo[5.3.0]decane scaffold were prepared from monomeric structures connected through a head–head (**8**), tail–tail (**9**) or head–tail (**10**) linker. The selection of appropriate decorating functions for the scaffolds, and of rigid and flexible linkers connecting them, is described. The synthesis, purification and analytical characterization of each prepared dimer **8–10** is thoroughly described.

1. Introduction

The apoptotic process of programmed cell death is dysfunctional in its regulation in a variety of human pathologies, among which cancer,[1–3] inflammation[4,5] and neurodegeneration,[6,7] where it has become the focus of extensive pharmaceutical research. Pathways leading to apoptosis include the extrinsic or death receptor-dependent path[8,9] and the intrinsic or mitochondrial path,[8,10] both caspase-dependent; and some caspase-independent mechanisms, involving other proteases as apoptosis executioners.[11]

In a complex scenario, hitting more than one putative significant target with a lead should maximize the chances of therapeutic success. Thus, we focused on targeting molecular entities involved in several apoptotic pathways, rather than extremely targeted agents. Such polypharmacology[12] approach is precedented in target classes such as kinases[13] and GPCRs.[14]

The family of Inhibitor of Apoptosis Proteins (IAPs)[15,16] is characterized by the presence of one or more Baculovirus IAP Repeat (BIR) domains. Since the discovery of the first viral *iap* gene and its linkage with apoptosis,[17] IAPs were considered putative targets for pro-apoptotic drugs in oncology.[18] The initial assumption of a common anti-apoptotic mechanism for the whole IAP target family through interference with caspase-dependent pathways[19,20] has been proven wrong, or at least only partially correct for other IAP proteins,[21,22] but their interest as oncology targets related to apoptosis has not been seriously challenged.[23]

The most caspase-connected IAP is the X-Inhibitor of Apoptosis Protein[24,25] (XIAP). XIAP is capable of binding caspase 9 (the initiator caspase) and both caspases 3 and 7 (the executioner caspases).[26] XIAP binding prevents activation of caspases and, consequently, prevents cells from entering apoptosis.

A protein released from mitochondria, the Second Mitochondria-derived Activator of Caspases (Smac)[27]/Direct IAP Binding protein with LOw pI (DIABLO)[28] binds XIAP as a dimer[29] on the same binding sites of caspase 9 (BIR3 domain).[30–32] Smac interferes also with the XIAP binding site of caspases 3 and 7 (linker-BIR2 domain),[33] promoting both the extrinsic and intrinsic apoptosis paths. The delicate balance of this binding equilibrium is altered in various diseases; for example, several tumor cell lines show overexpression of XIAP and, consequently, a caspase-dependent resistance to enter apoptosis.[34,35] Thus, XIAP inhibition via Smac mimetics' binding is considered a validated mechanism for intervention in cancer therapy.[36–38]

* Corresponding author. Tel.: +39 0250314060; fax: +39 0250314075.
E-mail address: pierfausto.seneci@unimi.it (P. Seneci).

0968-0896/$ - see front matter © 2012 Elsevier Ltd. All rights reserved.
http://dx.doi.org/10.1016/j.bmc.2012.09.020

Smac binding to other human IAP family members such as cIAP1[39] and cIAP2[40] through their BIR domains is also proven, although not related to their NF-κB activation-related anti-apoptotic properties.[41–43] Thus, Smac mimetics may modulate the pathological action of any IAP oncology target,[44–46] although the complex network of IAP-dependent interactions still needs to be fully elucidated to understand any drawback for the use of Smac mimetics in therapy.[47]

Several authors have shown how monomeric Smac mimetics/IAP inhibitors such as **1a** (Fig. 1, top left), inspired by the Smac N-terminal AVPI sequence and built on aza-containing bicycloalkane carboxylate scaffolds, bind XIAP, cIAP1 and cIAP2 on their BIR domains with sub-micromolar potency, induce rapid cIAP1 degradation, and affect apoptosis in tumor cells when given in combination with cytotoxic agents.[48] The same authors reported diazabicyclic scaffolds as potent, orally active pan-IAP antagonists.[49] Among them, **2a** (AT406, Fig. 1, bottom left) is in clinical development for the treatment of solid and hematological tumors.[50] Recently, another orally active clinical candidate **3a** (GDC-0152, Fig. 1, top right) was fully described.[51]

We have reported a structure-driven approach to potent, monomeric Smac mimetics/IAP inhibitors of general formula **4** (Fig. 1, middle), where introduction of a 4-substitution on the 1-aza-2-oxobicyclo[5.3.0]decane scaffold established novel molecular interactions with the binding linker-BIR2 and/or BIR3 sites.[52,53] Our early lead **4a**[52] (Fig. 1, bottom right) showed good in vitro—cell-free and cellular—potency. The optimized lead **4b**[54] (Fig. 1, bottom right) showed a significant improvement in solubility and penetration through biological membranes.

Dimeric Smac mimetics/IAP inhibitors such as **5–7** (Fig. 2) were also presented as bifunctional ligands able to simultaneously bind to BIR2 and BIR3 domains of XIAP, and to induce rapid cIAP1 and cIAP2 degradation.[55–57] Their structure includes two AVPI-related peptidomimetics connected through one (**5**, **7**) or two (**6**) linkers of varying length, rigidity and lipophilicity. The observed cytotoxic effects on selected cell lines[55] and significant activity in animal models[57] suggested a downstream developability for such 'non drug-like' dimers.

Here we report novel, dimeric Smac mimetics/IAP inhibitors **8**–**10** (Fig. 3) which take advantage of their characteristic 4-substitution to exploit three connection strategies. Labeling as 'head' the 4-substituent and 'tail' the C-terminus amide of the 1-aza-2-oxobicyclo[5.3.0]decane scaffold (Fig. 3), we have designed, synthesized and biologically characterized several head–head (**8**) and tail–tail homodimers (**9**), together with unprecedented heterodimeric head–tail compounds (**10**, Fig. 3). We aimed to introduce symmetrical and unsymmetrical substitution patterns on the two linker-connected monomer units, and to assess a few synthetic strategies fully compatible with a wide variety of functional groups. We reasoned that, if fully achieved, such goals should have allowed to understand the influence of structural modifications on in vitro and in vivo efficacy of dimeric Smac mimetics/IAP inhibitors **8**–**10**, and to select at least one suitable candidate for preclinical evaluation.

The rational design and the chemical synthesis of dimeric Smac mimetics/IAP inhibitors **8**–**10** is presented and discussed in this paper. Their structural and biological characterization, including NMR and X-ray studies, cell-free, cellular and in vivo efficacy testing on selected compounds, are reported in the following paper.[58]

2. Synthesis

2.1. Rationale

Some of us recently reported[52,59] an innovative synthesis strategy to access monomeric compounds of general formula **4**, which differ from known structures **1** for the additional 4-substitution on the 1-aza-2-oxobicyclo[5.3.0]decane scaffold (Fig. 1). Having secured synthetic access to such structures, and having established a preliminary SAR on the 4-position, we decided to study how two such structures could be connected, through a suitable linker attached onto a chemically modifiable functional group, to take advantage of a simultaneous interaction with two BIR domains, as previously reported by others.[55,57]

As to the connecting chemical function between the monomer unit and the linker, it has to be both chemically replaceable-modifiable, and compatible with preserving BIR-binding properties even after substantial structural modifications. Two such groups were known at the time when we designed our dimer assembly strategy: the C-terminus amide portion, used in several papers as an anchor point for dimer synthesis,[55,57] and the 4-substitution, which was proven by us to tolerate the introduction of various functional groups, including bulky substituents.[52] We named the latter compounds as head–head dimers **8**, while the former were labelled as tail–tail compounds **9**.

We reasoned that, in order to reach both binding sites in two BIR domains of a given IAP protein, the two monomeric AVPI mimetics would need to adopt specific—and possibly rather

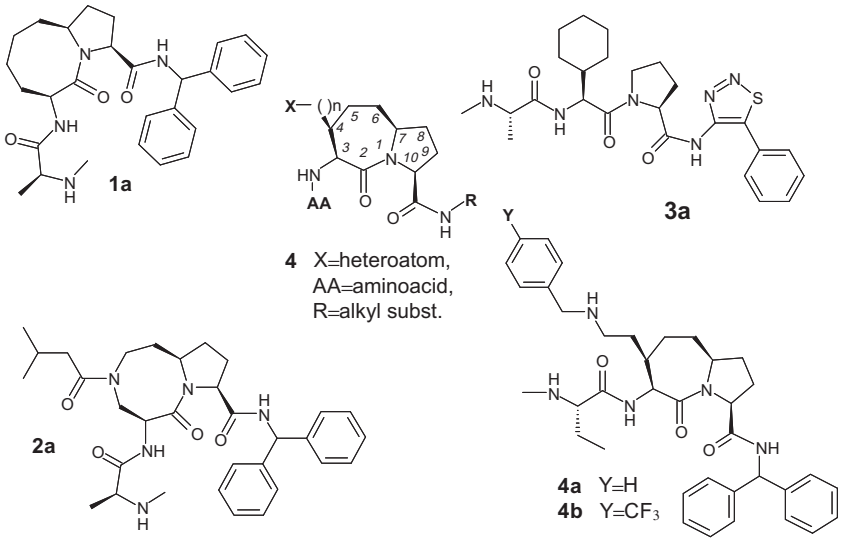

Figure 1. Monomeric Smac mimetics/IAP inhibitors.

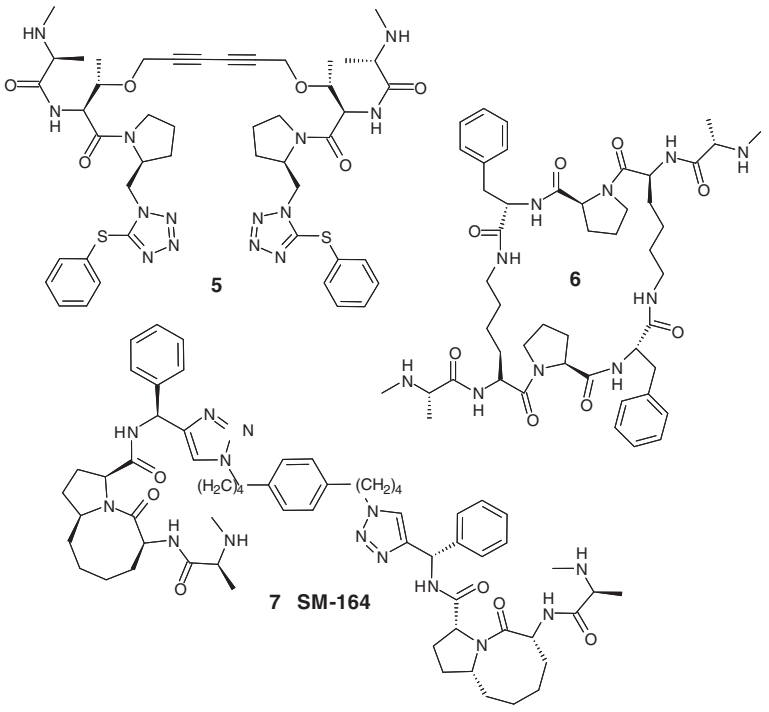

Figure 2. Previously reported dimeric Smac mimetics/IAP inhibitors.

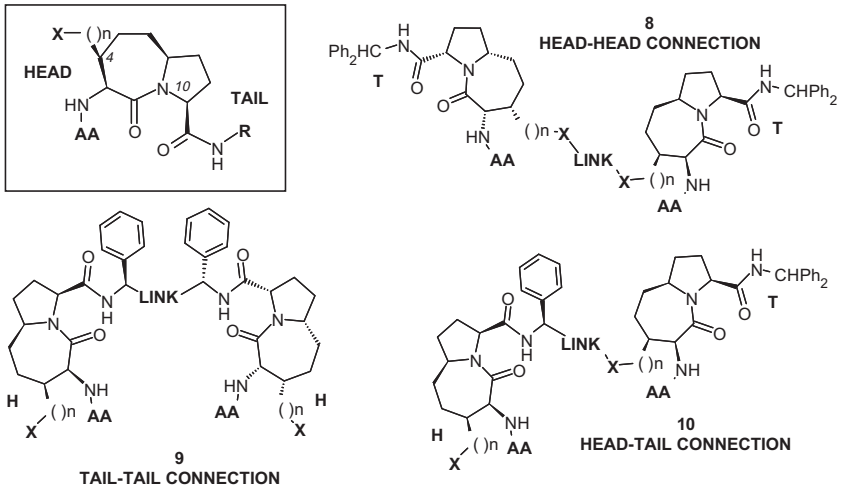

Figure 3. Head–head (**8**), tail–tail (**9**) and head–tail (**10**) dimeric Smac mimetics/IAP inhibitors based on the 1-aza-2-oxobicyclo[5.3.0]decane scaffold.

constrained—conformations. A graphically effective pictorial analogy of head–head, head–tail and tail–tail dimers is reported in Figure 4. It is likely that, to assume a relative orientation of both monomers in a given dimer **8** or **9** which would allow to bind simultaneously to two BIR targets, either one or both of the linked monomers should move away from their minimum energy state. It's also reasonable that their capability to reach such dimer binding conformation would be different, due to the constraints induced in dimer regions by a tail-tail or a head-head connection. We then reasoned that, if synthetically feasible, head-tail heterodimers **10** would also provide useful information in terms of binding modes, and obviously of dimers' structural requirements to maximize their pro-apoptotic effects (Fig. 4).

The linker unit, connecting two AVPI mimetics, is also going to influence the bi-functional binding potential of dimeric Smac mimetics. We selected several linking backbones, taking also advantage of reported efforts by other groups,[60] with the aim to explore how, *inter alia*, their length, flexibility and lipophilicity would influence the dimer activity. Some preferred linker structures are depicted in Figure 5.

2.2. Key monomers

Six monomeric intermediates were selected as synthetic gateways to our dimers. Their structure is shown in Figure 6, while their synthesis was previously reported.[52]

Namely, compound **4c** corresponds to the product of step ii, Scheme 1, Ref. 52; compound **4d** corresponds to the product of step iv, Scheme 1, Ref. 52; compounds **4e,f** and **4g,h** correspond, respectively, to compounds **8a,b** and **9a,b**, Scheme 1 in Ref. 52.

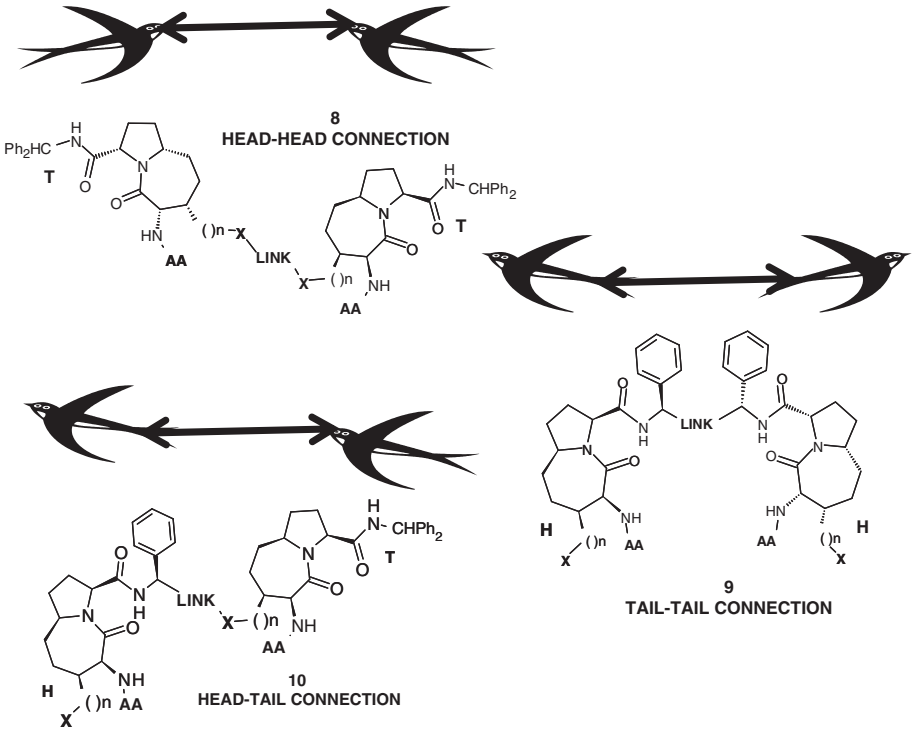

Figure 4. Heads, tails and swallows.

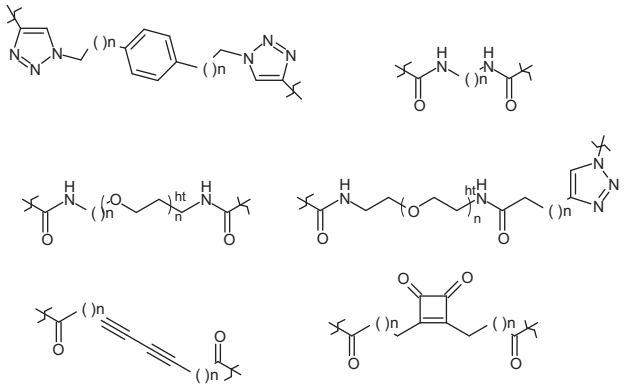

Figure 5. Preferred linker structures.

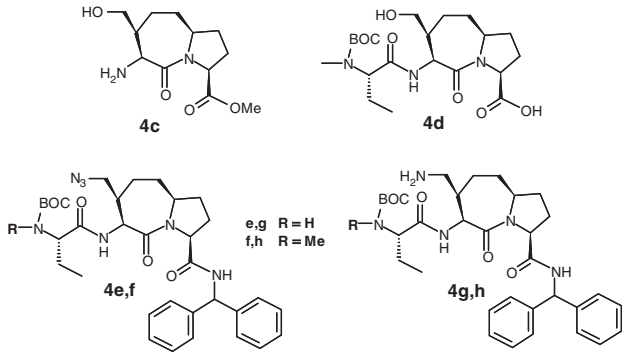

Figure 6. Key monomeric synthons for the synthesis of dimers **8**–**10**.

2.3. Head–head homodimers 8

Nine head–head homodimers **8** were synthesized. A diphenylmethylamide was the tail for all compounds **8**, while three of them contained (*S*)-ethylglycine and six contained *N*-methyl(*S*)-ethylglycine (AA, Fig. 3).

Amine **4g** was reacted with two alkynyl carboxylic acids (step a, Scheme 1) to provide high yields of 4-alkynyl amides **11a,b**. The amides were reacted with azide **4e** in a Cu-catalyzed click chemistry reaction (step b, Scheme 1) to provide good yields of *N*-Boc-protected dimers **12a**,**b**. Acidic deprotection with methanolic HCl (step c) provided high yields of head–head dimers **8a,b** as bishydrochlorides (Scheme 1). The unoptimized overall yields for **8a** and **8b** were, respectively, 38% and 42%.

Alkynylamide **11b** was oxidatively dimerized[55] in moderate yields (step a, Scheme 2) using copper (II) acetate, and the resulting symmetrical *N*-Boc-protected dimer **12c** was deprotected (step b) to provide quantitative yields of head–head dimer **8c** as a dihydrochloride (Scheme 2). The unoptimized overall yield for **8c** was 36%.

N-Methylamine **4h** was reacted with three biscarboxylates (step a, Scheme 3) to provide good yields of *N*-Boc-protected dimers **12d–f**. Acidic deprotection with TFA (step b) provided good to excellent yields of head–head dimers **8d–f** as bistrifluoroacetates (Scheme 3). The unoptimized overall yields for **8d**, **8e** and **8f** were, respectively, 44%, 53% and 39%.

N-Methylamine **4h** was also reacted with an alkynyl heptanoate (step a, Scheme 4) to provide *N*-methyl, 4-alkynyl amide **11c** in excellent yield. This was oxidatively dimerized[55] in excellent yields (step b) using copper (II) acetate, and the resulting symmetrical *N*-Boc-protected dimer **12g** was deprotected (step c) to provide moderate yields of head–head dimer **8g** as a dihydrochloride (Scheme 4). The unoptimized overall yield for **8g** was 30%.

The amide **11c** was also reacted with a known bis-azide[61] in a Cu-catalyzed click chemistry reaction (step a, Scheme 5) to provide moderate yields of the *N*-Boc-protected dimer **12h**. Acidic deprotection with TFA (step b) provided quantitative yields of the head–head dimer **8h** as a bistrifluoroacetate (Scheme 5). The unoptimized overall yield for **8h** was 29%.

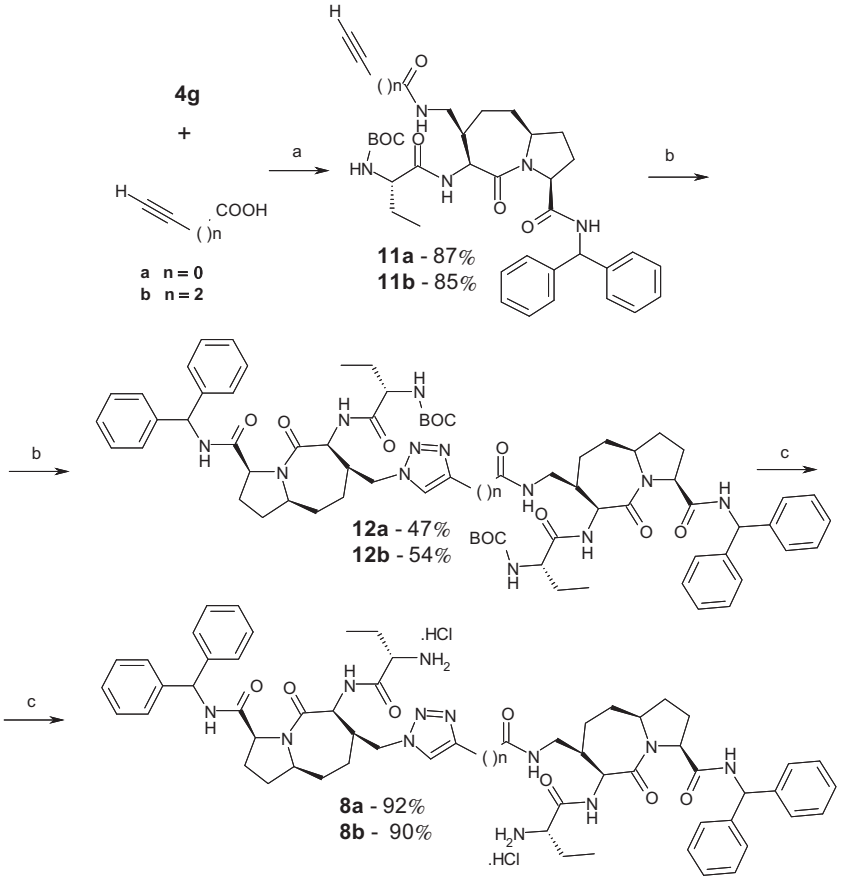

Scheme 1. Synthesis of head–head dimers **8a**,**b**.

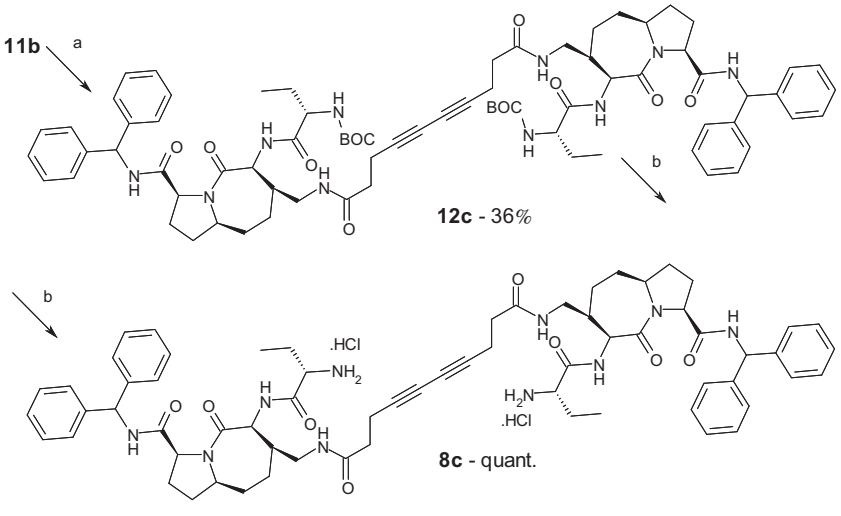

Scheme 2. Synthesis of head–head dimer **8c**.

Finally, *N*-methylamine **4h** was reacted with *N*-Cbz beta alanine (step a, Scheme 6) to provide *N*-methyl amide **11d** in quantitative yield. The amide was hydrogenolytically deprotected (step b) and reacted with diethyl squarate (step c) to give the symmetrical, *N*-Boc-protected dimer **12i** in excellent yield. Acidic deprotection with TFA (step d) provided excellent yields of the head–head dimer **8i** as a bistrifluoroacetate (Scheme 6). The unoptimized overall yield for **8i** was 75%.

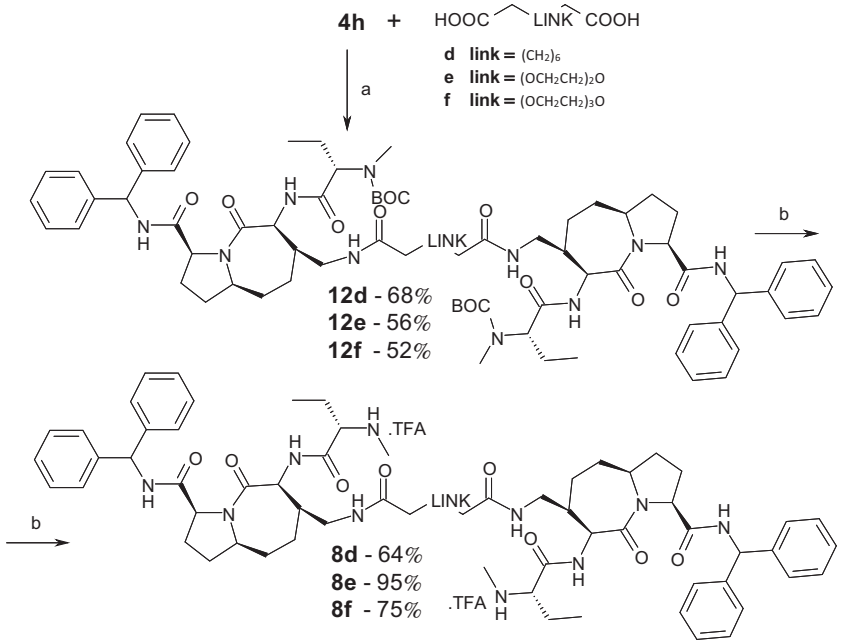

a, EDC, HOBt, DIPEA, CH_2Cl_2, rt, 2 hrs; b, TFA, CH_2Cl_2, rt, 4 hrs.

Scheme 3. Synthesis of head–head dimers **8d–f**.

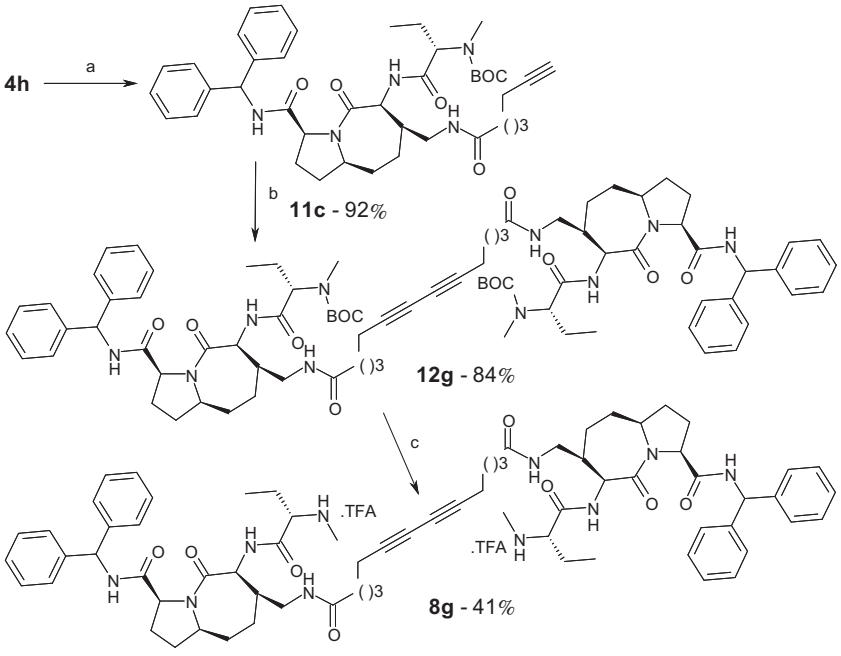

a, 6-heptynoic acid, EDC, HOBt, DIPEA, CH_2Cl_2, rt, 4 hrs; b, $Cu(OAc)_2$, CH_3CN, reflux, 0.5 hrs; c, TFA, CH_2Cl_2, rt, 4 hrs.

Scheme 4. Synthesis of head–head dimer **8g**.

2.4. Tail–tail homodimers 9

Seven tail–tail homodimers **9** were synthesized. *N*-methyl(*S*)-ethylglycine was present in all compounds **9** (AA, Fig. 3), while three different 4-substitutions (–CH_2OH in five compounds, -CH_2NHCH_2Ph and elongated –$CH_2CH_2NH_2$ in one compound) were introduced.

Carboxylic acid **4d** was reacted with an optically active alkynyl amine (step a, Scheme 7) to provide C-terminus-alkynyl amide **13a** in good yield. The amide was reacted with a known bis-azide[58] in a Cu-catalyzed click chemistry reaction (step b) to provide the *N*-Boc-protected dimer **14a** in good yield. Acidic deprotection with TFA (step c) provided tail–tail dimer **9a** as bistrifluoroacetate in good yield (Scheme 7). The unoptimized overall yield for **9a** was 29%.

A set of four tail–tail dimers **9b–e** was prepared by reaction of the same carboxylic acid **4d** with four bis-amine linkers **17a–d**. Such bis-amines were prepared from bis-amines **15a–d**[62] by

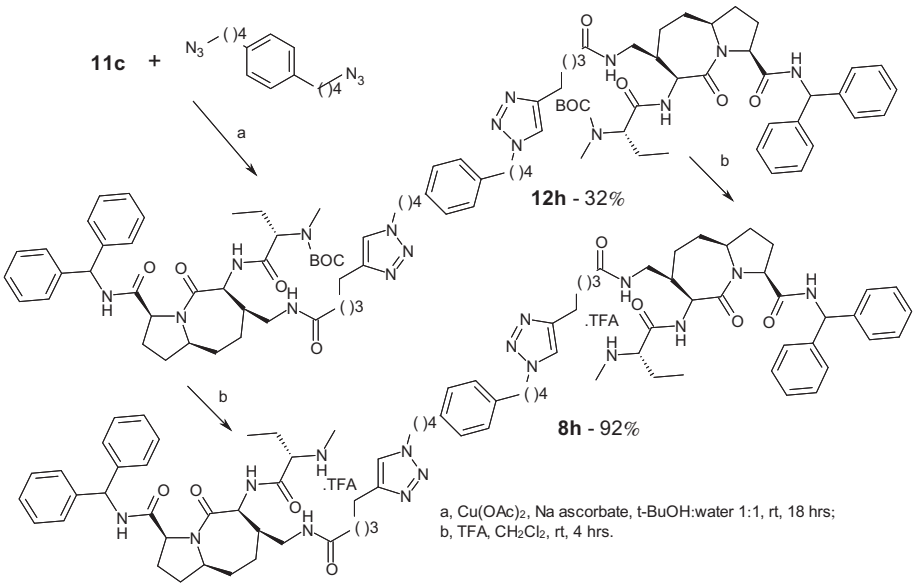

Scheme 5. Synthesis of head–head dimer **8h**.

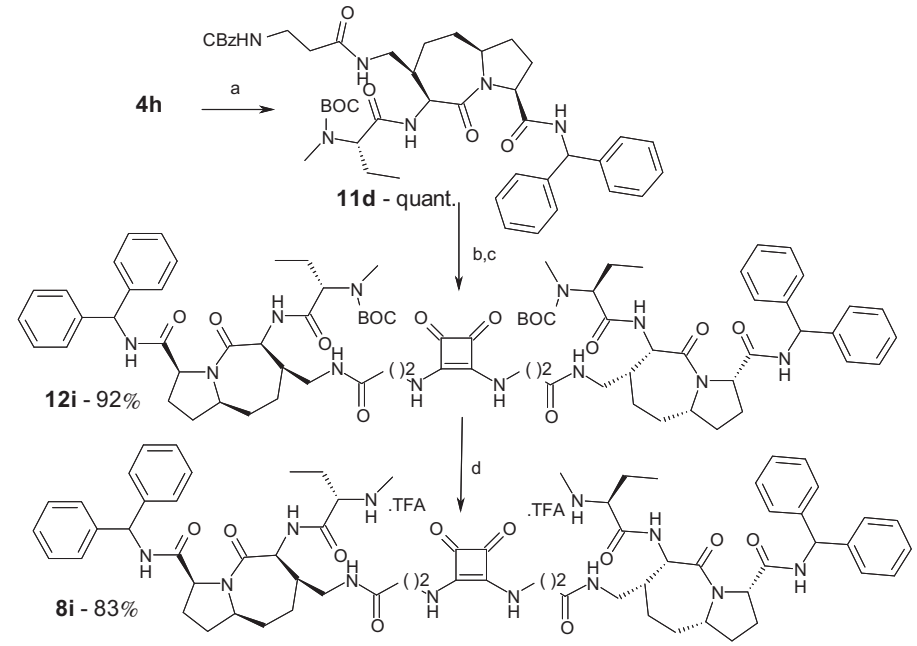

Scheme 6. Synthesis of head–head dimer **8i**.

condensation with (*S*)-phenylglycine (step a, Scheme 8) to give *N*-Boc protected compounds **16a–d** in excellent yields. Desired bis-amine linkers **17a–d** were obtained by TFA deprotection (step b) in quantitative yields (Scheme 8).

Carboxylic acid **4d** was reacted with four bis-amine linkers **17a–d** (step a, Scheme 9) to give, with good to excellent yields, *N*-Boc protected dimers **14b–e**. Acidic deprotection with TFA (step b) provided tail–tail dimers **9b–e** as bistrifluoroacetates in good to excellent yields (Scheme 9). The unoptimized overall yields for **9b–e**, starting from **4d** and **17a–d**, were, respectively, 53%, 73%, 31% and 56%.

N-Boc protected dimer **14a** was decorated on its 4-substitution to provide tail–tail dimer **9f** (Scheme 10). Namely, **14a** was mesylated and reacted with sodium azide (steps a, b) to give azide **14f** in good yield. The azide was reduced in a Staudinger reaction (step c) to give the amine **14g** in quantitative yield, and the amine was N-alkylated in a reductive amination protocol (step d) to provide the N-protected, benzylated dimer **14h** in moderate yields. Acidic

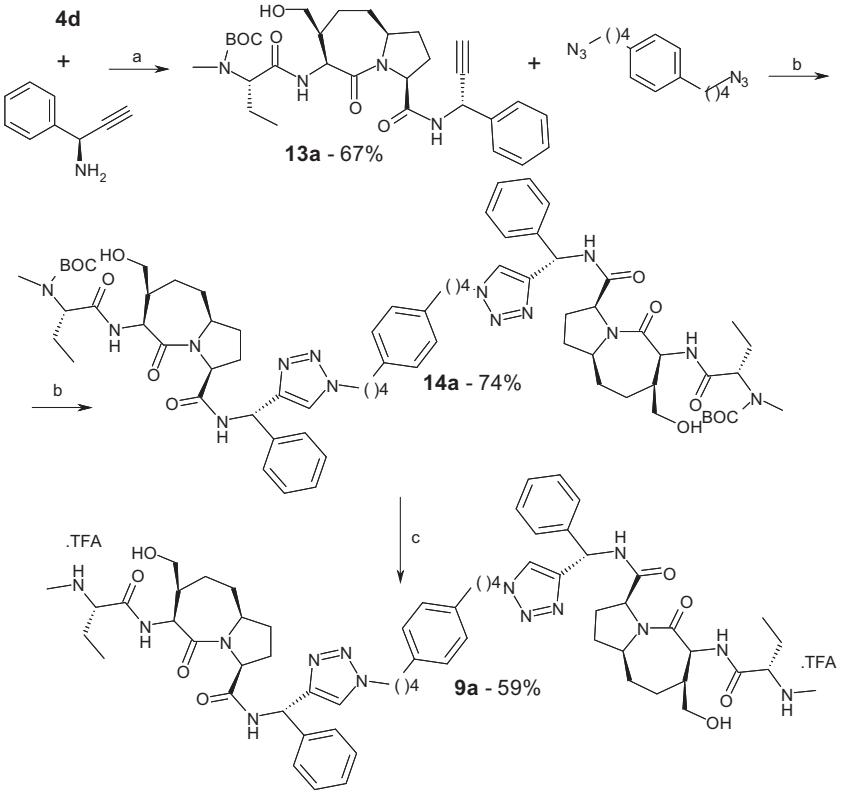

a, EDC, HOBt, DIPEA, dry CH_2Cl_2, rt, 2 hrs; b, $Cu(OAc)_2$, Na ascorbate, tBuOH:water 1:1, rt, 18 hrs; c,TFA, CH_2Cl_2, rt, 4 hrs.

Scheme 7. Synthesis of tail–tail dimer **9a**.

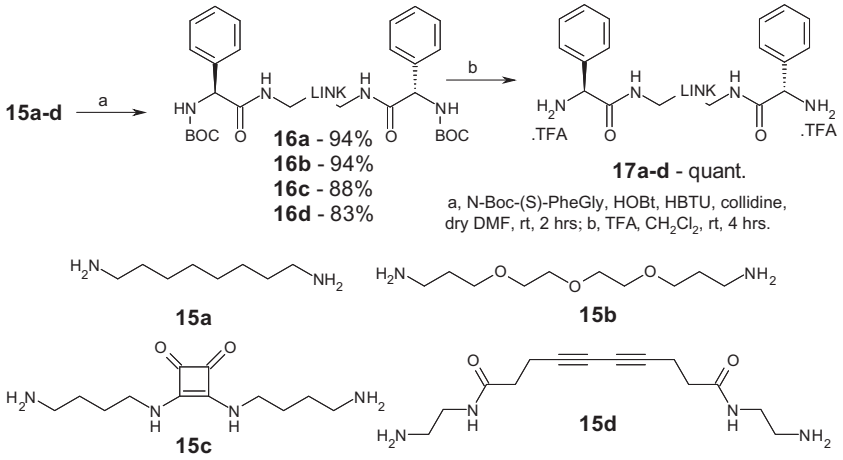

a, N-Boc-(S)-PheGly, HOBt, HBTU, collidine, dry DMF, rt, 2 hrs; b, TFA, CH_2Cl_2, rt, 4 hrs.

Scheme 8. Synthesis of bis-amine linkers **17a–d**.

deprotection with TFA (step e) provided tail–tail dimer **9f** as a tetratrifluoroacetate in good yield (Scheme 10). The unoptimized overall yield for **9f** from **14a** was 24%.

Finally, 4-hydroxymethyl methyl ester **4c** was *N*-Boc protected, mesylated and reacted with a tetraalkyl ammonium cyanide (steps a–c, Scheme 11) to provide the cyano compound **13b** in good yield. After N-deprotection and condensation with N-protected and methylated (*S*)-ethylglycine (steps d,e) to yield **13c**, the cyano group was reduced, and the resulting amine was protected with Boc in a one-pot reaction protocol (steps f,a) to give the *N*-Boc protected, elongated amine **13d** in moderate yield. After quantitative basic hydrolysis of the methyl ester (step g), the acid **13e** was reacted with previously described bis-amine **17b** (step h) to give tetra *N*-Boc protected dimer **14i** in good yields. Acidic deprotection with TFA (step i) provided elongated tail–tail dimer **9g** as a tetratrifluoroacetate in good yield (Scheme 11). The unoptimized overall yield for **9g** was 12%.

2.5. Head–tail heterodimers 10

Three head–tail heterodimers **10** were synthesized together with a hybrid heterodimeric structure. *N*-Methyl(*S*)-ethylglycine

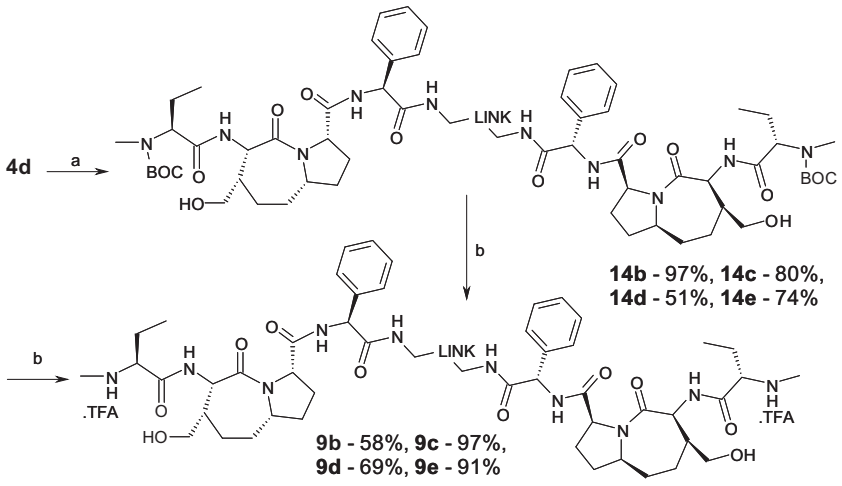

a, **17a-d**, HOBt, HBTU, collidine, dry DMF, 0° to rt, 2 hrs; b, TFA, CH_2Cl_2, rt, 4 hrs.

Scheme 9. Synthesis of tail–tail dimers **9b**–**e**.

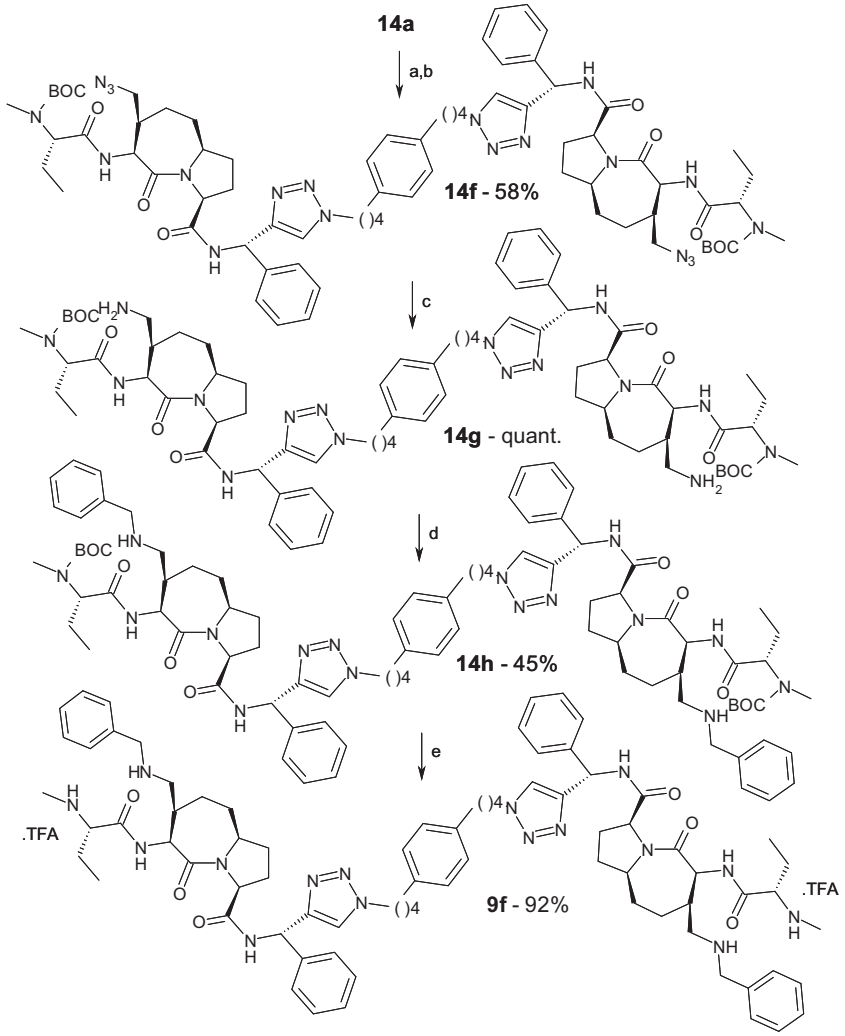

a, MsCl, TEA, dry CH_2Cl_2, 0° to rt, 2 hrs; b, NaN_3, dry DMF, 100° C, 0.5hrs; c, Me_3P, dry CH_2Cl_2, rt, 2 hrs; d, PhCHO, $NaBH(OAc)_3$, dry CH_2Cl_2, rt, 18 hrs; e, TFA, CH_2Cl_2, rt, 4 hrs.

Scheme 10. Synthesis of tail–tail dimer **9f**.

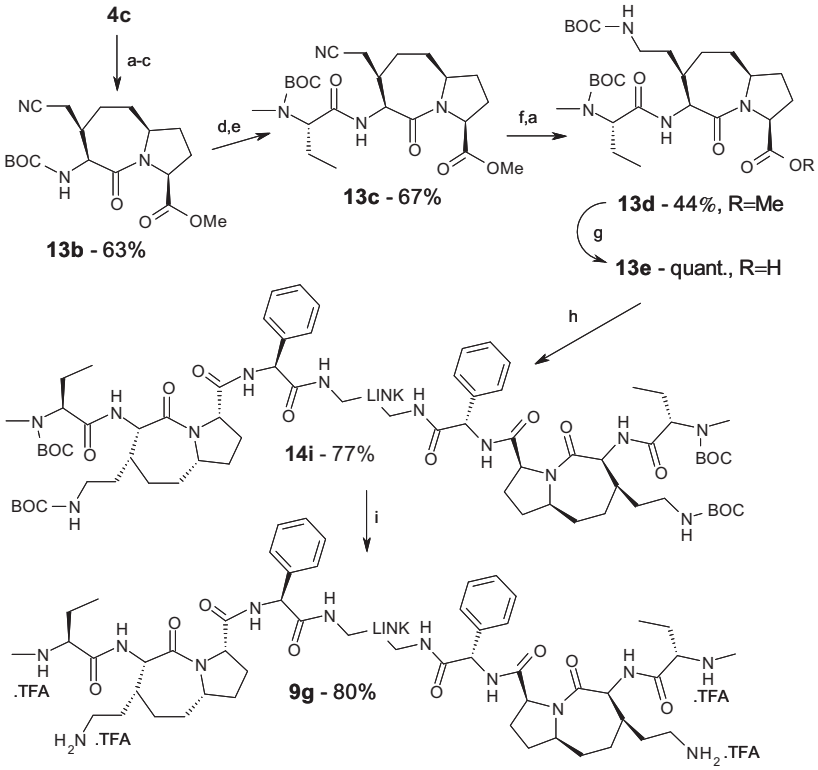

a, Boc_2O, TEA, CH_2Cl_2, rt, 2 hrs; b, MsCl, TEA, CH_2Cl_2, rt, 2 hrs; c, $nBu_4N^+CN^-$, DMF, microwave, 80°C, 1.5 hrs; d, 3N HCl in MeOH, rt, 18 hrs; e, N-Boc,N-Me-(S)-2aminobutanoic acid, EDC, HOBt, DIPEA, dry CH_2Cl_2, rt, 2 hrs; f, Ni Raney, EtOH, continuous flow, 60 bar, 60°C, 6 hrs; g, 2N LiOH, 1,4-dioxane:water, 0°C to rt, 1 hr; h, **17b**, HOBt, HBTU, collidine, dry DMF, rt, 18 hrs; i, TFA, CH_2Cl_2, rt, 4 hrs.

Scheme 11. Synthesis of tail–tail dimer **9g**.

(AA, Fig. 3), 4-CH_2OH substitution, and a diphenylmethyl amide tail were conserved in the three heterodimers, while the hybrid structure connected the head of a 1-aza-2-oxobicyclo[5.3.0]decane scaffold-based AVPI mimetic with a structurally different, known[55] monomeric unit.

Four key tail-linker monomeric intermediates **18a–d** were prepared as shown in Scheme 12. Commercially available azidoamine **15e** was first reacted with (*S*)-phenylglycine (step a) to give intermediate **16e** in good yield, then N-deprotected (step b). Coupling with **4d** (step c) provided the linker-bearing monomeric azide **18a** in excellent yield. After catalytic hydrogenation (step d) of the same azide to provide quantitatively the linker-bearing monomeric amine **18b**, the same amine was either coupled with 4-pentynyl-butanoic acid (step e) to give the linker-bearing monomeric alkyne **18c** with excellent yield, or with diglycolic anhydride (step f) to give the linker-bearing monomeric carboxylate **18d** (Scheme 12).

Linker-bearing monomeric azide **18a** was coupled in a click chemistry reaction with 4-alkynyl amide **11e** (step b, Scheme 13), this last prepared from **4h** (step a), to provide in good yield the N-protected head–tail heterodimer **19a**. Acidic deprotection with TFA (step c) provided head–tail heterodimer **10a** as a bistrifluoroacetate in excellent yield (Scheme 13). The unoptimized overall yield for **10a** was 55% from **18a**.

Linker-bearing alkyne **18c** was coupled in a click chemistry reaction with azide **4f** (step a, Scheme 14) to provide in very good yield the N-protected head–tail heterodimer **19b**. Acidic deprotection with TFA (step b) provided head–tail heterodimer **10b** as a bistrifluoroacetate in excellent yield (Scheme 14). The unoptimized overall yield for **10b** was 69% from **18c**.

Linker-bearing carboxylate **18d** was coupled with amine **4h** (step a, Scheme 15) to provide in very good yield the N-protected head–tail heterodimer **19c**. Acidic deprotection with TFA (step b) provided head–tail heterodimer **10c** as a bistrifluoroacetate in excellent yield (Scheme 15). The unoptimized overall yield for **10c** was 59% from **18d**.

Finally, a heterodimer containing two linker-connected AVPI mimetics based on different scaffolds was prepared as in Scheme 16. Namely, azide **4e** was coupled in a click chemistry reaction with N-protected alkyne-containing Smac mimetic **20a**[55] (step a) to give *N*-Boc, *N*-Fmoc protected heterodimer **19d** in good yield. Sequential deprotection in basic (step b) and acidic (step c) conditions produced the hybrid heterodimer **10d** in excellent yield. The unoptimized overall yield for **10d** was 51%.

3. Conclusions

The chemical feasibility of head head-**8**, tail tail-**9** and head tail-**10** dimers based on 4-substituted 1-aza-2-oxobicyclo[5.3.0]decane scaffolds was successfully proven through the synthesis of 20 compounds, bearing various 4-substitutions. The monomer units in each dimer were connected through linkers with varying length, lipophilicity and flexibility.

Extensive details regarding the biological activity of each prepared dimer, and the structural characterization of selected homodimers using NMR, X-ray crystallography and gel filtration are provided in the following paper.[58] Their activity profiling will drive our future synthetic efforts towards the more prospective homo- and heterodimers. Such efforts will be reported in due time.

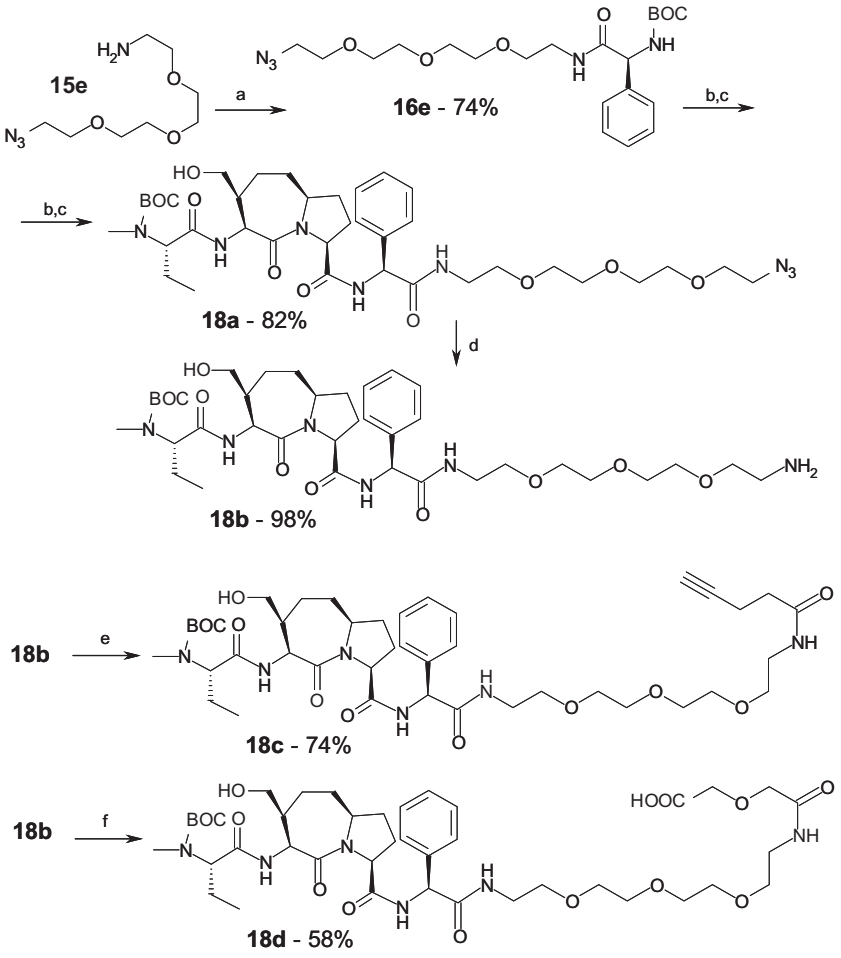

a, N-Boc-(S)-phenylglycine, HOBt, HBTU, collidine, dry DMF, 0° to rt, 2 hrs; b, TFA, CH_2Cl_2, rt, 4 hrs; c, **4d**, HOBt, HBTU, collidine, dry DMF, 0° to rt, 2 hrs; d, H_2, Pd/C, continuous flow, 10 bar, 35°C; e, 4-pentynoic acid, DCC, DMAP, dry CH_2Cl_2, 0° to rt, 4 hrs; f, diglycolic anhydride, pyridine, dry DMF, rt, 4 hrs.

Scheme 12. Synthesis of tail-linker monomeric intermediates **18a–d**.

4. Experimental part

4.1. General methods

^{1}H NMR spectra were recorded on a Bruker Avance instrument in $CDCl_3$, CD_3OD or D_2O as solvent at 400 or 600 MHz. ^{13}C NMR spectra were recorded in $CDCl_3$, CD_3OD or D_2O as solvent at 100 or 125 MHz. Coupling constants are given in Hertz, Hz, and are rounded to the nearest 0.1 Hz.

Purifications were carried out either by flash chromatography on silica gel (particle size 60 μm, 230–400 mesh), Kieselgel, or by Biotage™ flash chromatography [Biotage columns Si-12-M (150 × 12 mm; silica gel (40–63 lm), flow rate 12 mL/min); Si-25-M (150 × 25 mm; silica gel (40–63 μm), flow rate 25 mL/min)], or by Biotage™ C_{18} reverse phase chromatography [Biotage column C_{18}HS (150 × 25 mm; KP-C_{18}-HS (35–70 μm), flow rate 25 mL/min)]. Final products were purified by C_{18} reverse phase semi-preparative HPLC using either a Waters X-Terra RP_{18} OBD column (19 mm × 10.0 cm, 5 μm) or a Supelco Ascentis C_{18} column (21.2 mm × 15.0 cm, 5 μm).

LC–MS data were collected with an Agilent 1100 HPLC connected to a Bruker Esquire 3000$^+$ ion trap mass spectrometer through an ES interface.

Optical rotations $[\alpha]_{20}^{D}$ were measured in cells of 1 dm pathlength and 1 mL capacity with a Perkin Elmer 241 polarimeter.

Solvents were distilled and dried according to standard procedures, and reactions requiring anhydrous conditions were performed under nitrogen or argon. Solvents for the reactions were used directly from the bottle if not differently specified.

Standard dimers **3**[55] and **5**[57] were prepared according to the published procedure.

4.2. Head–head dimer 8a—Scheme 1

4.2.1. Compound 11a

A solution of DCC (20.6 mg, 0.10 mmol) and DMAP (2.4 mg, 0.02 mmol) in dry CH_2Cl_2 (10 mL) was added dropwise to a stirred solution of compound **4g (**59.2 mg, 0.10 mmol) and propiolic acid (6.2 μL, 0.10 mmol) in dry CH_2Cl_2 (10 mL) at 0 °C. After the addition, the reaction mixture was warmed to room temperature over a period of 1 h. After reaction completion, the reaction mixture was filtered, and the filtrate was washed with diethyl ether (2 × 10 mL). The combined organic phase was concentrated under reduced pressure, and the crude product was purified by Biotage™ flash chromatography, eluant conditions: 1% of MeOH and 99% of CH_2Cl_2 to 10% of MeOH and 90% of CH_2Cl_2. Yield 85% (55 mg, MW 644.32, 0.085 mmol) of pure **11a**. Analytical characterization: $[\alpha]_{20}^{D}$ −81.4 (c 0.75, MeOH); ^{1}H NMR (400 MHz, $CDCl_3$): δ: 7.91 (d, J = 8.8 Hz, 1H), 7.50–7.10 (m, 11H), 6.24 (d, J = 8.4 Hz, 1H), 5.00 (d, J = 6.4 Hz, 1H), 4.75 (d, J = 7.2 Hz, 1H), 4.64 (t, J = 9.2 Hz, 1H), 4.20 (dd,

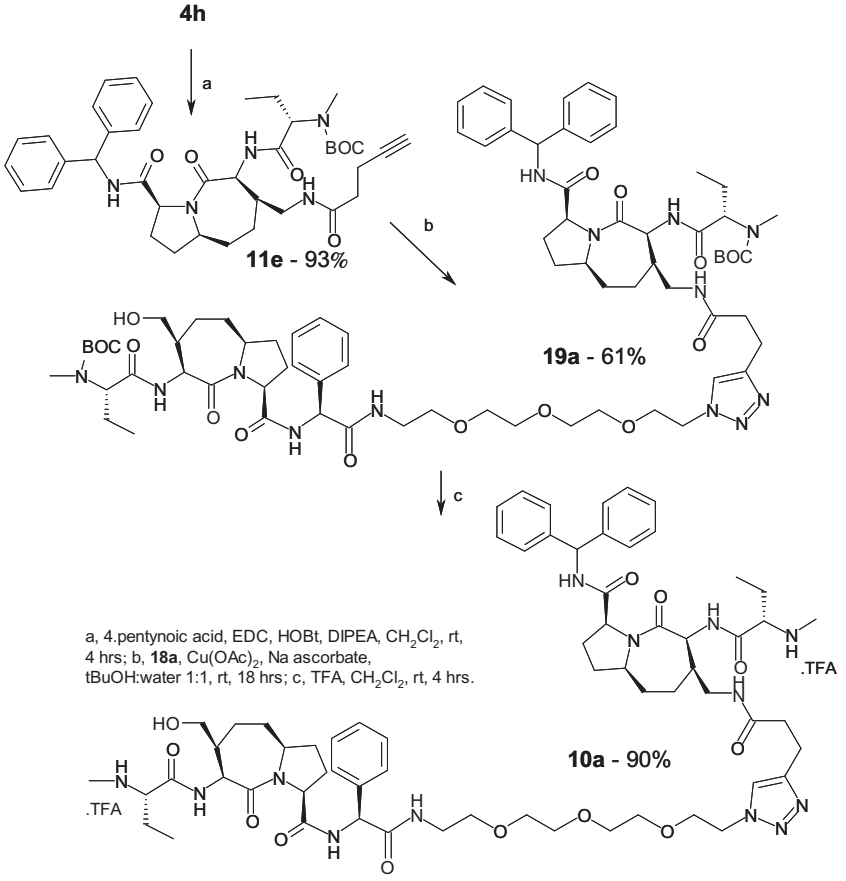

Scheme 13. Synthesis of head–tail dimer **10a**.

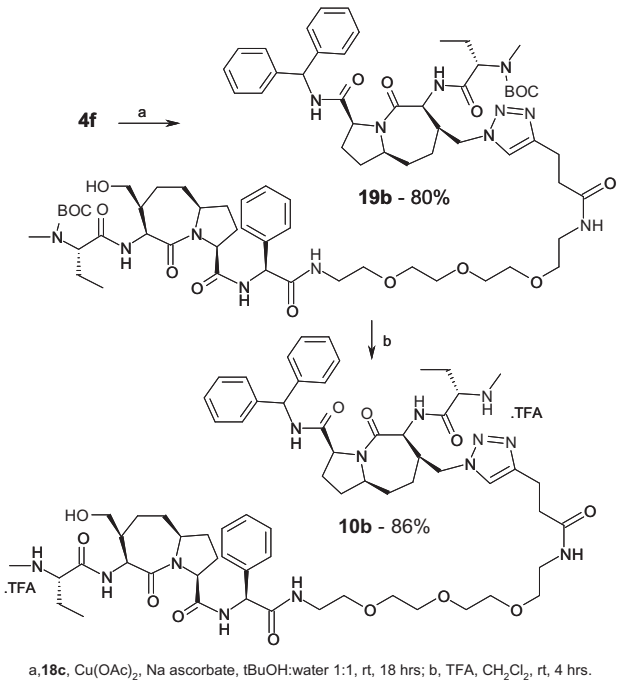

Scheme 14. Synthesis of head–tail dimer **10b**.

J = 10.8, 7.2 Hz, 1H), 4.06 (m, 2H), 3.85 (q, J = 8.4 Hz, 1H), 2.95 (s, 1H), 2.45 (m, 1H), 2.28 (m, 1H), 2.0–1.55 (m, 7H), 1.47 (s, 9H), 1.35–1.10 (m, 2H), 0.97 (t, J = 7.6 Hz, 3H); ^{13}C NMR (100 MHz, $CDCl_3$): δ: 172.4, 171.3, 169.5, 155.5, 152.2, 142.1, 141.1, 128.7, 127.3, 80.2, 74.6, 68.0, 61.0, 58.7, 56.8, 53.0, 39.1, 34.2, 33.3, 31.3, 28.3, 25.6, 10.4.

4.2.2. Compound 12a

A 0.9 M water solution of sodium ascorbate (45 μL, 0.4 mmol) and a 0.3 M water solution of $Cu(OAc)_2$ (65 μL, 0.02 mmol) were sequentially added to a stirred solution of compounds **4e** (61.8 mg, 0.10 mmol) and **11a** (64.4 mg, 0.10 mmol) in a 1:1 mixture of H_2O/^{t}BuOH (300 μL). The reaction mixture was stirred overnight at room temperature, and then the solvent was removed under reduced pressure. Finally, the residue was purified by Biotage™ flash chromatography, eluant conditions: 1% of MeOH and 99% of CH_2Cl_2 to 10% of MeOH and 90% of CH_2Cl_2. Yield 47% (59 mg, MW 1261.54, 0.047 mmol) of pure **11a**. Analytical characterization: $[\alpha]^D_{20}$ −64.3 (c 0.51, $CHCl_3$); ^{1}H NMR (400 MHz, $CDCl_3$): δ: 7.82 (d, J = 14.0, 1H), 7.73 (d, J = 8.4 Hz, 1H), 7.32–7.00 (m, 24H), 6.12 (t, J = 8 Hz, 2H), 5.07 (d, J = 5.6 Hz, 1H), 4.91 (d, J = 11.2 Hz, 1H), 4.64 (t, J = 6.4 Hz, 2H), 4.55 (m, 3H), 4.14 (t, J = 11.6 Hz, 1H), 3.98 (m, 2H), 3.73 (m, 3H), 3.14 (d, J = 12.0 Hz, 1H), 2.34 (m, 2H), 2.16 (m, 2H), 2.0–1.40 (m, 16H), 1.31 (s, 18H), 1.19 (s, 2H), 0.90 (m, 6H); ^{13}C NMR (100 MHz, $CDCl_3$): δ: 173.1, 171.7, 170.6, 169.4, 169.2, 160.4, 142.1, 141.8, 141.0, 128.8, 128.7, 127.7, 127.5, 127.4, 127.2, 127.1, 61.3, 61.1, 58.8, 56.8, 56.7, 54.0, 53.7, 40.7, 40.6, 40.2, 34.4, 33.8, 33.3, 33.2, 31.4, 25.7, 25.5, 25.4, 10.3.

4.2.3. Compound 8a

A 3 N solution of HCl in MeOH (0.5 mL) was added to a stirred solution of compound **12a** (7.6 mg, 0.006 mmol) in MeOH (2 mL). The reaction mixture was left stirring at room temperature overnight and then concentrated under reduced pressure. The

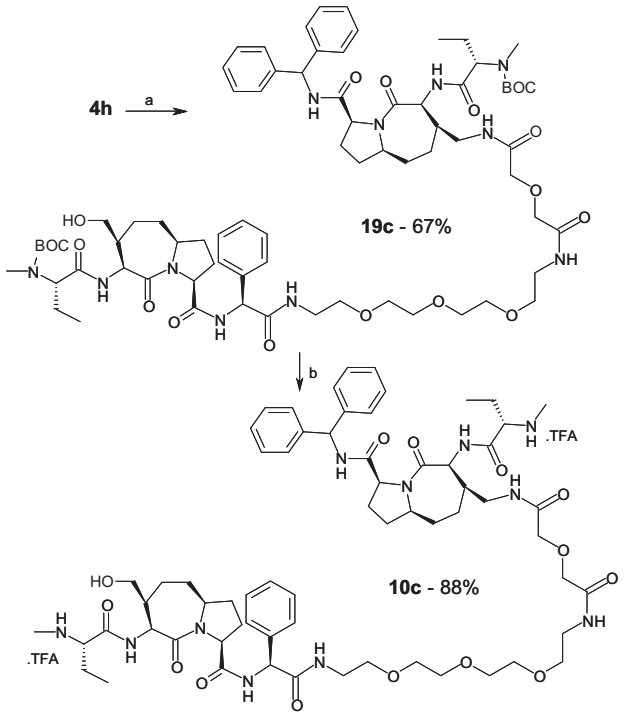

Scheme 15. Synthesis of head–tail dimer **10c**.

residue did not require any further purification, and was lyophilized. Yield 92% (6 mg, MW 1134.22, 0.0055 mmol) of pure **8a**. Analytical characterization: $[\alpha]_{20}^{D}$ −39.1 (*c* 0.23, H_2O); ^{1}H NMR (400 MHz, D_2O): δ: 8.35 (s, 1H), 7.32–7.18 (m, 20H), 5.97 (m, 2H), 4.61 (m, 3H), 4.48 (m, 2H), 4.35 (m, 1H), 3.9 (m, 4H), 3.50 (dd, *J* = 13.6, 8.4 Hz, 1H), 3.28 (dd, *J* = 12.8, 8.4 Hz,1H), 2.25–1.35 (m, 22H), 0.95 (m, 6H); ^{13}C NMR (100 MHz, D_2O): δ: 172.7, 170.5, 169.8, 169.7, 161.9, 142.2, 141.0, 140.9, 129.0, 128.9, 127.8, 127.4, 127.1, 61.9, 58.6, 58.4, 57.6, 54.5, 54.4, 54.3, 41.0, 38.6, 38.1, 32.4, 32.3, 27.8, 24.4, 8.5, 8.4. ESI-MS: m/z 1061.5 $[M+H]^+$1083.6 $[M+Na]^+$, 531.3 $[M+2H]^{2+}$.

4.3. Head–head dimer 8b—Scheme 1

The head–head dimer **8b** was prepared similarly to **8a**. The detailed synthetic protocol leading to its synthesis, and its full synthetic characterization are reported in the Supplementary data.

4.4. Head–head dimer 8c—Scheme 2

4.4.1. Compound 12c

A stirred suspension of compound **11b** (67.2 mg, 0.10 mmol) and $Cu(OAc)_2$ (127.1 mg, 0.70 mmol) in acetonitrile (20 mL) was refluxed for 30 min After reaction completion, the solvent was removed under reduced pressure, the residue was dissolved in CH_2Cl_2 and Cu(II) salts were removed by filtering over a short pad of silica gel eluting with 9/1 CH_2Cl_2/MeOH. Finally, the crude products was purified by Biotage™ flash chromatography, eluant conditions: 1% of MeOH and 99% of CH_2Cl_2 to 10% of MeOH and 90% of CH_2Cl_2. Yield 36% (48 mg, MW 1341.67, 0.036 mmol) of pure **12c**. Analytical characterization: $[\alpha]_{20}^{D}$ −69.3 (*c* 0.96, $CHCl_3$); ^{1}H NMR (400 MHz, $CDCl_3$): δ: 7.90 (d, J = 6.8 Hz, 2H), 7.36–7.16 (m, 25H), 6.22 (d, J = 8.0 Hz, 1H), 5.05 (bd, *J* = 6.4 Hz, 2H), 4.72 (d, *J* = 8.0 Hz, 2H), 4.49 (t, *J* = 9.6 Hz, 2H), 3.98 (dd, *J* = 13.6, 7.6 Hz, 2H), 3.81 (dd, *J* = 17.6, 8.8, 2H), 3.58 (m, 2H), 3.01 (m, 1H), 2.58 (m, 4H), 2.40 (m, 6H), 2.25 (m, 2H), 1.95–1.55 (m, 16H), 1.45 (s, 18H), 1.30–1.10 (m, 2H), 1.00 (t, *J* = 7.6 Hz, 6H); ^{13}C NMR13C NMR (100 MHz, $CDCl_3$): δ: 173.6, 171.7, 170.8, 169.4, 141.2, 140.8, 128.6, 127.5, 127.4, 127.2, 80.5, 66.0, 61.2, 58.9, 57.0, 56.8,

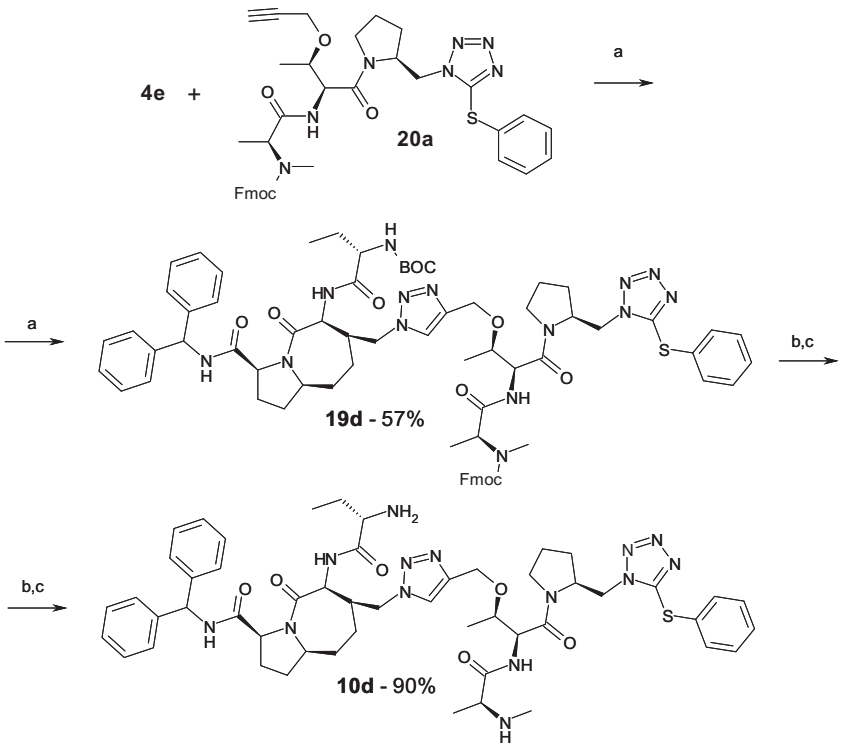

Scheme 16. Synthesis of head–tail dimer **10d**.

54.0, 41.3, 40.0, 35.3, 34.5, 33.2, 28.3, 25.7, 25.2, 15.9, 10.3. ESI-MS: m/z 1342.9 $[M+H]^+$, 1363.9 $[M+Na]^+$.

4.4.2. Compound 8c

A 3 N solution of HCl in MeOH (0.5 mL) was added to a stirred solution of compound **12c** (18.5 mg, 0.014 mmol) in MeOH (2 mL). The reaction mixture was left stirring at room temperature overnight and then concentrated under reduced pressure. The residue did not require any further purification, and was lyophilized. Quantitative yield (17 mg, MW 1214.35, 0.014 mmol) of pure **8c**. Analytical characterization: $[\alpha]_{20}^{D}$ −43.1 (*c* 0.90, H_2O); ^1H NMR (400 MHz, D_2O): δ: 7.35–7.20 (m, 20H), 5.95 (s, 2H), 4.56 (d, *J* = 10.4 Hz, 2H), 4.50 (dd, *J* = 7.6, 4.8 Hz, 2H), 3.98 (m, 4H), 3.23 (dd, *J* = 13.6, 3.2 Hz, 2H), 3.06 (m, 2H), 2.45–2.30 (m, 4H), 2.25–1.40 (m, 26H), 0.97 (t, *J* = 7.2 Hz, 6H); ^{13}C NMR (100 MHz, D_2O): δ: 174.3, 172.4, 170.4, 169.6, 141.1, 140.9, 129.0, 128.9, 127.9, 127.8, 127.4, 127.0, 65.8, 61.7, 58.4, 57.7, 54.5, 54.4, 40.7, 37.6, 34.3, 32.6, 30.7, 27.8, 24.4, 15.5, 8.5. ESI-MS: m/z 1163.3 $[M+Na]^+$, 571.1 $[M+2H]^{2+}$.

4.5. Head–head dimer 8d—Scheme 3

4.5.1. Compound 12d

EDC·HCl (23 mg, 0.12 mmol), HOBt (16.2 mg, 0.12 mmol) and DIPEA (69.7 μL, 0.40 mmol) were sequentially added to a stirred solution of 1,10-decanedioic acid (9.7 mg, 0.048 mmol) in dry CH_2Cl_2 (2 mL) at room temperature. The reaction mixture was left stirring for 15 min and then added to a stirred solution of **4h** (60.6 mg, 0.10 mmol) in dry CH_2Cl_2 (2 mL). The reaction mixture was stirred at room temperature overnight and then, after reaction completion, the solvent was removed under reduced pressure. The crude product was diluted with EtOAc (20 mL) and washed with a saturated solution of ammonium chloride (3 × 20 mL), saturated solution of sodium bicarbonate (3 × 20 mL) and brine (1 × 20 mL). The organic layer was dried over Na_2SO_4, and then the solvent removed under reduced pressure. The residue was purified by Biotage™ flash chromatography, eluant conditions: 1% of MeOH and 99% of CH_2Cl_2 to 10% of MeOH and 90% of CH_2Cl_2. Yield 68% (48 mg, MW 1376.71, 0.034 mmol) of pure **12d**. Analytical characterization: $[\alpha]_{20}^{D}$ −96 (*c* 1.34, $CHCl_3$); ^1H NMR (400 MHz, $CDCl_3$): δ: 7.82 (bs, 2H), 7.30–7.05 (m, 22H), 6.07 (m, 2H), 6.14 (d, *J* = 8.0 Hz, 2H), 4.66 (d, *J* = 7.2 Hz, 2H), 4,38 (m, 4H), 3.68 (m, 2H), 3.54 (m, 2H), 2.77 (m, 8H), 2.35 (m, 2H), 2.15 (m, 2H), 2.10 (m, 4H), 1.95–1.45 (m, 22H), 1.40 (s, 18H), 1.30–1.15 (m, 10H), 1.05 (m, 2H), 0.85 (m, 6H); ^{13}C NMR (100 MHz, $CDCl_3$): δ: 173.6, 172.8, 171.8, 169.3, 142.2, 128.6, 127.4, 127.3, 127.2, 61.1, 60.5, 58.9, 56.8, 53.7, 40.0, 37.0, 34.5, 33.2, 29.4, 28.3, 25.8, 25.5, 21.5, 10.7. ESI-MS: m/z 1377.4 $[M+H]^+$, 589.2 $[M+2H]^{2+}$.

4.5.2. Compound 8d

TFA (450 μL, 5.0 mmol) was added to a stirred solution of compound **12d** (37.8 mg, 0.028 mmol) in CH_2Cl_2 (2 mL). The reaction mixture was left stirring at room temperature overnight and then concentrated under reduced pressure. The residue was purified by chromatography on a C_{18} reverse phase semi-preparative hplc column, eluant conditions: from 70% of H_2O (0.2% TFA) and 30% of CH_3CN (0.2% TFA) to 30% of H_2O (0.2% TFA) and 70% of CH_3CN (0.2% TFA), flow rate 12 mL/min, 20 min runs. Yield 64% (25.3 mg, MW 1405.59, 0.018 mmol) of pure **8d**. Analytical characterization: $[\alpha]_{20}^{D}$ −61 (*c* 1.06, CH_3OH); ^1H NMR (400 MHz, D_2O): δ: 8.80 (m, 2H), 7.40–7.20 (m, 20H), 6.14 (s, 2H), 4.67 (m, 4H), 4.00 (m, 2H), 3.87 (bs, 2H), 3.44 (d, *J* = 13.6 Hz, 2H), 3.01 (t, *J* = 10 Hz, 2H), 2.70 (s, 6H), 2.85–2.70 (m, 6H), 2.70–1.75 (m, 16H), 1.70–1.55 (m, 8H), 1.32 (s, 8H), 1.05 (d, *J* = 7.0 Hz, 6H); ^{13}C NMR (100 MHz, D_2O): δ: 175.1, 171.6, 169.6, 167.5, 141.7, 141.5, 128.3, 128.1, 127.2, 127.1, 126.9, 62.6, 61.5, 58.2, 57.0, 54.3, 40.9, 38.2, 35.7, 32.7, 31.7, 31.0, 30.0, 28.9, 27.5, 25.6, 23.3, 8.0. ESI-MS: m/z 1177.6 $[M+H]^+$, 589.2 $[M+2H]^{2+}$.

4.6. Head–head dimers 8e,f—Scheme 3

The head–head dimers **8e** and **8f** were prepared similarly to **8d**. The detailed synthetic protocols leading to their synthesis, and their full synthetic characterization are reported in the Supplementary data.

4.7. Head–head dimer 8g—Scheme 4

4.7.1. Compound 11c

EDC·HCl (23 mg, 0.12 mmol), HOBt (16.2 mg, 0.12 mmol) and DIPEA (69.7 μL, 0.40 mmol) were sequentially added to a stirred solution of 6-heptynoic acid (15.2 μL, 0.12 mmol) in CH_2Cl_2 (2 mL) at room temperature. The reaction mixture was left stirring for 15 min and then added to a stirred solution of **4h** (60.6 mg, 0.10 mmol) in dry CH_2Cl_2 (2 mL). The reaction mixture was stirred at room temperature overnight and then, after reaction completion, the solvent was removed under reduced pressure. The crude product was diluted with EtOAc (20 mL) and washed with a saturated solution of ammonium chloride (3 × 20 mL), saturated solution of sodium bicarbonate (3 × 20 mL) and brine (1 × 20 mL). The organic layer was dried over Na_2SO_4, and then the solvent removed under reduced pressure. The residue was purified by Biotage™ flash chromatography, eluant conditions: from 50% of EtOAc and 50% of Petroleum ether to 100% of EtOAc. Yield 92% (65 mg, MW 713.42, 0.092 mmol) of pure **11c**. Analytical characterization: $[\alpha]_{20}^{D}$ −75 (*c* 0.90, $CHCl_3$); ^1H NMR (400 MHz, $CDCl_3$): δ: 7.92 (bs, 1H), 7.40–7.15 (m, 11H), 6.23 (d, *J* = 8.4 Hz, 1H), 4.75 (d, *J* = 7.6 Hz, 1H), 4.46 (m, 2H), 3.77 (m, 1H), 3.60 (m, 1H), 2.88 (s, 6H), 2.85 (m, 1H), 2.47 (m, 1H), 2.23 (m, 4H), 2.00–1.55 (m, 14H), 1.50 (s, 9H), 1.45–1.05 (m, 2H), 0.94 (m, 1H); ^{13}C NMR (100 MHz, $CDCl_3$): δ: 173.1, 172.9, 171.7, 169.3, 142.1, 128.5, 127.5, 127.4, 127.3, 127.2, 68.4, 61.1, 58.9, 56.8, 53.8, 40.0, 36.2, 34.5, 33.2, 28.4, 28.1, 25.5, 24.8, 21.6, 18.2, 10.8. ESI-MS: m/z 714.2 $[M+H]^+$.

4.7.2. Compound 12g

A stirred suspension of compound **11c** (71.4 mg, 0.10 mmol) and $Cu(OAc)_2$ (127.1 mg, 0.70 mmol) in acetonitrile (20 mL) was refluxed for 30 min. After reaction completion, the solvent was removed under reduced pressure. The crude product was diluted with EtOAc (20 mL) and washed with a saturated solution of amonium chloride (3 × 10 mL) and brine (1 × 10 mL). Finally, the crude product was purified by Biotage™ flash chromatography, eluant conditions: 1% of MeOH and 99% of CH_2Cl_2 to 10% of MeOH and 90% of CH_2Cl_2. Yield 84% (60 mg, MW 1425.83, 0.042 mmol) of pure **12g**. Analytical characterization: $[\alpha]_{20}^{D}$ −85 (*c* 1.1, $CHCl_3$); ^1H NMR (400 MHz, $CDCl_3$): δ: 7.83 (bs, 2H), 7.35–7.05 (m, 22H), 6.80 (m, 2H), 6.14 (m, 2H), 4.65 (bs, 2H), 4.37 (m, 4H), 3.68 (m, 2H), 3.52 (m, 2H), 2.78 (s, 6H), 2.66 (m, 2H), 2.36 (m, 2H), 2.25–2.10 (m, 10H), 1.95–1.45 (m, 22H), 1.40 (s, 18H), 1.35–1.00 (m, 4H), 0.87 (bs, 6H); ^{13}C NMR (100 MHz, $CDCl_3$): δ: 172.9, 171.7, 169.3, 142.1, 128.6, 127.5, 127.4, 127.3, 65.6, 61.1, 60.6, 58.9, 56.8, 53.7, 41.1, 40.0, 36.2, 34.5, 33.2, 31.8, 28.3, 28.0, 25.5, 24.9, 21.6, 19.0, 10.8. ESI-MS: m/z 1426.6 $[M+H]^+$, 613.2 $[M+2H]^{2+}$.

4.7.3. Compound 8g

TFA (450 μL, 5.0 mmol) was added to a stirred solution of compound **12g** (94.1 mg, 0.066 mmol) in CH_2Cl_2 (2 mL). The reaction mixture was left stirring at room temperature overnight and then concentrated under reduced pressure. The residue was purified by chromatography on a C_{18} reverse phase semi-preparative hplc column, eluant conditions: from 70% of H_2O (0.2% TFA) and 30% of CH_3CN (0.2% TFA) to 30% of H_2O (0.2% TFA) and 70% of CH_3CN (0.2% TFA), flow rate 12 mL/min, 20 min runs. Yield 41% (39 mg,

MW 1453.64, 0.027 mmol) of pure **8g**. Analytical characterization: $[\alpha]_{20}^{D}$ −84 (*c* 1.16, CH_3OH); ^1H NMR (400 MHz, D_2O): *δ*: 8.80 (m, 2H), 7.40–7.20 (m, 20H), 6.14 (s, 2H), 4.67 (m, 4H), 4.02 (bs, 2H), 3.87 (bs, 2H), 3.44 (d, *J* = 13.2 Hz, 2H), 3.07 (t, *J* = 11.2 Hz, 2H), 2.72 (s, 6H), 2.40–2.20 (m, 10H), 2.20–180 (m, 16H), 1.75–1.60 (m, 8H), 1.60–1.45 (m, 4H), 1.05 (d, *J* = 7.1 Hz, 6H); ^{13}C NMR (100 MHz, D_2O): *δ*: 174.6, 171.6, 169.6, 167.5, 141.7, 141.5, 128.3, 128.1, 127.3, 127.2, 127.0, 126.9, 76.3, 65.4, 62.6, 61.6, 58.3, 57.0, 54.3, 40.9, 38.3, 35.1, 32.7, 31.7, 31.0, 30.2, 27.7, 27.5, 24.8, 23.2, 18.1, 7.8. ESI-MS: m/z 1226.0 $[M+H]^+$, 613.7 $[M+2H]^{2+}$.

4.8. Head–head dimer 8h—Scheme 5

4.8.1. Compound 12h

A 0.9 M aqueous solution of sodium ascorbate (61 μL, 0.055 mmol) and a 0.3 M aqueous solution of $Cu(OAc)_2$ (83 μL, 0.025 mmol) were sequentially added to a stirred solution of compound **11c** (0.10 mmol) and 1,4-(4′-azidobutyl)benzene[61] (13.6 mg, 0.05 mmol) in a 1:1 mixture of H_2O/^{t}BuOH (300 μL). The reaction mixture was stirred overnight at room temperature and then the solvent was removed under reduced pressure. The crude product was diluted with EtOAc (20 mL) and washed with a saturated solution of amonium chloride (3 × 20 mL) and brine (1 × 20 mL). The residue was purified by Biotage™ flash chromatography, eluant conditions: 1% of MeOH and 99% of CH_2Cl_2 to 10% of MeOH and 90% of CH_2Cl_2. Yield 32% (27 mg, MW 1700.21, 0.016 mmol) of pure **12h**. Analytical characterization: $[\alpha]_{20}^{D}$ −84 (*c* 1.16, $CHCl_3$); ^1H NMR (400 MHz, $CDCl_3$): *δ*: 7.84 (bs, 2H), 7.37 (bs, 2H), 7.35–7.15 (m, 22H), 7.09 (d, *J* = 6.8 Hz, 2H), 6.98 (s, 4H), 6.13 (d, *J* = 7.6 Hz, 2H), 4.65 (d, *J* = 6.8 Hz, 2H), 4.48 (m, 4H), 4.20 (m, 4H), 3.70 (m, 2H), 3.46 (m, 2H), 2.78 (s, 6H), 2.75 (m, 2H), 2.65 (s, 4H), 2.53 (t, *J* = 6.4 Hz, 4H), 2.34 (m, 2H), 2.17 (m, 6H), 1.95–1.50 (m, 28H), 1.40 (s, 18H), 1.39 (m, 2H), 1.05 (m, 2H), 0.85 (bs, 6H); ^{13}C NMR (100 MHz, $CDCl_3$): *δ*: 174.9, 173.0, 171.8, 169.4, 150.0, 140.5, 139.0, 1.38.0, 138.6, 128.4, 127.5, 127.3, 120.6, 80.5, 61.2, 60.6, 59.0, 56.9, 53.8, 50.0, 41.3, 40.1, 36.3, 34.8, 34.4, 33.2, 31.8, 30.5, 29.8, 28.9, 28.3, 25.6, 25.3, 21.7, 20.7, 10.8. ESI-MS: m/z 1699.6 $[M+H]^+$, 850.8 $[M+2H]^{2+}$.

4.8.2. Compound 8h

TFA (450 μL, 5.0 mmol) was added to a stirred solution of compound **12h** (21.2 mg, 0.013 mmol) in CH_2Cl_2 (2 mL). The reaction mixture was left stirring at room temperature overnight and then concentrated under reduced pressure. The residue was purified by chromatography on a C_{18} reverse phase semi-preparative hplc column, eluant conditions: from 70% of H_2O (0.2% TFA) and 30% of CH_3CN (0.2% TFA) to 30% of H_2O (0.2% TFA) and 70% of CH_3CN (0.2% TFA), flow rate 12 mL/min, 20 min runs. Yield 92% (24 mg, MW 1728.01, 0.011 mmol) of pure **8h**. Analytical characterization: $[\alpha]_{D}^{20}$ −99 (*c* 1.16, CH_3OH); ^1H NMR (400 MHz, D_2O): *δ*: 8.80 (m, 2H), 7.76 (s, 2H), 7.40–7.15 (m, 20H), 7.06 (s, 4H), 6.14 (s, 2H), 4.66 (m, 4H), 4.37 (t, *J* = 6.4 Hz, 4H), 4.00 (m, 2H), 3.87 (m, 2H), 3.44 (d, *J* = 13.2 Hz, 2H), 3.05 (t, *J* = 11.6 Hz, 2H), 2–74–2.68 (m, 10H), 2.59 (t, *J* = 6.8 Hz, 4H), 2.26 (m, 6H), 2.15–1.75 (m, 21H), 1.70–1.50 (m, 17H), 1.06 (t, *J* = 7.2 Hz, 6H); ^{13}C NMR (100 MHz, D_2O): *δ*: 174.7, 171.6, 169.6, 167.5, 147.1, 141.7, 141.6, 139.2, 128.3, 128.1, 127.3, 127.1, 126.9, 122.2, 62.6, 61.6, 58.3, 57.1, 54.3, 50.0, 41.0, 38.3, 35.3, 34.2, 32.7, 31.7, 31.0, 30.2, 29.3, 28.5, 28.0, 27.6, 25.0, 24.3, 23.2, 7.8. ESI-MS: m/z 1500.2 $[M+H]^+$, 751.2 $[M+2H]^{2+}$.

4.9. Head–head dimer 8i—Scheme 6

4.9.1. Compound 11d

EDC·HCl (23 mg, 0.12 mmol), HOBt (16.2 mg, 0.12 mmol) and DIPEA (69.7 μL, 0.40 mmol) were sequentially added to a stirred solution of Cbz-β-Ala-OH (26.8 mg, 0.12 mmol) in CH_2Cl_2 (2 mL) at room temperature. The reaction mixture was left stirring for 15 min and then added to a stirred solution of **4h** (60.6 mg, 0.10 mmol) in dry CH_2Cl_2 (2 mL). The reaction mixture was stirred at room temperature overnight and then, after reaction completion, the solvent was removed under reduced pressure. The crude product was diluted with EtOAc (20 mL) and washed with a saturated solution of ammonium chloride (3 × 20 mL), saturated solution of sodium bicarbonate (3 × 20 mL) and brine (1 × 20 mL). The organic layer was dried over Na_2SO_4, and then the solvent removed under reduced pressure. The residue was purified by Biotage™ flash chromatography, eluant conditions: from 50% of EtOAc and 50% of Petroleum ether to 100% of EtOAc. Yield 99% (80 mg, MW 811.00, 0.099 mmol) of pure **11d**. Analytical characterization: $[\alpha]_{20}^{D}$ −118 (*c* 1.14, $CHCl_3$); ^1H NMR (400 MHz, $CDCl_3$): *δ*: 7.80 (d, *J* = 8.0 Hz, 2H), 7.30–7.15 (m, 14H), 7.10 (d, *J* = 7.6 Hz, 2H), 6.13 (d, *J* = 8.8 Hz, 2H), 5.02 (t, *J* = 12.0 Hz, 2H), 4.63 (d, *J* = 7.6 Hz, 1H), 4.31 (m, 2H), 3.62 (m, 1H), 3.40 (m, 3H), 2.75 (m, 3H), 2.35 (m, 3H), 2.12 (m, 1H), 1.90–1.50 (m, 8H), 1.39 (s, 9H), 1.35 (m, 1H), 1.05 (m, 1H), 0.85 (t , *J* = 6.8 Hz, 3H); ^{13}C NMR (100 MHz, $CDCl_3$): *δ*:.173.0, 171.6, 169.3, 156.4, 136.7, 128.7, 128.6, 128.4, 128.0, 127.4, 127.3, 127.2, 80.4, 66.5, 61.1, 60.8, 58.8, 56.8, 53.8, 41.3, 40.1, 37.3, 35.9, 34.5, 33.1, 32.0, 30.1, 28.4, 25.5, 21.8, 10.8. ESI-MS: m/z 811.6 $[M+H]^+$.

4.9.2. Compound 12i

A solution of compound **11d** (67.6 mg, 0.1 mmol) in EtOH/H_2O 9:1 (10 mL) was Cbz-deprotected by continuous flow hydrogenation using the H-Cube™ system. The hydrogenation was performed using a Pd/C catalyst cartridge column (CatCart™). The reactor pressure and temperature were fixed at 10 bar and 40 °C, and a flow rate of 0.8 ml/min was set. After reaction completion, the solvent was removed under reduced pressure.

The crude hydrogenation product was dissolved in EtOH (1 mL), and then diethyl squarate (7.1 μL, 0.048 mmol), Et_3N (55.8 μL, 0.4 mmol) and a catalytic amount of DMAP (1.2 mg, 0.01 mmol) were sequentially added at room temperature. The reaction mixture was left stirring overnight at room temperature. After reaction completion, the solvent was removed under reduced pressure, the crude product was diluted with EtOAc (20 mL) and washed with water (3 × 20 mL). The organic layer was dried over Na_2SO_4, and then the solvent was removed under reduced pressure. Finally, the crude product was purified by Biotage™ flash chromatography, eluant conditions: 1% of MeOH and 99% of CH_2Cl_2 to 10% of MeOH and 90% of CH_2Cl_2. Yield 92% (63 mg, MW 1431.75, 0.044 mmol) of pure **12i**. Analytical characterization: $[\alpha]_{20}^{D}$ −88 (*c* 1.60, $CHCl_3$); ^1H NMR (400 MHz, $CDCl_3$): *δ*: 7.76 (d, *J* = 8.4 Hz, 2H), 7.30–7.10 (m, 22H), 6.13 (d, *J* = 8.8 Hz, 2H), 4.63 (d, *J* = 7.2 Hz, 2H), 4.35 (m, 4H), 3.75 (m, 5H), 3.25 (bs, 2H), 2.95 (bs, 2H), 2.73 (s, 6H), 2.42 (bs, 4H), 2.30 (m, 2H), 2.18 (m, 2H), 1.95–1.60 (m, 14H), 1.50 (m, 2H), 1.40 (s, 18H), 1.20 (m, 2H), 0.84 (t, *J* = 6.8 Hz, 6H); ^{13}C NMR (100 MHz, $CDCl_3$): *δ*: 171.4, 169.6, 142.1, 141.2, 128.7, 127.4, 127.2, 61.2, 58.8, 56.8, 53.8, 41.5, 40.8, 39.9, 36.9, 34.0, 33.1, 31.8, 30.7, 25.8, 21.6, 10.5. ESI-MS: m/z 1432.0 $[M+H]^+$.

4.9.3. Compound 8i

TFA (450 μL, 5.0 mmol) was added to a stirred solution of compound **12i** (41.5 mg, 0.029 mmol) in CH_2Cl_2 (2 mL). The reaction mixture was left stirring at room temperature overnight and then concentrated under reduced pressure. The residue was purified by chromatography on a C_{18} reverse phase semi-preparative hplc column, eluant conditions: from 70% of H_2O (0.2% TFA) and 30% of CH_3CN (0.2% TFA) to 30% of H_2O (0.2% TFA) and 70% of CH_3CN (0.2% TFA), flow rate 12 mL/min, 20 min runs. Yield 83% (35 mg, MW 1459.56, 0.024 mmol) of pure **8i**. Analytical characterization: $[\alpha]_{20}^{D}$ −113 (*c* 1.20, CH_3OH); ^1H NMR (400 MHz, D_2O): *δ*:

7.35–7.25 (m, 20H), 6.00 (s, 2H), 4.57 (d, J = 10.0 Hz, 2H), 4.48 (dd, J = 7.6, 5.2 Hz, 2H), 3.95 (m, 2H), 3.88 (dd, J = 7.2, 5.2 Hz, 2H), 3.71 (m, 4H), 3.30 (dd, J = 13.6, 3.6 Hz, 2H), 2.99 (dd, J = 13.6, 9.6 Hz, 2H), 2.64 (s, 6H), 2.44 (m, 4H), 2.20–2.05 (m, 4H), 1.95–1.85 (m, 8H), 1.80–1.60 (m, 6H), 1.50–1.35 (m, 4H), 0.94 (t, J = 7.2 Hz, 6H); ^{13}C NMR (100 MHz, D_2O): δ: 181.7, 172.9, 172.0, 169.9, 168.4, 167.9, 141.3, 141.0, 128.8, 127.6, 127.5, 127.3, 127.0, 62.7, 61.6, 58.2, 57.4, 54.5, 40.7, 37.5, 37.0, 32.4, 31.6, 30.7, 27.7, 23.4, 8.3. ESI-MS: m/z 1231.9 $[M+H]^+$, 616.5 $[M+2H]^{2+}$.

4.10. Tail–tail dimer 9a—Scheme 7

4.10.1. Compound 13a

EDC·HCl (69 mg, 0.36 mmol), HOBt (48.6 mg, 0.36 mmol) and DIPEA (209 μL, 1.20 mmol) were sequentially added to a stirred solution of **4d** (132.5 mg, 0.3 mmol) in CH_2Cl_2 (10 mL) at room temperature. The reaction mixture was left stirring for 15 min and then added to a stirred solution of (*S*)-3-amino-3-phenylprop-1-yne (13.1 mg, 0.10 mmol) in dry CH_2Cl_2 (10 mL). The reaction mixture was stirred at room temperature overnight and then, after reaction completion, the solvent was removed under reduced pressure. The crude product was diluted with EtOAc (20 mL) and washed with a saturated solution of ammonium chloride (3 × 20 mL), saturated solution of sodium bicarbonate (3 × 20 mL) and brine (1 × 20 mL). The organic layer was dried over Na_2SO_4, and then the solvent was removed under reduced pressure. The residue was purified by Biotage™ flash chromatography, eluant conditions: 50% of EtOAc and 50% of Petroleum ether to 100% of EtOAc. Yield 67% (112 mg, MW 554.69, 0.201 mmol) of pure **13a**. Analytical characterization: $[\alpha]_{20}^{D}$ −116 (*c* 1.5, $CHCl_3$); ^{1}H NMR (400 MHz, $CDCl_3$): δ: 7.65 (d, J = 7.6 Hz, 1H), 7.36 (m, 3H), 7.20 (m, 3H), 5.87 (d, J = 6.8 Hz, 1H), 4.61 (d, J = 6.0 Hz, 1H), 4.42–4.30 (m, 2H), 3.67 (m, 1H), 3.47 (d, J = 11.6 Hz, 1H), 3.14 (d, J = 12.0, 1H), 2.78 (s, 3H), 2.42 (s, 1H), 2.36 (m, 1H), 2.18 (m, 1H), 2.00–1.70 (m, 4H), 1.70–1.55 (m, 3H), 1.44 (s, 9H), 0.97 (m, 1H), 0.84 (m, 4H); ^{13}C NMR (100 MHz, $CDCl_3$): δ: 171.7, 138.9, 128.9, 126.8, 73.0, 64.1, 60.8, 60.2, 58.7, 53.6, 44.4, 41.5, 34.6, 33.2, 31.0, 30.0, 28.4, 25.4, 21.4, 10.6. ESI-MS: m/z 555.4 $[M+H]^+$, 577.3 $[M+Na]^+$.

4.10.2. Compound 14a

A 0.9 M water solution of sodium ascorbate (61 μL, 0.055 mmol) and a 0.3 M water solution of $Cu(OAc)_2$ (83 μL, 0.025 mmol) were sequentially added to a stirred solution of compound **13a** (61 mg, 0.11 mmol) and 1,4-(4′-azidobutyl)benzene[61] (13.6 mg, 0.05 mmol) in a 1:1 mixture of H_2O/^{t}BuOH (300 μL). The reaction mixture was stirred overnight at room temperature and then the solvent was removed under reduced pressure. The crude product was diluted with EtOAc (20 mL) and washed with a saturated solution of ammonium chloride (3 × 20 mL) and brine (1 × 20 mL). The organic layer was dried over Na_2SO_4, and then the solvent was removed under reduced pressure. Finally, the residue was purified by Biotage™ flash chromatography, eluant conditions: 1% of MeOH and 99% of CH_2Cl_2 to 10% of MeOH and 90% of CH_2Cl_2. Yield 74% (51 mg, MW 1381.74, 0.037 mmol) of pure **14a**. Analytical characterization: $[\alpha]_{20}^{D}$ −83 (*c* 1.15, $CHCl_3$); ^{1}H NMR (400 MHz, $CDCl_3$): δ: 7.94 (m, 2H), 7.42 (m, 2H), 7.30–7.10 (m, 12H), 6.96 (s, 4H), 6.20 (d, J = 6.4 Hz, 2H), 4.64 (bs, 2H), 4.38 (m, 4H), 4.23 (bs, 4H), 3.70 (m, 2H), 3.53 (d, J = 12.0 Hz, 2H), 3.21 (d, J = 12.0 Hz, 2H), 2.79 (s, 6H), 2.53 (bs, 4H), 2.27 (m, 2H), 2.16 (m, 2H), 2.05–1.60 (m, 18H), 1.56 (m, 4H), 1.42 (s, 18H), 1.14 (m, 4H), 0.84 (bs, 6H); ^{13}C NMR (100 MHz, $CDCl_3$): δ: 173.0, 171.5, 169.6, 140.9, 139.0, 128.6, 128.4, 127.7, 127.1, 121.4, 80.0, 64.3, 61.2, 60.2, 58.8, 53.8, 50.2, 50.0, 41.6, 34.7, 34.5, 33.1, 31.1, 29.7, 28.4, 28.2, 26.0, 21.5, 10.7. ESI-MS: m/z 1382.1 $[M+H]^+$, 691.7 $[M+2H]^{2+}$.

4.10.3. Compound 9a

TFA (450 μL, 5.0 mmol) was added to a stirred solution of compound **14a** (30.4 mg, 0.022 mmol) in CH_2Cl_2 (2 mL). The reaction mixture was left stirring at room temperature overnight and then concentrated under reduced pressure. The residue was purified by chromatography on a C_{18} reverse phase semi-preparative hplc column, eluant conditions: from 90% of H_2O (0.2% TFA) and 10% of MeOH/^{i}PrOH 6:4 (0.2% TFA) to 100% of MeOH/^{i}PrOH 6:4 (0.2% TFA), flow rate 12 ml/min, 20 min runs. Yield 59% (18 mg, MW 1409.54, 0.013 mmol) of pure **9a**. Analytical characterization: $[\alpha]_{20}^{D}$ −110 (*c* 0.41, CH_3OH); ^{1}H NMR (400 MHz, D_2O): δ: 7.53 (s, 2H), 7.20–7.05 (m, 10H), 6.59 (s, 4H), 6.10 (s, 2H), 4.57 (d, J = 9.2 Hz, 2H), 4.38 (bs, 2H), 3.96 (bs, 4H), 3.81 (m, 4H), 3–49 (bs, 4H), 2.62 (s, 6H), 2.08 (bs, 4H), 2.00–1.80 (m, 10H), 1.75–1.55 (m, 8H), 1.50–1.35 (m, 8H), 1.08 (bs, 4H), 0.88 (d, J = 7.2 Hz, 6H); ^{13}C NMR (100 MHz, D_2O): δ: 172.3, 170.7, 168.0, 147.9, 139.4, 139.1, 128.8, 128.2, 128.0, 127.0, 123.0, 63.1, 62.7, 61.6, 58.5, 54.3, 50.0, 49.9, 39.0, 32.3, 31.5, 29.4, 28.9, 27.7, 27.5, 23.4, 8.3. ESI-MS: m/z 1181.9 $[M+H]^+$, 1204.2 $[M+Na]^+$, 591.8 $[M+2H]^{2+}$.

4.11. Tail–tail dimer 9b—Schemes 8 and 9

4.11.1. Compound 16a

HOBt (104 mg, 0.77 mmol), HBTU (292 mg, 0.77 mmol) and Sym-collidine (169.1 μL, 1.28 mmol) were sequentially added to a stirred solution of commercially available 15a (46.2 mg, 0.32 mmol) and *N*-Boc-(*S*)-2-Phenylglycine (200.9 mg, 0.80 mmol) in dry DMF (2 mL) at 0 °C. The reaction mixture was left stirring for 2 h and then, after reaction completion, the mixture was diluted with EtOAc (20 mL) and washed with a saturated solution of ammonium chloride (3 × 20 mL), saturated solution of sodium bicarbonate (3 × 20 mL) and brine (1 × 20 mL. The organic layers were dried over Na_2SO_4, and then the solvent was removed under reduced pressure. The residue was purified by Biotage™ flash chromatography, eluant conditions: from 1% of MeOH and 99% of CH_2Cl_2 to 10% of MeOH and 90% of CH_2Cl_2. Yield 94% (183 mg, MW 610.80, 0.30 mmol) of pure 16a. Analytical characterization: ^{1}H NMR (400 MHz, $CDCl_3$):δ: 7.38–7.25 (m, 10H), 5.76 (m, 2H), 5.25 (m, 2H), 3.32 (bs, 1H), 3.23 (m, 2H), 3.13 (bs, 1H), 1.57 (s, 4H), 1.42 (m, 18H), 1.21 (d, J = 11.2 Hz, 6H); ^{13}C NMR (100 MHz, $CDCl_3$): δ: 129.0, 128.9, 128.3, 127.2, 39.7, 39.7, 29.2, 28.8, 28.3, 26.4. ESI-MS: m/z 611.4 $[M+H]^+$.

4.11.2. Compound 17a

TFA (450 μL, 5.0 mmol) was added to a stirred solution of compound 16a (165 mg, 0.27 mmol) in CH_2Cl_2 (3 mL). The reaction mixture was left stirring at room temperature and then concentrated under reduced pressure to give a crude residue which was used without purification. Quantitative yield (172.4 mg, MW 638.56, 0.27 mmol) of 17a.

4.11.3. Compound 14b

HOBt (32.4 mg, 0.24 mmol), HBTU (91 mg, 0.24 mmol) and Sym-collidine (52.9 μL, 0.4 mmol) were sequentially added to a stirred solution of **4d** (110.4 mg, 0.25 mmol) and **17a** (63.9 mg, 0.10 mmol) in dry DMF (2 mL) at 0 °C. The reaction mixture was left stirring for 2 h and then, after reaction completion, the mixture was diluted with EtOAc (20 mL) and washed with a saturated solution of ammonium chloride (3 × 20 mL), saturated solution of sodium bicarbonate (3 × 20 mL) and brine (1 × 20 mL). The organic layers were dried over Na_2SO_4, and then the solvent was removed under reduced pressure. The residue was purified by Biotage™ flash chromatography, eluant conditions: 1% of MeOH and 99% of CH_2Cl_2 to 10% of MeOH and 90% of CH_2Cl_2. Yield 97% (122 mg, MW 1257.59, 0.094 mmol) of pure **14b**. Analytical characteriza-

tion: $[\alpha]_{20}^{D}$ −118 (*c* 1.23, $CHCl_3$); ^{1}H NMR (400 MHz, $CDCl_3$): δ: 8.43 (d, *J* = 8 Hz, 2H), 8.17 (t, *J* = 5.6 Hz, 2H), 7.86 (bs, 2H), 7.40–7.25 (m, 10H), 5.36 (d, *J* = 8 Hz, 2H), 4.61 (dd, *J* = 7.2, 4 Hz, 2H), 4.48–4.36 (m, 4H), 3.89 (m, 2H), 3.45 (bs, 2H), 3.25 (m, 2H), 3.00 (m, 4H), 2.70 (s, 6H), 2.16 (m, 2H), 2.14 (m, 2H), 2.00–1.75 (m, 8H), 1.70–1.45 (m, 10H), 1.40 (s, 18H), 1.35 (m, 4H), 1.15 (s, 8H), 0.80 (bs, 6H); ^{13}C NMR (100 MHz, $CDCl_3$): δ: 171.2, 170.3, 169.9, 139.4, 128.6, 127.8, 127.5, 79.5, 63.1, 61.1, 58.0, 56.8, 53.9, 41.0, 39.0, 33.2, 32.8, 30.2, 29.3, 29.0, 28.5, 28.1, 26.6, 11.2 . ESI-MS: m/z 1257.9 $[M+H]^+$.

4.11.4. Compound 9b

TFA (450 μL, 5.0 mmol) was added to a stirred solution of compound **14b** (93.1 mg, 0.074 mmol) in CH_2Cl_2 (2 mL). The reaction mixture was left stirring at room temperature overnight and then concentrated under reduced pressure. The residue was purified by chromatography on a C_{18} reverse phase semi-preparative hplc column, eluant conditions: from 70% of H_2O (0.2% TFA) and 30% of CH_3CN (0.2% TFA) to 30% of H_2O (0.2% TFA) and 70% of CH_3CN (0.2% TFA), flow rate 12 ml/min, 20 min runs. Yield 58% (55 mg, MW 1285.35, 0.043 mmol) of pure **9b**. Analytical characterization: $[\alpha]_{20}^{D}$ −94 (*c* 1.44, CH_3OH); ^{1}H NMR (400 MHz, D_2O): δ: 7.41 (m, 10H), 5.29 (s, 2H), 4.70 (m, 2H), 4.53 (dd, *J* = 8.0, 4.4 Hz, 2H), 4.05 (m, 2H), 3.88 (dd, *J* = 7.2, 5.2 Hz, 2H), 3.61 (m, 2H), 3.25 (m, 2H), 3.05 (m, 2H), 2.68 (s, 6H), 2.25 (m, 2H), 2.15 (m, 2H), 2.05 (m, 4H), 1.95 (m, 6H), 1.85 (m, 3H), 1.75 (m, 4H), 1.60 (m, 2H), 1.35 (m, 4H), 1.012(bs, 8H), 0.96 (t, *J* = 8.0 Hz, 6H); ^{13}C NMR (100 MHz, D_2O): δ: 173.2, 171.6, 171.2, 168.3, 136.1, 129.2, 129.0, 127.3, 63.2, 62.8, 61.8, 58.8, 58.2, 54.5, 39.3, 39.0, 32.4, 31.5, 31.4, 29.5, 28.1, 27.8, 25.6, 23.4, 8.2. ESI-MS: m/z 1057.9 $[M+H]^+$.

4.12. Tail–tail dimers 9c–e—Schemes 8 and 9

The tail–tail dimers **9c**, **9d** and **9e** were prepared similarly to **9b**. The detailed synthetic protocols leading to their synthesis, and their full synthetic characterization are reported in the Supplementary data.

4.13. Tail–tail dimer 9f—Scheme 10

4.13.1. Compound 14f

Dry TEA (83.6 μL, 0.6 mmol) and MsCl (46.4 μL, 0.6 mmol) were sequentially added to a stirred solution of compound **14a** (0.1 mmol) in dry CH_2Cl_2 (4 mL) under argon at 0 °C. The reaction mixture was stirred at room temperature for 2 h. After reaction completion, the resulting mixture was diluted with CH_2Cl_2 (20 mL) and washed with a saturated solution of ammonium chloride (3 × 20 mL). The combined organic layers were dried over Na_2SO_4, and then the solvent was removed under reduced pressure.

The crude mesylate was dissolved in dry DMF (10 mL) under argon at room temperature, and then NaN_3 (130 mg, 2 mmol) was added. The reaction mixture was heated at 100 °C for 30 min, while being irradiated in a microwave reactor. After reaction completion most of the DMF was removed under reduced pressure, the crude was diluted with EtOAc (20 mL) and washed with water (3 × 20 mL). The organic layer was dried over Na_2SO_4, and then the solvent was removed under reduced pressure. Finally, the crude product was purified by Biotage™ flash chromatography. eluant conditions: 1% of MeOH and 99% of CH_2Cl_2 to 10% of MeOH and 90% of CH_2Cl_2. Yield 58% (83 mg, MW 1431.77, 0.058 mmol) of pure **14f**. Analytical characterization: $[\alpha]_{20}^{D}$ −105 (*c* 1.31, $CHCl_3$); ^{1}H NMR (400 MHz, $CDCl_3$): δ: 8.03 (m, 2H), 7.40–7.20 (m, 12H), 7.05 (m, 6H), 6.29 (d, *J* = 7.6 Hz, 2H), 4.71 (d, *J* = 6.4 Hz, 2H), 4.58 (m, 2H), 4.49 (m, 2H), 4.33 (bs, 4H), 3.83 (m, 2H), 3.42 (bd, *J* = 11.6 Hz, 2H), 3.16 (t, *J* = 12.8 Hz, 2H), 2.86 (s, 6H), 2.62 (m, 4H), 2.36 (m, 2H), 2.23 (m, 2H), 2.05–2.60 (m, 22H), 1.55 (bs, 20H), 1.22 (m, 2H), 0.85 (bs, 6H) ; ^{13}C NMR (100 MHz, $CDCl_3$): δ: 171.5, 171.0, 169.6, 140.7, 139.0, 128.7, 128.4, 127.9, 127.1, 121.6, 61.0, 59.0, 58.7, 53.6, 53.2, 50.3, 50.0, 34.7, 34.1, 33.3, 32.1, 29.7, 28.4, 28.2, 26.0, 21.4, 10.6. ESI-MS: m/z 1433.1 $[M+H]^+$, 666.7 $[M+2H]^{2+}$.

4.13.2. Compound 14g

A 1 N solution of $(CH_3)_3P$ in toluene (105 μL, 0.105 mmol) was added dropwise to a stirred solution of compound **14f** (50.1 mg, 0.035 mmol) in dry CH_2Cl_2 (10 mL) under argon at room temperature. After 2 h, a 1 N HCl aqueous solution (10 mL) was added to the reaction mixture, and stirring at room temperature was continued for further 20 min. After reaction completion, the reaction mixture was neutralized with sodium bicarbonate and extracted with CH_2Cl_2 (3 × 20 mL). The organic layers were combined and dried over Na_2SO_4, and the solvent was removed under reduced pressure. The crude product did not require any further purification, and was characterized as such. Yield 99% (48 mg, MW 1379.77, 0.035 mmol) of pure **14g**. Analytical characterization: $[\alpha]_{20}^{D}$ −120 (*c* 0.48, $CHCl_3$); ^{1}H NMR (400 MHz, $CDCl_3$): δ: 8.35 (m, 4H), 7.88 (m, 2H), 7.35–7.15 (m, 12H), 6.93 (m, 4H), 6.14 (d, *J* = 6.4 Hz, 2H), 4.62 (bs, 2H), 4.40 (m, 4H), 4.24 (bs, 4H), 3.70 (m, 2H), 3.00–2.65 (m, 10H), 2.52 (bs, 4H), 2.30–2.05 (m, 4H), 2.00–1.55 (m, 20H), 1.54 (m, 4H), 1.39 (s, 18H), 1.19 (m, 4H), 0.84 (bs, 6H); ^{13}C NMR (100 MHz, $CDCl_3$): δ: 173.2, 171.7, 169.2, 141.9, 139.3, 129.6, 128.2, 127.5, 127.4, 122.4, 81.0, 64.5, 61.4, 60.1, 58.8, 53.8, 50.2, 50.0, 41.6, 35.7, 33.5, 33.1, 31.5, 29.7, 28.4, 28.2, 26.0, 21.5, 10.4. ESI-MS: m/z 1380.1 $[M+H]^+$, 691.2 $[M+2H]^{2+}$.

4.13.3. Compound 14h

$NaBH(OAc)_3$ (16.5 mg, 0.078 mmol) was added to a stirred solution of compound **14g** (41.4 mg, 0.03 mmol) and benzaldehyde (5.5 μL, 0.054 mmol) in dry CH_2Cl_2 (5 mL). The reaction mixture was stirred overnight at room temperature, and then the solvent was removed under reduced pressure. Finally, the crude product was purified by Biotage™ flash chromatography, eluant conditions: 1% of MeOH and 99% of CH_2Cl_2 to 10% of MeOH and 90% of CH_2Cl_2. Yield 45% (21 mg, MW 1560.32, 0.0135 mmol) of pure **14h**. Analytical characterization: $[\alpha]_{20}^{D}$ −150 (*c* 0.70, $CHCl_3$); ^{1}H NMR (400 MHz, $CDCl_3$): δ: 8.25 (bs, 2H), 8.03 (m, 2H), 7.40–7.24 (m, 20H), 7.18 (m, 2H), 7.05 (s, 4H), 6.28 (d, *J* = 7.6 Hz, 2H), 4,73 (bs, 2H), 4.49 (m, 4H), 4.30 (s, 4H), 3.95–3.75 (m, 6H), 2.95–2.75 (m, 6H), 2.70–2.50 (m, 8H), 2.35 (m, 2H), 2.23 (m, 2H), 2.25–1.55 (m, 22H), 1.49 (m, 20H), 1.24 (m, 2H), 0.93 (bs, 6H); ^{13}C NMR (100 MHz, $CDCl_3$): δ: 169.9, 147.8, 141.0, 139.1, 128.8, 128.6, 127.6, 127.2, 127.0, 121.5, 61.0, 58.4, 50.2, 50.0, 38.1, 34.7, 33.3, 33.2, 29.7, 28.5, 28.2, 26.0, 22.1, 10.6. ESI-MS: m/z 1561.4 $[M+H]^+$, 781.0 $[M+2H]^{2+}$.

4.13.4. Compound 9f

TFA (90 μL, 1.0 mmol) was added to a stirred solution of compound **14h** (20.3 mg, 0.013 mmol) in CH_2Cl_2 (2 mL). The reaction mixture was left stirring at room temperature overnight and then concentrated under reduced pressure. The residue was purified by chromatography on a C_{18} reverse phase semi-preparative hplc column, eluant conditions: from 90% of H_2O (0.2% TFA) and 10% of MeOH/^{i}PrOH 6:4 (0.2% TFA) to 100% of MeOH/^{i}PrOH 6:4 (0.2% TFA), flow rate 12 ml/min, 20 min runs. Yield 92% (19 mg, MW 1587.83, 0.012 mmol) of pure **9f**. Analytical characterization: $[\alpha]_{20}^{D}$ −121 (*c* 0.95, CH_3OH); ^{1}H NMR (400 MHz, D_2O): δ: 7.52 (s, 2H), 7.35 (s, 10H), 7.25–7.05 (m, 10H), 6.64 (s, 4H), 6.06 (s, 2H), 4.56 (d, *J* = 9.2 Hz, 2H), 4.37 (bs, 2H), 4.14 (s, 4H), 4.045 (bs, 4H), 3.89 (bs, 2H), 3.76 (bs, 2H), 3.03 (d, *J* = 12.0 Hz, 2H), 2.95 (t, *J* = 11.2 Hz, 2H), 2.49 (s, 6H), 2.15 (bs, 4H), 2.12–1.90 (m, 8H), 1.90–1.70 (m, 8H), 1.70–1.65 (m, 2H), 1.50 (bs, 8H), 1.13 (bs, 4H), 0.84 (t, *J* = 7.2 Hz, 6H); ^{13}C NMR (100 MHz, D_2O): δ: 172.5, 168.9,

168.7, 147.5, 139.3, 139.1, 130.1, 129.9, 129.8, 129.3, 128.9, 128.2, 128.1, 127.0, 132.2, 62.5, 61.7, 58.0, 54.1, 51.4, 50.2, 50.1, 47.8, 35.2, 33.7, 32.2, 31.5, 29.7, 28.7, 28.4, 27.9, 27.4, 23.4, 8.1. ESI-MS: m/z 1360.0 $[M+H]^+$, 680.6 $[M+2H]^{2+}$.

4.14. Tail–tail dimer 9g—Scheme 11

4.14.1. Compound 13b

Dry TEA (223 μL, 1.6 mmol) and Boc_2O (349.2 mg, 1.6 mmol) were sequentially added to a stirred solution of compound **4c** (205 mg, 0.8 mmol) in dry CH_2Cl_2 (4 mL). The reaction mixture was stirred at room temperature and monitored by LC–MS. After reaction completion, the solution was diluted with CH_2Cl_2 (5 mL) and washed once with 5% citric acid and saturated $NaHCO_3$. The organic layer was dried over Na_2SO_4 and evaporated under reduced pressure. The crude product was used as such in the next reaction step.

Dry TEA (335 μL, 2.4 mmol) and MsCl (92.9 μL, 1.2 mmol) were sequentially added to a stirred solution of crude alcohol (270 mg, 0.78 mmol) in dry CH_2Cl_2 (4 mL) under argon at 0 °C. The reaction mixture was stirred at room temperature overnight. After reaction completion, the resulting mixture was diluted with CH_2Cl_2 (20 mL) and washed with a saturated ammonium chloride solution (2 × 20 mL). The organic layer was dried over Na_2SO_4, and then the solvent was removed under reduced pressure.

The crude product was dissolved in dry DMF (10 mL) and treated with $Bu_4N^+CN^-$ (322.2 mg, 1.2 mmol). The reaction mixture was heated at 80 °C for 90 min in a microwave reactor. After reaction completion most of the DMF was removed under reduced pressure, the crude was diluted with EtOAc (20 mL) and washed with water (3 × 20 mL). The organic layer was dried over Na_2SO_4, and then the solvent was removed under reduced pressure. The crude product was purified by Biotage™ flash chromatography, eluant conditions: from 1% of MeOH and 99% of CH_2Cl_2 to 10% of MeOH and 90% of CH_2Cl_2. Yield 63% (245 mg, MW 365.0, 0.493 mmol) of pure **13b**. Analytical characterization: ^{1}H NMR (400 MHz, $CDCl_3$): δ: 5.83 (d, J = 6.8 Hz, 1H), 4.61 (dd, J = 8.0, 4.4 Hz, 1H), 4.25 (t, J = 9.6 Hz, 1H); 3.92 (dd, J = 14.8, 7.6 Hz, 1H), 3.77 (s, 3H), 2.76 (dd, J = 15.2, 4.4 Hz, 1H), 2.42–2.25 (m, 3H), 2.15–1.65 (m, 7H), 1.45 (s, 9H); ^{13}C NMR (100 MHz, $CDCl_3$): δ: 172.2, 169.5, 118.9, 80.2, 60.4, 58.7, 56.2, 52.4, 37.7, 34.0, 33.3, 32.8, 28.3, 27.7,20.9. ESI-MS: m/z 753.4 [2 M+Na]$^+$.

4.14.2. Compound 13c

Compound **13b** (0.49 mmol) was dissolved in 3 N methanolic HCl solution (3 mL). The resulting mixture was stirred at room temperature overnight, and then evaporated under reduced pressure. The crude product was re-dissolved in CH_2Cl_2 (20 mL) and washed once with a saturated solution of $NaHCO_3$. The organic layer was dried over Na_2SO_4, filtered and the solvent was removed under reduced pressure. The crude product was used as such in the next reaction step.

Dry DIPEA (341.4 μL, 1.96 mmol) was added to a solution of *N*-Boc, *N*-Me-(*S*)-ethylglycine (134.7 mg, 0.62 mmol), EDC·HCl (115 mg, 0.6 mmol) and HOBt (73.3 mg, 0.6 mmol) in dry CH_2Cl_2 (3 mL) at room temperature under a nitrogen atmosphere. The solution was stirred for 10 min before adding a solution of the crude amine (180 mg, 0.49 mmol) in CH_2Cl_2 (2 mL). The reaction mixture was stirred at room temperature and monitored by LC–MS. After reaction completion, the solution was diluted with CH_2Cl_2 (20 mL) and washed once with 5% citric acid and saturated $NaHCO_3$. The organic layer was dried over Na_2SO_4 and evaporated under reduced pressure. The crude product was purified by flash chromatography, eluant conditions: from 1% of MeOH and 99% of CH_2Cl_2 to 10% of MeOH and 90% of CH_2Cl_2. Yield 67% (152 mg, MW 464.57, 0.327 mmol) of pure **13c**. Analytical characterization: ^{1}H NMR (400 MHz, $CDCl_3$): δ: 7.14 (d, J = 7.2 Hz, 1H); 4.62 (dd, J = 7.6, 4.0, 1H), 4.56 (t, J = 9.6 Hz, 1H), 4.38 (bs, 1H), 3.97 (dd, J = 14.8, 7.2 Hz, 1H), 3.78 (s, 3H), 2.87 (s, 3H), 2.65 (bd, 1H), 2.45–2.28 (m, 3H), 2.20–1.70 (m, 9H), 1.50 (s, 9H), 0.92 (t, J = 7.6 Hz, 3H); ^{13}C NMR (100 MHz, $CDCl_3$): δ: 172.3, 169.0, 60.4, 58.6, 54.4, 52.5, 37.5, 33.9, 33.4, 32.7, 28.4, 27.7, 21.6, 20.8, 10.7. ESI-MS: m/z 465.5 $[M+H]^{+\cdot}$.

4.14.3. Compound 13d

A solution of nitrile **13c** (0.31 mmol) in EtOH (4 mL), and the was flowed through a Raney Nickel catalyst cartridge (hydrogen pressure 60 bar, temperature 60 °C, flow rate 0.5 mL/min) in a continuous flow hydrogenation H-Cube™ system. After reaction completion, the solvent was removed under reduced pressure and the crude was used as such in the next reaction step.

Dry TEA (86.4 μL, 0.62 mmol) and Boc_2O (135.3 mg, 0.62 mmol) were sequentially added to a stirred solution of the crude amine in dry CH_2Cl_2 (3 mL). The reaction mixture was stirred at room temperature and monitored by LC–MS. After reaction completion, the solution was diluted with CH_2Cl_2 (5 mL) and washed once with 5% citric acid and saturated $NaHCO_3$. The organic layer was dried over Na_2SO_4 and evaporated under reduced pressure. The crude product was purified by flash chromatography, eluant conditions: from 10% of EtOAc and 90% of petroleum ether to 100% of EtOAc. Yield 44% (78 mg, MW 568.60, 0.137 mmol) of pure **13d**. Analytical characterization: ^{1}H NMR (400 MHz, $CDCl_3$): δ: 6.88 (d, J = 4.8 Hz, 1H), 4.57 (m, 2H), 4.41 (dd, J = 9.2, 6.0 Hz, 1H), 4.94 (bd, J = 8.4 Hz, 1H), 3.75 (s, 3H), 3.06 (bs, 2H), 2.84 (s, 3H), 2.25 (m, 1H), 2.20–2.03 (m, 3H), 2.0–1.85 (m, 2H), 1.80–1.55 (m, 6H), 1.49 (s, 9H), 1.43 (s, 9H), 1.28 (t, J = 7.2 Hz, 1H), 0.91 (t, J = 7.2 Hz, 3H); ^{13}C NMR (100 MHz, $CDCl_3$): δ: 172.5, 170.7, 155.9, 79.0, 60.2, 58.5, 55.0, 52.3, 38.4, 37.2, 33.5, 32.8, 32.3, 28.4, 27.8, 21.7, 21.0, 14.2, 10.7. ESI-MS: m/z 569.5 $[M+H]^+$.

4.14.4. Compound 13e

A 2 N aqueous LiOH solution (0.5 mL) was slowly added to an iced cooled, stirred solution of **13d** (74 mg, 0.13 mmol) in 1,4-dioxane (1 mL). The reaction mixture was then stirred at room temperature until complete hydrolysis of the starting material. After reaction completion, the cloudy solution was concentrated, the residue was taken up in CH_2Cl_2 (10 mL) and water (10 mL), and acidified to pH ≈3 with 2 N aqueous HCl. The mixture was extracted with CH_2Cl_2 (2 × 10 mL), the combined organic layers were dried over Na_2SO_4, and then the solvent was removed under reduced pressure. Crude **13e** was used without purification in the next reaction step.

4.14.5. Compound 14i

HOBt (16.2 mg, 0.12 mmol), HBTU (45.5 mg, 0.12 mmol) and Sym-collidine (26.4 μL, 0.2 mmol) were sequentially added to a stirred solution of **17b** (39.3 mg, 0.055 mmol) and crude **13e** (72.1 mg, 0.13 mmol) in dry DMF (2 mL) at 0 °C. The reaction mixture was left stirring and monitored by LC–MS. After reaction completion, the mixture was diluted with EtOAc (20 mL) and sequentially washed with 5% aqueous citric (20 mL) acid, saturated aqueous sodium bicarbonate (20 mL) and brine (2 × 20 mL). The organic layer was dried over Na_2SO_4, and then the solvent removed under reduced pressure. The residue was purified by Biotage™ flash chromatography, eluant conditions: from 10% of EtOAc and 90% of petroleum ether to 100% of EtOAc. Yield 77% (66 mg, MW 1559.97, 0.042 mmol) of pure **7**. Analytical characterization: ^{1}H NMR (400 MHz, $CDCl_3$): δ: 8.03 (d, J = 4.5 Hz, 2H), 7.32–7.02 (m, 10H), 7.01 (d, J = 8.4 Hz, 2H), 6.85 (bs, 2H), 5.32 (d, J = 4.5 Hz, 2H), 4.68 (d, J = 7.2 Hz, 2H), 4.48 (bs, 2H), 4.45 (dd, J = 9.6, 4.0 Hz, 2H), 3.86 (m, 2H), 3.62–3.25 (m, 16H), 3.10 (m, 4H), 2.86 (s, 6H), 2.32–2.15 (M, 4H), 2.05–1.60 (m, 24H), 1.52 (s, 18H), 1.43 (s, 18H), 1.28 (m, 2H), 0.93 (t, J = 7.2 Hz, 6H); ^{13}C NMR (100 MHz,

$CDCl_3$): δ: 171.9, 169.4, 156.0, 138.4, 128.9, 128.8, 128.2, 128.1, 127.2, 70.5, 70.0, 69.6, 61.2, 58.7, 57.3, 54.8, 38.1, 37.3, 34.5, 33.2, 28.5, 26.6, 10.8. ESI-MS: m/z 1559.9 $[M+H]^+$.

4.14.6. Compound 9g

TFA (270 μL, 3.0 mmol) was added to a stirred solution of compound **14i** (61 mg, 0.04 mmol) in CH_2Cl_2 (5 mL). The reaction mixture was left stirring at room temperature overnight and then concentrated under reduced pressure. The residue was purified by chromatography on a C_{18} reverse phase semi-preparative hplc column, eluant conditions: from 70% of H_2O (0.2% TFA) and 30% of CH_3CN (0.2% TFA) to 30% of H_2O (0.2% TFA) and 70% of CH_3CN (0.2% TFA), flow rate 12 ml/min, 20 min runs. Yield 80% (52 mg, MW 1615.57, 0.032 mmol) of pure **9g**. Analytical characterization: ^{1}H NMR (400 MHz, D_2O): δ: 7.47 (m, 10H), 5.28 (s, 2H), 4.60 (d, J = 9.6 Hz, 2H), 4.49 (dd, J = 8.0, 5.2 hz, 2H), 4.05 (m, 2H), 3.50 (dd, J = 6.4, 3.2 Hz, 4H), 3.43 (dd, J = 5.2, 3.2 Hz, 4H), 3.32 (t, J = 6.4 Hz, 4H), 3.29 (t, J = 6.8 Hz, 2H), 3.20–3.00 (m, 4H), 2.95 (m, 2H), 2,67 (s, 6H), 2.25 (m, 2H), 2.15 (m, 2H), 2.03 (m, 4H), 1.90 (m, 6H), 1.85–1.55 (m, 16H), 0.92 (t, J = 7.6, Hz, 6H); (100 MHz, D_2O): δ: 173.3, 171.8, 170.4, 168.6, 135.9, 129.3, 127.3, 69.4, 69.3, 68.0, 62.6, 61.6, 58.4, 58.3, 56.1, 37.3, 36.4, 35.1, 32.4, 31.6, 30.5, 29.8, 29.1, 28.1, 27.9, 23.5, 8.1. ESI-MS: m/z 580.6 $[M+H]^{2+}$, 1159.7 $[M+H]^+$.

4.15. Head–tail dimer 10a—Schemes 12 and 13

4.15.1. Compound 16e

HOBt (81 mg, 0.6 mmol), HBTU (227.5 mg, 0.6 mmol) and Sym-collidine (132.1 μL, 1 mmol) were sequentially added to a stirred solution of commercially available **15e** (110 mg, 0.503 mmol) and *N*-Boc-(*S*)-2-Phenylglycine (158 mg, 0.63 mmol) in dry DMF (3 mL) at 0 °C . The reaction mixture was left stirring and monitored by LC–MS. After reaction completion, the mixture was diluted with EtOAc (20 mL) and sequentially washed with 5% aqueous citric acid (20 mL), saturated aqueous sodium bicarbonate (20 mL) and brine (2 × 20 mL). The organic layer was dried over Na_2SO_4, and then the solvent was removed under reduced pressure. The residue was purified by Biotage™ flash chromatography, eluant conditions: from 1% of MeOH and 99% of CH_2Cl_2 to 10% of MeOH and 90% of CH_2Cl_2. Yield 74% (167 mg, MW 451.53, 0.37 mmol) of pure **16e**. Analytical characterization: ^{1}H NMR (400 MHz, $CDCl_3$): δ: 7.32.7.20 (m, 5H), 6.28 (bs, 1H), 5.77 (bs, 1H), 5.07 (bs, 1H), 3.6–3.28 (m, 16H), 1.35 (s, 9H); ^{13}C NMR (100 MHz, $CDCl_3$): δ: 129.0, 128.3, 127.2, 70.7, 70.6, 70.5, 70.3, 70.0, 69.6, 68.8, 58.5, 50.7, 39.6, 28.3. ESI-MS: m/z 452.5 $[M+H]^+$, 474.5 $[M+Na]^+$.

4.15.2. Compound 18a

TFA (900 μL, 10 mmol) was added to a stirred solution of compounds **16e** (95 mg, 0.27 mmol) in CH_2Cl_2 (3 mL). The reaction mixture was left stirring at room temperature and then concentrated under reduced pressure. The crude product was used in the next reaction step without further purification.

HOBt (74.6 mg, 0.55 mmol), HBTU (208.6 mg, 0.55 mmol) and sym-collidine (132.1 μL, 1 mmol) were sequentially added to a stirred solution of the crude residue (theoretically 0.27 mmol) and compound **4d** (150 mg, 0.034 mmol) in dry DMF (3 mL) at 0 °C. The reaction mixture was left stirring and monitored by LC–MS. After reaction completion, the mixture was diluted with EtOAc (20 mL) and washed with 5% aqueous citric acid (20 mL), saturated aqueous sodium bicarbonate (20 mL) and brine (2 × 20 mL). The organic layer was dried over Na_2SO_4, and then the solvent was removed under reduced pressure. The residue was purified by Biotage™ flash chromatography, eluant conditions: from 1% of MeOH and 99% of CH_2Cl_2 to 10% of MeOH and 90% of CH_2Cl_2. Yield 82% (170 mg, MW 774.92, 0.220 mmol) of pure **18a**. Analytical characterization: ^{1}H NMR (400 MHz, $CDCl_3$): δ: 7.93 (d, J = 6.8 Hz, 1H), 7.51 (d, J = 8.0 Hz, 1H), 7.36–7.27 (m, 5H), 6.37 (bs, 1H), 5.38 (d, J = 7 Hz, 1H), 4.71 (d, J = 6.8 Hz, 1H), 4.48 (m, 2H), 3.68 (m, 1H), 3.65 (m, 8H), 3.55 (m, 4H), 3.45 (m, 4H), 3.38 (m, 2H), 3.32 (m, 1H), 2.87 (s, 3H), 2.32 (m 1H), 2.22 (m, 1H), 2.10–1.40 (m, 3H), 1.35–1.70 (m, 5H), 1.52 (s, 9H), 1.30 (m, 2H), 0.93 (t, J = 7 Hz, 3H); ^{13}C NMR (100 MHz, $CDCl_3$): δ: 173.2, 172.4, 171.4, 170.0, 169.5, 138.2, 128.9, 128.2, 127.2, 70.7, 70.6, 70.5, 70.3, 70.0, 69.5, 64.3, 61.4, 61.0, 59.1, 58.8, 57.4, 53.9, 50.6, 41.6, 39.7, 34.4, 33.0, 32.8, 30.4, 28.4, 26.4, 21.6, 10.7 . ESI-MS: m/z 775.5 $[M+H]^+$, 797.5 $[M+Na]^+$.

4.15.3. Compound 11e

DCC (22.7 mg, 0.11 mmol) and DMAP (2.4 mg, 0.02 mmol) were sequentially added to a stirred solution of compound **4h** (60 mg, 0.1 mmol) and 4-pentynoic acid (9.8 mg, 0.1 mmol) in dry CH_2Cl_2 (4 mL) at 0 °C. The reaction mixture was warmed to room temperature over a period of 1 h. After reaction completion, the reaction mixture was filtered, and the filtrate was washed with diethyl ether. The organic phase was removed under reduced pressure, and the crude product was purified by Biotage™ flash chromatography, eluant conditions: from 1% of MeOH and 99% of CH_2Cl_2 to 10% of MeOH and 90% of CH_2Cl_2. Yield 93% (64 mg, MW 685.87, 0.093 mmol) of pure **11e**. Analytical characterization: $[\alpha]_{20}^{D}$ −116.0 (c 0.90, $CHCl_3$); ^{1}H NMR (400 MHz, $CDCl_3$): δ: 7.90 (d, J = 6.8 Hz, 1H), 7.28–7.09 (m, 11H), 6.13 (d, J = 8.0 Hz, 1H), 4.64 (d, J = 7.0 Hz, 1H), 4.45 (bs, 1H), 4.34 (m, 1H), 3.67 (m, 1H), 3.35 (m, 1H), 3.00–2.60 (m, 4H), 2.50–2.30 (m, 5H), 2.15 (m, 1H), 2.00–1.50 (m, 9H), 1.45 (m, 1H), 1.40 (s, 9H), 1.35–1.05 (m, 1H), 0.91 (t, J = 7.6 Hz, 3H); ^{13}C NMR (100 MHz, $CDCl_3$): δ: 172.8, 171.7, 171.3, 169.3, 142.0, 141.2, 128.7, 128.6, 127.5, 127.4, 127.3, 127.2, 80.7, 69.0, 62.0, 58.9, 56.8, 54.0, 41.8, 39.9, 35.4, 34.5, 33.3, 33.0, 32.0, 28.3, 27.5, 25.5, 21.9, 15.1, 10.8. ESI-MS: m/z 686.5 $[M+H]^+$, 703.5 $[M+Na]^+$.

4.15.4. Compound 19a

A 0.9 M aqueous solution of sodium ascorbate (70 μL) and a 0.3 M aqueous solution of $Cu(OAc)_2$ (50 μL) were sequentially added to a stirred solution of compound **18a** (44 mg, 0.057 mmol) and compound **11e** (38 mg, 0.057 mmol) in a 1:1 mixture of H_2O/^{t}BuOH (1 mL). The reaction mixture was stirred overnight at room temperature and then the solvent was removed under reduced pressure. The residues were purified by Biotage™ flash chromatography, eluant conditions: from 1% of MeOH and 99% of CH_2Cl_2 to 10% of MeOH and 90% of CH_2Cl_2. Yield 61% (51 mg, MW 1460.79, 0.035 mmol) of pure **19a**. Analytical characterization: ^{1}H NMR (400 MHz, $CDCl_3$): δ: 7.95 (d, J = 6.8 Hz, 2H), 7.51 (m, 2H), 7.35–7.20 (m, 15H), 7.16 (d, J = 9.2 Hz, 2H), 6.75 (bs, 1H), 6.22 (d, J = 6.8 Hz, 1H), 5.43 (d, J = 7.2 Hz, 1H), 4.72 (dd, J = 16, 7.6 Hz, 2H), 4.48 (m, 6H), 3.82 (m, 4H), 3.70–3.30 (m, 15H), 3.07 (t, J = 7.6 Hz, 2H), 2.85 (m, 6H), 2,.67 (m, 3H), 2.48 (m, 1H), 2.25 (m, 3H), 2.05 (m, 1H), 2.00–1.80 (m, 5H), 1.80–1.65 (m, 7H), 1.52 (s, 9H), 1.48 (s, 9H), 1.35 (m, 1H), 1.25 (m, 2H), 1.10 (m, 1H), 0.94 (t, J = 7.2 Hz, 6H); ^{13}C NMR (100 MHz, $CDCl_3$): δ: 173.1, 171.4, 169.6, 169.4, 146.1, 142.1, 138.4, 128.8, 128.7, 128.6, 127.3, 127.2, 127.1, 123.0, 70.5, 70.4, 70.2, 69.5, 69.3, 64.3, 61.4, 61.1, 58.8, 57.2, 56.8, 53.9, 53.7, 50.4, 41.7, 39.6, 35.5, 34.5, 33.2, 33.0, 31.2, 28.4, 28.3, 26.4, 25.6, 21.6, 21.3, 10.7. ESI-MS: m/z 1461.7 $[M+H]^+$, 1482.7 $[M+Na]^+$.

4.15.5. Compound 10a

TFA (270 μL, 3.0 mmol) was added to a stirred solution of compound **19a** (54 mg, 0.030 mmol) in CH_2Cl_2 (5 mL). The reaction mixture was left stirring at room temperature overnight and then concentrated under reduced pressure. The residue was purified by chromatography on a C_{18} reverse phase semi-preparative hplc

column, eluant conditions: from 40% of H_2O (0.1% TFA) and 60% of CH_3CN (0.1% TFA) to 25% of H_2O (0.1% TFA) and 75% of CH_3CN (0.1% TFA), flow rate 15 ml/min, 22 min runs. Yield 90% (41 mg, MW 1488.60, 0.027 mmol) of pure **10a**. Analytical characterization: ^{1}H NMR (400 MHz, D_2O): δ: 8.77 (s, 1H), 7.39–7.29 (m, 15H), 6.04 (s, 1H), 5.33 (s, 1H), 4.67 (d, J = 10.0 Hz, 2H), 4.60–4.40 (m, 5H), 4.00 (m, 2H), 3.90 (m, 2H), 3.79 (m, 2H), 3.58 (d, J = 3.6 Hz, 2H), 3.55–38 (m, 11H), 3.35–3.20 (m, 2H), 2.96 (m, 3H), 2.67 (s, 6H), 2.57 (t, J = 7.2 Hz, 2H), 2.23 (m, 2H), 2.12 (m, 2H), 2.07–1.85 (m, 8H), 1.85–1.62 (m, 7H), 1.55 (m, 1H), 1.50–1.30 (m, 2H), 0.95 (m, 6H); ^{13}C NMR (100 MHz, D_2O): δ:174.8, 173.2, 172.7, 171.8, 171.1, 169.9, 168.4, 168.2, 146.0, 141.0, 140.8, 135.9, 129.2, 129.0, 128.8, 127.8, 127.3, 127.1, 123.9, 69.5, 69.4, 68.7, 68.6, 63.2, 62.7, 62.6, 61.7, 58.7, 58.3, 58.0, 57.6, 54.5, 54.4, 50.0, 40.7, 39.2, 38.9, 37.2, 35.1, 32.4, 31.5, 31.4, 30.1, 29.4, 27.9, 27.7, 23.4, 21.0, 8.2. ESI-MS: m/z 631.3 $[M+H]^{2+}$, 1260.8 $[M+H]^+$, 1282.7 $[M+Na]^+$.

4.16. Head–tail dimer 10b—Schemes 12 and 14

4.16.1. Compound 18b

A 1.0 M aqueous citric acid solution (250 μL) was added to a solution of **18a** (170 mg, 0.220 mmol) in H_2O/EtOH 1:9 (3 mL**).** The solution was hydrogenated by flowing through a 10% Pd/C catalyst cartridge (hydrogen pressure 10 bar, temperature 35 °C, flow rate 0.5 mL/min) using the H-Cube™ system. After reaction completion, the solvent was removed under reduced pressure. The crude product was used without any further purification, and only an analytical sample was purified by semi-preparative HPLC reverse phase chromatography, eluant conditions: from 90% H_2O (1% CH_3COOH) and 10% CH_3CN (1% CH_3COOH) to 100% CH_3CN (1% CH_3COOH). Yield 98% (162 mg, MW 748.95, 0.219 mmol) of pure **18b**. Analytical characterization: ^{1}H NMR (400 MHz, CD_{3OD}): $_\delta$: 8.6 (bs, 1H), 7.44–7.33 (m, 5H), 5.40 (s, 1H), 4.67 (dd, J = 5.2, 2.8 Hz, 1H), 4.53 (m, 2H), 4.01 (m, 1H), 3.67 (m, 5H), 3.65–3.47 (m, 8H), 3.39 (m, 2H), 3.09 (bs, 2H), 2.85 (s, 3H), 2.27 (m, 1H), 2.16 (m, 1H), 2.10- 1.88 (m, 4H), 1.82–1.65 (m, 4H), 1.55 (m, 1H), 1.50 (s, 9H), 1.42 (bs, 2H), 0.94 (t, J = 7.2 Hz, 3H); ^{13}C NMR (100 MHz, CD_3OD): δ: 172.3, 171.8, 171.0, 137.6, 128.4, 127.9, 127.2, 70.1, 69.8, 69.0, 67.4, 63.9, 61.4, 58.5, 57.3, 40.3, 39.6, 39.2, 33.2, 32.8, 30.7, 29.5, 27.3, 27.2, 26.9, 9.6. ESI-MS: m/z 749.6 $[M+H]^+$, 771.7 $[M+Na]^+$.

4.16.2. Compound 18c

DCC (24.8 mg, 0.12 mmol) and DMAP (3 mg, 0.025 mmol) were sequentially added to a stirred solution of compound **18b (**83 mg, 0.11 mmol) and 4-pentynoic acid (0.11 mmol) in dry CH_2Cl_2 (4 mL) at 0 °C. The reaction mixture was warmed to room temperature over a period of 1 h. After reaction completion, the reaction mixture was filtered, and washed with diethyl ether. The combined solvents were removed under reduced pressure, and the crude product was purified by Biotage™ flash chromatography, eluant conditions: : from 1% of MeOH and 99% of CH_2Cl_2 to 10% of MeOH and 90% of CH_2Cl_2. Yield 74% (67 mg, MW 829.01, 0.081 mmol) of pure **18c**. Analytical characterization: ^{1}H NMR (400 MHz, $CDCl_3$): δ: 7.98 (d, J = 7.0 Hz, 1H), 7.51 (d, J = 6.8 Hz, 1H), 7.45–7.25 (m, 5H), 6.68 (bs, 1H), 5.43 (d, J = 7.2 Hz, 1H), 4.71 (d, J = 6.8 Hz, 1H); 4.48 (bs, 2H), 3.8 (m, 1H), 3.70- 3.30 (m, 18H), 2.87 (s. 3H), 2.48 (m, 2H), 2.40–2.15 (m, 4H), 2.15–1.65 (m, 9H), 1.52 (s, 9H), 1.40–1.25 (m, 2H), 0.93 (t, J = 7.2 Hz, 3H); ^{13}C NMR (100 MHz, $CDCl_3$): δ: 173.4, 173.2, 171.4, 171.3, 170.1, 169.5, 138.2, 128.8, 128.2, 127.2, 83.2, 70.6, 70.5, 70.4, 70.3, 70.1, 69.8, 69.5, 69.2, 64.3, 61.4, 58.8, 57.2, 53.9, 41.6, 39.7, 39.6, 39.1, 35.1, 34.5, 33.0, 31.2, 28.4, 26.6, 21.6, 20.6, 14.8, 10.6. ESI-MS: m/z 829.6 $[M+H]^+$, 851.5 $[M+Na]^+$.

4.16.3. Compound 19b

A 0.9 M aqueous solution of sodium ascorbate (60 μL) and a 0.3 M aqueous solution of $Cu(OAc)_2$ (40 μL) were sequentially added to a stirred solution of compound **19c** (37 mg, 0.045 mmol) and compound **4f** (29 mg, 0.045 mmol) in a 1:1 mixture of H_2O/^{t}BuOH (750 μL). The reaction mixture was stirred overnight at room temperature and then the solvent was removed under reduced pressure. The residues were purified by Biotage™ flash chromatography, eluant conditions: from 1% of MeOH and 99% of CH_2Cl_2 to 10% of MeOH and 90% of CH_2Cl_2. Yield 80% (52 mg, MW 1460.79, 0.036 mmol) of pure **19b**. Analytical characterization: ^{1}H NMR (400 MHz, $CDCl_3$): δ: 7.89 (d, J = 6.8 Hz, 1H), 7.71 (d, J = 7.0 Hz, 1H), 7.47 (m, 1H), 7.35–7.12 (m, 15H), 7.08 (d, J = 7.2 Hz, 1H), 6.85 (bs, 1H), 6.55 (bs, 1H), 6.10 (d, J = 8.8 Hz, 1H), 5.36 (d, J = 7.2 Hz, 1H), 4.56 (m, 3H), 4.38 (m, 4H), 4.10 (bs, 1H), 3.75 (m, 2H), 3.60–3.20 (m, 18H), , 2.97 (bs, 2H), 2.75 (s, 6H), 2.55 (m, 3H), 2.32 (m, 1H), 2.15 (m, 3H), 1.95–1.60 (m, 13H), 1.43 (s, 9H), 1.38 (s, 9H); 1.35–1.15 (m, 3H), 1.02 (m, 1H), 0.85 (t, J = 7.2 Hz, 6H); ^{13}C NMR (100 MHz, $CDCl_3$): δ: 171.9, 171.4, 170.7, 169.6, 141.8, 141.2, 138.4, 128.8, 128.7, 128.1, 127.6, 127.5, 127.3, 127.2, 127.1, 70.4, 70.1, 69.9, 69.8, 69.5, 64.3, 61.4, 61.3, 58.8, 57.2, 56.9, 53.9, 53.6, 41.6, 40.4, 39.6, 39.2, 34.4, 33.6, 33.3, 33.0, 31.1, 28.4, 28.3, 26.5, 25.9, 21.7, 21.2, 10.7. ESI-MS: m/z 681.2 $[M+H]^{2+}$,1461.0 $[M+H]^+$, 1483.0 $[M+Na]^+$.

4.16.4. Compound 10b

TFA (180 μL, 2.0 mmol) was added to a stirred solution of compound **19b** (30 mg, 0.022 mmol) in CH_2Cl_2 (4 mL). The reaction mixture was left stirring at room temperature overnight and then concentrated under reduced pressure. The residue was purified by chromatography on a C_{18} reverse phase semi-preparative hplc column, eluant conditions: from 40% of H_2O (0.1% TFA) and 60% of CH_3CN (0.1% TFA) to 25% of H_2O (0.1% TFA) and 75% of CH_3CN (0.1% TFA), flow rate 15 ml/min, 22 min runs. Yield 86% (28 mg, MW 1488.60, 0.019 mmol) of pure **10b**. Analytical characterization: ^{1}H NMR (400 MHz, D_2O): δ: 7.78 (s, 1H), 7.37–7.28 (m, 15H), 6.04 (s, 1H), 5.34 (s, 1H), 4.78 (d, J = 10.4 Hz, 1H), 4.66 (m, 1H), 4.53 (m, 3H), 4.36 (m, 1H), 4.03 (m, 2H), 3.88 (t, J = 6.0 Hz, 2H), 3.60–3.25 (m, 16H), 3.28 (m, 3H), 2.94 (t, J = 14.4 Hz, 2H), 2.70 (s, 3H), 2.58 (s, 3H), 2.56 (t, J = 7.2 Hz, 2H), 2.35–2.05 (m, 5H), 2.05–1.88 (m, 9H), 1.85–1.65 (m, 6H), 1.62–1.46 (m, 3H), 0.95 (m, 6H); ^{13}C NMR (100 MHz, D_2O): δ: 174.9, 173.2, 172.7, 171.1, 169.5, 168.7, 146.5, 141.0, 140.9, 136.0, 129.2, 129.0, 128.9, 127.8, 127.4, 127.3, 127.1, 69.6, 69.4, 68.8, 68.7, 63.2, 62.8, 62.6, 61.9, 61.8, 58.7, 58.2, 58.0, 57.6, 54.5, 54.4, 52.0, 39.3, 39.0, 38.1, 35.0, 32.4, 32.3, 31.8, 31.5, 27.9, 27.7, 23.5, 23.4, 20.9, 8.2, 8.1. ESI-MS: m/z 631.1 $[M+H]^{2+}$, 1260.8 $[M+H]^+$, 1282.7 $[M+Na]^+$.

4.17. Head–tail dimer 10c—Schemes 12 and 15

4.17.1. Compound 18d

Diglycolic anhydride (25.5 mg, 0.22 mmol) and pyridine (36.4 μL, 0.45 mmol) were sequentially added to a stirred solution of compound **18b (**83 mg, 0.11 mmol) in DMF (3 mL). The reaction mixture was stirred at room temperature for 4 h. After reaction completion, water (20 mL) was added to the reaction mixture. The mixture was diluted with EtOAc (20 mL) and washed with 5% aqueous citric acid (20 mL), saturated aqueous sodium bicarbonate (20 mL) and brine (2 × 20 mL). The combined organic layer was dried over Na_2SO_4, and then the solvent was removed under reduced pressure. Finally, the crude product was purified by flash chromatography on a Biotage™ C_{18} reverse phase column, eluant conditions: from 90% H_2O (1% CH_3COOH) and 10% CH_3CN (1% CH_3COOH) to 100% CH_3CN (1% CH_3COOH). Yield 58% (55 mg, MW 865.00, 0.064 mmol) of pure **18d**. Analytical characterization: ^{1}H

NMR (400 MHz, $CDCl_3$): δ: 8.01 (d, J = 7.0 Hz, 1H), 7.61 (bs, 1H), 7.53 (d, J = 6.8 Hz, 1H), 7.40–7.28 (m, 5H), 6.98 (bs, 1H), 4.52 (d, J = 7.2 Hz, 1H), 4.71 (d, J = 6.8 Hz, 1H), 4.5 (m, 2H), 4.10 (m, 3H), 3.82 (m, 1H); 3.70–3.30 (m, 18H), 2.88 (s, 3H), 2.25 (m, 2H), 2.08 (s, 2H), 2.05–1.70 (m, 8H), 1.51 (s, 9H), 1.39 (m, 2H), 0.93 (t, J = 7.2 Hz, 3H); ^{13}C NMR (100 MHz, $CDCl_3$): δ: 175.2, 173.0, 171.9, 171.4, 169.8, 169.8, 137.9, 128.8, 128.3, 127.2, 77.3, 77.0, 76.8, 71.4, 70.4, 70.0, 69.7, 69.5, 69.2, 64.3, 61.6, 58.9, 57.2, 54.0, 41.5, 39.7, 38.8, 34.3, 33.0, 31.2, 28.4, 26.7, 21.6, 20.6, 10.6. ESI-MS: m/z 865.4 $[M+H]^+$, 887.4 $[M+Na]^+$.

4.17.2. Compound 19c

HOBt (9.5 mg, 0.078 mmol), HBTU (29.6 mg, 0.078 mmol) and sym-collidine (33 μL, 0.25 mmol) were sequentially added to a stirred solution of compound **18d** (54 mg, 0.063 mmol) and compound **4h** (52 mg, 0.08 mmol) in dry DMF (1 mL) at 0 °C. The reaction mixture was left stirring and monitored by LC–MS. After reaction completion, the mixture was diluted with EtOAc (20 mL) and washed with 5% aqueous citric acid (20 mL), saturated aqueous sodium bicarbonate (20 mL) and brine (2 × 20 mL). The organic layer was dried over Na_2SO_4, and then the solvent was removed under reduced pressure. The residue was purified by Biotage™ flash chromatography, eluant conditions: from 1% of MeOH and 99% of CH_2Cl_2 to 10% of MeOH and 90% of CH_2Cl_2. Yield 67% (61 mg, MW 1457.77, 0.042 mmol) of pure **19c**. Analytical characterization: ^{1}H NMR (400 MHz, $CDCl_3$): δ: 7.87 (d, J = 7.2 Hz, 1H), 7.76 (d, J = 6.8 Hz, 1H), 7.63 (d, J = 6.0 Hz, 1H), 7.46 (m, 2H), 7.35–7.10 (m, 15H), 6.72 (bs, 1H), 6.15 (d, J = 8.4 Hz, 1H), 5.35 (d, J = 7.2 Hz, 1H), 4.64 (dd, J = 19.2, 7.2 Hz, 2H), 4.40 (m, 4H), 3.95 (m, 4H), 3.72 (m, 3H), 3.6–3.20 (m, 18H), 2.79 (s, 3H), 2.75 (s, 3H), 2.52 (m, 2H), 2.35 (m, 1H), 2.18 (m, 2H), 1.90–1.55 (m, 14H), 1.43 (s, 9H), 1.41 (s, 9H), 1.30–1.10 (m, 4H), 0.85 (m, 6H); ^{13}C NMR (100 MHz, $CDCl_3$): δ: 172.7, 171.3, 169.6, 168.9, 168.9, 142.2, 138.4, 128.8, 128.6, 128.5, 128.1, 127.4, 127.3, 127.2, 70.7, 70.5, 70.4, 70.3, 70.1, 69.6, 69.5, 64.3, 61.7, 61.4, 61.3, 60.5, 58.9, 58.8, 57.2, 56.8, 53.9, 53.5, 41.6, 40.0, 39.7, 39.6, 38.7, 34.4, 34.3, 33.1, 33.0, 31.1, 28.4, 28.3, 26.4, 25.7, 21.7, 21.3, 10.7, 10.6. ESI-MS: m/z 1452.9 $[M+H]^+$, 1475.0 $[M+Na]^+$.

4.17.3. Compound 10c

TFA (360 μL, 4.0 mmol) was added to a stirred solution of compound **19c** (58 mg, 0.040 mmol) in CH_2Cl_2 (5 mL). The reaction mixture was left stirring at room temperature overnight and then concentrated under reduced pressure. The residue was purified by chromatography on a C_{18} reverse phase semi-preparative hplc column, eluant conditions: from 40% of H_2O (0.1% TFA) and 60% of CH_3CN (0.1% TFA) to 25% of H_2O (0.1% TFA) and 75% of CH_3CN (0.1% TFA), flow rate 15 ml/min, 22 min runs. Yield 88% (55 mg, MW 1480.57, 0.037 mmol) of pure **10c**. Analytical characterization: ^{1}H NMR (400 MHz, D_2O): δ: 7.41–7.30 (m, 15H), 6.06 (s, 1H), 5.36 (s, 1H), 4.67 (d, J = 8.4 Hz, 2H), 4.55 (m, 2H), 4.10 (d, J = 5.2 hz, 4H), 4.05 (m, 2H), 3.93 (t, J = 6.4 Hz, 1H), 3.89 (t, J = 5.6 Hz, 1H), 2.70 (s, 3H), 2.69 (s, 3H), 2.25 (m, 2H), 2.15 (m, 2H), 2.08–1-68 (m, 17H), 1.65–1.50 (m, 3H), 0.97 (m, 6H) ; ^{13}C NMR (100 MHz, D_2O): δ: 172.8, 171.8, 171.7, 171.1, 170.1, 168.5, 168.3, 141.0, 140.9, 129.2, 129.0, 128.9, 127.8, 127.4, 127.3, 127.2, 70.0, 69.9, 69.6, 69.4, 68.8, 68.7, 63.2, 62.8, 62.7, 61.9, 61.8, 58.8, 58.5, 58.0, 57.7, 54.6, 54.5, 40.7, 39.3, 39.0, 38.6, 37.4, 32.4, 31.6, 31.5, 30.5, 29.5, 29.0, 27.9, 27.7, 23.4, 8.2, 8.1. ESI-MS: m/z 627.1 $[M+H]^{2+}$, 1252.8 $[M+H]^+$, 1274.8 $[M+Na]^+$.

4.18. Head–tail dimer 10d—Schemes 12 and 16

4.18.1. Compound 19d

A 0.9 M aqueous solution of sodium ascorbate (45 μL, 0.4 mmol) and a 0.3 M aqueous solution of $Cu(OAc)_2$ (65 μL, 0.02 mmol) were added to A stirred solution of compound **4e** (61.8 mg, 0.10 mmol) and of the alkyne **20a**[55] (70.8 mg, 0.10 mmol) in a 1:1 mixture of H_2O/^{t}BuOH (300 μL). The reaction mixture was stirred overnight at room temperature, and then the solvent was removed under reduced pressure. Finally, the residue was purified by flash chromatography, eluant conditions: isocratic, CH_2Cl_2/MeOH 95/5. Yield 57% (76 mg, MW 1324.62, 0.057 mmol) of pure **19d**. Analytical characterization: $[\alpha]_{20}^{D}$ −55.6 (c 0.54, MeOH); ^{1}H NMR (400 MHz, $CDCl_3$): δ: 7.83 (d, J = 7.2 Hz, 1H), 7.76 (d, J = 7.2 Hz, 2H), 7.57 (m, 5H), 7.49 (bd, 1H), 7.45–7.13 (m, 18H), 6.17 (d, J = 8.2 Hz, 1H), 5.23 (bd, J = 7.2 Hz, 1H), 4.80–4.30 (m, 9H), 4.30–3.90 (m, 6H), 3.90–3.50 (m, 4H), 2.87 (s, 3H), 2.38 (m, 1H), 2.21 (m, 1H), 2.02 (m, 1H), 1.94–1.45 (m, 10H), 1.43–1.32 (m, 11H), 1.30–1.05 (m, 6H), 0.93 (t, 3H); ^{13}C NMR (100 MHz, $CDCl_3$): δ: 173.0, 171.2, 170.7, 169.4, 169.3, 155.7, 153.3, 143.9, 141.8, 141.3, 133.0, 129.8, 128.8, 127.7, 127.4, 127.3, 127.2, 127.1, 125.0, 120.0, 80.1, 74.6, 68.0, 62.6, 61.2, 58.7, 56.8, 56.3, 54.9, 54.6, 53.7, 51.8, 48.4, 47.7, 47.2, 40.4, 33.5, 33.2, 31.1, 28.5, 27.2, 26.0, 25.6, 24.0, 16.3, 10.2. ESI-MS: m/z 1325.4 $[M+H]^+$, 1347.4 $[M+Na]^+$.

4.18.2. Compound 10d

Compound **19d** (59.7 mg, 0.045 mmol) was dissolved into a 20% solution of piperidine in CH_2Cl_2 (2 mL). The reaction mixture was stirred for 30 min at room temperature. and then concentrated in vacuo. The residue was used as such in the next reaction step.

A 3 N solution of HCl in MeOH (0.5 mL) was added to a stirred solution of crude (theoretically 0.045 mmol) in MeOH (2 mL). The reaction mixture was left stirring at room temperature overnight and then concentrated under reduced pressure. The residue was purified by chromatography on a C_{18} reverse phase semi-preparative hplc column, eluant conditions: from 80% of H_2O (0.1% TFA) and 20% of CH_3CN (0.1% TFA) to 50% of H_2O (0.1% TFA) and 50% of CH_3CN, flow rate 20 ml/min, 10 min runs. Yield 90% (45 mg, MW 1231.29, 0.040 mmol) of pure **10d**. Analytical characterization: $[\alpha]_{20}^{D}$ −29.0 (c 0.88, H_2O); ^{1}H NMR (400 MHz, D_2O): δ: 7.86 (s, 1H); 7.43–7.05 (m, 15H), 5.91 (s, 1H), 4.63–4.10 (m, 10H), 3.95–3.80 (m, 4H), 3.48 (m, 2H), 2.59 (s, 3H), 2.25–1.38 (m, 16H), 1.23 (m, 2H), 1.14 (m, 3H), 0.96 (m, 3H); ^{13}C NMR (100 MHz, D_2O): δ: 172.0, 169.7, 169.5, 154.7, 144.5, 141.2, 141.0, 134.0, 133.3, 130.2, 130.0, 128.7, 127.6, 127.3, 127.0, 126.6, 125.2, 74.0, 61.5, 58.1, 57.4, 57.0, 56.5, 56.0, 54.3, 54.1, 51.8, 48.9, 47.6, 38.6, 32.3, 31.0, 29.6, 28.6, 27.7, 26.9, 24.4, 23.5, 16.0, 15.3, 8.4. ESI-MS: m/z 1025.7 $[M+Na]^+$, 502.4 $[M+2H]^{2+}$.

Acknowledgment

The authors are thankful to 'FONDAZIONE CARIPLO' for financing through Project 2009-2534, titled 'Inhibitors of Apoptosis Proteins (IAPs) as anticancer therapeutics'.

Supplementary data

Supplementary data associated with this article can be found, in the online version, at http://dx.doi.org/10.1016/j.bmc.2012.09.020.

References and notes

1. Fulda, S.; Debatin, K. M. *Curr. Cancer Drug Targets* **2004**, *4*, 569.
2. Kim, R. *Nat. Rev. Cancer* **2005**, *103*, 1551.
3. Cotter, T. G. *Nat. Rev. Cancer* **2009**, *9*, 501.
4. Damgaard, R. B.; Gyrd-Hansen, M. *Discov. Med.* **2011**, *11*, 221.
5. Nagata, S. *Ann. N. Y. Acad. Sci.* **2010**, *1209*, 10.
6. Okouchi, M.; Ekshyyan, O.; Maracine, M.; Aw, T. Y. *Antioxid. Redox Signal.* **2007**, *9*, 1059.
7. Baratchi, S.; Kanwar, R. K.; Kanwar, J. R. *Crit. Rev. Biochem. Mol. Biol.* **2010**, *45*, 535.
8. Fulda, S.; Debatin, K. M. *Oncogene* **2006**, *25*, 4798.
9. Wiezorek, J.; Holland, P.; Graves, J. *Clin. Cancer Res.* **2010**, *16*, 1701.

10. Brenner, D.; Mak, T. W. *Curr. Opin. Cell Biol.* **2009**, *21*, 871.
11. Constantinou, C.; Papas, K. A.; Constantinou, A. I. *Curr. Cancer Drug Targets* **2009**, *9*, 717.
12. Metz, J. T.; Hajduk, P. J. *Curr. Opin. Chem. Biol.* **2010**, *14*, 498.
13. Knight, Z. A.; Lin, H.; Shokat, K. M. *Nat. Rev. Cancer* **2010**, *10*, 130.
14. Allen, J. A.; Roth, B. A. *Annu. Rev. Pharmacol. Toxicol.* **2011**, *51*, 117.
15. Danson, S.; Dean, E.; Dive, C.; Ranson, M. *Curr. Cancer Drug Targets* **2007**, *7*, 785.
16. Altieri, D. C. J. *Biochem.* **2010**, *430*, 199.
17. Crook, N. E.; Clem, R. J.; Miller, L. K. *J. Virol.* **1993**, *67*, 2168.
18. Hunter, M.; LaCasse, E. C.; Korneluk, R. G. *Apoptosis* **2007**, *12*, 1543.
19. Shi, Y. *Protein Sci.* **2004**, *13*, 1979.
20. Eckelman, P.; Salvesen, G. S.; Scott, F. L. *EMBO Rep.* **2006**, *7*, 988.
21. Srinivasula, S. M.; Ashwell, J. D. *Mol. Cell* **2008**, *30*, 123.
22. Dubrez-Daloz, L.; Dupoux, A.; Cartier, J. *Cell Cycle* **2008**, *7*, 1036.
23. Gyrd-Hansen, M.; Meier, P. *Nat. Rev. Cancer* **2010**, *10*, 561.
24. Mufti, R.; Burstein, E.; Duckett, C. S. *Arch. Biochem. Biophys.* **2007**, *463*, 168.
25. Kashar, H. *Clin. Cancer Res.* **2010**, *16*, 4496.
26. Deveraux, Q. L.; Leo, E.; Stennicke, H. R.; Welsh, K.; Salvesen, G. S.; Reed, J. C. *EMBO J.* **1999**, *18*, 5242.
27. Du, M.; Fang, Y.; Li, L.; Wang, X. *Cell* **2000**, *102*, 33.
28. Verhagen, M.; Ekert, P. G.; Pakusch, M.; Silke, J.; Connolly, L. M.; Reid, G. E.; Moritz, R. L.; Simpson, R. J.; Vaux, D. L. *Cell* **2000**, *102*, 43.
29. Chai, J.; Du, C.; Wu, J.-W.; Kyin, S.; Wang, X.; Shi, Y. *Nature* **2000**, *406*, 855.
30. Liu, Z.; Sun, C.; Olejniczak, E. T.; Meadows, R. P.; Betz, S. F.; Oost, T.; Herrmann, J.; Wu, J. C.; Fesik, S. W. *Nature* **2000**, *408*, 1004.
31. Wu, G.; Chai, J.; Suber, T. L.; Wu, J. W.; Du, C.; Wang, X.; Shi, Y. *Nature* **2000**, *408*, 1008.
32. Shiozaki, N.; Chai, J.; Rigotti, D. J.; Riedl, S. J.; Li, P.; Srinivasula, S. M.; Alnemri, E. S.; Fairman, R.; Shi, Y. *Mol. Cell* **2003**, *11*, 519.
33. Riedl, S. J.; Renatus, M.; Schwarzenbacher, R.; Zhou, Q.; Sun, C.; Fesik, S. W.; Liddington, R. C.; Salvesen, G. S. *Cell* **2001**, *104*, 791.
34. Shi, Z.; Liang, Y. J.; Chen, Z. S.; Wang, X. H.; Ding, Y.; Chen, L. M. L.; Fu, W. *Oncol. Rep.* **2007**, *17*, 969.
35. Mizutani, Y.; Nakanishi, H.; Li, Y. N.; Matsubara, H.; Yamamoto, K.; Sato, N.; Shiraishi, T.; Nakamura, T.; Mikami, K.; Okihara, K.; Takaha, N.; Ukimura, O.; Kawauchi, A.; Nonomura, N.; Bonavida, B.; Miki, T. *Int. J. Oncol.* **2007**, *30*, 919.
36. Holcik, M.; Gibson, H.; Korneluk, R. G. *Apoptosis* **2001**, *6*, 253.
37. Dean, J.; Ranson, M.; Blackhall, F.; Dive, C. *Expert Opin. Ther. Targets* **2007**, *11*, 1459.
38. Rajapakse, H. A. *Curr. Top. Med. Chem.* **2007**, *7*, 966.
39. Rothe, M.; Pan, M. G.; Henzel, W. J.; Ayres, T. M.; Goeddel, D. V. *Cell* **1995**, *83*, 1243.
40. Baud, V.; Karin, M. *Nat. Rev. Drug Disc.* **2009**, *8*, 33.
41. Eckelman, B. P.; Salvesen, G. S. *J. Biol. Chem.* **2006**, *281*, 3254.
42. Bertrand, M. J. M.; Milutinovic, S.; Dickson, K. M.; Ho, W. C.; Boudreault, A.; Durkin, J.; Gillard, J. W.; Jaquith, J. B.; Morris, S. J.; Barker, A. P. *Mol. Cell* **2008**, *30*, 689.
43. Bertrand, M. J. M.; Doiron, K.; Labbè, K.; Korneluk, R. G.; Barker, A. P.; Saleh, M. *Immunity* **2009**, *30*, 789.
44. Chen, D. J.; Huerta, S. *Anticancer Drugs* **2009**, *20*, 646.
45. Mannhold, R.; Fulda, S.; Carosati, E. *Drug Discovery Today* **2010**, *15*, 210.
46. Flygare, J. A.; Fairbrother, W. J. *Expert Opin. Ther. Pat.* **2010**, *20*, 251.
47. Krieg, A.; Reed, C. J. *Cell Cycle* **2010**, *9*, 426.
48. Sun, H.; Nikolovska-Coleska, Z.; Lu, J.; Qiu, S.; Yang, C.-Y.; Gao, W.; Meagher, J.; Stuckey, J.; Wang, S. *J. Med. Chem.* **2006**, *49*, 7916.
49. Peng, Y.; Sun, H.; Nikolovska-Coleska, Z.; Qiu, S.; Yang, C.-Y.; Lu, J.; Cai, Q.; Yi, H.; Kang, S.; Yang, D.; Wang, S. *J. Med. Chem.* **2008**, *51*, 8158.
50. Cai, Q.; Sun, H.; Peng, Y.; Lu, J.; Nikolovska-Coleska, Z.; McEachern, D.; Liu, L.; Qiu, S.; Yang, C.-Y.; Miller, R.; Yi, H.; Zhang, T.; Sun, D.; Kang, S.; Guo, M.; Leopold, L.; Yang, D.; Wang, S. *J. Med. Chem.* **2011**, *54*, 2714.
51. Flygare, J. A.; Beresini, M.; Budha, N.; Chan, H.; Chan, I. T.; Cheeti, S.; Cohen, F.; Deshayes, K.; Doerner, K.; Eckhardt, S. G.; Elliott, L. O.; Feng, B.; Franklin, M. C.; FrankovitzReisner, S.; Gazzard, L.; Halladay, J.; Hymowitz, S. G.; La, H.; LoRusso, P.; Maurer, B.; Murray, L.; Plise, E.; Quan, C.; Stephan, J.-P.; Young, S. G.; Tom, J.; Tsui, V.; Um, J.; Varfolomeev, E.; Vucic, D.; Wagner, A. J.; Wallweber, H. J. A.; Wang, L.; Ware, J.; Wen, Z.; Wong, H.; Wong, J. M.; Wong, M.; Wong, S.; Yu, R.; Zobel, K.; Fairbrother, W. J. *J. Med. Chem.* **2012**, *55*, 4101.
52. Seneci, P.; Bianchi, A.; Battaglia, C.; Belvisi, L.; Bolognesi, M.; Caprini, A.; Cossu, F.; De Franco, E.; De Matteo, M.; Delia, D.; Drago, C.; Khaled, A.; Lecis, D.; Manzoni, L.; Marizzoni, M.; Mastrangelo, E.; Milani, M.; Motto, I.; Potenza, D.; Rizzo, V.; Servida, F.; Turlizzi, E.; Varrone, M.; Vasile, F.; Scolastico, C. *Bioorg. Med. Chem.* **2009**, *17*, 5834.
53. Cossu, F.; Malvezzi, F.; Canevari, G.; Mastrangelo, E.; Lecis, D.; Delia, D.; Seneci, P.; Scolastico, C.; Bolognesi, M.; Milani, M. *Protein Sci.* **2010**, *17*, 2418.
54. Bianchi, A.; Ugazzi, M.; Ferrante, L.; Lecis, D.; Scavullo, C.; Mastrangelo, E.; Seneci, P. *Bioorg. Med. Chem. Lett.* **2012**, *22*, 2204.
55. Li, L.; Thomas, R. M.; Suzuki, H.; De Brabander, J. K.; Wang, X.; Harran, P. G. *Science* **2004**, *305*, 1471.
56. Nikolovska-Coleska, Z.; Meagher, J. L.; Jiang, S.; Yang, C.-Y.; Qiu, S.; Roller, P. P.; Stuckey, J. A.; Wang, S. *Biochemistry* **2008**, *47*, 9811.
57. Lu, J.; Bai, L.; Sun, H.; Nikolovska-Coleska, Z.; McEachern, D.; Qiu, S.; Miller, R. S.; Yi, H.; Shangary, S.; Sun, Y.; Meagher, J. L.; Stuckey, J. A.; Wang, S. *Cancer Res.* **2008**, *68*, 9384.
58. Lecis, D.; Mastrangelo, E.; Belvisi, L.; Bolognesi, M.; Civera, M.; Cossu, F.; De Cesare, M.; Delia, D.; Manenti, G.; Manzoni, L.; Milani, M.; Moroni, E.; Perego, P.; Potenza, D.; Rizzo, V.; Scavullo, C.; Scolastico, C.; Servida, F.; Vasile, F.; Seneci, P. *Bioorg. Med. Chem.* **2012**.
59. Manzoni, L.; Arosio, D.; Belvisi, L.; Bracci, A.; Colombo, M.; Invernizzi, D.; Scolastico, C. *J. Org. Chem.* **2005**, *70*, 4124.
60. Sun, H.; Liu, L.; Lu, J.; Bai, L.; Li, X.; Nikolovska-Coleska, Z.; McEachern, D.; Yang, C.-Y.; Qiu, S.; Yi, H.; Sun, D.; Wang, S. *J. Med. Chem.* **2011**, *54*, 3306.
61. Sun, H.; Nikolovska-Coleska, Z.; Lu, J.; Meagher, J. L.; Yang, C.-Y.; Qiu, S.; Tomita, Y.; Ueda, Y.; Yiang, S.; Krajewski, K.; Roller, P. P.; Stuckey, J. A.; Wang, S. *J. Am. Chem. Soc.* **2007**, *129*, 15279.
62. Bis-amino linkers **15a** and **15b** are commercially available. The synthesis of compounds **15c** and **15d** is described in the Section 4.

OPEN

Cell Death and Differentiation (2014) 21, 491–502

www.nature.com/cdd

Selective CDK9 inhibition overcomes TRAIL resistance by concomitant suppression of cFlip and Mcl-1

J Lemke[1,2], S von Karstedt[1], M Abd El Hay[1], A Conti[1,3], F Arce[4], A Montinaro[1], K Papenfuss[1], MA El-Bahrawy[5] and H Walczak*[,1]

Tumor necrosis factor-related apoptosis-inducing ligand (TRAIL) can induce apoptosis in many cancer cells without causing toxicity *in vivo*. However, to date, TRAIL-receptor agonists have only shown limited therapeutic benefit in clinical trials. This can, most likely, be attributed to the fact that 50% of all cancer cell lines and most primary human cancers are TRAIL resistant. Consequently, future TRAIL-based therapies will require the addition of sensitizing agents that remove crucial blocks in the TRAIL apoptosis pathway. Here, we identify PIK-75, a small molecule inhibitor of the p110α isoform of phosphoinositide-3 kinase (PI3K), as an exceptionally potent TRAIL apoptosis sensitizer. Surprisingly, PI3K inhibition was not responsible for this activity. A kinome-wide *in vitro* screen revealed that PIK-75 strongly inhibits a panel of 27 kinases in addition to p110α. Within this panel, we identified cyclin-dependent kinase 9 (CDK9) as responsible for TRAIL resistance of cancer cells. Combination of CDK9 inhibition with TRAIL effectively induced apoptosis even in highly TRAIL-resistant cancer cells. Mechanistically, CDK9 inhibition resulted in downregulation of cellular FLICE-like inhibitory protein (cFlip) and Mcl-1 at both the mRNA and protein levels. Concomitant cFlip and Mcl-1 downregulation was required and sufficient for TRAIL sensitization by CDK9 inhibition. When evaluating cancer selectivity of TRAIL combined with SNS-032, the most selective and clinically used inhibitor of CDK9, we found that a panel of mostly TRAIL-resistant non-small cell lung cancer cell lines was readily killed, even at low concentrations of TRAIL. Primary human hepatocytes did not succumb to the same treatment regime, defining a therapeutic window. Importantly, TRAIL in combination with SNS-032 eradicated established, orthotopic lung cancer xenografts *in vivo*. Based on the high potency of CDK9 inhibition as a cancer cell-selective TRAIL-sensitizing strategy, we envisage the development of new, highly effective cancer therapies.

Cell Death and Differentiation (2014) **21,** 491–502; doi:10.1038/cdd.2013.179; published online 20 December 2013

Introduction

De novo and acquired resistance to conventional chemotherapy remains the major obstacle in treating many cancers today. Intrinsic apoptosis resistance of cancer cells often involves disabling of the intrinsic apoptotic machinery.[1] Therefore, targeting cancer cells via the extrinsic cell death machinery involving death receptors of the tumor necrosis factor (TNF) superfamily has become an attractive approach in cancer research. However, attempts to use cell death-inducing CD95L or TNF for systemic therapy were hampered by severe toxicity.[2,3] In contrast, TNF-related apoptosis-inducing ligand (TRAIL) can induce apoptosis selectively in tumor cells *in vitro* and *in vivo*.[4,5]

Based on these findings, TRAIL-receptor (TRAIL-R) agonists, comprising recombinant soluble TRAIL and agonistic TRAIL-R antibodies, are currently evaluated in clinical trials. However, so far these trials only showed very limited therapeutic benefit.[6] It has emerged that, although TRAIL is capable of inducing apoptosis in many cancer cell lines *in vitro* and *in vivo*, about 50% of cancer cell lines and the majority of primary tumor cells are TRAIL resistant.[7] The limited success of clinical trials conducted so far is likely to be attributable to this fact. However, combinatorial treatment with sensitizing agents can break TRAIL apoptosis resistance resulting in synergistic and selective killing of tumor cells.[4] These findings have encouraged extensive research into identifying potent TRAIL-sensitizing agents that do not sensitize non-transformed cells.

Binding of TRAIL to cognate apoptosis-inducing TRAIL-R1 (DR4)[8] and/or TRAIL-R2 (DR5)[9] results in receptor trimerization. The adaptor protein FAS-associated protein with death domain (FADD) is recruited to the death domain (DD) of trimerized TRAIL-Rs and, in turn, enables caspase-8 and -10 recruitment to and activation at the death-inducing signaling complex (DISC).[10–14] In type-I cells, activation of caspase-8 and -10 at the DISC results in sufficient activation of the effector caspase-3, ultimately resulting in apoptosis. In type-II

[1]Centre for Cell Death, Cancer and Inflammation, UCL Cancer Institute, University College London, 72 Huntley Street, London WC1E 6DD, UK; [2]Clinic of General and Visceral Surgery, University of Ulm, Albert-Einstein-Allee 23, 89081 Ulm, Germany; [3]Department of Experimental Oncology and Molecular Medicine, Fondazione IRCCS Istituto Nazionale dei Tumori, 20133 Milan, Italy; [4]Cancer Immunology Unit, University College London, 72 Huntley Street, London WC1E 6DD, UK and [5]Department of Histopathology, Imperial College London, Du Cane Road, London W12 0NN, UK

*Corresponding author: H Walczak, Centre for Cell Death, Cancer and Inflammation, UCL Cancer Institute, University College London, 72 Huntley Street, London WC1E 6DD, UK. Tel: +44 207 67946471; Fax: +44 207 679 6925; E-mail: h.walczak@ucl.ac.uk

Keywords: CDK9; TRAIL; NSCLC; PIK-75; SNS-032

Abbreviations: AST, aspartate transaminase; CDK, cyclin-dependent kinase; cFlip, cellular FLICE-like inhibitory protein; DD, death domain; DISC, death-inducing signaling complex; FADD, Fas-associated protein with death domain; IAP, inhibitor of apoptosis proteins; NSCLC, non-small cell lung cancer; PI3K, phosphoinositide-3 kinase; PHH, primary human hepatocytes; P-TEFb, positive transcription elongation factor b; RNA Pol II, RNA-polymerase II; TNF, tumor necrosis factor; TRAIL, tumor necrosis factor-related apoptosis-inducing ligand; WT, wild-type; XIAP, X-linked inhibitor of apoptosis

Received 29.6.13; revised 07.10.13; accepted 05.11.13; Edited by T Mak; published online 20.12.13

cells, additional activation of the mitochondrial pathway is required to neutralize X-linked inhibitor of apoptosis protein (XIAP)-mediated effector caspase inhibition via release of Smac/DIABLO from mitochondria.[15]

In order to prevent excessive apoptosis induction by TRAIL, several mechanisms that negatively regulate the TRAIL apoptosis pathway have evolved that are frequently exacerbated by cancer cells. The cellular FLICE-like inhibitory protein (cFlip) competes with caspase-8 for binding to FADD, thereby preventing caspase-8 activation and, consequently, apoptosis induction.[16] Other cellular factors that antagonize apoptosis induction by TRAIL include the inhibitor of apoptosis proteins (IAPs).[17] Among these, XIAP has been shown to have a major role in mediating resistance to TRAIL-induced apoptosis.[18] In type-II cells, resistance to TRAIL-induced apoptosis can be mediated by high expression of anti-apoptotic Bcl-2 family members such as Bcl-2, Bcl-xL and Mcl-1 that antagonize truncated Bid-triggered Bax/Bak-mediated mitochondrial outer membrane permeabilization and the consequent release of the pro-apoptotic factors cytochrome *c* and Smac/DIABLO.[19]

Kinase inhibitors have emerged as a novel class of targeted small molecule agents with great therapeutic potential in cancer treatment. This is owed to the fact that kinases are crucial components of most cellular signaling pathways that promote tumor cell survival, growth, migration, invasion and metastasis. Several inhibitors of the phosphoinositide-3 kinase (PI3K) pathway are currently in clinical trials[20] and, interestingly, pan-PI3K inhibitors, inhibiting all four catalytic isoforms (p110α, β, γ and δ), have been shown to sensitize to TRAIL-induced apoptosis.[21,22] Activating mutations of the α-isoform of PI3K (p110α) occur with frequencies of up to 30% in cancer[23] and, recently, mutated p110α was suggested to render cancer cell lines resistant to TRAIL-induced apoptosis.[24] Therefore, we set out to test whether specific inhibition of p110α would render cancer cells sensitive to TRAIL-induced apoptosis.

Results

The p110α inhibitor PIK-75 potently sensitizes tumor cells to TRAIL-induced apoptosis independently of PI3K inhibition. To investigate whether inhibition of one of the PI3K isoforms is sufficient to sensitize cancer cells to TRAIL-induced apoptosis, we treated HeLa cells with TRAIL in the presence or absence of pharmacological inhibitors that have been reported to be isoform specific (PIK-75 (p110α), TGX-221 (p110β), AS-252424 (p110γ) and IC-87114 (p110δ)) (for IC50 values see Supplementary Figure S1a). Whereas co-treatment with inhibitors of the β-, γ- and δ-isoforms of PI3K showed only marginal effects, co-treatment with PIK-75 profoundly increased TRAIL sensitivity of HeLa cells shifting the sensitivity of these cells by 3–4 orders of magnitude (Figure 1a and Supplementary Figure S1b). HeLa cells are sensitive to higher concentrations of TRAIL; however, many other cancer cell lines and most primary cancer cells are TRAIL resistant.[7] Therefore, we next tested whether the exceptionally potent TRAIL sensitization exerted by PIK-75 in HeLa cells would translate into sensitization of the highly TRAIL resistant non-small cell lung cancer (NSCLC) cell line A549. Indeed, when treated with PIK-75 A549 cells became sensitive to apoptosis induction by TRAIL, even at concentrations of TRAIL as low as 10 ng/ml (Supplementary Figure S1c). Intriguingly, when examining clonogenic survival, we observed that this novel combination almost completely obliterated clonogenic survival of A549 cells (Figure 1b).

Having shown that PIK-75, a potent inhibitor of p110α, is a very effective TRAIL sensitizer, we next investigated whether specific inhibition of the p110α isoform of PI3K was capable of breaking TRAIL resistance in cancer cells and, hence, responsible for the PIK-75-mediated effect. To this end, we performed RNAi-mediated silencing of p110α as compared to p110β and DNA-PK, which has been shown to be inhibited by PIK-75 in addition to p110α.[25] Surprisingly, silencing of p110α, p110β and DNA-PK, or any combination thereof, did not sensitize HeLa cells to TRAIL-induced apoptosis (Figure 1c, knockdown efficiency in Supplementary Figure S1d). In order to test the possibility that very low amounts of protein remaining after knockdown may be sufficient to maintain resistance, we also used two pan-PI3K inhibitors, GDC-0941 and BEZ-235, which both inhibit p110α with even lower IC50s than PIK-75.[26,27] In addition, we also used A66, a novel p110α-specific inhibitor[28] (for IC50 values see Supplementary Figure S1e). However, when testing these three compounds, we found that none of them reproduced the extent of sensitization observed with PIK-75 co-treatment (Figure 1d). Interestingly, BEZ-235 was more efficient than PIK-75 at suppressing PI3K activity as assessed by phosphorylation of AKT (Supplementary Figure S1f). Moreover, concentrations of up to 10 μM of A66 were not able to suppress pan-PI3K activity in HeLa cells, which have been reported to harbor wild-type (WT) PI3K p110α (Supplementary Figure S1f). This is in line with a recent report that selective inhibition of p110α using A66 is only efficient in preventing phosphorylation of AKT in cells with activating mutations in p110α.[28]

These results were unexpected but led us to conclude that PIK-75 sensitizes cancer cells to TRAIL-induced apoptosis either independently of p110α or by inhibiting p110α and (an) additional kinase(s). We therefore used PIK-75 in an *in vitro* screen testing its capability to inhibit a panel of 451 kinases (80% of the kinome). This revealed that, in addition to p110α, PIK-75 potently inhibited 27 other kinases when used at 200 nM (Figure 1e), a concentration at which it effectively sensitizes cancer cells to TRAIL. In conclusion, we established that PIK-75 potently breaks TRAIL resistance, but its p110α-inhibitory activity is either not responsible or alone not sufficient to sensitize cancer cells to TRAIL.

CDK9 is the PIK-75-target responsible for TRAIL sensitization. To evaluate which of the 27 kinases inhibited, or which combination thereof, was responsible for PIK-75-mediated sensitization to TRAIL-induced apoptosis, we screened all 27 kinases identified in the *in vitro* screen by siRNA knockdown for sensitization to TRAIL (Supplementary Figure S2a). Knockdown of 26 of these kinases did not affect sensitivity to TRAIL. Silencing of cyclin-dependent kinase 9 (CDK9), however, potently sensitized HeLa and A549 cells to TRAIL-induced apoptosis (Figures 2a and b). CDK9 is a member of the family of CDKs, which are mainly known for their function in cell cycle regulation.[29] Recently, it was

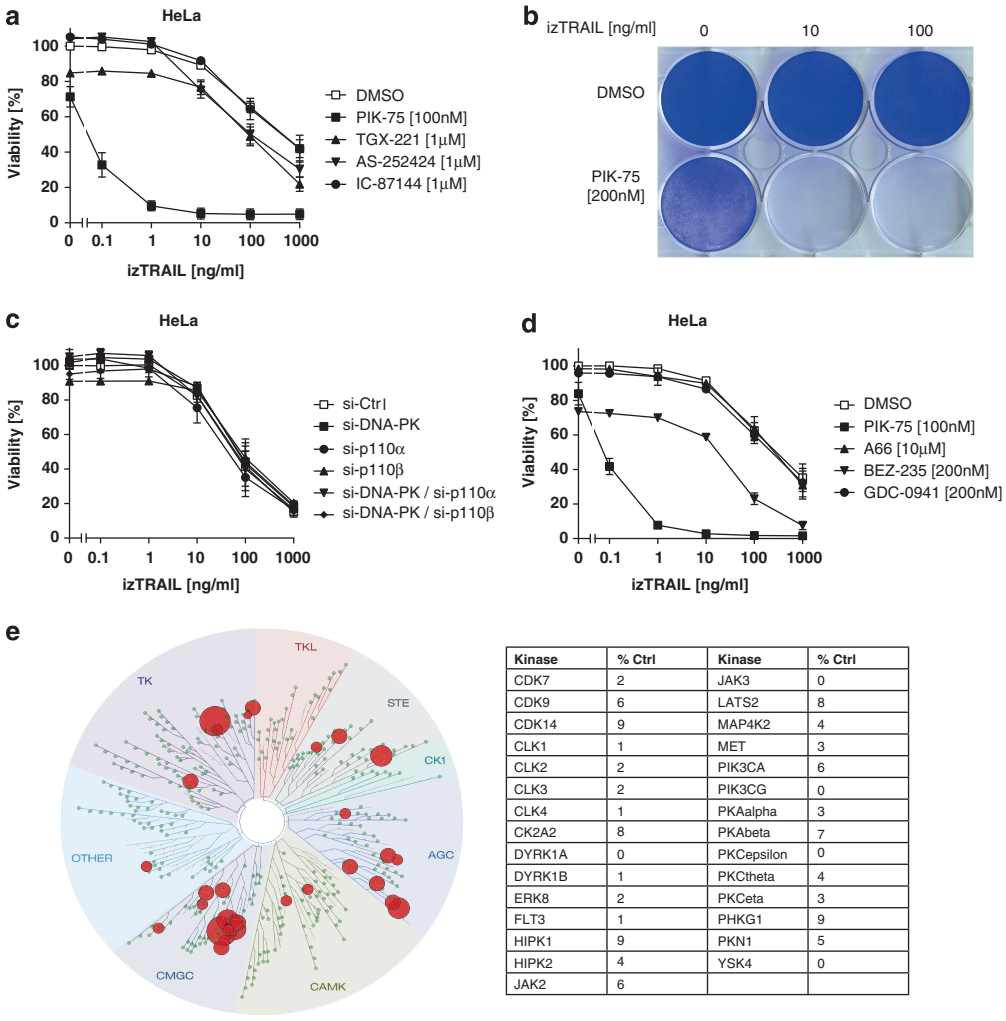

Kinase	% Ctrl	Kinase	% Ctrl
CDK7	2	JAK3	0
CDK9	6	LATS2	8
CDK14	9	MAP4K2	4
CLK1	1	MET	3
CLK2	2	PIK3CA	6
CLK3	2	PIK3CG	0
CLK4	1	PKAalpha	3
CK2A2	8	PKAbeta	7
DYRK1A	0	PKCepsilon	0
DYRK1B	1	PKCtheta	4
ERK8	2	PKCeta	3
FLT3	1	PHKG1	9
HIPK1	9	PKN1	5
HIPK2	4	YSK4	0
JAK2	6		

Figure 1 PIK-75 profoundly sensitizes cancer cells to TRAIL-induced apoptosis independently of PI3K inhibition. (**a**) HeLa cells were preincubated for 1 h with the indicated PI3K inhibitors and subsequently stimulated with izTRAIL at the indicated concentrations. Cell viability was quantified after 24 h. (**b**) A549 cells were treated with DMSO or PIK-75 (200 nM) for 1 h and subsequently stimulated with izTRAIL for 24 h. Long-term survival was visualized after 7 days by crystal violet staining. One of two independent experiments is shown. (**c**) HeLa cells were transfected with the indicated siRNAs. After 48 h, cells were stimulated with izTRAIL at different concentrations. Cell viability was analyzed 24 h later. (**d**) HeLa cells were preincubated for 1 h with the different PI3K inhibitors at the indicated concentrations and subsequently stimulated with izTRAIL at different concentrations. Cell viability was quantified after 24 h. (**e**) The capacity of PIK-75 at 200 nM to bind to a panel of 451 human kinases was determined by analyzing the binding interaction (%) compared with DMSO (= 100%) using Kinomescan. Hits (< 10% remaining activity) are visualized (red circles) and listed in the table. Values (**a**, **c** and **d**) are means ± S.E.M. of three independent experiments

shown that a subset of CDKs, namely CDK7 and CDK9 regulate transcription.[30,31] Our screen revealed that PIK-75 also inhibits CDK7. However, a role of CDK7 in mediating TRAIL resistance could be excluded, as CDK7 knockdown did not sensitize to TRAIL-induced apoptosis (Figures 2a and b). Moreover, a contributing role of the most prominent members of the cell cycle-regulating CDKs, CDK1, 2, 4 and 6 could also be excluded by knockdown experiments (Supplementary Figures S2b and c).

CDK9 inhibition by SNS-032 potently sensitizes to TRAIL-induced apoptosis. Several CDK inhibitors targeting different subsets of CDKs are currently evaluated in clinical trials.[32] Among them, SNS-032 (BMS-387032) appears to be the most selective CDK9 inhibitor. It inhibits CDK2, CDK7 and CDK9 selectively over other CDKs and kinases, but its inhibitory capacity is about 10-fold selective for CDK9 (IC50 = 4 nM) over CDK2 (IC50 = 38 nM) and 15-fold over CDK7 (IC50 = 62 nM).[33] CDK9, in a complex with its partner Cyclin-T/K, constitutes the positive transcription elongation factor b (P-TEFb) that promotes transcriptional elongation by phosphorylation of substrates.[34,35] The most important substrate of P-TEFb is the carboxy-terminal domain of RNA-polymerase II (RNA-Pol II), which is phosphorylated by CDK9 at Ser-2. Analysis of Ser-2 phosphorylation of RNA-Pol II showed that PIK-75 and SNS-032 exerted similar inhibitory activity towards CDK9 (Supplementary Figure S3a). We next evaluated a novel combinatorial therapy consisting of the clinically used CDK9 inhibitor SNS-032 and TRAIL. Indeed, SNS-032 markedly sensitized HeLa and A549 cells to TRAIL-induced cell death (Figure 3a). Sensitized cells died apoptotically (Figure 3b) and this cell

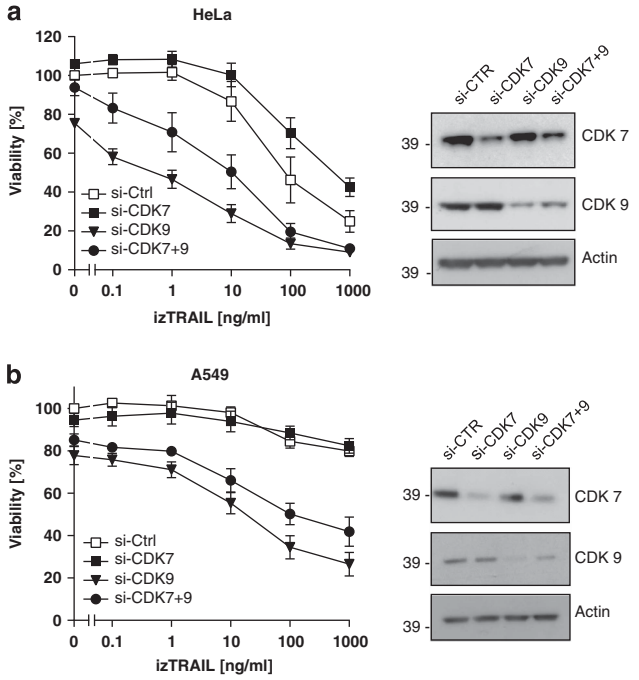

Figure 2 CDK9 is the PIK-75-target that is responsible for TRAIL sensitization. HeLa (**a**) or A549 cells (**b**) were transiently transfected with the indicated siRNAs for 48 h and subsequently stimulated with izTRAIL at different concentrations. Cell viability was determined 24 h later. Representative western blots of knockdown efficiency are shown. All values are means ± S.E.M. of three independent experiments

death was prevented by the caspase-inhibitor zVAD (Supple mentary Figure S3b). Finally, SNS-032 in combination with TRAIL almost completely abrogated clonogenic survival of A549 cells (Figure 3c). These data demonstrate that cancer cell lines can be strongly sensitized to TRAIL-induced apoptosis via CDK9 inhibition using SNS-032, a small molecule inhibitor that is already undergoing clinical testing.

In line with these findings, cancer cells treated with TRAIL in the presence of SNS-032 showed a drastic increase in the cleavage of caspase-8, Bid, caspase-9, -3 and poly ADP ribose polymerase (PARP) (Figure 3d and Supplementary Figure S3c). Moreover, cells in which CDK9 was silenced using siRNA also showed increased activation of the apoptotic caspase cascade (Supplementary Figure S3d). As expected from this finding, DISC analysis upon CDK9 inhibition using SNS-032 (Figure 3e) or upon CDK9 knockdown (Supplementary Figure S3e) revealed that caspase-8 cleavage generating the p18 fragment was enhanced upon CDK9 inhibition or suppression at the DISC (Figure 3e, Supplementary Figure S3e). Thus, CDK9 inhibition facilitates initiation of the caspase cascade at the DISC as part of its sensitization mechanism.

CDK9 mediates TRAIL resistance by promoting concomitant transcription of cFlip and Mcl-1. Having established that CDK9 inhibition efficiently sensitizes cancer cell lines to TRAIL-induced apoptosis, we next addressed which molecular changes are responsible for this effect. Upregulation of TRAIL-R1 and/or TRAIL-R2 often correlates with, and sometimes also contributes to, TRAIL apoptosis sensitization.[36] However, treatment of HeLa or A549 cells with PIK-75 or SNS-032 did not alter TRAIL-R1/R2 surface expression (Figure 4a), in line with similar recruitment of TRAIL-R1/2 in the DISC analysis (Figure 3e). Consequently, TRAIL sensitization by CDK9 inhibition is likely to require changes in intracellular modulators of the TRAIL apoptosis pathway that should enhance DISC activity and possibly additional downstream steps in the pathway. We, therefore, next investigated whether known components of the TRAIL–DISC and the downstream apoptosis pathway it activates are regulated by PIK-75 or SNS-032 treatment. Whereas the majority of the DISC components and downstream pro- and anti-apoptotic proteins remained unchanged, cFlip and Mcl-1 protein levels were rapidly suppressed by pharmacological CDK9 inhibition by SNS-032 or PIK-75 (Figure 4b and Supplementary Figure S4a). Because siRNA-mediated suppression of CDK9, performed in the presence or absence of pan-caspase inhibition to exclude a possible impact of CDK9-silencing-induced apoptosis, also resulted in down-regulation of cFlip and Mcl-1, we can conclude that CDK9 is required to maintain high expression of these anti-apoptotic proteins in cancer cells (Figure 4c).

CDK9 is known for its role in transcriptional elongation, suggesting that the observed downregulation of cFlip and Mcl-1 protein levels could be caused by suppression of their transcripts. In line with this hypothesis, SNS-032 treatment rapidly decreased the amount of mRNA for cFlip and Mcl-1 (Figure 4d). The effect was a consequence of direct inhibition of transcription, because co-treatment with SNS-032 and the transcriptional inhibitor actinomycin D[37] did not further reduce mRNA levels (Supplementary Figure S4b). Moreover, preincubation with the translational inhibitor cycloheximide before SNS-032 treatment did not inhibit SNS-032-mediated mRNA suppression (Supplementary Figure S4b). Co-incubation with actinomycin D and cycloheximide induced a steady-state level of mRNA. Additional treatment with SNS-032 did not reduce Mcl-1 mRNA, showing that SNS-032 does not induce degradation of mRNA. Next, we analyzed cFlip and Mcl-1 mRNA upon CDK9 knockdown. In slight contrast to CDK9 inhibition using SNS-032, prolonged silencing of CDK9 using siRNA also strongly affected mRNA levels of housekeeping genes. Therefore, we normalized mRNA amounts to cell numbers used for RNA extraction. The amplification of cFlip and Mcl-1 transcripts by real-time PCR (RT-PCR) required a higher cycle threshold, demonstrating that their transcripts are indeed suppressed when normalized to the cell number (Supplementary Figure S4c). We conclude that SNS-032-induced suppression of cFlip and Mcl-1 is mediated by direct inhibition of global transcription that will preferentially affect expression levels of short-lived proteins such as cFlip and Mcl-1.

Concomitant downregulation of cFlip and Mcl-1 is sufficient and required for CDK9 inhibition-induced TRAIL sensitization. To evaluate whether concomitant suppression of cFlip and Mcl-1 was sufficient for CDK9 inhibition-mediated TRAIL sensitization, we silenced cFlip and/or Mcl-1 in HeLa and A549 cells. Hela cells were sensitized to die by Mcl-1 knockdown alone only when high

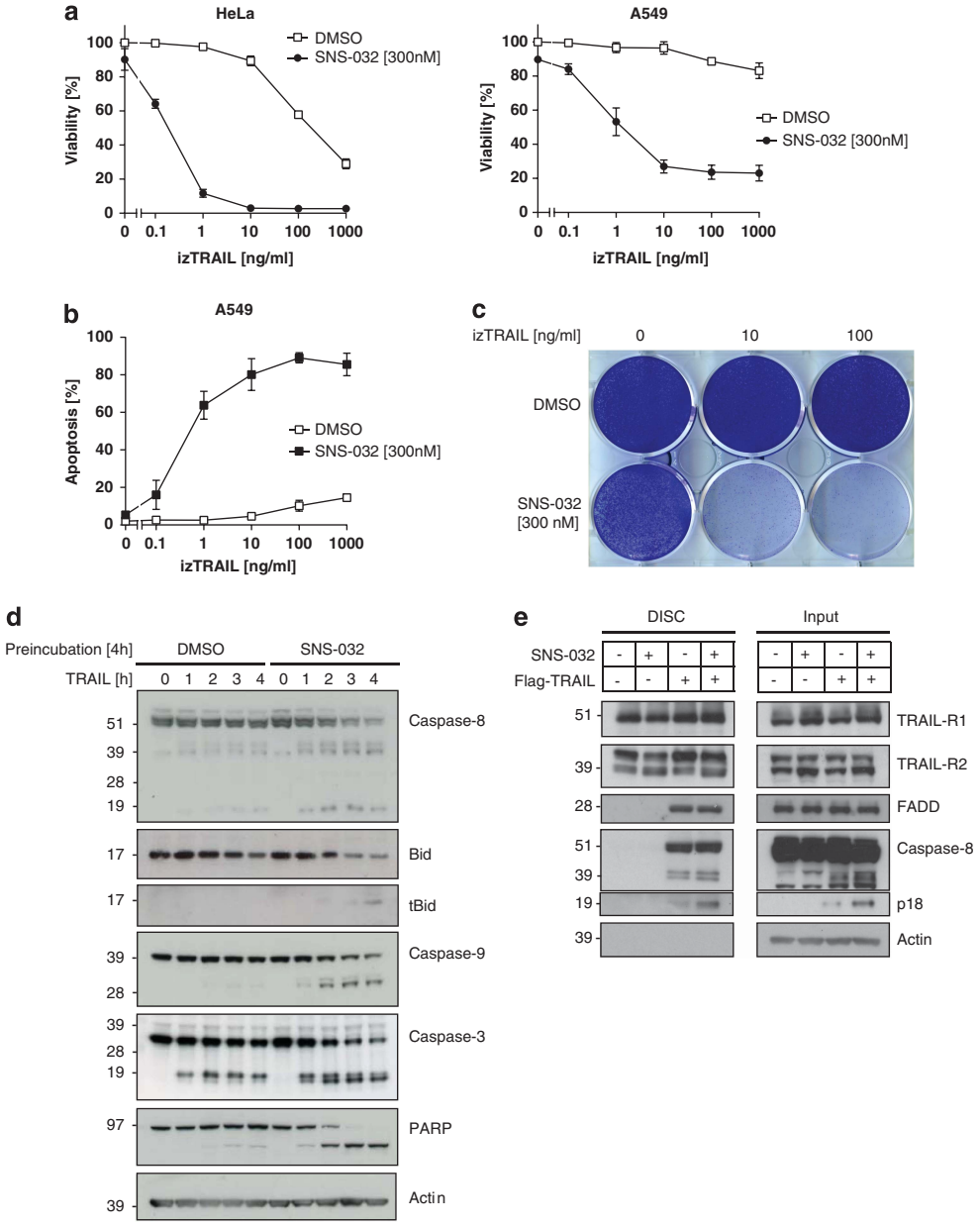

Figure 3 CDK9 inhibition by SNS-032 potently synergizes with TRAIL to kill cancer cells. (**a**) HeLa and A549 cells were preincubated with DMSO or SNS-032 (300 nM) for 1 h and subsequently stimulated with izTRAIL at the concentrations indicated. Cell viability was determined after 24 h. (**b**) A549 cells were preincubated with DMSO or SNS-032 (300 nM) for 1 h and subsequently stimulated with indicated concentrations of izTRAIL. Apoptosis was determined after 24 h. (**c**) A549 cells were treated with DMSO or SNS-032 (300 nM) for 1 h and subsequently stimulated for 24 h with izTRAIL (10 or 100 ng/ml). Long-term survival was visualized after 7 days by crystal violet staining. One of two independent experiments is shown. (**d**) A549 cells were preincubated with DMSO or SNS-032 (300 nM) for 4 h and subsequently stimulated with izTRAIL (100 ng/ml) for the indicated times. Cells were lysed and subjected to western blotting. One representative of two independent experiments is shown. (**e**) A549 cells were preincubated with SNS-032 (300 nM) for 12 h, stimulated with Flag-TRAIL (1 μg/ml) for 1 h and subsequently the TRAIL–DISC was immunoprecipitated via M2-coupled beads and analyzed by western blotting. One representative of two independent experiments is shown. All other values are means ± S.E.M. of three independent experiments

concentrations of TRAIL were used. Knockdown of cFlip, in turn, sensitized at lower TRAIL concentrations, whereas at higher TRAIL concentrations HeLa cells were rendered more resistant by cFlip knockdown (Figure 5a). The latter may be attributable to the interesting observation that knockdown of cFlip brought about the upregulation of Mcl-1. In A549 cells, silencing of neither cFlip nor Mcl-1 alone was sufficient to sensitize to TRAIL-induced apoptosis (Figure 5b). Combined knockdown of both components, however, resulted in a striking synergistic sensitization rendering both, HeLa and A549 cells, highly susceptible to TRAIL-induced apoptosis (Figures 5a and b). Thus, combined downregulation of cFlip and Mcl-1 is sufficient to break TRAIL resistance.

To further investigate the interesting observation that silencing of either cFlip or Mcl-1 resulted in the inverse upregulation of the respective other protein, we also analyzed transcripts of cFlip and Mcl-1 upon knockdown. Silencing of cFlip, Mcl-1 or the combination thereof resulted in comparable

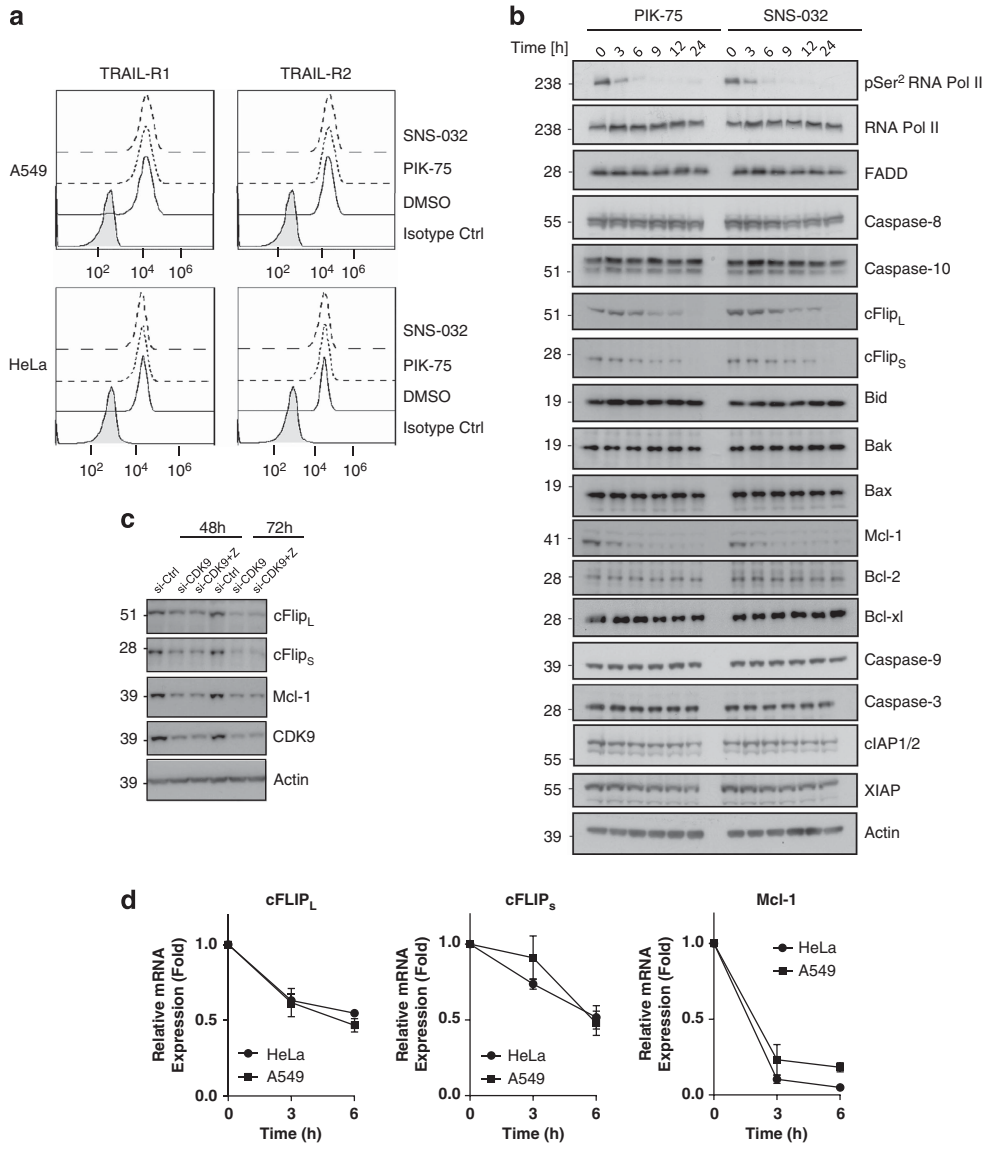

Figure 4 CDK9 mediates TRAIL resistance by promoting concomitant transcription of cFlip and Mcl-1. (**a**) A549 or HeLa cells were incubated with SNS-032 (300 nM) or PIK-75 (100 nM) for 6 h and subsequently stained for surface expression of TRAIL-R1 and TRAIL-R2. One representative of two independent experiments is shown. (**b**) A549 cells were treated with PIK-75 (100 nM) or SNS-032 (300 nM) for the indicated times. Cells were lysed and subjected to western blotting. One representative of two independent experiments is shown. (**c**) HeLa cells were subjected to the indicated knockdowns for 48 or 72 h. zVAD was added at 20 μM 24 h after transfection where indicated. Cells were lysed and subjected to western blotting. One representative of two independent experiments is shown. (**d**) A549 and HeLa cells were incubated with SNS-032 (300 nM) for different times. $cFlip_L$, $cFlip_S$ and Mcl-1 mRNA expression was quantified by RT-PCR. Values are means ± S.E.M. of three independent experiments. Z, zVAD

and efficient suppression of the respectively targeted transcripts (Supplementary Figure S5a). Interestingly, the inverse upregulation we observed on the protein level was also apparent on the transcriptional level (Supplementary Figure S5a), suggesting that this phenomenon is, at least partially, regulated on the transcriptional level.

To test whether cFlip and/or Mcl-1 were responsible for the block of TRAIL-induced apoptosis that is specifically removed by CDK9 inhibition, we overexpressed cFlip and/or Mcl-1 in HeLa cells before treatment with SNS-032 and TRAIL. Transfection was highly efficient (Supplementary Figure S5b) and nontoxic to the cells (Supplementary Figure S5c). Overexpression of cFlip or Mcl-1 alone rendered these cells slightly more TRAIL resistant but could only marginally inhibit SNS-032-mediated sensitization (Figure 5c). Combined overexpression, however, rendered HeLa cells almost completely resistant to TRAIL-induced apoptosis and prevented SNS-032-mediated sensitization (Figure 5c). Thus, SNS-032 sensitizes cancer cell lines to TRAIL-induced apoptosis by concomitant suppression of cFlip and Mcl-1.

We next investigated whether CDK9 inhibition-induced TRAIL sensitization requires activation of the mitochondrial pathway. To do so, we used the isogenic HCT-116 colon carcinoma cell lines in which Bax and Bak are either both expressed (parental HCT-116 WT cells) or both genetically deleted (BAX/BAK-deficient HCT-116 cells). HCT-116 WT cells were partially TRAIL sensitive but profoundly sensitized by co-treatment with SNS-032 (Supplementary Figure S5d).

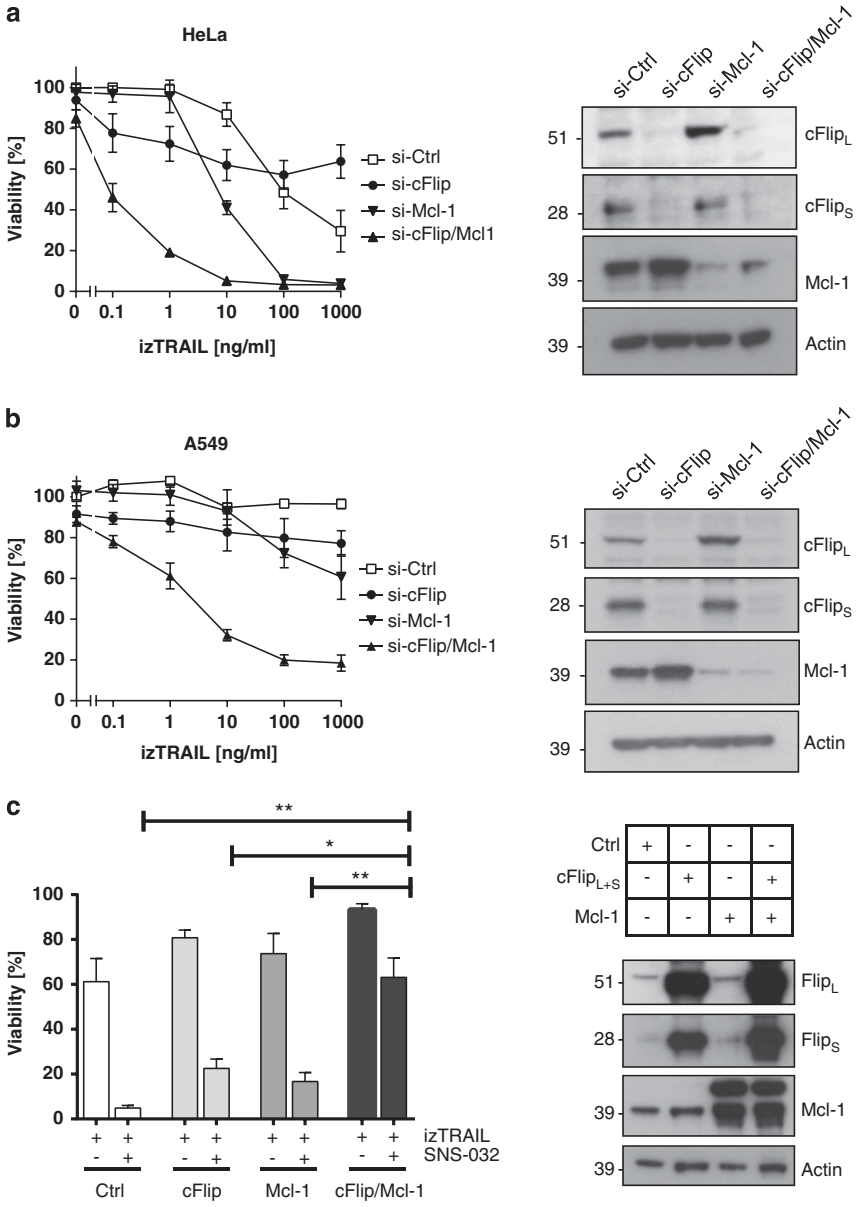

Figure 5 Concomitant downregulation of cFlip and Mcl-1 is required and sufficient for CDK9 inhibition-induced TRAIL sensitization. HeLa (**a**) and A549 cells (**b**) were transfected with siRNA-targeting cFlip and/or Mcl-1 for 48 h and subsequently stimulated with izTRAIL at the indicated concentrations. Cell viability was determined after 24 h. (**c**) HeLa cells were transfected with expression plasmids for cFlip and/or Mcl-1 or empty vector control. Twenty four hours later, cells were stimulated with izTRAIL (10 ng/ml) for 24 h and cell viability was determined. All values are means ± S.E.M. of three independent experiments. Representative western blots are shown. $^*P<0.05$; $^{**}P<0.01$; Student's *t*-test

Their Bax/Bak-deficient counterparts, however, were completely resistant to SNS-032-mediated TRAIL sensitization. Thus, TRAIL sensitization mediated by CDK9 inhibition uses a type-II apoptosis pathway that requires both, effective DISC-mediated caspase-8 activation with consequent Bid cleavage, enabled by cFlip downregulation, and efficient triggering of the mitochondrial apoptosis pathway by cleaved Bid, enabled by Mcl-1 downregulation.

Combined CDK9 inhibition and TRAIL selectively kills NSCLC cell lines but not primary human hepatocytes within a therapeutic window. On all cancer cell lines tested, including primarily TRAIL-resistant A549 cells, already low concentrations of TRAIL (1–10 ng/ml) in the presence of SNS-032 (300 nM) were sufficient to reach maximum efficiency in killing these cells. To investigate whether this was a coincidence or may be applicable more broadly, we extended our study to an established panel of NSCLC cell lines.[38] This panel includes cells that are mutated in *KRAS* and/or *p53* (Supplementary Figure S6a). The majority of the cell lines were TRAIL resistant, resembling TRAIL sensitivity of primary cancer cells (Figure 6a and Supplementary Figure S6b). However, all cell lines tested were potently sensitized to 10 ng/ml of TRAIL by co-treatment with SNS-032 at 300 nM, irrespective of their oncogenic mutations (Figure 6a and Supplementary

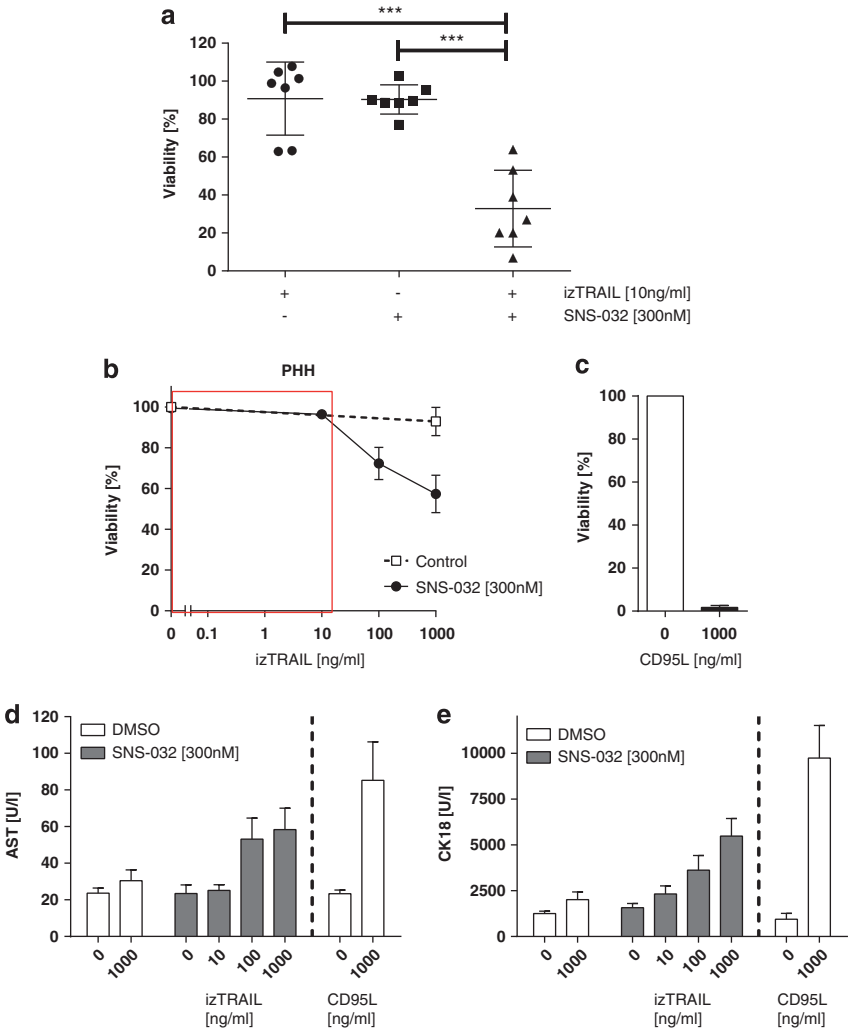

Figure 6 Combination of TRAIL and CDK9 inhibition selectively kills NSCLC cell lines but not PHH within a therapeutic window. (**a**) Seven NSCLC cell lines were preincubated with SNS-032 (300 nM) for 1 h and subsequently stimulated with izTRAIL (10 ng/ml). Cell viability was quantified after 24 h. Values are means of ± S.D. Individual dots represent means of three independent experiments of one cell line. (**b**) On day 4 of culture, PHH of three different donors were preincubated with DMSO or SNS-032 (300 nM) for 1 h and stimulated with izTRAIL at the indicated concentrations. Cell viability was analyzed after 24 h. (**c**) PHH were treated with CD95L (1 μg/ml) as positive control. Supernatants of treated PHH were used to determine levels of AST (**d**) and caspase-cleaved cytokeratin 18 (**e**). Values are means of three independent experiments ± S.E.M. ***$P < 0.001$; Student's *t*-test

Figure S6b). Thus, SNS-032/TRAIL co-treatment enables efficient killing in a broad range of cancer cell lines, irrespective of their *p53*-status.

Considering the remarkable sensitization observed with combination of TRAIL and SNS-032, we next tested the cancer selectiveness of this new combination. Hepatotoxicity is a major concern for the clinical application of novel cancer therapeutics and special care should be taken in the development of therapies containing TNF superfamily members.[3] We therefore next assessed the effect of TRAIL and/or SNS-032 treatment on primary human hepatocytes (PHH). In line with our previous results,[39] the recombinant form of TRAIL used in our study (izTRAIL) did not reduce viability of PHH (Figure 6b). In contrast, PHH were readily killed by recombinant CD95L that served as a control (Figure 6c). Treatment of PHH with SNS-032 at 300 nM in combination with TRAIL used at different concentrations revealed that at high concentrations of TRAIL (100 ng/ml and 1000 ng/ml) hepatocytes died when co-treated with SNS-032 (Figure 6b). However, co-treatment with SNS-032 at 300 nM and TRAIL at 10 ng/ml, the concentrations at which these drugs were highly efficient at killing cancer cells when combined, did not affect viability of hepatocytes. The same nontoxic window was confirmed for the levels of aspartate transaminase (AST), which is released when liver cells are damaged (Figure 6d), and the levels of caspase-cleaved cytokeratin 18 (Figure 6e). Therefore, our novel therapeutic combination can be applied within a considerable therapeutic window. At the same time, toxicity would be expected at higher levels of TRAIL.

TRAIL combined with CDK9 inhibition eradicates established orthotopic lung tumors. Having established an applicable therapeutic window for our newly identified combination of TRAIL with SNS-032 *in vitro*, we next assessed this combination's potency in an orthotopic model of lung cancer *in vivo*. To this end, we induced lung tumors

via tail vein injection of A549 cells stably expressing luciferase (A549-luc). After 7 days, mice were randomized to create treatment groups of mice with comparable tumor burden in each group (Supplementary Figure S7). Subsequently, a 4-day treatment regime was started with either vehicle, TRAIL, SNS-032 or the combination of SNS-032 and TRAIL (Figure 7a). Whereas TRAIL treatment alone had a slight growth inhibitory effect, and SNS-032 only marginally affected lung tumor burden, combined treatment with TRAIL and SNS-032 induced a drastic antitumor effect. TRAIL/SNS-032 treatment completely eradicated established lung tumors in most mice, as determined by *in vivo* bioluminescence imaging (Figure 7b) and subsequent histopathological inspection of lung sections (Figure 7c). Strikingly, and in line with the bioluminescence data, seven out of eight mice that had received TRAIL combined with SNS-032 were histologically tumor free after a 4-day treatment cycle.

Discussion

We found that the supposedly p110α-specific inhibitor PIK-75 potently sensitizes to TRAIL-induced apoptosis. Surprisingly, however, PI3K inhibition was not responsible for this effect. A kinome-wide screen revealed that PIK-75 strongly inhibits 27 kinases in addition to p110α. Off-target activity is a common feature among kinase inhibitors, as most inhibitors are ATP-competitive compounds and the ATP-binding pocket is highly conserved among the human kinome.[40,41] We show that

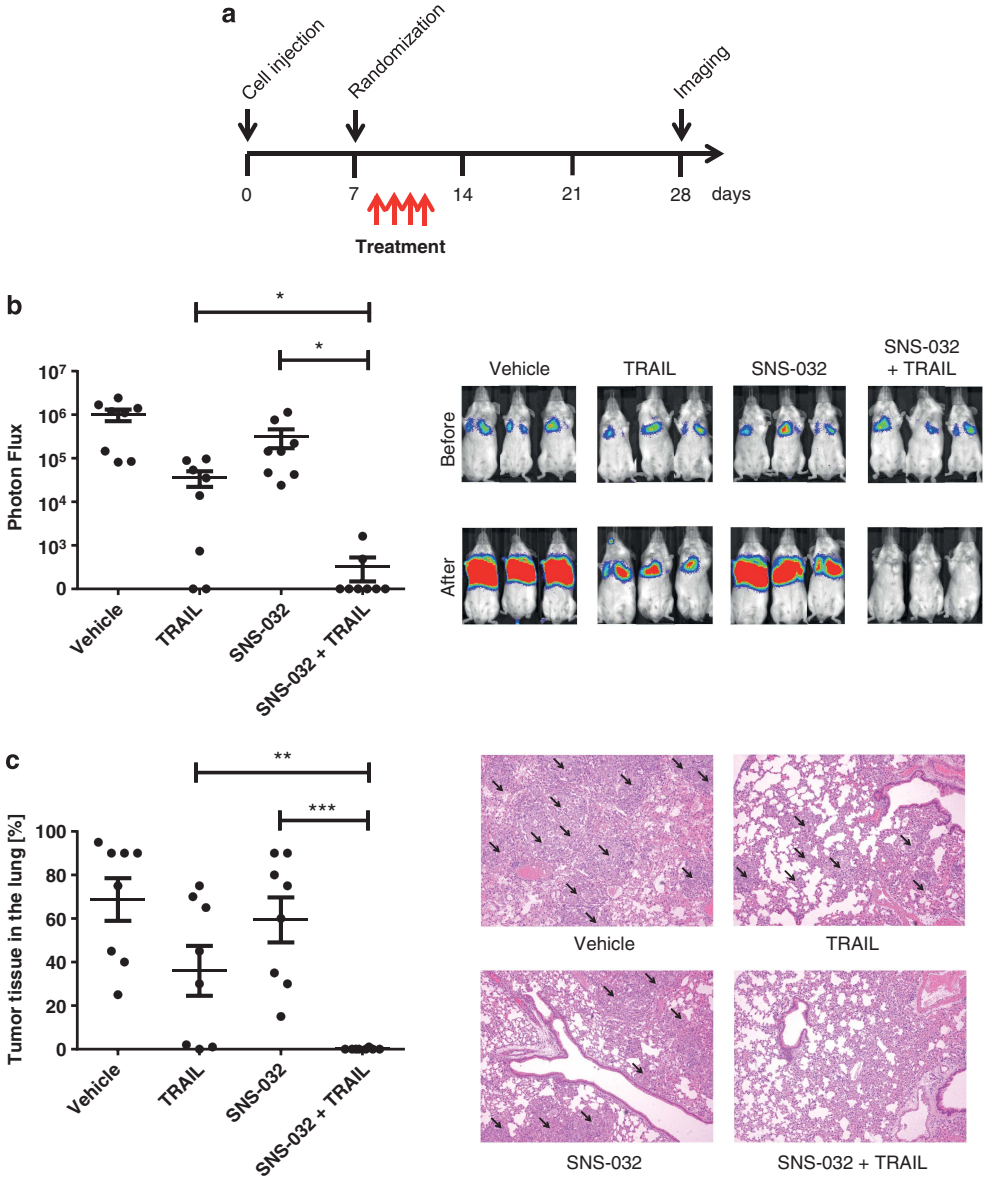

Figure 7 SNS-032 and TRAIL co-treatment eradicates established lung tumors *in vivo*. (**a**) Experimental treatment schedule is shown. (**b**) In week three after treatment tumor burden was quantified by bioluminescence imaging (Photon Flux). Values are means ± S.E.M. Dots represent individual mice ($n = 8$ per group). Three representative mice from each group are shown. (**c**) Paraffin sections of lungs from all mice were stained with H&E and subjected to microscopical analysis quantifying the percentage of total lung area occupied by tumour tissue. Values are means ± S.E.M. Dots represent lungs from individual mice, ($n = 8$ per group). Representative histological images are shown (arrows indicate tumor tissue). $^{*}P < 0.05$; $^{**}P < 0.01$, $^{***}P < 0.001$; Student's *t*-test

PIK-75 exerts off-target effects toward CDK7 and CDK9. This is in line with a recent report on the effects of PIK-75 on acute myeloid leukemia.[42] Moreover, we demonstrate that PIK-75's activity to sensitize cancer cells to TRAIL-induced apoptosis is exclusively due to inhibition of CDK9. CDKs are mainly known for their regulatory role in cell cycle, and development of CDK inhibitors for cancer therapy is aimed at suppressing exacerbated cell cycle progression.[43] Recently, a subset of CDKs, namely CDK7 and CDK9, has been implicated in regulating transcription.[30,31] CDK9 inhibition has been shown to block transcriptional elongation, thereby suppressing expression of short-lived proteins such as Mcl-1 that can result in induction of apoptosis in cancer cells.[30] This finding has paved the way for targeting transcriptional CDKs in addition to cell cycle-regulating CDKs in cancer therapy. Here we provide evidence that selective inhibition of CDK9 achieves an exceptionally potent sensitization to TRAIL-induced apoptosis. Interestingly, the pan-CDK inhibitors Flavopiridol[44–46] and Roscovitine (Seliciclib)[47–49] have previously been shown to synergize with TRAIL. However, so far, it remained unclear which CDK, inhibited by these pan-CDK inhibitors, was responsible for these effects. When combining our result with the fact that Flavopiridol and Roscovitine also inhibit CDK9, it appears reasonable to assume that their previously described TRAIL-sensitizing capacity is likely owed to their CDK9-inhibitory capacity.

Inhibition of certain CDKs can potentially cause toxicity, and CDK1 inhibition is currently thought to be most problematic in this respect.[50] To avoid potential dose-limiting toxicity, we devised a novel combinatorial therapy consisting of TRAIL and SNS-032, an inhibitor targeting CDK9 preferentially over cell cycle CDKs.[33] Importantly, the safety of SNS-032 was already confirmed in clinical trials[51,52] and SNS-032 has been shown to be more potent in inhibiting transcription than Flavopiridol and Roscovitine.[53] The fact that CDK9 inhibition was found to be nontoxic in clinical trials implies that normal cells have possibly developed coping mechanisms that might not be present in transformed cells. In line with this notion, our results show that CDK9 inhibition in combination with TRAIL can selectively kill tumor cells, but not PHH within a significant therapeutic window. Of note, the concentration at which SNS-032 effectively sensitizes cancer cells to TRAIL-induced apoptosis, 300 nM, is commonly reached and sustained in the plasma of patients.[51]

Investigating the underlying mechanism of how CDK9 inhibition sensitizes to TRAIL-induced apoptosis revealed that Mcl-1 downregulation is required, but not sufficient, for TRAIL sensitization. In addition, CDK9 inhibition-induced suppression of another short-lived protein, cFlip, was required to achieve potent TRAIL sensitization. Hence, the synergistic effect of CDK9 inhibition and TRAIL is due to a dual mechanism: downregulation of cFlip enables caspase-8 activation at the DISC and downregulation of Mcl-1 facilitates activation of the mitochondrial apoptosis pathway for enhanced caspase-9 and, ultimately, caspase-3 activation. As a consequence, the combination of TRAIL and CDK9 inhibition is exquisitely powerful in killing tumor cells with a cFlip-imposed block to initiator caspase activation at the DISC and an Mcl-1-imposed block to activation of the mitochondrial apoptosis pathway.

Chemotherapy mostly induces apoptosis by induction of DNA damage that is sensed by p53.[54] However, impairment of functional p53, either by mutation or loss of expression, is frequently detected in cancer. Therefore, therapies that function independently of *p53*-status are likely to be more effective than chemotherapy. Importantly, we determined that CDK9 inhibition sensitizes cancer cells to TRAIL irrespective of their *p53*-status, thereby providing a therapeutic option also for cancers with mutated *p53* in which conventional chemotherapy is largely ineffective. Moreover, the high efficacy of the newly devised treatment combination was also apparent *in vivo*. In an orthotopic lung cancer xenograft model, the combination of SNS-032 with TRAIL eradicated established lung tumors after a 4-day treatment cycle. This striking result provides further support for the high therapeutic potential of combinations of TRAIL-R agonists with CDK9 inhibitors.

Recent reports on first clinical trials with TRAIL and other TRAIL-R agonists showed, on the one hand, that these biotherapeutics were well tolerated but, on the other, that the clinical activity they exerted, even when combined with standard chemotherapy, was rather limited.[6] Cancer cell resistance to TRAIL-induced apoptosis is likely to be a significant factor in this outcome, indicating that a TRAIL-comprising therapy will only be effective when a potent TRAIL sensitizer is applied in combination with a TRAIL-R agonist. Based on our results, we propose CDK9 inhibition as an effective means to overcome TRAIL resistance in a cancer-selective manner.

Materials and Methods

Reagents. Antibodies: α-RNA-Pol II, α-pSer2 and α-pSer5 were purchased from Covance (Princeton, NJ, USA); α-Caspase-3 and α-cIAP from R&D Systems (Abingdon, UK); α-cFlip (NF6) and α-Caspase-8 (C15) are available from Enzo (Exeter, UK); α-PARP was purchased from BD Biosciences (Oxford, UK); α-FADD was purchased from BD Biosciences (IgG1) or Santa Cruz (Heidelberg, Germany) (rabbit). α-Caspase-10 and α-Caspase-9 from MBL (Woburn, MA, USA); α-β-Actin from Sigma (Gillingham, UK) and α-DNA-PK, α-p110α, α-p110β, α-Bak, α-Bax, α-Mcl-1, α-Bcl-2, α-Bcl-xL, α-XIAP, α-CDK1, α-CDK2, α-CDK4, α-CDK6, α-CDK7, α-CDK9, α-AKT and α-pAKT(Ser473) from Cell Signaling (Danvers, MA, USA); α-Bid was obtained from or Cell Signaling (rabbit) or R&D Systems (goat). HS101 and HS201 were used for surface staining of TRAIL-R1/–R2 and are available from Enzo (Exeter, UK). Recombinant TRAIL was used as an isoleucine zipper-tagged version of the extracellular domain of human TRAIL (izTRAIL) as described previously.[39] PIK-75, TGX-221 AS-252424, IC-87144, A66, BEZ-235, GDC-0941 and SNS-032 were purchased from Selleck Chemicals (Houston, TX, USA); actinomycin D from Merck Millipore (Darmstadt, Germany); cycloheximide and crystal violet from Sigma, z-VAD(OMe)-FMK from Abcam (Cambridge, UK) and D-Luciferin from Caliper Life Science (Waltham, MA, USA).

Cell lines. The human lung adenocarcinoma panel (H460, H522, H322, H441, Calu-1 and H23) was kindly provided by J Downward and cultured in RPMI supplemented with 10% FCS. A549-luc cells were purchased from Caliper Life Science and cultured in RPMI supplemented with 10% FCS. HeLa cells were cultured in DMEM supplemented with 5% FCS. HCT-116 WT and HCT-116 $^{Bax-/-Bak-/-}$ were kindly provided by B Vogelstein and R Youle and were cultured in DMEM supplemented with 10% FCS. PHHs were purchased from Gibco/Invitrogen (Paisley, UK) and cultured according to the manufacturer's instructions.

RNA interference. siRNA pools (ON-TARGET plus) containing four different siRNA sequences targeting each gene of interest were purchased from Dharmacon/Thermo Scientific (Loughborough, UK). Cells were transfected using Dharmafect reagent according to the manufacturer's instructions. Cells were used for further analysis at 48 or 72 h after transfection. Knockdown efficiency was assessed by western blot in parallel.

Cell viability and cell death assays. Cell viability was determined using the Cell Titer Glo assay (Promega, Southampton, UK) according to the manufacturer's instructions. As a direct measurement of apoptotic cell death,

DNA fragmentation was quantified as described before.[55] To analyze long-term survival (clonogenic assay), cells were seeded into six-well plates. The next day, cells were preincubated with DMSO, PIK-75 or SNS-032 for 1 h before izTRAIL was added. After 24 h, dead cells were washed away and surviving cells were cultured for additional 6 days in fresh medium without any treatment. After 7 days, cells were washed twice with PBS, fixed with 10% formaldehyde in PBS for 30 min at room temperature and stained with crystal violet (1% in 50% ethanol).

Western blot analysis. Cells were treated as indicated and then lysed in lysis buffer (30 mM Tris-HCl; pH 7.4, 150 mM NaCl, 2 mM EDTA, 2 mM KCl, 10% glycerol, 1% Triton X-100 and 1 × complete protease-inhibitor cocktail (Roche, Burgess Hill, UK)). Proteins were separated by SDS-PAGE (NuPAGE) and analyzed by western blotting. Membranes were stripped with 50 mM glycine (pH 2.3) before reprobing with other antibodies.

DISC analysis. We performed ligand affinity precipitations using Flag-tagged TRAIL in combination with M2 beads (Sigma). Cells were incubated for 1 h at 37 °C in the presence or absence of 1 μg/ml Flag-TRAIL. For the precipitation of the non-stimulated receptors, Flag-TRAIL was added to the lysates prepared from non-stimulated cells. Precipitates were prepared as described previously.[56]

TRAIL-R surface staining. Cells were detached using Accutase (Sigma) and counted. Cells (2×10^5) were incubated with 10 μg/ml anti-TRAIL-R1 (HS101) or anti-TRAIL-R2 (HS201) or IgG1 isotype control antibody in 2% BSA in 100 μl PBS (BSA/PBS) for 30 min on ice. Cells were washed twice with ice-cold BSA/PBS before incubation with secondary goat–anti-mouse-APC (BioLegend, London, UK) at a dilution of 1:200 in BSA/PBS for 20 min on ice. Cells were washed three times in ice-cold BSA/PBS and surface expression was assessed by flow cytometry.

Overexpression of cFlip and Mcl-1. HeLa cells were transfected with control, PEGZ-cFlip, pEF 3xFLAG-hMcl-1 or both using Lipofectamine LTX (Invitrogen, Paisley, UK) according to the manufacturer's instructions. Cells were left untreated for 24 h before any treatment to ensure efficient expression of the respective protein. Efficient expression of the respective protein was controlled by SDS-PAGE and subsequent western blot. Furthermore, cells were transfected with a GFP-containing plasmid and transfection efficiency was quantified by flow cytometry.

Determination of AST values. Supernatant (30 μl) of treated PHHs was used to determine AST levels using a Reflovet Analyzer (Roche) and Reflotron GOT test strips according to the manufacturer's instructions.

Caspase-cleaved CK 18-ELISA. Supernatant (50 μl) of treated PHHs was used in the M30 Apoptosense ELISA (Peviva, Bromma, Sweden) according to the manufacturer's instructions.

High-Throughput kinase selectivity profiling (Kinomescan). High-throughput kinase selectivity profiling assay (Kinomescan, DiscoveRx, Fremont, CA, USA) was used to determine the promiscuity of PIK-75 as a kinase inhibitor. The capacity of PIK-75 to bind to a panel of 451 human kinases was determined by analyzing the binding interaction (%) compared with DMSO (= 100%). We chose to use PIK-75 at 200 nM in this screen because this was twice the concentration of this agent required to sensitize cancer cells to TRAIL. Hits were visualized using the TREEspot visualization tool provided by DiscoveRx. Kinases were considered hits if their activity was inhibited by >90% leaving <10% remaining activity.

RNA analysis by RT-PCR. RNA was extracted using the RNeasy Kit (Qiagen, Manchester, UK) and treated with the TURBO DNA-free Kit (Ambion, Paisley, UK) according to the manufacturer's instructions. cDNA was generated using the RevertAid H Minus Strand cDNA Synthesis Kit (Thermo Scientific, Loughborough, UK) and used in combination with the FastStart Universal ProbeLibrary Mastermix (Roche) for the RT-PCR. Quantification of gene products was performed using the Eppendorf Mastercycler. When fold changes are shown, the gene product was normalized to GAPDH as a housekeeping gene and were calculated using the method described by Pfaffl *et al*.[57]

Primers for RT-PCR. Primers and probe combinations were determined using the Universal ProbeLibrary Design Center (Roche) and are as follows.

cFLIP(s) forward: 5′–TTGGAAATTGTTCCATGTGATT-3′
cFLIP(s) reverse: 5′-GCAACAAGAAAGGGCTAAACA-3′
cFLIP(s) Essay Universal ProbeLibrary Number: 34
cFLIP(l) forward: 5′-GCTCACCATCCCTGTACCTG-3′
cFLIP(l) reverse: 5′-CAGGAGTGGGCGTTTTCTT-3′
cFLIP(l) Essay Universal ProbeLibrary Number: 14
CDK9 forward: 5′-TTCGGGGAGGTGTTCAAG-3′
CDK9 reverse: 5′-ATCTCCCGCAAGGCTGTAAT-3′
CDK9 Essay Universal ProbeLibrary Number: 21
MCL-1 forward: 5′-AAGCCAATGGGCAGGTCT-3′
MCL-1 reverse: 5′-TGTCCAGTTTCCGAAGCAT-3′
MCL-1 Essay Universal ProbeLibrary Number: 49
GAPDH forward: 5′-AGCCACATCGCTCAGACAC-3′
GAPDH reverse: 5′-GCCCAATACGACCAAATCC-3′
GAPDH Essay Universal ProbeLibrary Number: 60

Orthotopic lung cancer xenograft. Female Fox Chase SCID Beige Mice (6–12 week old; Charles River, Germany) were injected with 2×10^6 A549-luc cells via the lateral tail vein. After 1 week, all mice were imaged for bioluminescence using the Ivis Spectrum (Caliper Life Science). Photons per second (Photon Flux) were quantified using the Ivis Spectrum software. Mice with established tumor burden were included in the study and randomized into the treatment groups (eight mice/group). Subsequently, mice were treated for 4 consecutive days with daily i.p. injections of 600 μg SNS-032 (30 mg/kg) and/or 100 μg izTRAIL or 200 μl buffer as control. After 3 weeks, tumor burden was quantified by bioluminescence imaging. For preparation of lung tissue sections, mice were killed according to Guidance on Operation of Animals (Scientific Procedures) Act 1986. Lungs were removed, fixed in 10% formalin for 1 week and then transferred to 70% ethanol. Paraffin embedding, preparation of sections and H&E stainings were performed as part of a histological staining service at the National Heart & Lung Institute. H&E stainings were examined and quantified by an experienced pathologist (MAE-B) who was blinded to the study. Tumor burden was quantified as percentage of tumor tissue in the lung. SCID beige mice were maintained in individually ventilated cages, received autoclaved food, water and bedding according to the institutional guidelines under a UK Home Office project license. The required risk assessments were obtained for this study.

Statistical analysis. Data were analyzed using GraphPad Prism 6 software (GraphPad Software). Statistical significance between groups was determined using Student's *t*-test. Significant *P*-values are denoted as $^*P<0.05$; $^{**}P<0.01$; $^{***}P<0.001$.

Conflict of Interest

HW is co-founder, scientific advisor and shareholder of Apogenix GmbH (Heidelberg, Germany), a company that develops apoptosis-based drugs. The remaining authors declare no conflict of interest.

Acknowledgements. We thank J Downward, B Vogelstein and R Youle for providing cell lines; and M Leverkus and A Villunger for providing plasmids. This work was supported by a Cancer Research UK program grant awarded to HW. JL was supported by the Dr Mildred-Scheel Stiftung/Deutsche Krebshilfe; and AC was supported by the Italian Foundation for Cancer Research (FIRC).

Author contributions

HW and JL designed the research. JL, SvK and HW co-wrote the manuscript. JL performed most of the experiments; SvK, MAEH, AC, AM, FA and KP contributed experimentally. MAE-B. performed histopathological examinations of tumor tissues in a blinded manner.

1. Pommier Y, Sordet O, Antony S, Hayward RL, Kohn KW. Apoptosis defects and chemotherapy resistance: molecular interaction maps and networks. *Oncogene* 2004; **23**: 2934–2949.
2. Creagan ET, Kovach JS, Moertel CG, Frytak S, Kvols LK. A phase I clinical trial of recombinant human tumor necrosis factor. *Cancer* 1988; **62**: 2467–2471.
3. Ogasawara J, Watanabe-Fukunaga R, Adachi M, Matsuzawa A, Kasugai T, Kitamura Y *et al*. Lethal effect of the anti-Fas antibody in mice. *Nature* 1993; **364**: 806–809.

4. Ashkenazi A, Pai RC, Fong S, Leung S, Lawrence DA, Marsters SA *et al.* Safety and antitumor activity of recombinant soluble Apo2 ligand. *J Clin Invest* 1999; **104**: 155–162.
5. Walczak H, Miller RE, Ariail K, Gliniak B, Griffith TS, Kubin M *et al.* Tumoricidal activity of tumor necrosis factor-related apoptosis-inducing ligand in vivo. *Nat Med* 1999; **5**: 157–163.
6. Micheau O, Shirley S, Dufour F. Death receptors as targets in cancer. *Br J Pharmacol* 2013; **169**: 1723–1744.
7. Todaro M, Lombardo Y, Francipane MG, Alea MP, Cammareri P, Iovino F *et al.* Apoptosis resistance in epithelial tumors is mediated by tumor-cell-derived interleukin-4. *Cell Death Differ* 2008; **15**: 762–772.
8. Pan G, O'Rourke K, Chinnaiyan AM, Gentz R, Ebner R, Ni J *et al.* The receptor for the cytotoxic ligand TRAIL. *Science* 1997; **276**: 111–113.
9. Walczak H, Degli-Esposti MA, Johnson RS, Smolak PJ, Waugh JY, Boiani N *et al.* TRAIL-R2: a novel apoptosis-mediating receptor for TRAIL. *EMBO J* 1997; **16**: 5386–5397.
10. Kischkel FC, Lawrence DA, Chuntharapai A, Schow P, Kim KJ, Ashkenazi A. Apo2L/TRAIL-dependent recruitment of endogenous FADD and caspase-8 to death receptors 4 and 5. *Immunity* 2000; **12**: 611–620.
11. Kischkel FC, Lawrence DA, Tinel A, LeBlanc H, Virmani A, Schow P *et al.* Death receptor recruitment of endogenous caspase-10 and apoptosis initiation in the absence of caspase-8. *J Biol Chem* 2001; **276**: 46639–46646.
12. Sprick MR, Rieser E, Stahl H, Grosse-Wilde A, Weigand MA, Walczak H. Caspase-10 is recruited to and activated at the native TRAIL and CD95 death-inducing signalling complexes in a FADD-dependent manner but can not functionally substitute caspase-8. *EMBO J* 2002; **21**: 4520–4530.
13. Sprick MR, Weigand MA, Rieser E, Rauch CT, Juo P, Blenis J *et al.* FADD/MORT1 and caspase-8 are recruited to TRAIL receptors 1 and 2 and are essential for apoptosis mediated by TRAIL receptor 2. *Immunity* 2000; **12**: 599–609.
14. Dickens LS, Boyd RS, Jukes-Jones R, Hughes MA, Robinson GL, Fairall L *et al.* A death effector domain chain DISC model reveals a crucial role for caspase-8 chain assembly in mediating apoptotic cell death. *Mol Cell* 2012; **47**: 291–305.
15. Jost PJ, Grabow S, Gray D, McKenzie MD, Nachbur U, Huang DC *et al.* XIAP discriminates between type I and type II FAS-induced apoptosis. *Nature* 2009; **460**: 1035–1039.
16. Krueger A, Schmitz I, Baumann S, Krammer PH, Kirchhoff S. Cellular FLICE-inhibitory protein splice variants inhibit different steps of caspase-8 activation at the CD95 death-inducing signaling complex. *J Biol Chem* 2001; **276**: 20633–20640.
17. Salvesen GS, Duckett CS. IAP proteins: blocking the road to death's door. *Nat Rev Mol Cell Biol* 2002; **3**: 401–410.
18. Deveraux QL, Takahashi R, Salvesen GS, Reed JC. X-linked IAP is a direct inhibitor of cell-death proteases. *Nature* 1997; **388**: 300–304.
19. Reed JC. Regulation of apoptosis by bcl-2 family proteins and its role in cancer and chemoresistance. *Curr Opin Oncol* 1995; **7**: 541–546.
20. Rodon J, Dienstmann R, Serra V, Tabernero J. Development of PI3K inhibitors: lessons learned from early clinical trials.. *Nat Rev Clin Oncol* 2013; **10**: 143–153.
21. Bagci-Onder T, Wakimoto H, Anderegg M, Cameron C, Shah K. A dual PI3K/mTOR inhibitor, PI-103, cooperates with stem cell-delivered TRAIL in experimental glioma models. *Cancer Res* 2011; **71**: 154–163.
22. Opel D, Naumann I, Schneider M, Bertele D, Debatin KM, Fulda S. Targeting aberrant PI3K/Akt activation by PI103 restores sensitivity to TRAIL-induced apoptosis in neuroblastoma. *Clin Cancer Res* 2011; **17**: 3233–3247.
23. Samuels Y, Wang Z, Bardelli A, Silliman N, Ptak J, Szabo S *et al.* High frequency of mutations of the PIK3CA gene in human cancers. *Science* 2004; **304**: 554.
24. Ehrenschwender M, Siegmund D, Wicovsky A, Kracht M, Dittrich-Breiholz O, Spindler V *et al.* Mutant PIK3CA licenses TRAIL and CD95L to induce non-apoptotic caspase-8-mediated ROCK activation. *Cell Death Differ* 2010; **17**: 1435–1447.
25. Marone R, Cmiljanovic V, Giese B, Wymann MP. Targeting phosphoinositide 3-kinase: moving towards therapy. *Biochim Biophys Acta* 2008; **1784**: 159–185.
26. Folkes AJ, Ahmadi K, Alderton WK, Alix S, Baker SJ, Box G *et al.* The identification of 2-(1H-indazol-4-yl)-6-(4-methanesulfonyl-piperazin-1-ylmethyl)-4-morpholin-4-yl-t hieno [3,2-d]pyrimidine (GDC-0941) as a potent, selective, orally bioavailable inhibitor of class I PI3 kinase for the treatment of cancer. *J Med Chem* 2008; **51**: 5522–5532.
27. Maira SM, Stauffer F, Brueggen J, Furet P, Schnell C, Fritsch C *et al.* Identification and characterization of NVP-BEZ235, a new orally available dual phosphatidylinositol 3-kinase/mammalian target of rapamycin inhibitor with potent *in vivo* antitumor activity. *Mol Cancer Ther* 2008; **7**: 1851–1863.
28. Jamieson S, Flanagan JU, Kolekar S, Buchanan C, Kendall JD, Lee WJ *et al.* A drug targeting only p110alpha can block phosphoinositide 3-kinase signalling and tumour growth in certain cell types. *Biochem J* 2011; **438**: 53–62.
29. Malumbres M, Barbacid M. Cell cycle, CDKs and cancer: a changing paradigm. *Nat Rev Cancer* 2009; **9**: 153–166.
30. Wang S, Fischer PM. Cyclin-dependent kinase 9: a key transcriptional regulator and potential drug target in oncology, virology and cardiology. *Trends Pharmacol Sci* 2008; **29**: 302–313.
31. Fisher RP. Secrets of a double agent: CDK7 in cell-cycle control and transcription. *J Cell Sci* 2005; **118**(Pt 22): 5171–5180.
32. Shapiro GI. Cyclin-dependent kinase pathways as targets for cancer treatment. *J Clin Oncol* 2006; **24**: 1770–1783.
33. Conroy A, Stockett DE, Walker D, Arkin MR, Hoch U, Fox JA *et al.* SNS-032 is a potent and selective CDK 2, 7 and 9 inhibitor that drives target modulation in patient samples. *Cancer Chem Pharmacol* 2009; **64**: 723–732.
34. Marshall NF, Peng J, Xie Z, Price DH. Control of RNA polymerase II elongation potential by a novel carboxyl-terminal domain kinase. *J Biol Chem* 1996; **271**: 27176–27183.
35. Peterlin BM, Price DH. Controlling the elongation phase of transcription with P-TEFb. *Mol Cell* 2006; **23**: 297–305.
36. Newsom-Davis T, Prieske S, Walczak H. Is TRAIL the holy grail of cancer therapy? *Apoptosis* 2009; **14**: 607–623.
37. Bensaude O. Inhibiting eukaryotic transcription: which compound to choose? How to evaluate its activity? *Transcription* 2011; **2**: 103–108.
38. Kumar MS, Hancock DC, Molina-Arcas M, Steckel M, East P, Diefenbacher M *et al.* The GATA2 transcriptional network is requisite for RAS oncogene-driven non-small cell lung cancer. *Cell* 2012; **149**: 642–655.
39. Ganten TM, Koschny R, Sykora J, Schulze-Bergkamen H, Buchler P, Haas TL *et al.* Preclinical differentiation between apparently safe and potentially hepatotoxic applications of TRAIL either alone or in combination with chemotherapeutic drugs. *Clin Cancer Res* 2006; **12**: 2640–2646.
40. Huang D, Zhou T, Lafleur K, Nevado C, Caflisch A. Kinase selectivity potential for inhibitors targeting the ATP binding site: a network analysis. *Bioinformatics* 2010; **26**: 198–204.
41. Manning G, Whyte DB, Martinez R, Hunter T, Sudarsanam S. The protein kinase complement of the human genome. *Science* 2002; **298**: 1912–1934.
42. Thomas D, Powell JA, Vergez F, Segal DH, Nguyen NY, Baker A *et al.* Targeting acute myeloid leukemia by dual inhibition of PI3K signalling and Cdk9-mediated Mcl-1 transcription. *Blood* 2013; **122**: 738–748.
43. Lapenna S, Giordano A. Cell cycle kinases as therapeutic targets for cancer. *Nat Rev Drug Disc* 2009; **8**: 547–566.
44. Fandy TE, Ross DD, Gore SD, Srivastava RK. Flavopiridol synergizes TRAIL cytotoxicity by downregulation of FLIPL. *Cancer Chem Pharmacol* 2007; **60**: 313–319.
45. Kim DM, Koo SY, Jeon K, Kim MH, Lee J, Hong CY *et al.* Rapid induction of apoptosis by combination of flavopiridol and tumor necrosis factor (TNF)-alpha or TNF-related apoptosis-inducing ligand in human cancer cell lines. *Cancer Res* 2003; **63**: 621–626.
46. Palacios C, Yerbes R, Lopez-Rivas A. Flavopiridol induces cellular FLICE-inhibitory protein degradation by the proteasome and promotes TRAIL-induced early signaling and apoptosis in breast tumor cells. *Cancer Res* 2006; **66**: 8858–8869.
47. Kim EH, Kim SU, Shin DY, Choi KS. Roscovitine sensitizes glioma cells to TRAIL-mediated apoptosis by downregulation of survivin and XIAP. *Oncogene* 2004; **23**: 446–456.
48. Molinsky J, Klanova M, Koc M, Beranova L, Andera L, Ludvikova Z *et al.* Roscovitine sensitizes leukemia and lymphoma cells to tumor necrosis factor-related apoptosis-inducing ligand-induced apoptosis. *Leuk Lymphoma* 2013; **54**: 372–380.
49. Ortiz-Ferron G, Yerbes R, Eramo A, Lopez-Perez AI, De Maria R, Lopez-Rivas A. Roscovitine sensitizes breast cancer cells to TRAIL-induced apoptosis through a pleiotropic mechanism. *Cell Res* 2008; **18**: 664–676.
50. Guha M. Cyclin-dependent kinase inhibitors move into Phase III. *Nat Rev Drug Disc* 2012; **11**: 892–894.
51. Heath EI, Bible K, Martell RE, Adelman DC, Lorusso PM. A phase 1 study of SNS-032 (formerly BMS-387032), a potent inhibitor of cyclin-dependent kinases 2, 7 and 9 administered as a single oral dose and weekly infusion in patients with metastatic refractory solid tumors. *Invest New Drugs* 2008; **26**: 59–65.
52. Tong WG, Chen R, Plunkett W, Siegel D, Sinha R, Harvey RD *et al.* Phase I and pharmacologic study of SNS-032, a potent and selective Cdk2, 7, and 9 inhibitor, in patients with advanced chronic lymphocytic leukemia and multiple myeloma. *J Clin Oncol* 2010; **28**: 3015–3022.
53. Chen R, Wierda WG, Chubb S, Hawtin RE, Fox JA, Keating MJ *et al.* Mechanism of action of SNS-032, a novel cyclin-dependent kinase inhibitor, in chronic lymphocytic leukemia. *Blood* 2009; **113**: 4637–4645.
54. Lowe SW, Bodis S, McClatchey A, Remington L, Ruley HE, Fisher DE *et al.* p53 status and the efficacy of cancer therapy *in vivo*. *Science* 1994; **266**: 807–810.
55. Nicoletti I, Migliorati G, Pagliacci MC, Grignani F, Riccardi C. A rapid and simple method for measuring thymocyte apoptosis by propidium iodide staining and flow cytometry. *J Immunol Methods* 1991; **139**: 271–279.
56. Walczak H, Haas TL. Biochemical analysis of the native TRAIL death-inducing signaling complex. *Methods Mol Biol* 2008; **414**: 221–239.
57. Pfaffl MW. A new mathematical model for relative quantification in real-time RT-PCR. *Nucleic Acids Res* 2001; **29**: e45.

Supplementary Information accompanies this paper on Cell Death and Differentiation website (http://www.nature.com/cdd)

KRAS-driven cancer progression, invasion and metastasis require the endogenous TRAIL/TRAIL-R2 system

Silvia von Karstedt,[1] Annalisa Conti,[1,2] Johannes Lemke,[1] Max Nobis,[3] Antonella Montinaro,[1] Hartwig Torsten,[1] Karen Legler,[4] Franka Annewanter,[4] Andrew D. Campbell,[3] Lucia Taraborrelli,[1] Anne Grosse-Wilde,[5,6] Johannes F. Coy,[5,7] Mona A. El-Bahrawy,[8] Frank Bergmann,[9] Ronald Koschny,[10] Jens Werner,[11] Tom M. Ganten,[10] Thomas Schweiger,[12,13] Konrad Hoetzenecker,[13] Istvan Kenessey,[14] Balazs Hegedüs,[12,14] Michael Bergmann,[12] Jan-Hendrik Egberts,[15] Charlotte Hauser,[15] Thomas Becker,[15] Christoph Röcken,[16] Holger Kalthoff,[4] Anna Trauzold,[4,15] Kurt I. Anderson,[3] Owen J. Sansom[3] and Henning Walczak[1,*]

[1]Centre for Cell Death, Cancer and Inflammation, UCL, 72 Huntley Street, London WC1E 6DD, UK

[2]Department of Experimental Oncology and Molecular Medicine, Fondazione IRCCS Istituto Nazionale dei Tumori, 20133 Milan, Italy

[3]Beatson Institute for Cancer Research, Switchback Road, Bearsden, Glasgow G61 1BD, UK

[4]Division of Molecular Oncology, Institute for Experimental Cancer Research, University of Kiel, Kiel D-24105, Germany

[5]German Cancer Research Centre (DKFZ), Im Neuenheimer Feld 580, 69120 Heidelberg, Germany

[6]Institute for Systems Biology, 401 Terry Ave N, Seattle WA 98109, USA

[7]TAVARLIN AG, Biotechpark Pfungstadt, Reißstraße 1a, 64319 Pfungstadt, Germany

[8]Department of Histopathology, Imperial College London, Du Cane Road, London W12 0NN, UK

[9] Institute of Pathology, University Hospital Heidelberg, Im Neuenheimer Feld 224, 69120 Heidelberg, Germany

[10]Department of Gastroenterology, University Hospital Heidelberg, Im Neuenheimer Feld 410, 69120 Heidelberg, Germany

[11]Department of Surgery, University Hospital Heidelberg, Im Neuenheimer Feld 110, 69120 Heidelberg, Germany

[12]Department of Thoracic Surgery, Medical University of Vienna, Waehringer Guertel 18-20, A-1090 Vienna, Austria

[13]Christian Doppler Laboratory for Cardiac and Thoracic Diagnosis and Regeneration, Medical University of Vienna, Waehringer Guertel 18-20, A-1090 Vienna, Austria

[14]2nd Department of Pathology, Semmelweis University Budapest, Ulloi ut 93, H-1091 Budapest, Hungary

[15]Department of General Surgery, Visceral, Thoracic, Transplantation and Pediatric Surgery, University Hospital Schleswig-Holstein, Kiel, Germany

[16]Department of Pathology, Christian-Albrechts-University, Kiel, Germany

[*]Correspondence: Henning Walczak, E-mail: h.walczak@ucl.ac.uk, phone: +44 207 67946471;

FAX: +44 207 679 6925

Running title: TRAIL/TRAIL-R2 promote KRAS-driven cancer progression

Highlights:

- TRAIL-R2 promotes tumor growth, migration, invasion and metastasis
- Endogenous TRAIL/TRAIL-R2 constitutively activate Rac1/ PI3K
- mTRAIL-R promotes *KRAS*-driven lung and pancreatic cancer and metastasis
- TRAIL-R2 expression positively correlates with onset of metastasis in patients

Abstract

Many cancers harbor oncogenic mutations of *KRAS*. Effectors mediating cancer progression, invasion and metastasis in *KRAS*-mutated cancers are only incompletely understood. An apparently unrelated observation is that many cancers highly express TRAIL-receptors (TRAIL-Rs), which seems counterintuitive given that the main function ascribed to TRAIL-Rs is induction of apoptosis. Here we identify cancer-cell-expressed TRAIL-R2 as a mediator of KRAS-driven cancer progression, invasion and metastasis. This cancer-cell-autonomous signal originates from the membrane-proximal domain (MPD) of TRAIL-R2, a domain with previously unknown function. Cancer-cell-autonomous TRAIL-R2 stimulation promotes activation of a Rac1/PI3K signaling axis responsible for increased migration. Cancer-cell-restricted deletion of murine TRAIL-R in autochthonous models of lung and pancreatic cancer (LsL-*KRASG12D* and LsL-*KRASG12D*/LsL-*p53R172H*) reduces tumor growth, consequently substantially prolonging survival, and blunts metastasis. Consistent with this, high TRAIL-R2 expression in pancreatic cancer patients correlates with tumor invasion into lymph vessels and with shortened metastasis-free survival of *KRAS*-mutated colorectal cancer patients.

OPEN

Citation: Cell Death and Disease (2013) 4, e920; doi:10.1038/cddis.2013.449

www.nature.com/cddis

Smac mimetics induce inflammation and necrotic tumour cell death by modulating macrophage activity

D Lecis*[,1], M De Cesare[1], P Perego[1], A Conti[1], E Corna[1], C Drago[2], P Seneci[3,4], H Walczak[5], MP Colombo[1], D Delia[1] and S Sangaletti*[,1]

Smac mimetics (SMs) comprise a class of small molecules that target members of the inhibitor of apoptosis family of pro-survival proteins, whose expression in cancer cells hinders the action of conventional chemotherapeutics. Herein, we describe the activity of SM83, a newly synthesised dimeric SM, in two cancer ascites models: athymic nude mice injected intraperitoneally with IGROV-1 human ovarian carcinoma cells and immunocompetent BALB/c mice injected with murine Meth A sarcoma cells. SM83 rapidly killed ascitic IGROV-1 and Meth A cells *in vivo* (prolonging mouse survival), but was ineffective against the same cells *in vitro*. IGROV-1 cells in nude mice were killed within the ascites by a non-apoptotic, tumour necrosis factor (TNF)-dependent mechanism. SM83 administration triggered a rapid inflammatory event characterised by host secretion of TNF, interleukin-1β and interferon-γ. This inflammatory response was associated with the reversion of the phenotype of tumour-associated macrophages from a pro-tumoural M2- to a pro-inflammatory M1-like state. SM83 treatment was also associated with a massive recruitment of neutrophils that, however, was not essential for the antitumoural activity of this compound. In BALB/c mice bearing Meth A ascites, SM83 treatment was in some cases curative, and these mice became resistant to a second injection of cancer cells, suggesting that they had developed an adaptive immune response. Altogether, these results indicate that, *in vivo,* SM83 modulates the immune system within the tumour microenvironment and, through its pro-inflammatory action, leads cancer cells to die by necrosis with the release of high-mobility group box-1. In conclusion, our work provides evidence that SMs could be more therapeutically active than expected by stimulating the immune system.
Cell Death and Disease (2013) **4,** e920; doi:10.1038/cddis.2013.449; published online 14 November 2013
Subject Category: Cancer

Resistance to death is a hallmark of cancer cells[1] that renders them unresponsive to chemotherapy. Chemoresistance is often attributed to the inhibitor of apoptosis (IAP) proteins that control many aspects of cellular life, including the response to environmental stimuli, the regulation of cell death[2] and cellular motility.[3,4] X-linked IAP (XIAP) is the only IAP to directly interact with caspases, which occurs through conserved domains named baculoviral IAP repeats.[5] This interaction hinders the activity of both initiator caspase-9[6] and effector caspases-3 and -7.[7] XIAP activity is antagonised by second mitochondria-derived activator of caspases/direct IAP-binding protein with low pI (Smac/DIABLO), which binds to its baculoviral IAP repeats, thereby releasing the caspases[6] and favouring the apoptotic cascade. Starting from this observation, many groups have designed small peptidomimetics that mimic the structure of the N-terminal tetrapeptide (AVPI) of Smac/DIABLO in order to prevent XIAP from inhibiting caspases.[8–10] These compounds, referred to as Smac mimetics (SMs), enhanced the antitumour activity of radiation or chemotherapeutic treatments in combination experiments.[11] Furthermore, they have been shown to potentiate the cytotoxic effects of 'death ligands', in particular, than that of tumour necrosis factor (TNF)-related apoptosis-inducing ligand (TRAIL).[9,12–14] Therefore, these compounds have been proposed as novel cancer treatments and are currently being tested, as part of combination therapies, in clinical trials.[2]

Despite the ability of SMs to enhance the cytotoxicity of other compounds, they are often ineffective in monotherapy. Still, some cancer cell lines undergo a TNF-dependent apoptotic process in response to the administration of a SM alone. In fact, although these compounds were designed to target XIAP, they also bind other IAPs, such as cellular IAP1 (cIAP1) and cIAP2, leading to their self-ubiquitination[15,16] and rapid proteasomal degradation.[17,18] As cIAPs are negative regulators of NF-κB-inducing kinase, their SM-triggered depletion results in the stabilisation of NF-κB-inducing kinase[19] with consequent induction of the non-canonical NF-κB pathway.[17] In cell lines sensitive to these compounds, this event is sufficient to trigger the secretion of high

[1]Department of Experimental Oncology and Molecular Medicine, Fondazione IRCCS Istituto Nazionale dei Tumori, Milan 20133, Italy; [2]Institute of Biomolecular Chemistry, National Research Council, Catania 25126, Italy; [3]Department of Chemistry, University of Milan, Viale Golgi 19, Milan 20133, Italy; [4]CISI scrl, Via Fantoli 16/15, Milan 20138, Italy and [5]Centre for Cell Death, Cancer and Inflammation, University College London, London WC1E 6BT, UK
*Corresponding author: D Lecis or S Sangaletti, Department of Experimental Oncology and Molecular Medicine, Fondazione IRCCS Istituto Nazionale dei Tumori, Via Amadeo 42, Milan 20133, Italy. Tel: +39-02-23902846; Fax: +39-02-23903073; E-mail: daniele.lecis@istitutotumori.mi.it (DL) or Tel: +39-02-23903229; Fax: +39-02-23903073; E-mail: sabina.sangaletti@istitutotumori.mi.it (SS)
Keywords: Smac mimetics; ovarian cancer ascites; IAPs; innate immunity; inflammation
Abbreviations: SM, smac mimetic; IAP, inhibitor of apoptosis; TNF, tumour necrosis factor; XIAP, X-linked inhibitor of apoptosis; TRAIL, TNF-related apoptosis-inducing ligand; PARP, poly (ADP-ribose) polymerase; LPS, lipopolysaccharides; HMGB-1, high-mobility group box-1; TNF-R1, TNF-receptor-1; TLR, toll-like receptor; BMDM, bone marrow-derived macrophages; PMN, polymorphonuclear leucocytes
Received 10.6.13; revised 11.10.13; accepted 15.10.13; Edited by M Piacentini

levels of TNF, thus killing the cells through an autocrine or paracrine mechanism.[17,18] Despite the clear *in vitro* assessment of this process, the role of TNF in SM-induced cell death *in vivo* is still controversial. In fact, the employment of these compounds in pre-clinical models, either as monotherapy or in combination with other drugs, has resulted in conflicting evidence,[11,20,21] indicating a need to clarify the mechanism of action of SMs *in vivo*.

One way to study the mechanisms of action of antitumoural agents involves the use of animal models of cancer ascites. The formation of ascites characterises the advanced-stage of various types of tumours, especially ovarian carcinomas. This condition depends on a mechanical constriction exerted by the tumour and is determined by a peritoneal increase of fluid production associated with decreased lymphatic absorption. Ascites is often the cause of death for ovarian cancer patients, while rarely there is metastatic spread of tumour cells outside the peritoneum.[22] In peritoneal ovarian carcinomatosis, the ascitic fluid represents the microenvironment in which soluble factors are interchanged between cancer and stromal and inflammatory cells, in order to support tumour growth and invasion. This microenvironment also promotes immunosuppression favouring tumour escape from immune control. Thus, although the ascitic fluid is normally enriched in immune cells, they are often anergic and unable to elicit an antitumour immune response. Animal models of cancer ascites facilitate the study of immune cells such as macrophages in response to antitumoural treatments.

Macrophages are plastic cells characterised by different states of activation.[23] Classically activated macrophages (M1) and 'alternatively' activated macrophages (M2) represent the two extremes in the spectrum of the macrophage phenotype. Tumour-associated macrophages are classified as M2 macrophages because of their cytokine expression profile;[24] they produce high amounts of immunosuppressive cytokines such as interleukin-10 (IL-10) and, mostly in solid tumours, share some tissue repair functions with fibroblasts.[23,25] In contrast, M1 macrophages produce large amounts of pro-inflammatory cytokines including interferon-γ (IFNγ) and IL-12, and can be involved in the elicitation of an effective antitumour immune response. The plasticity of macrophages has suggested new therapeutic approaches aiming to revert the M2 phenotype[26] especially in tumours that strictly relies on the macrophage infiltration such as ovarian carcinomas. Accordingly, macrophages have been reprogrammed in a mouse ovarian ascites model by modulating NF-κB signalling.[27]

We recently described the synthesis of novel dimeric molecules that target XIAP, cIAP1 and cIAP2.[28,29] One of these molecules, SM83, inhibited the growth of SM-sensitive human mammary adenocarcinoma MDA-MB231 and rhabdomyosarcoma Kym-1, but not of other cell lines. Here, we use two murine xenograft models of cancer ascites to show that SM83, when administered in monotherapy, increases the survival of these mice by targeting tumour-associated macrophages. Through TNF, SM83 rapidly induces necrosis of the intraperitoneally (i.p.) injected cancer cells, which are otherwise completely resistant *in vitro* to the antitumoural effects of SM83. Therefore, our work shows that SM83 displays different mechanisms of action *in vitro* and *in vivo*, and that *in vivo* it exerts its antitumoural activity by stimulating the immune system.

Results

SM83 sensitises the IGROV-1 ovarian carcinoma cell line to the apoptotic effects of TRAIL. SM83 (Figure 1a) is a novel inhibitor of XIAP, cIAP1 and cIAP2. When administered to human IGROV-1 ovarian carcinoma cells, SM83 in monotherapy at two doses had no inhibitory effect on cell growth (Figure 1b). Instead, when administered together with TRAIL, cell growth was substantially reduced to about 50 (2 ng/ml TRAIL) and 28% (10 ng/ml TRAIL) of that of untreated cells, without a dose-dependent effect for SM83. TRAIL treatment alone had a negligible effect at this concentration, whereas SM83 monotherapy was ineffective on a panel of other human cancer cell lines (A2780, H460, SW48, HCT-116 and DLD-1 cells; data not shown). The apoptotic effects of these treatments on IGROV-1 cells at 3 and 24 h were assessed by western blotting (Figure 1c). Treatment with SM83 alone decreased cIAP1 and cIAP2 to almost undetectable levels already at 3 h. Treatment with SM83 and TRAIL, at 24 h, strongly increased cleaved poly (ADP-ribose) polymerase (PARP), a marker of activated apoptosis. Similar results were obtained when cells were treated with SM59 (Figure 1d). These results suggest that SMs sensitise IGROV-1 cells to TRAIL-induced cell death without causing death themselves.

SMs in monotherapy increase the survival of mice bearing cancer ascites. SM83 and SM59 were then tested *in vivo* using a murine xenograft model in which IGROV-1 cells are injected i.p. into athymic nude mice, leading to ascites and death. Treatment with both SM83 (Figure 2a) and SM59 (Figure 2b) increased mouse survival ($P<0.05$ *versus* control mice), but SM83 was slightly more effective than SM59 (T/C% 180 *versus* 164). Furthermore, SM83 administration significantly reduced the formation of the ascites (Figure 2c). Treatment with TRAIL alone did not increase mouse survival, and the combination of TRAIL plus SM83 had no additive effect (Figure 2a). These findings, which are contrary to the *in vitro* results, suggest that SMs alone slow the progression of ovarian ascites but are not curative in these mice, whereas TRAIL alone is ineffective at the concentration used.

To test whether the *in vivo* activity of SM83 was cell line-specific or limited to immunodeficient mice, we used another ascites model in which murine Meth A sarcoma cells are injected i.p. into immunocompetent syngeneic BALB/c mice. Similar to IGROV-1 cells, Meth A cells were not growth-inhibited by SM83 *in vitro* (data not shown). In mice, SM83 reduced the progression of the ascites, seen as a smaller increase in body weight (Figure 2d), and augmented the median survival time from 15 days for untreated animals to 26 days ($P=0.0721$; Figure 2e). Also in this model, combination with TRAIL was not beneficial (data not shown). Moreover, when mice cured by SM83 (4 of 14 mice tested) were challenged with a new injection of 4×10^5 Meth A cells (twice that of the first administration) none formed new ascites

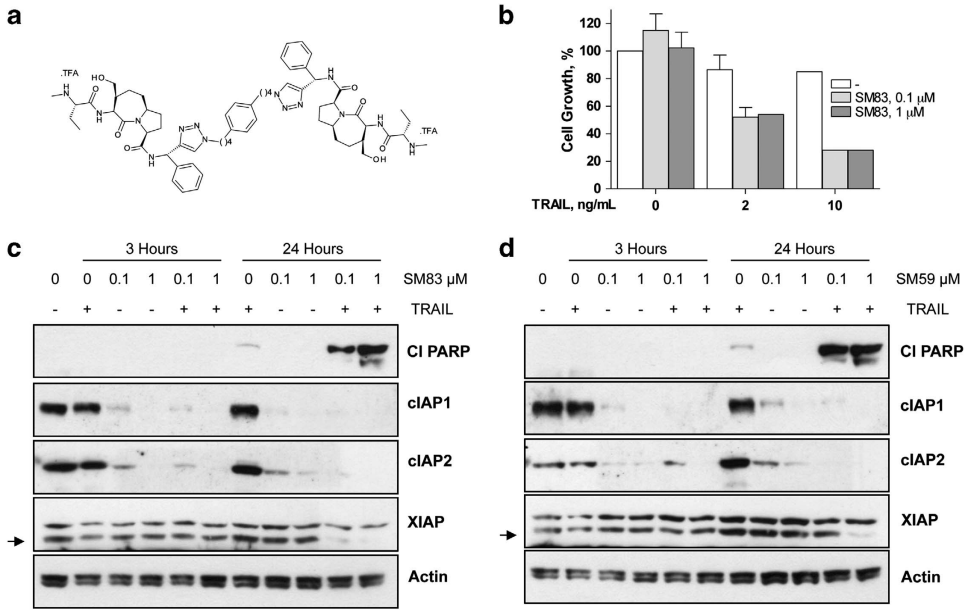

Figure 1 SM83 induces apoptosis *in vitro* when combined with TRAIL. (**a**) Chemical structure of the dimeric SM SM83. (**b**) IGROV-1 cells were treated with 0.1 or 1.0 μM SM83 alone or in combination with 2 or 10 ng/ml TRAIL. Cell growth is expressed as a percentage relative to cells mock-treated with vehicle. Values are mean and S.D. from one experiment representative experiment of three performed. (**c** and **d**) Western blot analysis of XIAP, cIAP1, cIAP2 and cleaved PARP (Cl PARP) in IGROV-1 cells treated 3 or 24 h with SM83 (**c**) or SM59 (SM-164) (**d**) in the absence or presence of 10 ng/ml TRAIL. Actin is shown as loading control. Arrow, specific XIAP band

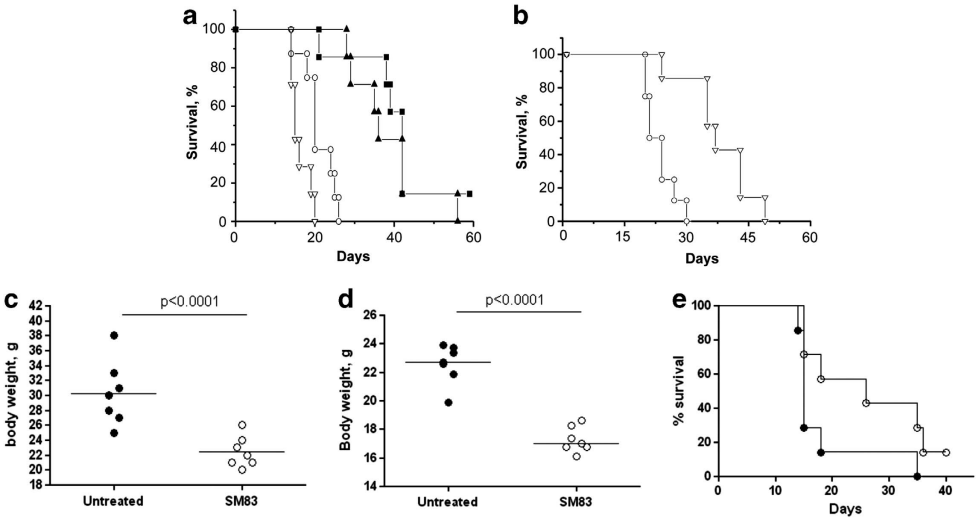

Figure 2 Treatment with SM83 in monotherapy increases the survival of mice bearing cancer ascites. (**a**) Nude mice were injected i.p. with IGROV-1 cells and left untreated (○) or treated 5 times a week, for 2 consecutive weeks starting the day after injection, with 5 mg/kg SM83 (▲), 2.5 mg/kg TRAIL (▽) or with the same doses of SM83 and TRAIL together (■). One experiment representative of two performed is shown. Each treatment group contained seven mice. Survival curve for SM83-treated mice and controls. (**b**) Survival curve for SM59-treated and control mice. Untreated (○) or treated with SM SM59 (▽). (**c**) The formation of ascites was checked by monitoring body weight on day 17. (**d** and **e**) BALB/c mice were injected with Meth A cells and, starting on day 7, were treated daily with 5 mg/kg SM83. (**d**) The formation of ascites was checked by monitoring body weight on day 13. The horizontal line represents the mean. (**e**) Survival curve for untreated (●) or SM83-treated mice (○) starting from day 7

(data not shown). These results strongly suggest that these animals developed an adaptive immunity.

SM83 rapidly kills cancer cells floating in the ascites by a non-apoptotic mechanism. To investigate the mechanism of SM83 activity *in vivo*, the ascitic fluid from mice injected with IGROV-1 cells and treated or not with SM83 for 3, 6 or 24 h was collected and tumour cells were counted. The results showed a striking decrease ($P<0.001$) in the total number of ascites tumour cells in SM83-treated mice at 24 h compared with control untreated mice, without appreciable changes at 3 or 6 h (Figure 3a). Autopsy revealed no adhesion of single cancer cells to the peritoneal wall nor migration outside the peritoneum. Furthermore, we detected a significant increase of human cytokeratin-18 ($P<0.0001$), a protein released from dying human epithelial cells, in the

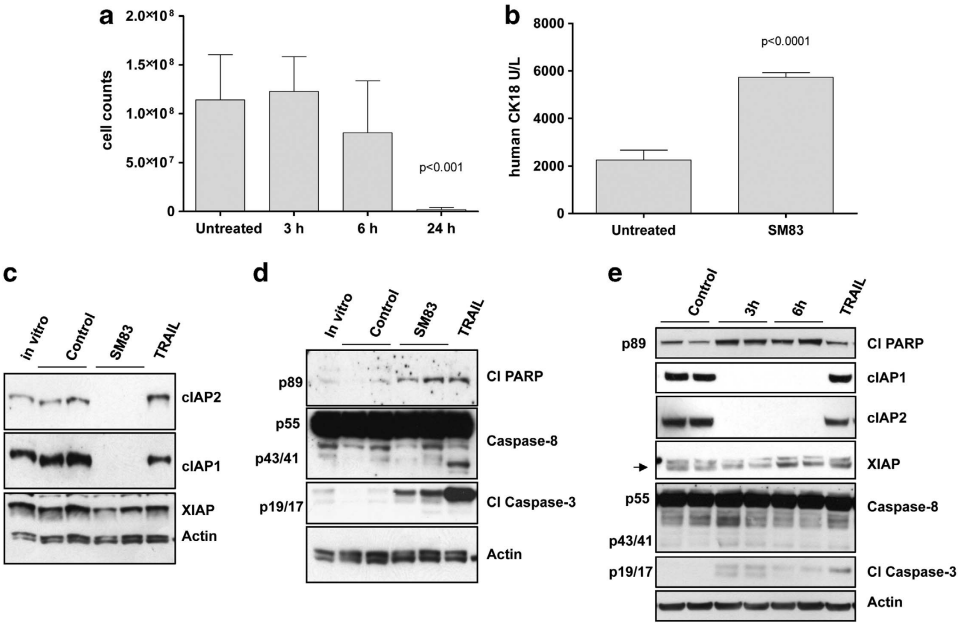

Figure 3 SM83 kills ascites tumour cells through a rapid, non-apoptotic event. Ascitic fluids were collected from nude mice injected with IGROV-1 cells and left untreated or treated with a single injection of SM83 (5 mg/kg). (**a**) Number of tumour cells within the ascites of untreated animals ($n = 11$) or of animals treated for 3 ($n = 4$), 6 ($n = 4$) and 24 h ($n = 9$). Data are mean and S.D. (**b**) Levels of human cytokeratin-18 in the serum collected 24 h after a single dose of SM83 (5 mg/kg) or no treatment. (**c**) Western blot of apoptosis markers in IGROV-1 cells cultured *in vitro* or recovered from the ascites of control mice ($n = 2$) or mice treated with SM83 ($n = 2$) or TRAIL for 24 h. (**d**) Western blot to detect activated apoptosis markers cleaved PARP (p89), caspase-8 (precursor p55 and cleaved form p43/41) and cleaved caspase-3 (p19/p17) in IGROV-1 cells cultured *in vitro* or recovered from the ascites (24 h) of control mice ($n = 2$) and of mice treated with 5 mg/kg SM83 ($n = 2$) or 10 mg/kg TRAIL. (**e**) Western blot of apoptotic markers in tumour cells collected from the ascites of untreated mice ($n = 2$) or from mice treated for 3 or 6 h with SM83 ($n = 2$ for both) or with TRAIL for 24 h. Arrow, specific band for XIAP

serum of mice treated for 24 h (Figure 3b), suggesting that SM83 triggered tumour cell death. Corroborating these *in vivo* findings, western blot analysis of proteins from floating tumour cells within the ascites confirmed that SM83 induced the degradation of cIAP1 and cIAP2, but not of XIAP (Figure 3c).

To understand the mechanism of cell death accounting for the decrease in the number of floating tumour cells within ascites, we examined the expression of mediators of apoptosis in these cells at different time points. At 24 h, SM83 treatment led to only a faint increase of cleaved PARP, no evidence of cleaved, active caspase-8 (which was expected because these cells are killed *in vivo* by SM monotherapy[30]) and only a modest effect on cleavage of caspase-3 (Figure 3d). In contrast, cells treated with TRAIL showed a greater activation of these apoptotic markers even though TRAIL was ineffective in reducing the ascitic cell number (Supplementary Figure S1). In an attempt to detect the apoptotic events, western blotting was done on the cells collected after 3 and 6 h of treatment (Figure 3e). Also in this case, SM83 caused the complete degradation of cIAP1 and cIAP2, but there was only a faint accumulation of the cleaved forms of PARP, caspase-8 and caspase-3. This low activation of the apoptotic cascade suggested that the cause of death of the ascites tumour cells was not primarily apoptotic.

To assess the possibility that autophagy – another mechanism that can cause cell death when abnormally and continuously activated – was responsible for the loss of ascites tumour cells, we measured the levels of beclin-1 and cleaved LC3B. Treatment with SM83 did not increase the levels of these proteins (Supplementary Figure S2), suggesting that autophagy is not involved in SM83-induced tumour cell death.

SM83 triggers an inflammatory event *in vivo*. Having excluded apoptosis and autophagy in SM83-mediated cell death, we investigated the involvement of necrosis by measuring the levels of murine inflammatory cytokines in the ascites. There was a basal level of murine TNF in the ascites of untreated mice, whereas in mice treated with SM83, the level of murine TNF was significantly higher at 3 and 6 h but not at 24 h (Figure 4a). On the contrary, human TNF was not affected by SM83 treatment (Supplementary Figure S3). We tested the relevance of TNF in this model by pretreating mice with two inhibitors of TNF, etanercept and infliximab. Etanercept at the higher dose tested completely blocked the cytotoxic effects of SM83 (Figure 4b), without preventing SM83-triggered degradation of cIAPs (Figure 4c). Pretreatment of mice with infliximab, instead, did not block the cytotoxic effects of SM83 on ascites tumour cells (data not shown), probably owing to its lower affinity for mouse TNF or to an insufficient concentration. Overall, these data suggest that SMs are effective *in vivo* by stimulating the release of murine TNF that activates the TNF receptor leading to the creation of a pro-inflammatory microenvironment. Accordingly, the murine inflammatory cytokines IL-1β (Figure 4d) and IFN-γ (Figure 4e) were upregulated in the peritoneal ascites in response to SM83 administration.

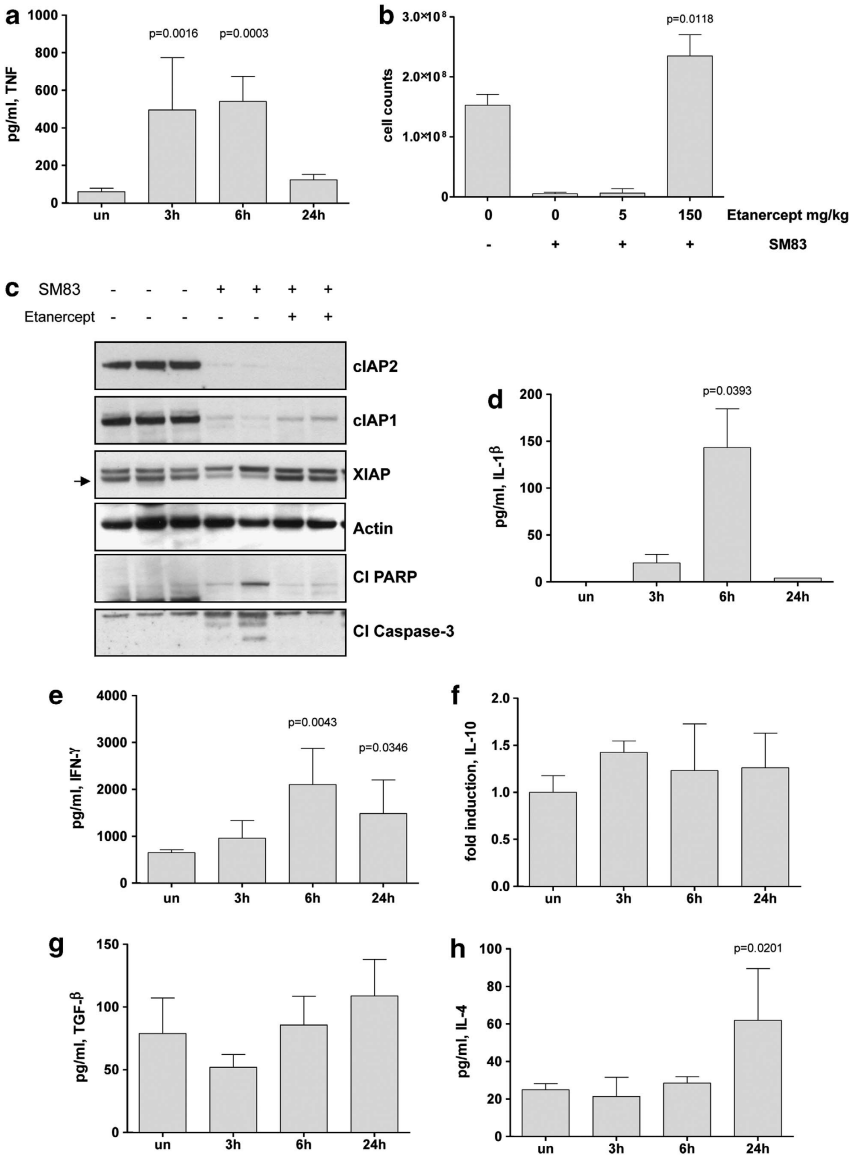

Figure 4 SM83 treatment induces the expression of inflammatory cytokines *in vivo*. Nude mice were injected i.p. with IGROV-1 cells and treated or not with a single dose of 5 mg/kg SM83; ascites was collected 3, 6 and 24 h after SM83 administration. (**a**) SM83 transiently increased the level of murine TNF measured by ELISA. (**b**) SM83 treatment reduced ascites cell counts but this action was blocked when TNF was sequestered with the higher dose of etanercept ($P = 0.0118$ relative to treated with SM83 alone). (**c**) Western blots of ascites tumour cell protein from untreated mice and mice treated with SM83 alone or in combination with 150 mg/kg etanercept. Arrow, specific band for XIAP. (**d–h**) ELISA results for IL-1β (**d**), IFN-γ (**e**), IL-10 (**f**), transforming growth factor-β (TGF-β) (**g**) and IL-4 (**h**) in the ascitic fluid of mice treated as above. Results for IL-10 are shown as fold induction owing to the lack of recombinant protein standard

In contrast, levels of the immunosuppressive cytokines IL-10 (Figure 4f), transforming growth factor-β (Figure 4g) and IL-4 (Figure 4h) remained mostly unchanged, with the exception of IL-4 that increased significantly at 24 h; this increase could be explained by the anti-inflammatory role of this cytokine, secreted after 24 h to restrain the strong inflammation in process.

SM83 promotes macrophage activation towards an M1-like phenotype. To evaluate whether the pro-inflammatory effect of SM83 depends on the activation of tumour-associated macrophages, bone marrow (BM)-derived macrophages (BMDM) from BALB/c mice were treated *in vitro* with SM83, and the cell supernatants were assayed for TNF and IL-1β. SM83 induced the secretion of TNF starting at 6 h (Figure 5a) and of IL-1β at 24 h (Figure 5b). Moreover, as macrophage activation is regulated by NF-κB, we checked whether SM83 activated this pathway using a macrophage cell line stably expressing a luciferase reporter gene under control of the NF-κB-response element. NF-κB activation was detectable after 3 h of treatment with SM83 but returned to basal levels at 24 h (Figure 5c). In agreement with an earlier study,[31] SM83 treatment also promoted the death of BMDM through necroptosis, which was seen 24 h after treatment both morphologically (Figure 5d, second panel) and with the CellTiter-Glo assay

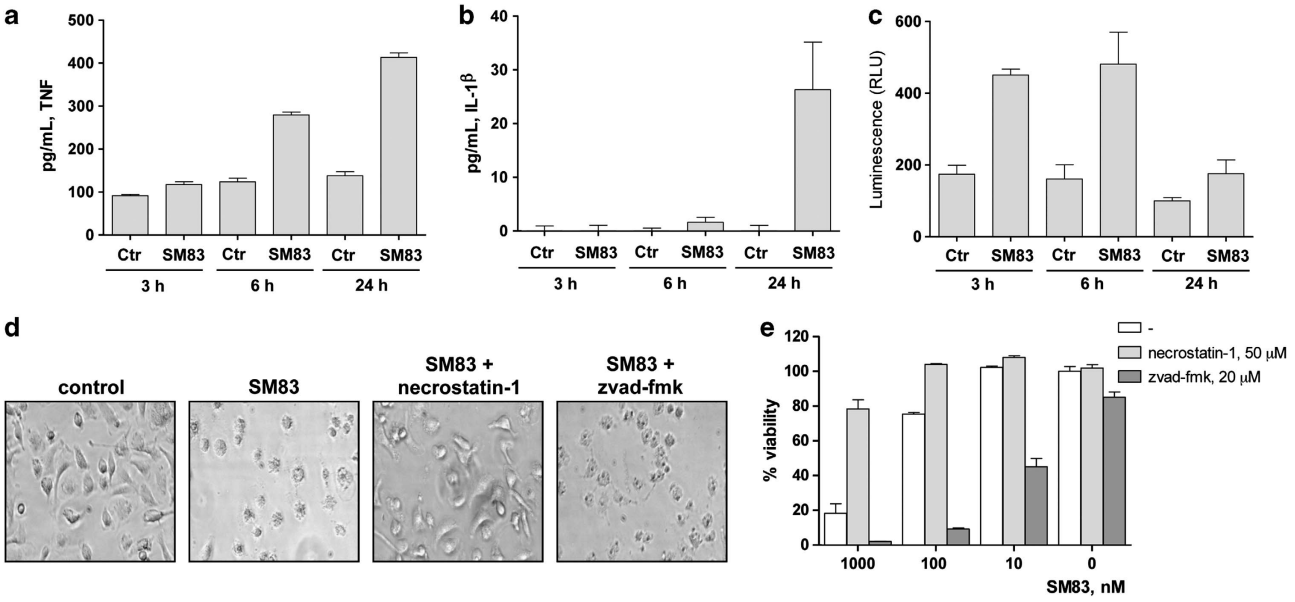

Figure 5 SM treatment activates macrophage and sensitises them to necroptotic death. (**a** and **b**) BALB/c BMDM (5×10^5) were seeded in 96-well plates, left to adhere for 16 h and treated or not with 1 μM SM83 for up to 24 h. SM83 treatment promoted the secretion of the pro-inflammatory cytokines TNF (**a**) and IL-1β (**b**). (**c**) NF-κB activation by SM83 evaluated in the macrophage cell line RAW stably transfected with a NF-κB luciferase reporter gene. One representative experiment of two performed is shown. Values are mean and S.D.; $n = 3$. (**d** and **e**) BALB/c BMDM were seeded in six-well plates, left to adhere for 16 h and treated with serial dilutions of SM83 in the absence or presence of necrostatin-1 or z-vad-fmk to inhibit necroptosis or apoptosis, respectively. (**d**) Representative images showing cell morphology after 24 h of treatment. (**e**) Cell viability after treatments evaluated using the CellTiter-Glo assay

(Figure 5e, first bar). This cytotoxicity was prevented by pretreatment with necrostatin-1, a specific inhibitor of receptor-interacting protein-1 (a crucial mediator of necroptosis), but not by the pan-caspase inhibitor z-vad-fmk, which actually increased BMDM death (Figures 5d and e). Overall, these data suggest that macrophages could be the first target of SM83 activity that fosters their production of pro-inflammatory M1-like molecules such as TNF and IL-1β.

To exclude the possibility that the SM83-induced IL-1β secretion was due to contamination with lipopolysaccharides (LPS), by the stimulation of toll-like receptor-4 (TLR4[32]), we prepared BMDM from TLR4-knockout (KO) mice and found that IL-1β was secreted to a similar extent as it was secreted from BALB/c cells (Supplementary Figure S4). Furthermore, SM83 preparations for injection were found to not contain detectable levels of LPS on the Endosafe-PTS (Charles River Laboratories, Calco, Italy) test (data not shown). These results indicate that the SM83-induced IL-1β production was not due to LPS contamination.

Bystander accumulation of neutrophils in the ascites. Having demonstrated a pro-inflammatory effect of SM83 in the tumour microenvironment, we next evaluated whether SM83 treatment affected the innate immune cells infiltrating the ascites. To this end, we used immunofluorescence to examine the expression of leucocyte antigens on cells harvested from the ascites of nude mice. This assay allowed us to identify both macrophages ($CD11b^+$ $Gr\text{-}1^-$) and neutrophils ($CD11b^+$ $Gr\text{-}1^+$) in mice that were either untreated or treated for 3 and 6 h before harvesting (Figure 6a), without noticeable differences in cell density. However, after 24 h of treatment, neutrophils (but not macrophages) had massively accumulated in the ascitic fluid (Figure 6a, Supplementary Figure S5). Neutrophils had also infiltrated the tumour nodules (Supplementary Figure S6). This massive neutrophil recruitment was likely because of the presence, in the ascites, of high-mobility group box-1 (HMGB-1; Figures 6b and c) and TNF (Figure 4a). HMGB-1, which is released during necrosis and immunogenic cell death, behaves as an 'alarmin' that, together with TNF, attracts and activates neutrophils.[33] In our IGROV-1 model, HMGB-1 was detected in the ascitic fluid starting 6 h after SM83 treatment (Figure 6b) and was located within the cytoplasm of dying tumour cells (Figure 6c).

Next, neutrophils were isolated from spleens of BALB/c (wild-type) and TNF-receptor-1 (TNF-R1)-deficient mice to investigate *in vitro* the role of neutrophils in the antitumoural activity of SM83. In Transwell assays, the migration of wild-type neutrophils towards ascites from SM83-treated mice was greater than that from untreated mice (Figure 6d). The HMGB-1 inhibitor partially reduced the migration, whereas neutrophils from TNF-R1-deficient mice did not migrate in response to ascites from SM83-treated mice. Ascites from mice treated with SM83 activated wild-type neutrophils to produce superoxide even in the presence of the TNF blocker etanercept, whereas glycyrrhizin completely blocked such activity (Figure 6e). These findings suggest that neutrophil migration in the presence of ascites from SM83-treated mice is stimulated by TNF while activation is attributable to HMGB-1. The importance of TNF in neutrophil migration was also shown *in vivo*, where etanercept pretreatment blocked the recruitment of these cells into the ascites (Supplementary Figure S5).

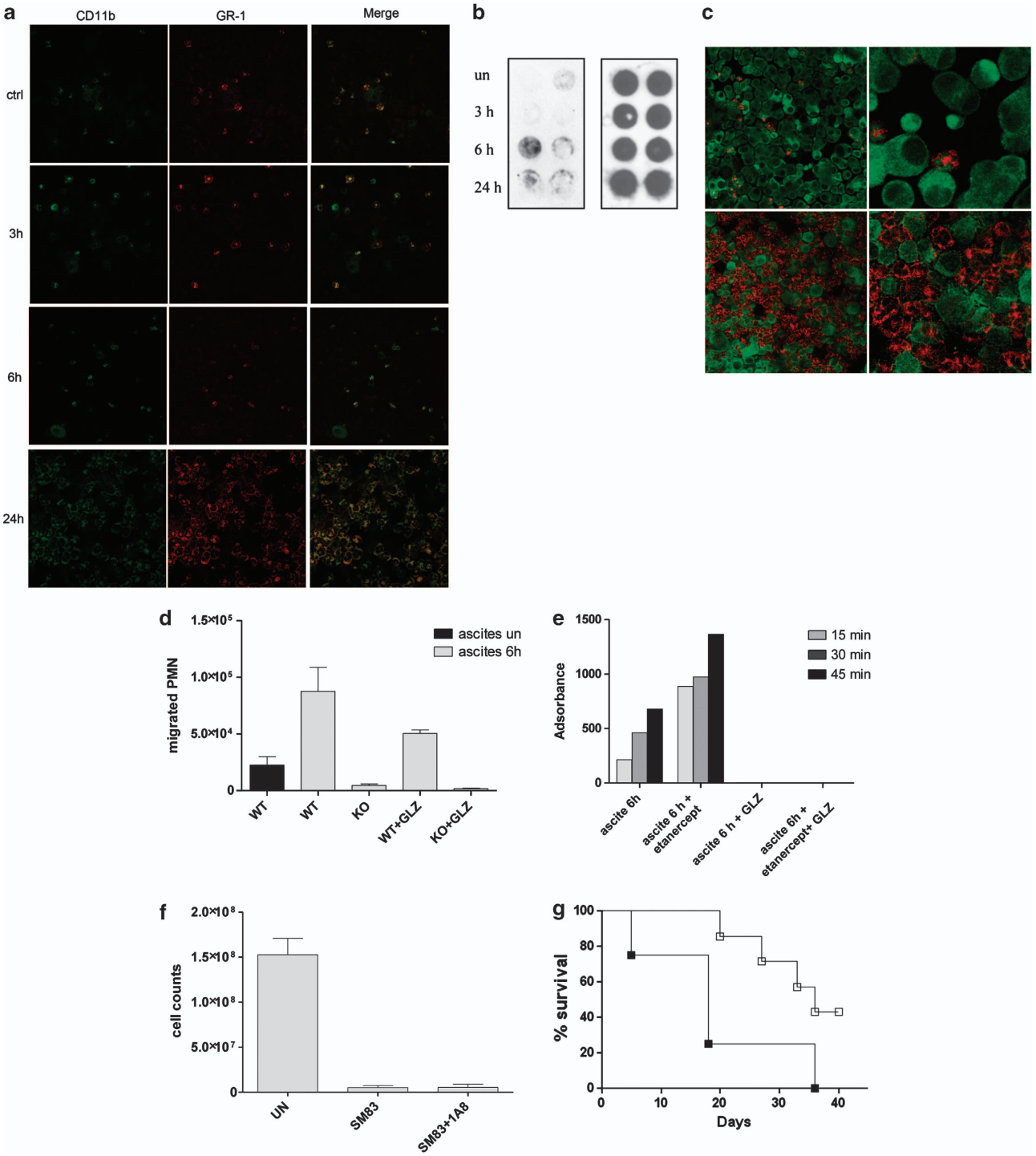

Figure 6 SM83 treatment promotes peritoneal neutrophil recruitment and activation. Cells were harvested from the ascitic fluid of mice treated with 5 mg/kg SM83. (**a**) Immunofluorescence for CD11b (green) and Gr-1 (red) was performed on Cytospin cell preparations. SM83 treatment induced a massive recruitment of neutrophils ($CD11b^+$ $Gr\text{-}1^+$) at 24 h but not at earlier time points. (**b**) Dot blot of HMGB-1 (left panel) was performed on cleared ascitic fluids collected from untreated (un) or treated mice at 3, 6 and 24 h after a single injection of 5 mg/kg SM83. Right panel, loading control. (**c**) Infiltration of neutrophils (Gr-1; red) and HMGB-1 expression in dying tumour cells (green) in ascites untreated (upper row) and treated for 24 h (lower row) with a single injection of SM83. Left and right panels show two different magnifications ($\times$ 10 and $\times$ 40). (**d**) PMN migration assessed by Transwell assay. Wild-type PMN from BALB/c mice (WT) or TNF-R1-deficient PMN from TNF-R1-KO mice (KO) were seeded into the upper chamber in the absence or presence of the HMGB-1 inhibitor glycyrrhizin (GLZ), whereas the ascitic fluid of mice untreated or treated for 6 h (1:20 in medium) was added to the lower chamber of the Transwell insert. PMN were left to migrate overnight, harvested and counted. (**e**) Activation of wild-type PMNs was colorimetrically evaluated on the basis of the ability of cells to oxidise the cytochrome *c* in presence of the ascitic fluid collected from mice 6 h after treating with a single injection of SM83. The experiment was also performed in the presence of GLZ and the TNF inhibitor etanercept. (**f**) Tumour cell counts in the ascites of untreated mice (UN), mice treated with a single injection of SM83 alone or mice treated with SM83 24 h after depletion of neutrophils by injection with the 1A8 mAb. (**g**) BALB/c mice were injected i.p. with Meth A cells and treated with 1A8 alone (■) or in combination with 5 mg/kg SM83 (□), starting from day 7

Considering that, in certain conditions, neutrophils can be responsible for tumour cell killing,[34,35] we depleted ascites-bearing mice of neutrophils before SM83 treatment. In nude mice bearing IGROV-1 ascites, neutrophil depletion did not impede the ability of SM83 to reduce the number of floating tumour cells in the ascites (Figure 6f). Furthermore, in immunocompetent BALB/c mice bearing Meth A ascites, depletion of neutrophils (Supplementary Figure S7) did not prevent SM83 from prolonging survival (Figure 6g), even though these mice have CD8+ T cells that are known to support the activity of neutrophils.[36] On the contrary, neutrophil depletion improved the efficacy of SM83 treatment by significantly augmenting the overall survival of mice treated with SM83 ($P=0.0458$ *versus* 1A8 alone). These results support the notion that, in our models, neutrophil recruitment is a bystander effect due to SM83-induced TNF secretion. The accumulation of neutrophils has no role in SM-dependent cancer cell killing but rather, at least in the Meth A model, could be in some way detrimental to the host.

In conclusion, our work shows that SM83 acts *in vivo* in cancer ascites by reverting macrophages from an M2-like phenotype, supporting the tumour, to an M1-like phenotype, endowed with antitumour activity. M1 macrophages secrete cytokines such as TNF, IL-1β and IFNγ that cause a rapid TNF-dependent necrotic death of the ascites cancer cells (Figure 7); subsequently, the dying cells release HMGB-1 that, together with TNF, stimulates a massive infiltration of neutrophils.

Discussion

In this study, we describe the *in vivo* activity of newly synthesised SM SM83 in two murine xenograft models of cancer ascites. We show that SM83 is active as monotherapy *in vivo* on human and murine cancer cells that are refractory to SMs *in vitro*, and demonstrate that these cells die through a non-apoptotic, TNF-dependent mechanism. We also provide evidence that SM83 exerts its activity by inducing inflammation and immune cell activation, resulting in immunogenic death of cancer cells. Moreover, our study shows that the activity of SM83 (and possibly other SMs) in the complex *in vivo* environment is different from that already observed *in vitro*.

The activity of SMs *in vitro* has been widely shown to depend on the secretion of TNF from tumour cells leading to apoptosis in an autocrine manner.[17,18] Our *in vivo* work confirms that the antitumoural activity of SM83 depends on TNF production. However, in our xenograft models, TNF originated primarily from the host rather than from the tumour cells. TNF was secreted by the immune cells, and by macrophages in particular, and this effect was preceded temporally by activation of the NF-κB-response element. Following SM83 treatment, macrophages acquired an M1-like phenotype characterised by the release of pro-inflammatory cytokines such as TNF and IL-1β. Both cytokines have been associated with the cytotoxic activity of macrophages on tumour cells.[23,37] Our experiments show that SM83 treatment increased the concentration of these cytokines in the ascites without a major influx of macrophages. Thus, SM83 treatment may revert existing M2 macrophages to the M1 phenotype rather than recruit new macrophages to the ascites. A mechanistic interpretation of these results (Figure 7) is that the cytokines secreted by M1 macrophages cause necrotic death of the ascites cancer cells; the dying cells release HMGB-1 that, together with TNF, recruits neutrophils as a side effect rather than a needed step in the antitumoural activity of SM83.

In tumour microenvironment, including ovarian cancer, macrophages acquire an M2-like phenotype.[38,39] Nevertheless, some authors have proposed various strategies[23,24] that are able to interchange the status of macrophages towards an efficient antitumour response. On this line, it has also been

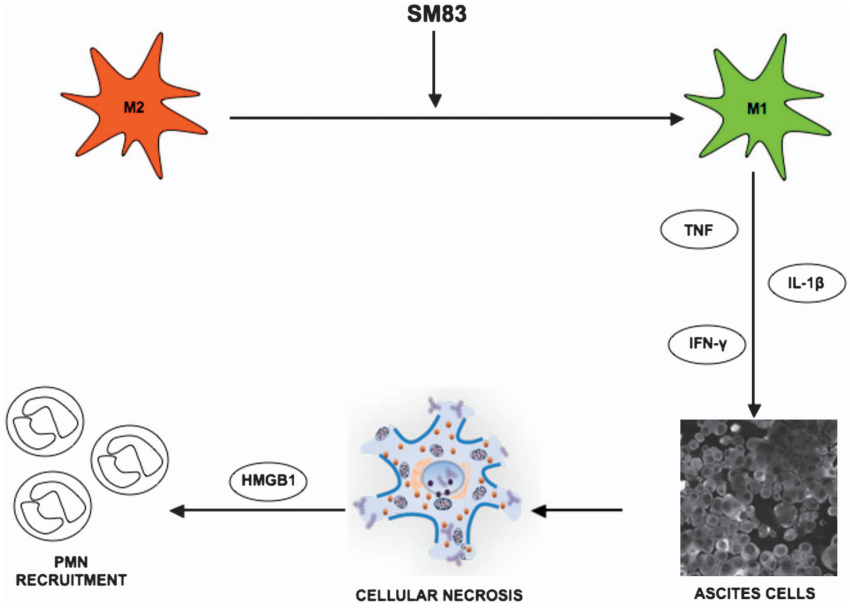

Figure 7 Proposed mechanism of action of SM83 in cancer ascites. SM83 stimulates the reversal of macrophages from M2 to M1 phenotype. TNF secreted by M1 macrophages triggers necrotic death of the cancer cells within the ascitic fluid; the dying cells release HMGB-1 that, together with TNF, recruits neutrophils

shown the possibility of increasing efficacy of standard therapies interfering with M2 macrophages,[40] particularly in tumours whose progression strictly relies on their support such as ovarian carcinomas. These tumours establish a complex relationship with the associated immune cells within the ascites,[41] developing an immunosuppressive microenvironment elicited by macrophages. Thus, in ovarian cancer, the re-polarisation of macrophages or the inhibition of their recruitment could be a new effective therapeutic strategy.

Our results suggest that SMs regulate the immune response to cancer ascites by polarising macrophages and thus have therapeutic potential. In fact, Smac/DIABLO[42] and its mimetic SM83, as shown here, trigger necrotic or necroptotic cell death. Necrotic cells, different from apoptotic ones, release a non-oxidised, immunogenic form of the alarmin HMGB-1[43] that activates dendritic cells by engaging receptor for advanced glycation endproducts, TLR4, TLR7 and TLR9 receptors.[44] Furthermore, necrotic cells can prime CD4 + T cells, essential for the development of an adaptive immune response.[45] The possibility that SM83-induced necrosis primed an adaptive immune response is raised by our results using BALB/c-immunocompetent mice bearing Meth A ascites. Some of these mice were cured by SM83 treatment and, when challenged with a new, double dose of Meth A cells, they did not form another ascites, suggesting that they were immune to Meth A sarcoma cells.

In conclusion, our data demonstrate that the SM SM83 is active in monotherapy by promoting inflammation and immunogenic cell death. These observations provide an explanation for why SMs increase the effectiveness of standard therapies, namely by stimulating the immune system. Finally, the evidence that SMs can induce an inflammatory response and activate the immune system provides an interpretation of why SMs can be more effective *in vivo* than *in vitro*,[11,46] and our results in cancer cell killing.

Materials and Methods

SMs, cell lines and mice strains. The compounds used in this study were SM83 (called 9a elsewhere[29,47]), SM59 (also called SM-164[48]) and TRAIL. Recombinant TRAIL was purchased from Enzo Life Sciences (Farmingdale, NY, USA), whereas SM83 and SM59 were synthesised by CISI scrl (purity > 99%). Synthesis and chemical structure of these SMs have been described elsewhere.[28,29]

Human ovarian carcinoma IGROV-1 and A2780, lung cancer H460, colon cancer SW48, HCT-116 and DLD-1, and murine sarcoma Meth A cell lines were cultured *in vitro* with RPMI plus 10% foetal calf serum. The murine macrophage cell line RAW 264.7, stably transfected with an NF-κB luciferase reporter plasmid, was cultured in DMEM plus 10% foetal calf serum.

KO C57/BL6 mice strains deficient in TNF-R1 (TNF-R1-KO[49]) or in TLR4-KO[50] and female athymic Swiss nude mice, all 8–10 weeks of age (Charles River Laboratories), were maintained in laminar flow rooms keeping temperature and humidity constant. Female BALB/c mice 7–8 weeks of age (Charles River Laboratories) were housed in filter-top cages. Room sentinels were checked for pathogens every 6 months by Charles River Laboratories staff. Experiments were approved by the Ethics Committee for Animal Experimentation of the Fondazione IRCCS Istituto Nazionale dei Tumori of Milan according to institutional guidelines.

Cell treatments and assays. Cells were plated at a density of about 60% and grown overnight before being treated with SM83 or SM59 in the absence or presence of 2 or 10 ng/ml TRAIL. Cell growth was determined after 3 days by cell counting, whereas viability was tested using the CellTiter-Glo (Promega Italia srl, Milan, Italy) assay for ATP after 24 h of treatment. For apoptosis assays, cells were harvested after 3 or 24 h of treatment and used in western blotting.

Western blotting. Cells were harvested at the end of the treatment and lysed in 125 mM Tris HCl pH 6.8, 5% SDS by boiling; protein concentration was quantified. Lysates (50 μg) were fractionated by SDS-PAGE and proteins were blotted onto PVDF membranes. Free protein-binding sites were blocked with 5% non-fat dry milk in phosphate-buffered saline (PBS) and the membranes were incubated overnight with primary antibodies diluted in non-fat dry milk-PBS. The primary antibodies used were directed against: cleaved caspase-3, beclin-1, cleaved PARP and LC3B (Cell Signaling Technology, Danvers, MA, USA); caspase-8 (Enzo Life Sciences); XIAP and cIAP2 (BD Biosciences, Milan, Italy), β-actin (Sigma, Rome, Italy); and cIAP1 (R&D Systems, Minneapolis, MN, USA). After washing, the membranes were exposed to horseradish peroxidase-linked secondary antibody (GE Healthcare, Milan, Italy) for 1 h and the bound antibodies were detected using ECL (Thermo Scientific, Rockford, IL, USA).

Animal models of cancer ascites. The *in vivo* effects of SMs were tested using two murine xenograft models of ovarian cancer. In one model, human ovarian carcinoma IGROV-1 cells are injected i.p. into athymic nude mice.[51] The cells adapt to grow i.p. and are maintained by i.p. serial passages of ascitic cells. Mice develop haemorrhagic ascites and diffuse carcinomatosis and eventually die.[51] In order to assess the effects of SMs on survival, mice were inoculated i.p. with 2.5×10^6 cells in 0.2 ml saline and, starting the day after cell injection, injected i.p. with the compounds (dissolved in saline) at 5 mg/kg body weight, once daily for 5 days per week for 2 weeks (qdx5/wx2w). The animals were inspected and weighed daily. The progression of ascites was assessed from an increase in body weight (measured on day 17). For ethical reasons, they were killed before impending death, recognised by their suffering status and loss of reactivity to external stimuli. The day of killing was taken as the day of death for calculating the median survival time. The antitumour activity of treatments was expressed as the ratio of median survival time in treated mice to that of untreated control mice $\times$ 100 (T/C%).

In the other ascites model, murine Meth A cells are injected i.p. into immunocompetent syngeneic BALB/c mice.[52] Here, 2×10^5 Meth A cells were injected i.p., and treatment, starting 7 days later, consisted of five consecutive daily i.p. injections of SM83 at a dose of 5 mg/kg body weight. The progression of ascites was assessed from both an increase in body weight (measured on day 13) and overall survival, as calculated above. Mice in whom the ascites resolved and did not relapse within 60 days were considered to be cured, and were challenged with a new injection of 4×10^5 Meth A cells.

To assess the effects of SMs on ascites tumour cells, athymic nude mice were injected with IGROV-1 cells as above. Ten days after IGROV-1 inoculation, ascites-bearing mice were treated with a single injection of SM83 (5 mg/kg) or left untreated; in some experiments, mice were pretreated 1 h before SM83 administration by i.p. injection with one of two TNF inhibitors: 5 or 150 mg/kg etanercept (Wyeth Pharmaceuticals, Collegeville, PA, USA)[53] or 5 mg/kg infliximab (Schering-Plough, Milan, Italy). Mice were killed 3, 6 or 24 h after SM83 treatment, and ascitic fluid was collected with a heparinised syringe, transferred to a centrifuge tube on ice and centrifuged to pellet the cells for blotting. The supernatant was removed and stored at $-80\,^{\circ}$C until it was assayed for cytokines (human and murine TNF, and murine IL-1β, IL-4, IL-10, IFNγ and transforming growth factor-β enzyme-linked immunosorbent assay (ELISA) kits (Affymetrix, San Diego, CA, USA) or used in blotting and in neutrophil assays. The pellet was suspended in 0.17 M ammonium chloride for 10 min at 41 $^{\circ}$C to lyse red blood cells; after washing in saline, the remaining tumour cells were counted using the trypan blue exclusion assay and used in immunofluorescence. Death of IGROV-1 cells was also checked by quantifying human cytokeratin-18, a cytokeratin released by dying cells, in the serum collected from killed ascites-bearing mice using M65 ELISA (Enzo Life Sciences).

Animals were subjected to autopsy to search for adherent tumour cells or extraperitoneal migration. As IGROV-1 cells injected i.p. in nude mice also form solid nodules, these were collected and fixed in formalin. After 24 h, tumours were washed in PBS and kept in 70% ethanol until they were embedded in paraffin and prepared for haematoxylin and eosin staining.

To deplete neutrophils, nude mice bearing IGROV-1 ascites were injected i.p. with the anti-Ly-6G antibody (clone 1A8; Affymetrix) 24 h before SM83 administration. In the Meth A model, mice were injected with 20 μg 1A8 antibody every second day, for 14 consecutive days, starting one day before SM83 treatment (day 7). The efficiency of polymorphonuclear leucocytes (PMNs) depletion in nude mice was tested by sampling the bone marrow (BM) 24 h after injection of the anti-Ly-6G antibody. Cells were double-stained with anti-CD11b/Ly-6G and cell populations were quantified by flow cytometry.[54]

Macrophage primary cultures and reporter gene assays. BM precursors were obtained from BALB/c and TLR4-KO mice and used to isolate macrophages as previously described.[26] Briefly, macrophages were isolated from the precursors by cultivation in RPMI medium 10% foetal calf serum containing 5 ng/ml macrophage colony-stimulating factor. On day 5, the medium was replaced with fresh medium containing macrophage colony-stimulating factor. On day 7, adherent cells were harvested and phenotypically characterised by immunofluorescence using mAb to the macrophage markers CD11b and F4/80 (BD Biosciences). Up to 90% of the adherent population consisted of BMDM.

For *in vitro* experiments, 5×10^5 BMDM were seeded in six-well plates, allowed to attach for 1 h at 37 °C and then treated or not with 1 μM SM83. The release of TNF and IL-1β to the culture medium, after 3, 6 and 24 h, was evaluated using ELISA kits (Affymetrix). In viability experiments, 1×10^4 cells were seeded in 96-well plates and exposed to serial dilutions of SM83 in the absence or presence of either 50 μM necrostatin-1 (Enzo Life Sciences) or 20 μM z-vad-fmk (Enzo Life Sciences). After 24 h, cells were examined morphologically by microscopy and tested for viability using the CellTiter-Glo (Thermo Scientific) assay.

In other experiments, 10^4 RAW 264.7 macrophages were plated in 96-well plates, grown for 16 h and then treated or not with 1 μM SM83 for up to 24 h. The activation of the NF-κB promoter was assayed using the Dual-Luciferase Reporter Assay System (Thermo Scientific).

Immunofluorescence and dot blotting. Floating cells harvested from the ascites were prepared for double-marker immunofluorescence by centrifugation on slides using a Cytospin cytocentrifuge. Briefly, acetone-fixed cells were re-hydrated in PBS and incubated 1 h with a primary antibody. Cells were then washed in PBS and incubated for 30 min with the appropriate Alexa Fluor 488-conjugated secondary antibody. After washing, slides were incubated for 30 min with another primary antibody, washed and incubated for 30 min with an Alexa Fluor 546-conjugated secondary antibody. The primary antibodies used were: rat anti-mouse CD11b mAb (1:200; BD Biosciences); rat anti-mouse Ly-6G mAb (1:200; BD Biosciences); and rabbit anti-HMGB-1 Ab (1:400; Abcam, Cambridge, UK). In some experiments, nuclei were stained with 4′,6-diamidino-2-phenylindole. Slides were mounted with Prolong medium (Life Technologies, Monza, Italy) and examined under a RADiance-2000 (Bio-Rad, Milan, Italy) Nikon-TE300 laser scanning confocal microscope (Nikon Instruments S.p.A, Florence, Italy).

For dot blotting, ascitic fluid samples cleared of cells were spotted on PDVF membranes and let to dry. After saturation with non-fat dry milk-PBS, filters were hybridised with anti-HMGB-1 Ab (Abcam, 1:2000). The HMGB-1 was then detected as for western blotting.

Spleen neutrophil preparation and assays. Neutrophils were obtained from BALB/c (wild-type) or TNF-R1-KO mice through immunomagnetic cell separation of a spleen cell suspension, using the Anti-Ly-6G MicroBead Kit (Miltenyi Biotec, Bologna, Italy), as already described.[54]

Migration of neutrophils PMNs was tested using the Transwell system (Corning, Tewksbury, MA, USA). Briefly, 5×10^5 PMNs were placed in serum-free RPMI in the upper chamber of the Transwell insert. The lower chamber was filled with ascites (1:20) or TNF in serum-free DMEM. PMNs were allowed to migrate for 24 h and then collected from the lower chamber. In some cases, experiments were performed by adding 100 μM of the HMGB-1 inhibitor glycyrrhizin (Sigma-Aldrich, St. Louis, MO, USA) to the top chamber.[55]

Neutrophil activation by cleared ascites was evaluated by measuring the rate of formation of superoxide. Briefly, neutrophils (2×10^6/0.1 ml cells/PBS solution) were incubated with 20 μl of cytochrome c (0.1 mM final, bovine, Sigma), 20 μl of ascites or 10 μg/ml of PMA (as positive control for the neutrophil stimuli) in 1.76 ml PiCM-G buffer (138 mM NaCl, 2.7 mM KCl, 0.6 mM CaCl2, 1.0 mM MgCl2, 5 mM glucose and 10 mM NaH_2PO_4/Na_2HPO_4, pH 7.4). The mixture was added to cuvettes for spectrophotometer and absorbance was read at 550 nm every 15 min as described.[56]

Statistical analyses. For survival analyses, the percent survivorship over time was estimated using the two-sided Kaplan–Meier product method; differences between groups were compared using the log-rank test. In other analyses, differences between groups were tested for significance using a two-tailed unpaired *t*-test. A value of $P < 0.05$ indicated significance. The analyses were performed using Graphpad Prism v.5.02 (GraphPad Software, La Jolla, CA, USA).

Conflict of Interest

The authors declare no conflict of interest.

Acknowledgements. We thank Vinci-Biochem for the gift of the M65 ELISA kit, Dr. C Tripodo for the evaluation of immunohistochemistry, Dr. A Coliva for testing for LPS in SM preparations, Dr. P Casalini for confocal immunofluorescence analyses, Professor C Carlo-Stella for providing reagents, the Immunohistochemistry Facility of the Fondazione IRCCS Istituto Nazionale dei Tumori for sample preparation and staining, and Professor E Berti for providing infliximab and etanercept. Valerie Matarese provided scientific editing. This work was financially supported by grants of the CARIPLO Foundation (Project 2009-2534, IAPs as anticancer therapeutics) and the Italian Association for Cancer Research (AIRC Special Program Molecular Clinical Oncology – 5 per mille – Project 2010-9998; My First Grant no 12810 to SS).

Author Contributions

Conception and design: DL, MDC, PP, MPC, DD and SS. Development of methodology: DL, MDC, AC, EC and SS. Acquisition of data: DL, MDC, PP and SS. Analysis and interpretation of data: DL, MDC, PP, PS, MPC, DD and SS. Writing, review and/or revision of the manuscript: DL, MDC, PP, PS, HW, DD, SS and MPC. Administrative, technical or material support: CD and PS. Study supervision: PP, PS, HW, MPC, DD.

1. Hanahan D, Weinberg RA. Hallmarks of cancer: the next generation. *Cell* 2011; **144**: 646–674.
2. Gyrd-Hansen M, Meier P. IAPs: from caspase inhibitors to modulators of NF-kappaB, inflammation and cancer. *Nat Rev Cancer* 2010; **10**: 561–574.
3. Lopez J, John SW, Tenev T, Rautureau GJ, Hinds MG, Francalanci F *et al.* CARD-mediated autoinhibition of cIAP1's E3 ligase activity suppresses cell proliferation and migration. *Mol Cell* 2011; **42**: 569–583.
4. Fingas CD, Blechacz BR, Smoot RL, Guicciardi ME, Mott J, Bronk SF *et al.* A smac mimetic reduces TNF related apoptosis inducing ligand (TRAIL)-induced invasion and metastasis of cholangiocarcinoma cells. *Hepatology* 2010; **52**: 550–561.
5. Takahashi R, Deveraux Q, Tamm I, Welsh K, Assa-Munt N, Salvesen GS *et al.* A single BIR domain of XIAP sufficient for inhibiting caspases. *J Biol Chem* 1998; **273**: 7787–7790.
6. Srinivasula SM, Hegde R, Saleh A, Datta P, Shiozaki E, Chai J *et al.* A conserved XIAP-interaction motif in caspase-9 and Smac/DIABLO regulates caspase activity and apoptosis. *Nature* 2001; **410**: 112–116.
7. Deveraux QL, Takahashi R, Salvesen GS, Reed JC. X-linked IAP is a direct inhibitor of cell-death proteases. *Nature* 1997; **388**: 300–304.
8. Oost TK, Sun C, Armstrong RC, Al-Assaad A, Betz SF, Deckwerth TL *et al.* Discovery of potent antagonists of the antiapoptotic protein XIAP for the treatment of cancer. *J Med Chem* 2004; **47**: 4417–4426.
9. Li L, Thomas RM, Suzuki H, De Brabander JK, Wang X, Harran PG. A small molecule smac mimic potentiates TRAIL- and TNF{alpha}-mediated cell death. *Science* 2004; **305**: 1471–1474.
10. Seneci P, Bianchi A, Battaglia C, Belvisi L, Bolognesi M, Caprini A *et al.* Rational design, synthesis and characterization of potent, non-peptidic Smac mimics/XIAP inhibitors as proapoptotic agents for cancer therapy. *Bioorg Med Chem* 2009; **17**: 5834–5856.
11. Probst BL, Liu L, Ramesh V, Li L, Sun H, Minna JD *et al.* Smac mimetics increase cancer cell response to chemotherapeutics in a TNF-alpha-dependent manner. *Cell Death Differ* 2010; **17**: 1645–1654.
12. Vogler M, Walczak H, Stadel D, Haas TL, Genze F, Jovanovic M *et al.* Small molecule XIAP inhibitors enhance TRAIL-induced apoptosis and antitumor activity in preclinical models of pancreatic carcinoma. *Cancer Res* 2009; **69**: 2425–2434.
13. Lecis D, Drago C, Manzoni L, Seneci P, Scolastico C, Mastrangelo E *et al.* Novel SMAC-mimetics synergistically stimulate melanoma cell death in combination with TRAIL and Bortezomib. *Br J Cancer* 2010; **102**: 1707–1716.
14. Lu J, McEachern D, Sun H, Bai L, Peng Y, Qiu S *et al.* Therapeutic potential and molecular mechanism of a novel, potent, nonpeptide, Smac mimetic SM-164 in combination with TRAIL for cancer treatment. *Mol Cancer Ther* 2011; **10**: 902–914.
15. Feltham R, Bettjeman B, Budhidarmo R, Mace PD, Shirley S, Condon SM *et al.* SMAC-mimetics activate the E3 ligase activity of cIAP1 by promoting RING dimerisation. *J Biol Chem* 2011; **286**: 17015–17028.
16. Darding M, Feltham R, Tenev T, Bianchi K, Benetatos C, Silke J *et al.* Molecular determinants of Smac mimetic induced degradation of cIAP1 and cIAP2. *Cell Death Differ* 2011; **18**: 1376–1386.
17. Vince JE, Wong WW, Khan N, Feltham R, Chau D, Ahmed AU *et al.* IAP antagonists target cIAP1 to induce TNFα-dependent apoptosis. *Cell* 2007; **131**: 682–693.
18. Varfolomeev E, Blankenship JW, Wayson SM, Fedorova AV, Kayagaki N, Garg P *et al.* IAP antagonists induce autoubiquitination of c-IAPs, NF-κB activation, and TNFα-dependent apoptosis. *Cell* 2007; **131**: 669–681.
19. Moulin M, Anderton H, Voss AK, Thomas T, Wong WW, Bankovacki A *et al.* IAPs limit activation of RIP kinases by TNF receptor 1 during development. *EMBO J* 2012; **31**: 1679–1691.

20. Eschenburg G, Eggert A, Schramm A, Lode HN, Hundsdoerfer P. Smac mimetic LBW242 sensitizes XIAP-overexpressing neuroblastoma cells for TNF-alpha independent apoptosis. *Cancer Res* 2012; **72**: 2645–2656.
21. Greer RM, Peyton M, Larsen JE, Girard L, Xie Y, Gazdar AF *et al.* SMAC mimetic (JP1201) sensitizes non-small cell lung cancers to multiple chemotherapy agents in an IAP-dependent but TNF-alpha-independent manner. *Cancer Res* 2011; **71**: 7640–7648.
22. Lengyel E. Ovarian cancer development and metastasis. *Am J Pathol* 2010; **177**: 1053–1064.
23. Sica A, Mantovani A. Macrophage plasticity and polarization: *in vivo* veritas. *J Clin Invest* 2012; **122**: 787–795.
24. Sica A, Schioppa T, Mantovani A, Allavena P. Tumour-associated macrophages are a distinct M2 polarised population promoting tumour progression: potential targets of anti-cancer therapy. *Eur J Cancer* 2006; **42**: 717–727.
25. Martinez FO, Helming L, Gordon S. Alternative activation of macrophages: an immunologic functional perspective. *Annu Rev Immunol* 2009; **27**: 451–483.
26. Guiducci C, Vicari AP, Sangaletti S, Trinchieri G, Colombo MP. Redirecting *in vivo* elicited tumor infiltrating macrophages and dendritic cells towards tumor rejection. *Cancer Res* 2005; **65**: 3437–3446.
27. Hagemann T, Lawrence T, McNeish I, Charles KA, Kulbe H, Thompson RG *et al.* "Re-educating" tumor-associated macrophages by targeting NF-κB. *J Exp Med* 2008; **205**: 1261–1268.
28. Manzoni L, Belvisi L, Bianchi A, Conti A, Drago C, de Matteo M *et al.* Homo- and heterodimeric Smac mimetics/IAP inhibitors as *in vivo*-active pro-apoptotic agents. Part I: synthesis. *Bioorg Med Chem* 2012; **20**: 6687–6708.
29. Lecis D, Mastrangelo E, Belvisi L, Bolognesi M, Civera M, Cossu F *et al.* Dimeric Smac mimetics/IAP inhibitors as *in vivo*-active pro-apoptotic agents. Part II: Structural and biological characterization. *Bioorg Med Chem* 2012; **20**: 6709–6723.
30. Gaither A, Porter D, Yao Y, Borawski J, Yang G, Donovan J *et al.* A Smac mimetic rescue screen reveals roles for inhibitor of apoptosis proteins in tumor necrosis factor-{alpha} signaling. *Cancer Res* 2007; **67**: 11493–11498.
31. Muller-Sienerth N, Dietz L, Holtz P, Kapp M, Grigoleit GU, Schmuck C *et al.* SMAC mimetic BV6 induces cell death in monocytes and maturation of monocyte-derived dendritic cells. *PLoS One* 2011; **6**: e21556.
32. Qureshi ST, Lariviere L, Leveque G, Clermont S, Moore KJ, Gros P *et al.* Endotoxin-tolerant mice have mutations in Toll-like receptor 4 (Tlr4). *J Exp Med* 1999; **189**: 615–625.
33. Sitia G, Iannacone M, Muller S, Bianchi ME, Guidotti LG. Treatment with HMGB1 inhibitors diminishes CTL-induced liver disease in HBV transgenic mice. *J Leukoc Biol* 2007; **81**: 100–107.
34. Colombo MP, Modesti A, Parmiani G, Forni G. Local cytokine availability elicits tumor rejection and systemic immunity through granulocyte-T-lymphocyte cross-talk. *Cancer Res* 1992; **52**: 4853–4857.
35. Granot Z, Henke E, Comen EA, King TA, Norton L, Benezra R. Tumor entrained neutrophils inhibit seeding in the premetastatic lung. *Cancer Cell* 2011; **20**: 300–314.
36. Stoppacciaro A, Melani C, Parenza M, Mastracchio A, Bassi C, Baroni C *et al.* Regression of an established tumor genetically modified to release granulocyte colony-stimulating factor requires granulocyte-T cell cooperation and T cell-produced interferon gamma. *J Exp Med* 1993; **178**: 151–161.
37. Bonta IL, Ben-Efraim S. Involvement of inflammatory mediators in macrophage antitumor activity. *J Leukoc Biol* 1993; **54**: 613–626.
38. Heusinkveld M, de Vos van Steenwijk PJ, Goedemans R, Ramwadhdoebe TH, Gorter A, Welters MJ *et al.* M2 macrophages induced by prostaglandin E2 and IL-6 from cervical carcinoma are switched to activated M1 macrophages by CD4+ Th1 cells. *J Immunol* 2011; **187**: 1157–1165.
39. Said NA, Elmarakby AA, Imig JD, Fulton DJ, Motamed K. SPARC ameliorates ovarian cancer-associated inflammation. *Neoplasia* 2008; **10**: 1092–1104.
40. Coward J, Kulbe H, Chakravarty P, Leader D, Vassileva V, Leinster DA *et al.* Interleukin-6 as a therapeutic target in human ovarian cancer. *Clin Cancer Res* 2011; **17**: 6083–6096.
41. Jeon BH, Jang C, Han J, Kataru RP, Piao L, Jung K *et al.* Profound but dysfunctional lymphangiogenesis via vascular endothelial growth factor ligands from CD11b+ macrophages in advanced ovarian cancer. *Cancer Res* 2008; **68**: 1100–1109.
42. Emeagi PU, Van Lint S, Goyvaerts C, Maenhout S, Cauwels A, McNeish IA *et al.* Proinflammatory characteristics of SMAC/DIABLO-induced cell death in antitumor therapy. *Cancer Res* 2012; **72**: 1342–1352.
43. Kazama H, Ricci JE, Herndon JM, Hoppe G, Green DR, Ferguson TA. Induction of immunological tolerance by apoptotic cells requires caspase-dependent oxidation of high-mobility group box-1 protein. *Immunity* 2008; **29**: 21–32.
44. Sims GP, Rowe DC, Rietdijk ST, Herbst R, Coyle AJ. HMGB1 and RAGE in inflammation and cancer. *Annu Rev Immunol.* 2010; **28**: 367–388.
45. Bartholomae WC, Rininsland FH, Eisenberg JC, Boehm BO, Lehmann PV, Tary-Lehmann M. T cell immunity induced by live, necrotic, and apoptotic tumor cells. *J Immunol* 2004; **173**: 1012–1022.
46. Dineen SP, Roland CL, Greer R, Carbon JG, Toombs JE, Gupta P *et al.* Smac mimetic increases chemotherapy response and improves survival in mice with pancreatic cancer. *Cancer Res* 2010; **70**: 2852–2861.
47. Cossu F, Milani M, Vachette P, Malvezzi F, Grassi S, Lecis D *et al.* Structural insight into inhibitor of apoptosis proteins recognition by a potent divalent smac-mimetic. *PLoS One* 2012; **7**: e49527.
48. Sun H, Nikolovska-Coleska Z, Lu J, Meagher JL, Yang CY, Qiu S *et al.* Design, synthesis, and characterization of a potent, nonpeptide, cell-permeable, bivalent Smac mimetic that concurrently targets both the BIR2 and BIR3 domains in XIAP. *J Am Chem Soc* 2007; **129**: 15279–15294.
49. Sangaletti S, Tripodo C, Ratti C, Piconese S, Porcasi R, Salcedo R *et al.* Oncogene-driven intrinsic inflammation induces leukocyte production of tumor necrosis factor that critically contributes to mammary carcinogenesis. *Cancer Res* 2010; **70**: 7764–7775.
50. Calcaterra C, Sfondrini L, Rossini A, Sommariva M, Rumio C, Menard S *et al.* Critical role of TLR9 in acute graft-versus-host disease. *J Immunol* 2008; **181**: 6132–6139.
51. De Cesare M, Sfondrini L, Campiglio M, Sommariva M, Bianchi F, Perego P *et al.* Ascites regression and survival increase in mice bearing advanced-stage human ovarian carcinomas and repeatedly treated intraperitoneally with CpG-ODN. *J Immunother* 2010; **33**: 8–15.
52. Watanabe N, Niitsu Y, Sone H, Neda H, Urushizaki I, Yamamoto A *et al.* Therapeutic effect of endogenous tumor necrosis factor on ascites Meth A sarcoma. *J Immunopharmacol* 1986; **8**: 271–283.
53. Scallon B, Cai A, Solowski N, Rosenberg A, Song XY, Shealy D *et al.* Binding and functional comparisons of two types of tumor necrosis factor antagonists. *J Pharmacol Exp Ther* 2002; **301**: 418–426.
54. Sangaletti S, Tripodo C, Chiodoni C, Guarnotta C, Cappetti B, Casalini P *et al.* Neutrophil extracellular traps mediate transfer of cytoplasmic neutrophil antigens to myeloid dendritic cells toward ANCA induction and associated autoimmunity. *Blood* 2012; **120**: 3007–3018.
55. Mollica L, De Marchis F, Spitaleri A, Dallacosta C, Pennacchini D, Zamai M *et al.* Glycyrrhizin binds to high-mobility group box 1 protein and inhibits its cytokine activities. *Chem Biol* 2007; **14**: 431–441.
56. Clark RA, Nauseef WM. Isolation and Functional Analysis of Neutrophils. *Current Protocols in Immunology.* John Wiley & Sons, Inc, 2001.

Supplementary Information accompanies this paper on Cell Death and Disease website (http://www.nature.com/cddis)

Bioorganic & Medicinal Chemistry Letters 24 (2014) 2374–2378

Contents lists available at ScienceDirect

Bioorganic & Medicinal Chemistry Letters

journal homepage: www.elsevier.com/locate/bmcl

SPION-Smac mimetic nano-conjugates: Putative pro-apoptotic agents in oncology

Pierfausto Seneci [a,*], Mattia Rizzi [a], Luigi Ballabio [a], Daniele Lecis [b], Annalisa Conti [b], Claudio Carrara [a], Emanuela Licandro [a,*]

[a] Università degli Studi di Milano, Dipartimento di Chimica, Via Golgi 19, I-20133 Milan, Italy
[b] Fondazione IRCCS Istituto Nazionale dei Tumori, Dipartimento di Oncologia Sperimentale e Medicina Molecolare, Via Amadeo 42, I-20133 Milan, Italy

ARTICLE INFO

Article history:
Received 27 January 2014
Revised 16 March 2014
Accepted 17 March 2014
Available online 25 March 2014

Keywords:
SPION nanoparticles
Smac mimetics
Pro-apoptotics
Oncology
Peptidomimetics

ABSTRACT

Non-covalent (**NP-1/3**) and covalent (**NP-A-1/3**) pro-apoptotic SPION-Smac mimetic nano-conjugates antitumor agents are reported. The solution synthesis of key Smac mimetics, their support onto SPIONs through non-covalent adsorption (**NP-1/3**) or APTES-mediated covalent binding (**NP-A-1/3**), the analytical characterization of SPION-Smac mimetic conjugates, their target affinity in cell-free assays, and their cytotoxicity against tumor cells are thoroughly described.

Nanoparticles are popular tools in cancer detection and treatment, due to major advancements in nanosynthesis, bioengineering and imaging technology.[1] Super Paramagnetic Iron Oxide Nanoparticles (SPIONs) are particularly attractive as diagnostics (e.g. biomarker-targeted magnetic resonance imaging/MRI contrast agents) and therapeutics (e.g. magnetic nanoparticle-enhanced hyperthermia).[2] Their large surface areas to conjugate targeting ligands and load therapeutic agents,[3] their unique magnetic properties,[4] their biocompatibility[5] and low toxicity[6] make them suitable technology platforms in oncology.

Anti-apoptotic Inhibition of Apoptosis Proteins (IAPs)[7] bind Cysteine ASPartic acid-specific proteASEs (caspases, CASP),[8] the major apoptotic effectors, through their baculovirus inhibitor repeat (BIR) domains. CASP-IAP interactions inactivate caspases and block apoptosis. The endogenous Smac protein[9] (Second Mitochondria-derived Activator of Caspases) binds to IAPs through its N-terminus AVPI sequence. The tetrapeptide binds to BIR3, the CASP-9 binding domain of IAPs, and prevents linker-BIR2-CASP-3/7 interactions through a weaker interaction.[10] Thus, Smac is a pro-apoptotic IAP ligand that restores caspase-dependent apoptosis in cancer cells.

We introduced 4-substituted, aza-bicyclo [5.3.0] decane (ABD)-based *N*-AVPI mimetics as potent, pro-apoptotic cytotoxic agents (see Fig. 1 for ABD structure and numbering). Monomers such as **1** (Smac136, Fig. 1) are potent, orally available BIR3 binders with moderate cytotoxicity.[11] Dimers such as **2** (Smac83, Fig. 1) bind IAPs on both BIR domains, resulting in a stronger cytotoxic activity, but possess a sub-optimal PK profile and cannot be administered orally.[12]

We reasoned that SPION-Smac mimetic nano-conjugates may take advantage of nanoparticle-specific access to cytosolic compartments (e.g. receptor-mediated endocytosis, macropinocytosis).[13] The spatial arrangement of monomeric Smac mimetics on the surface of SPIONs may allow, or even promote, the binding of two SPION-grafted Smac mimetics to a single IAP molecule (dimer-like binding). Finally, a single SPION-Smac mimetic nano-conjugate may bind several IAPs (multi-presentation mode). Thus, we decided to synthesize and biologically characterize a small library of SPION-Smac mimetic nano-conjugates.

4-CH_2OR and 4-$CH_2NR_1R_2$-substituted ABD Smac mimetics possess strong BIR/IAP affinity.[11] *N*-Boc-protected hydroxyacid **4** and *N*-Boc-protected aminoamide **5** were prepared from the tricyclic intermediate **3**[14] as previously reported[11a] (Scheme 1), although several reaction conditions were optimized. 4-Connected Smac-linker carboxylate constructs (**6**, ester connection, and **7**, amide connection) were obtained in good yields respectively from compounds **4** and **5** (Scheme 1).

* Corresponding authors. Tel.: +39 02 5031 4060; fax: +39 02 5031 4072.
E-mail addresses: pierfausto.seneci@unimi.it (P. Seneci), emanuela.licandro@unimi.it (E. Licandro).

http://dx.doi.org/10.1016/j.bmcl.2014.03.048
0960-894X/

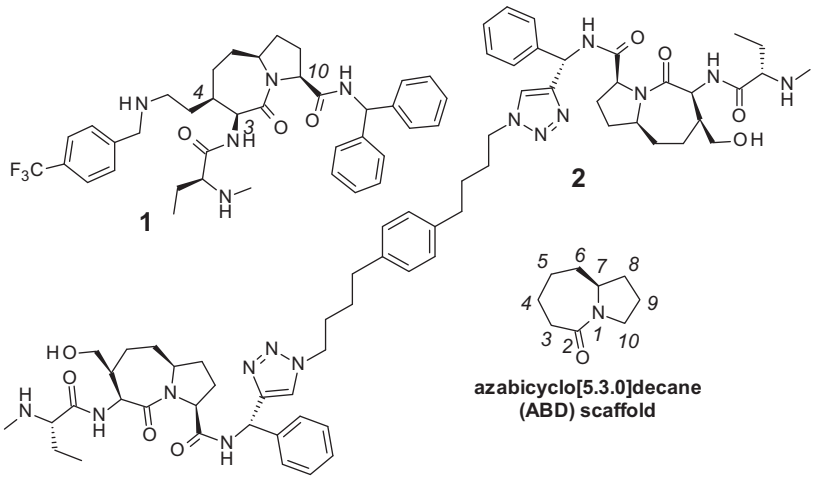

Figure 1. Monomeric and dimeric Smac mimetics.

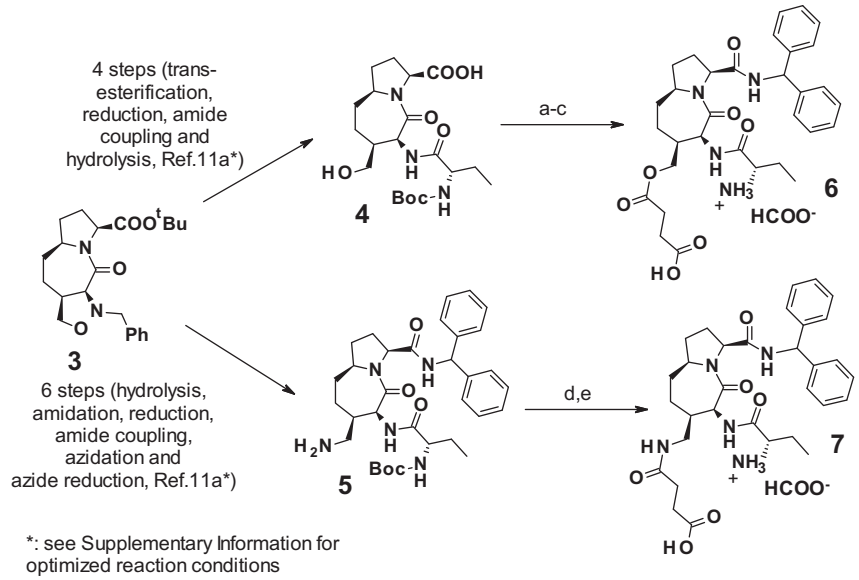

a) Ph_2CHNH_2.HCl, EDC.HCl, HOBt, DIPEA, dry CH_2Cl_2, N_2, rt, 24hrs, 51%; b) succinic anhydride, cat. DMAP, DIPEA, dry CH_2Cl_2, N_2, rt, 20hrs, 85%; c) neat HCOOH, rt, 3hrs, 75%; d) as in a), 53%; e) as in c), quantitative.

Scheme 1. Synthesis of 4-connected Smac-linker carboxylate constructs **6** and **7**.

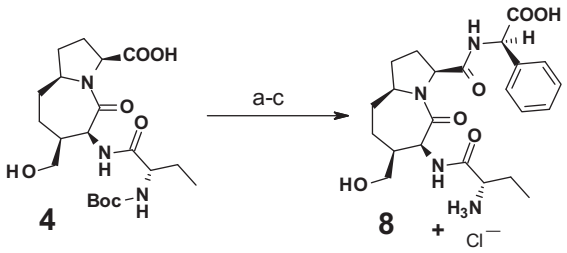

a) (R)-PheGlyOMe, EDC.HCl, HOBt, DIPEA, dry CH_2Cl_2, N_2, rt, 24hrs, 48%; b) 3N HCl in MeOH, rt, 20hrs, 95%; c) LiOH, H2O/1,4-dioxane, rt, 3hrs, then 2N aq. HCl, quantitative.

Scheme 2. Synthesis of C terminus-connected Smac-linker carboxylate construct **8**.

BIR3 affinity is also preserved when the C terminus diphenylmethyl amide of Smac mimetic **1** is replaced by an (R)-phenylglycine amide. N-protected hydroxyacid **4** was used to prepare in good yields the C terminus-connected Smac-linker carboxylate construct **8** (Scheme 2).

Smac-linker constructs **6**–**8** and all previously unreported intermediates were analytically and spectroscopically characterized (LC–MS, ^1H and ^{13}C NMR).

The carboxy group of Smac-linker constructs **6**–**8** is used to non-covalently adsorb the compounds onto surface-exposed OH

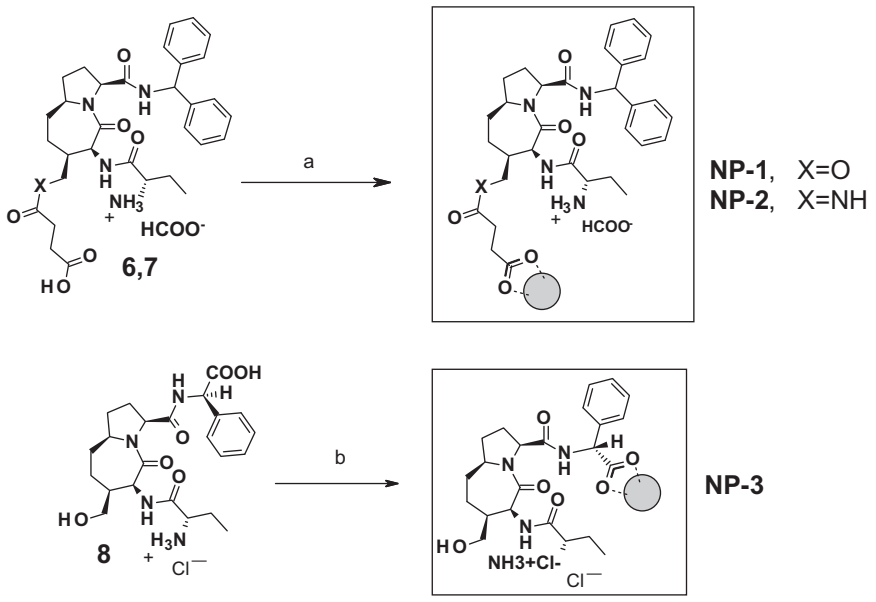

a) Naked SPIONs, H_2O, sonication, 60°C, 4hrs, loading 0.272 mmol/g_{SPION} (**NP-1**), 0.485 mmol/g_{SPION} (**NP-2**);
b) Naked SPIONs, dry toluene, sonication, 60°C, 4hrs, loading 0.168 mmol/g_{SPION}.

Scheme 3. Synthesis of non-covalent SPION-Smac mimetic nano-conjugates **NP-1/3**.

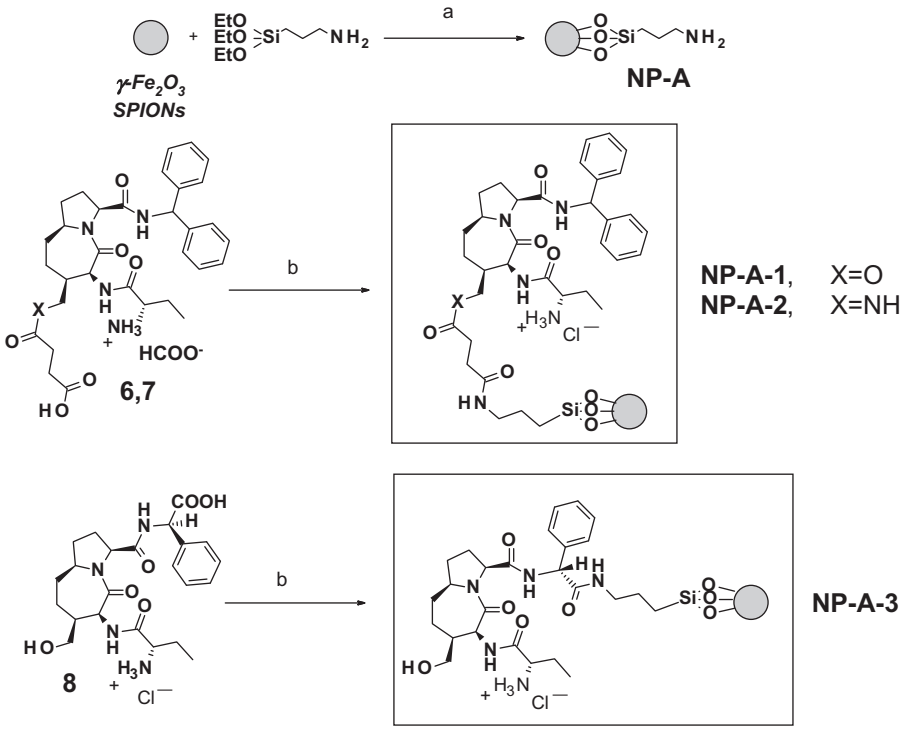

a) Naked SPIONs, dry toluene, N_2, sonication, 60°C, 4hrs, loading 0.836 mmol/g_{SPION} ; b) **NP-A**, EDC.HCl, dry CH_3CN, N_2, sonication, 60°C, 4hrs, loading 0.167 mmol/g_{SPION}(**NP-A-1**), 0.308 mmol/g_{SPION}(**NP-A-2**), 0.718 mmol/g_{SPION}(**NP-A-3**).

Scheme 4. Synthesis of covalent SPION-Smac mimetic nano-conjugates **NP-A-1/3**.

groups of commercial SPIONs. Non-covalent nano-conjugates **NP-1/3** are obtained with moderate to good Smac mimetic loadings (Scheme 3), as judged by elemental analysis.

Commercially available- maghemite γ-Fe_2O_3 SPIONs may be reacted with 3-aminopropyl triethoxysilane (APTES) to give the high loading SPION-APTES-NH_2 construct **NP-A** (Scheme 4). **NP-A** is then covalently coupled with the carboxy group of Smac-linker constructs **6**–**8**. Covalent nano-conjugates **NP-A-1/3** are obtained with moderate to good Smac loadings (Scheme 4) in unoptimized reaction conditions.

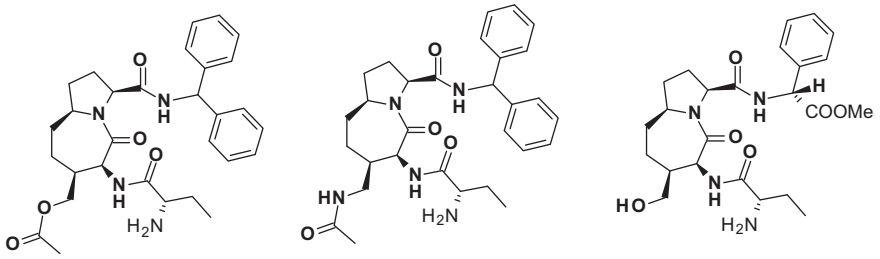

Figure 2. Reference Smac mimetics.

Non-covalent and covalent SPION-Smac mimetic nano-conjugates **NP-1/3** and **NP-A-1/3** were analytically and spectroscopically characterized (FT-IR, elemental analysis). Single reaction runs for each nanoconjugate often lead to good loadings (0.272–0.718 mmol/g_{SPION}; **NP-1**, **NP-2**, **NP-A-2**, **NP-A-3**). Observed moderate loadings (<0.200 mmol/g_{SPION}) could be improved by repeating the synthetic procedure for **NP-3** and **NP-A-1**.

The affinity of the six SPION-Smac mimetic nano-conjugates for mono-functional (BIR3 domains from X-linked IAP/XIAP, and from cellular IAPs/cIAP1 and cIAP2) and bi-functional IAP constructs (linker-BIR2-BIR3 multi-domain region from XIAP) was measured in a *cell-free* assay format. Standard reference compounds 4-acetoxymethyl/**9**, 4-acetamidomethyl/**10** and C terminus (*R*)-phenylglycinamide methyl ester/**11** (Fig. 2) were prepared in solution as previously described.[11a] They were biologically tested as soluble analogues respectively of non covalent/covalent SPION-Smac mimetic nano-conjugate pairs **NP-1/A-1** (**9**), **NP-2/A-2** (**10**) and **NP-3/A-3** (**11**).

The IC_{50} values determined for ABD-based Smac mimetics **9**–**11** and SPION-Smac mimetic non-covalent (**NP-1/3**) and covalent (**NP-A-1/3**) nano-conjugates are listed in Table 1.

SPION-Smac mimetic nano-conjugates generally maintain the nanomolar binding affinity of reference compounds **9**–**11** for single BIR3 domains from IAPs. Both non-covalent adsorption and covalent drafting of Smac mimetics onto SPIONs are compatible with IAP binding (Table 1). For example, the non-covalent conjugate **NP-1** and the reference standard **9** show similar binding strength in presence of BIR3 from XIAP and L-BIR2-BIR3 from XIAP; and the same behavior is shown by covalent conjugate **NP-A-3** and reference standard **11** (Table 1). Loading may influence affinity, as **NP-3** and **NP-A-1** (loading <0.2 mmol/g_{SPION}) show extremely reduced affinity for IAP proteins. Unfortunately, there is no evidence of a dimer-like binding/increase of affinity (expected IC_{50} < 10 nM for dimer-like compounds) for any nano-conjugate against the bifunctional L-BIR2-BIR3 construct from XIAP.

The cytotoxicity of cell free-active **NP-1/2** and **NP-A-2/3** nano-conjugates was tested on three human tumor cell lines (breast cancer, MDA-MB-231, ovarian carcinoma, IGROV-1, cervical cancer, HeLa cells). The nano-conjugates were generally inactive against tumor cells, with slight signs of cytotoxicity at the highest concentrations (≈25 μM). **NP-1/2** and **NP-A-2/3** show monomer-like cell free binding to IAP constructs, and reference monomers **9**–**11** show moderate cytotoxicity (IC_{50} between 10 and 25 μM against MDA-MB-231 cells). Thus, the weak cytotoxicity of nano-conjugates is likely due to a surprising lack of multimeric behavior that prevents their expected, dimer-like interaction with multiple bifunctional L-BIR2-BIR3 construct from XIAP.

Table 1
Binding affinity on BIR domains, IC_{50} (nM)

Compd	BIR3 XIAP	BIR3 cIAP1	BIR3 cIAP2	L-BIR2-3 XIAP
9	400	NT[a]	NT	320
NP-1	360	38	78	300
NP-A-1	>2000	>2000	>2000	>2000
10	330	NT	NT	190
NP-2	560	150	62	240
NP-A-2	230	38	NT	120
11	760	160	180	190
NP-3	>2000	1400	>2000	410
NP-A-3	580	270	180	410

[a] Not tested.

In summary, we report here the synthesis, the spectroscopical and biological characterization of non-covalent (**NP-1/3**) and covalent (**NP-A-1/3**) SPION-Smac mimetic nano-conjugates as IAP-targeted pro-apoptotic agents. SPION-Smac mimetic nano-conjugates behave as their soluble monomer analogues, retaining monomer-like cell free binding affinity for IAP targets, while being almost inactive in cellular assays. Further efforts will aim to achieve cellular and in vivo activity for SPION-Smac mimetic nano-conjugates in suitable cellular apoptosis/oncology models. Namely, we will vary the connection between Smac mimetics and SPIONs (chemical bond, linker/spacer length, hydro/lipophilicity, etc.), and we will decorate SPIONs with more potent monomeric and dimeric Smac mimetics.

Acknowledgments

We are grateful for the financial support from Cariplo Foundation, Bando 2011, grant title: '*Inter-cellular delivery, trafficking, and toxicity of engineered magnetic nanoparticles in macrophages and CNS cells*'; and from Associazione Italiana Ricerca sul Cancro (AIRC, MCO—9998, D.D.).

Supplementary data

Supplementary data (experimental procedures for the synthesis in solution of Smac mimetics **6**–**8** and **11**. LC–MS and NMR characterization of Smac mimetics **6**–**8** and **11**. Experimental procedures for the preparation of non-covalent (**NP-1/3**) and covalent (**NP-A-1/3**) SPION-Smac mimetic nano-conjugates. Elemental analysis and FT-IR of **NP-1/3** and **NP-A-1/3**. Experimental procedures for cell-free testing/binding affinity determination of soluble Smac mimetics and SPION-Smac mimetic nano-conjugates in presence of BIR domains/constructs from IAPs. Experimental procedures for cellular cytotoxicity testing of SPION-Smac mimetic nano-conjugates against human tumor cell lines) associated with this article can be found, in the online version, at http://dx.doi.org/10.1016/j.bmcl.2014.03.048.

References and notes

1. For selected reviews, see: (a) Sengupta, S.; Kulkarni, A. *ACS Nano* **2013**, *7*, 2878; (b) Cheng, Z.; Al Zaki, A.; Hui, J. Z.; Muzykantov, V. R.; Tsourkas, A. *Science* **2012**,

338, 903; (c) Ahmed, N.; Fessi, H.; Elaissari, A. *Drug Discovery Today* **2012**, *17*, 928.
2. For selected reviews, see: (a) Ling, D.; Hyeon, T. *Small* **2013**, *9*, 1450; (b) Hilger, I.; Kaiser, W. A. *Nanomedicine* **2012**, *7*, 1443; (c) Wahauddin; Arora, S. *Int. J. Nanomed.* **2012**, *7*, 3445; (d) Lin, C.; Cai, S.; Feng, J. *J. Nanomat.* **2012**, 734842.
3. Fang, C.; Kievit, F. M.; Veiseh, O.; Stephen, Z. R.; Wang, T.; Lee, D.; Ellenbogen, R. G.; Zhang, M. *J. Controll. Rel.* **2012**, *162*, 233.
4. Hasany, S. F.; Rehman, A.; Jose, R.; Ahmed, I. *AIP Conf. Proc.* **2012**, *1502*, 298.
5. Mahdavi, M.; Bin Ahmad, M.; Haron, M. J.; Namvar, F.; Nadi, B.; Ab Rahman, M. Z.; Amin, J. *Molecules* **2013**, *18*, 7533.
6. Liu, G.; Gao, J.; Ai, H.; Chen, X. *Small* **2013**, *9*, 1533.
7. For selected reviews, see: (a) De Almagro, M. C.; Vucic, D. *Exp. Oncol.* **2012**, *34*, 200; (b) Fulda, S.; Vucic, D. *Nat. Rev. Drug Disc.* **2012**, *11*, 109; (c) Lopez, J.; Meier, P. *Curr. Opin. Cell Biol.* **2010**, *22*, 872.
8. For selected reviews, see: (a) Evans, C.; Megeney, L. *Apoptosis* **2010**, 55; (b) Riedl, S. J.; Shi, Y. *Nat. Rev. Mol. Cell Biol.* **2004**, *5*, 897.
9. (a) Martinez-Ruiz, G.; Maldonado, V.; Ceballos-Cancino, G.; Grajeda, J. P. R.; Melendez-Zajgla, J. *J. Exp. Clin. Cancer Res.* **2008**, *27*, 48; (b) Du, C.; Fang, M.; Li, Y.; Li, M.; Wang, X. *Cell* **2000**, *102*, 33; (c) Verhagen, A. M.; Ekert, P. G.; Pakusch, M.; Silke, J.; Connolly, L. M.; Reid, G. E.; Moritz, R. L.; Simpson, R. J.; Vaux, D. L. *Cell* **2000**, *102*, 43.
10. (a) Scott, F. L.; Denault, J.-B.; Riedl, S. J.; Shin, H.; Renatus, M.; Salvesen, G. S. *EMBO J.* **2005**, *24*, 645; (b) Srinivasula, S. M.; Hegde, R.; Saleh, A.; Datta, P.; Shiozaki, E.; Chal, J.; Lee, R.-A.; Robbins, P. D.; Fernandes-Alnemri, T.; Shi, Y.; Alnemri, E. S. *Nature* **2001**, *410*, 112.
11. (a) Seneci, P.; Bianchi, A.; Battaglia, C.; Belvisi, L.; Bolognesi, M.; Caprini, A.; Cossu, F.; de Franco, E.; de Matteo, M.; Delia, D.; Drago, C.; Khaled, A.; Lecis, D.; Manzoni, L.; Marizzoni, M.; Mastrangelo, E.; Milani, M.; Motto, I.; Potenza, D.; Rizzo, V.; Servida, F.; Turlizzi, E.; Varrone, M.; Vasile, F.; Scolastico, C. *Bioorg. Med. Chem.* **2009**, *17*, 5834; (b) Bianchi, A.; Ugazzi, M.; Ferrante, L.; Lecis, D.; Scavullo, C.; Mastrangelo, E.; Seneci, P. *Bioorg. Med. Chem. Lett.* **2012**, *22*, 2204.
12. (a) Manzoni, L.; Belvisi, L.; Bianchi, A.; Conti, A.; Drago, C.; de Matteo, M.; Ferrante, L.; Mastrangelo, E.; Perego, P.; Potenza, D.; Scolastico, C.; Servida, F.; Timpano, G.; Vasile, F.; Rizzo, V.; Seneci, P. *Bioorg. Med. Chem.* **2012**, *20*, 6687; (b) Lecis, D.; Mastrangelo, E.; Belvisi, L.; Bolognesi, M.; Civera, M.; Cossu, F.; De Cesare, M.; Delia, D.; Drago, C.; Manenti, G.; Manzoni, L.; Milani, M.; Moroni, E.; Perego, P.; Potenza, D.; Rizzo, V.; Scavullo, C.; Scolastico, C.; Servida, F.; Vasile, F.; Seneci, P. *Bioorg. Med. Chem.* **2012**, *20*, 6709.
13. For selected reviews, see: (a) Vranic, S.; Boggetto, N.; Contremoulins, V.; Mornet, S.; Reinhardt, N.; Marano, F.; Baeza-Squiban, A.; Boland, S. *Particle Fibre Tox.* **2013**, *10*, 2; (b) Wu, Y.-L.; Putcha, N.; Ng, K. W.; Leong, D. T.; Lim, C. T.; Loo, S. C. J.; Chen, X. *Acc. Chem. Res.* **2013**, *46*, 782; (c) Duan, X.; Li, Y. *Small* **2013**, *9*, 1521; For selected examples, see: (a) Panariti, A.; Lettiero, B.; Alexandrescu, R.; Collini, M.; Sironi, L.; Chanana, M.; Morjan, I.; Wang, D.; Chirico, G.; Miserocchi, G.; Bucci, C.; Rivolta, I. *J. Biotech. Nanomed.* **2013**, *9*, 1556; (b) Luther, E. M.; Petters, C.; Bulcke, F.; Kaltz, A.; Thiel, K.; Bickmeyer, U.; Dringen, R. *Acta Biomater.* **2013**, *9*, 8454; (c) Hirsch, V.; Kinnear, C.; Moniatte, M.; Rothen-Rutishauser, B.; Clift, M. J. D.; Fink, A. *Nanoscale* **2013**, *5*, 3723.
14. Manzoni, L.; Arosio, D.; Belvisi, L.; Bracci, A.; Colombo, M.; Invernizzi, D.; Scolastico, C. *J. Org. Chem.* **2005**, *70*, 4124.